pH RESPONSIVE CAPSULES CONTAINING COMPOSITE COATINGS FOR CORROSION INHIBITION IN METAL ALLOYS

A Dissertation
Submitted to the Graduate Faculty
of the
North Dakota State University
of Agriculture and Applied Science

By

Kiran Bhat Kashi

In Partial Fulfillment of the Requirements
for the Degree of
DOCTOR OF PHILOSOPHY

Major Department:
Coatings & Polymeric Materials

July 2014

Fargo, North Dakota

North Dakota State University
Graduate School

Title

pH RESPONSIVE CAPSULES CONTAINING COMPOSITE COATINGS FOR CORROSION INHIBITION IN METAL ALLOYS

By

Kiran Bhat Kashi

The Supervisory Committee certifies that this ***disquisition*** complies with North Dakota State University's regulations and meets the accepted standards for the degree of

DOCTOR OF PHILOSOPHY

SUPERVISORY COMMITTEE:

Dr. Victoria J. Gelling
Chair

Dr. Dean C. Webster

Dr. Stuart G. Croll

Dr. Yechun Wang

Approved:

06/29/2015	Dr. Dean C. Webster
Date	Department Chair

ABSTRACT

Hexavalent chromes have be used as effective corrosion inhibitors due to their high inhibitor efficiency and low cost for the protection of several metal alloys. However, owing to their toxicity federal legislations restrict the use and distribution of these highly toxic materials. The need for an environmentally friendly yet effective alternative to the chrome based corrosion inhibitors has led to the investigation of rare earth metals as potential candidates. Cerium is one such rare earth metal that has received considerable attention as an alternative to hexavalent chromes. However, the high water solubility of some of the cerium salts makes it difficult for the incorporation of such salts in coatings.

In this work, pH responsive microcapsules containing cerium salts were synthesized using an internally phase separated emulsion polymerization technique. Core shell microcapsule consisting of a water core containing dissolved cerium salts were synthesized. The synthesized capsules were characterized using characterization techniques such as Fourier Transform Infrared (FTIR) spectroscopy, UV-vis spectroscopy, Dynamic Mechanical Analysis (DMA), Thermo-Gravimetric Analysis (TGA), and Inductively Coupled Plasma Optical Emission Spectroscopy (ICP-OES). The structure and morphology of the capsules were studied using electron microscopy techniques. The synthesized capsules were dispersed in 2K epoxy coatings and applied on aluminum alloy 2024 T-3 and cold rolled steel substrates. These coatings were exposed to salt spray (ASTM B117) and electrochemically evaluated using electrochemical impedance spectroscopy (EIS), potentio-dynamic(PD) polarization, cyclic voltammetry(CV), open circuit potential(OCP) measurements. Localized corrosion assessment was also performed on the coated metal alloys using Scanning electrochemical microscopy (SECM) to understand the mechanism of corrosion inhibition using cerium encapsulated microcapsules.

ACKNOWLEDGMENTS

First and foremost I want to thank my advisor Dr. Victoria J. Gelling. I appreciate all her contributions in the form of time, ideas and motivation to make my Ph.D. experiences very simulating and memorable. I would like to thank her for not only for allowing me to grow as a researcher but also sharing her valuable experiences to help with my career. I'd like to thank my committee members Dr. Dean Webster, Dr. Stuart Croll and Dr. Yechun Wang for their suggestions.

The members of the Gelling group have contributed immensely to my personal and professional growth during my time at the Department of Coatings & Polymeric Materials. This group has provided some very memorable friendships in addition to great advice and collaborations. I am especially thankful to the following group members for being a constant source of encouragement and valuable resources from whom I have learnt a lot from: Dr. Niteen G. Jadhav, Dr. Abhijeet Suryawanshi, Christopher Vetter, Kenneth Croes, Subramanyam Kasisomayajula and Drew Pavlacky. I would like to acknowledge Dr. Mark Jenson from the Department of Chemistry at Concordia College, Moorhead, MN who worked with the Gelling group on a sabbatical in 2013. I very much appreciate his willingness, creativity and enthusiasm in helping with and designing the Scanning Electrochemical Microscopy (SECM) experiments for the detection of cerium and Rotating Disc Electrode (RDE) experiments. I'd also like to thank the undergraduate research assistants for their help in the synthesis and characterization of microcapsules: Jeff Garty, Austin Maples and Mariah Jorda.

In my work with Scanning Electron Microscopy and elemental analysis work I am particularly indebted to Scott Payne and Jayma Moore. Without their expertise and patience, the incorporation of cerium within the capsules could not have been visualized. I’d like to also thank

Dr. Donna Jacob, Assistant Director of the Wet Ecosystems Research Group, at the Department of Biology at North Dakota State University for helping with Inductively Couple Plasma (ICP) experiments at her laboratory.

I gratefully acknowledge the founding sources that made my Ph.D. work possible. I would like to acknowledge the support for this research by U.S. Army Research Laboratory under grant no. W911NF-09-2-0014, W911NF-10-2-0082, and W911NF-11-2-0027.

My time at North Dakota State University was made enjoyable by a large group of friends and certain families in Fargo who will be missed dearly. I am also grateful to the students, staff, and faculty of Department of Coatings and Polymeric Materials at North Dakota State University for providing me a wonderful ambiance to work.

Lastly, I would like to thank my family for all their love and encouragement in letting me pursue my dreams. Special thanks to my dad who I have always looked up to and who has been my inspiration.

TABLE OF CONTENTS

LIST OF TABLES

LIST OF FIGURES

LIST OF APPENDIX TABLES

LIST OF APPENDIX FIGURES

CHAPTER 1. FUNCTIONAL COATINGS: USING POLYMER ENCAPSULATION FOR CORROSION INHIBITION

1.1. Introduction

We live in a highly metal - based society and our dependence on metals and their alloys is ever increasing. There are 85 metals in the periodic table and common metals, whatever be their end use, tend to interact with their environment to different extents and at different rates. The interaction with the environment, which causes deterioration in their physical and chemical properties due to electrochemical oxidation, is termed as corrosion. According to American Society of Testing Materials' corrosion glossary, corrosion is defined as "the chemical or electrochemical reaction between material, usually a metal, and its environment that produces a deterioration of the material and its properties."[1] In other words, corrosion is the extractive metallurgy in reverse,[2] thus making it impossible to avoid.

Like natural hazards such as earthquakes or severe weather disturbances, damage caused by corrosion can be dangerous and expensive. In a study entitled "Corrosion Costs and Preventative Strategies in the United States," the total annual estimated direct cost of corrosion in the U.S. was estimated a staggering $276 billion equaling approximately 3.1% of the nation's Gross Domestic Product (GDP).[3] The expenditure incurred is divided into two costs (a) avoidable cost, which are costs that can be reduced by the effective use of the existing corrosion technology and (b) unavoidable costs which are a result of presently unavoidable losses. It has also been reported that the cost of corrosion could be reduced as much as by 15% by the use of proper use of existing technology[4] such as proper design, selection of material, coatings and linings, cathodic protection and inhibitors. Even though corrosion management in the U.S. has improved in the past decade there still remains better ways to support and implement optimum corrosion control practices. One of the most common corrosion preventative techniques is the use of corrosion inhibitors. Compared to other techniques, use of corrosion inhibitors is very convenient due to the ease of application either by themselves or within a protective coating.

The focus of this work is on the use of encapsulation technique as a viable route for the delivery of water soluble corrosion inhibitors which have the potential to replace chromates in a coating system for corrosion inhibition in metal alloys. Thus this chapter, after a brief introduction to general corrosion, details corrosion inhibition with emphasis on the lanthanide series of elements as potential environmentally-friendly corrosion inhibitors followed by a detailed review of encapsulation techniques that have been employed in designing self-healing coatings.

1.2. Metal corrosion in an electrolyte

Corrosion is an electrochemical process i.e. it does not occur by direct chemical reaction of a metal with its environment but through coupled electrochemical half-cell reactions. For any metal to corrode there are four basic requirements that need to be met. They are:

a) an anodic reaction,

b) a cathodic reaction,

c) a conductive path between the anodic and cathodic sites,

d) and the presence of an electrolyte.

An anode is the site on the metal surface where the metal dissolution occurs with the liberation of electrons and metal ions. These generated electrons travel to the cathode via an electrical path through the metal where they reduce the positively charged ions. This sets up a complete electrical circuit with current flowing from anode to cathode ionically and from cathode to anode electrically.

A typical corroding system is often times complex. Several factors in addition to the four basic requirements affect corrosion reactions. Examples of the factors are temperature, pH, dissolved oxygen content, stirring effect and salt concentration in the electrolyte. In a simple electrochemical setup with metal immersed in an electrolyte, reaction (1.1) represents the anodic reaction whereas based on the pH of the media; several different cathodic reactions are possible.

$$M \rightarrow M^{n+} + ne^- \tag{1.1}$$

$$O_2 + 2H^+ + 2e^- \rightarrow 2H_2O \text{ ; pH = 0} \tag{1.2}$$

$$2H_2O + 2e^- \rightarrow H_2 + 2OH^-\text{; pH = 7} \tag{1.3}$$

$$2H_2O + O_2 + 4e^- \rightarrow 4OH^- \text{ ; pH = 14} \tag{1.4}$$

In these complicated situations, a Pourbaix diagram (potential vs. pH) gives clear thermodynamic information of the system in terms of favored corrosion products at a given potential and pH. As stated before, the process of corrosion involves simultaneous charge transfer and mass transfer across the metal/solution interface. The link between charge transfer and mass transfer is given by Faraday's law. To obtain the corrosion rate, mass loss due to corrosion (m) is related to current flow using Faraday's law given by:

$$m = \frac{ItA}{nF} \tag{1.5}$$

where I is the current in amperes, t is the time in seconds, A is the atomic weight of the metal, F is Faradays constant (96458.34 C mol^{-1}) and n is the number of equivalents transferred per mole of the metal. Another method to calculate corrosion rate is using a polarization experiment. A polarization experiment with its resultant Tafel plots can be used to extract the equilibrium corrosion potential and the current density. The overall corrosion reaction in a system with multiple possible redox reactions can be used to determine the equilibrium potential using mixed potential theory.

The two most commonly used metals in structural applications are alloys of steel and aluminum, due to their cost, strength, ease in fabrication, load bearing capacities etc. However, one of the major issues of using these metals is the problem of corrosion. If this issue is addressed then optimal performance can be extracted from these materials.

Steel is the most important and widely used structural material. For a civil engineer involved in the planning and design of steel structures, in addition to accounting for tensile and compressive stresses, it becomes important to consider corrosion as one of the key aspects of design of metal structures. Steel structures may be exposed to a variety of corrosive environments and a clear understanding of corrosion processes is essential to understand steps to inhibit corrosion. In the presence of water/moisture, salts and oxygen, steel (iron) corrodes to form oxides and mixed species which acts as a barrier. However, such an oxide layer is loosely bound to the metal and unable to protect the metal from further corrosion. Iron corrodes rapidly in at pH below 9 and is passive at pH above 9.

Pure aluminum is light and soft metal that demonstrates excellent corrosion resistance due to the formation of a passive oxide layer. Pure aluminum shows pH dependent corrosion. As the pH increases the corrosion rate decreases up to a pH of 7.5. However, at a pH of ~8 the corrosion rate begins to increase again.   Due to its “soft” nature its use had been limited until alloying came to existence. To enhance the mechanical properties aluminum is alloyed with elements such as copper, zinc, magnesium, manganese etc. However, this strength increase comes at the price of galvanic coupling of various alloy components leading to localized corrosion. Due to these inherent defects in metals, the protection of these alloys from corrosion becomes important not only to increase the service lifetimes of the structures made from these alloys but also increase the safety of using these structures.

1.3. Corrosion inhibition

Corrosion protection can be employed by either changing the electrode potential of the metal surface or changing the nature of the metal itself. Cathodic protection and anodic protection are two methods of corrosion control by changing the electrode potential. The use of metallic coatings or use of corrosion-resistant alloy is a way to prevent corrosion by changing the nature of the metal. In a market driven by cost, very often the choice of a corrosion resistant alloy is not the most economical alternative. In such cases, the use of corrosion inhibitors becomes a possible means of corrosion control. A corrosion inhibitor is defined as a chemical substance or combination of substances that, when present in the proper concentration and forms in the environment, prevents or reduces corrosion.[1] Inhibitors function in many ways to control corrosion, namely by adsorbing as a thin film on the metal surface or by forming a thick corrosion product that is impervious to further attack by the environment or by changing the characteristics of the environment and making it less aggressive to the metal surface. Corrosion inhibitors are used in various industrial applications such as potable water [6, 7], automobile engine coolants[8, 9], acid pickling[10], surface treatment of various metal alloys [11, 12]to name a few.

Corrosion inhibitors are classified in several different ways. Depending on the mechanism there are two broad classifications (i) adsorption inhibitors and (ii) film forming inhibitors. Adsorption inhibitors for a chemisorbed layer with the metal surface and impede the electrochemical dissolution reaction. Film – forming inhibitors are divided into two types (i) passivating inhibitors and (ii) precipitation inhibitors. Passivating inhibitors promote the formation of a passivating layer on the surface of the metal whereas precipitation inhibitors aid in the formation of a barrier between the corroding metal and the environment by participating in a precipitation reaction between the metal cations. Another classification of corrosion inhibitors is by the electrochemical reaction that they affect. The common classifications of corrosion inhibitors are listed below.

a) Anodic Inhibitors: compounds that reduce the rate of metal dissolution i.e. inhibit the anodic reaction.

b) Cathodic Inhibitors: compounds that reduce the rates of cathodic reactions such as hydrogen evolution or oxygen reduction reactions.

c) Mixed inhibitors: compounds that reduce the anodic and cathodic reactions by adsorption covering the entire surface.

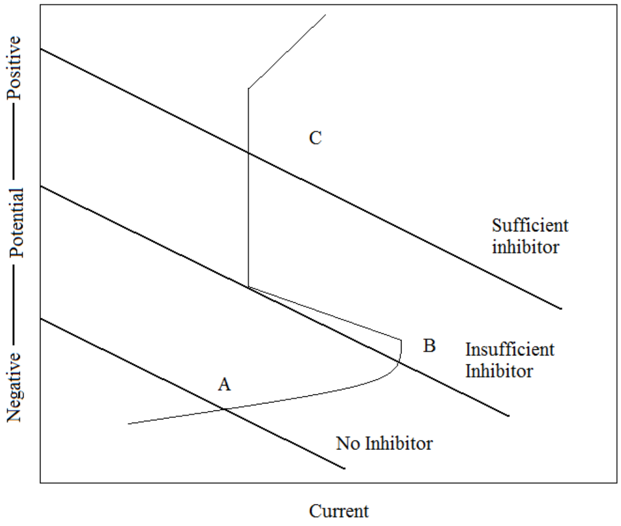

Figure 1.1. Polarization curve of active-passive metal showing dependence of corrosion current on inhibitor concentration. Reprinted from reference 13 Revie, R. W., Corrosion protection. In *Uhlig's Corrosion Handbook*, John Wiley & Sons: 2011; pp 1094. Copyright© 2011 John Wiley & Sons Inc. This material is reproduced with permission of John Wiley & Sons, Inc.

Anodic inhibitors are used in near neutral solutions where the corrosion product such as oxides, hydroxides or salts are sparingly soluble, thus forming a passivating film that inhibits further metal dissolution. The mechanism of anodic inhibition can be better explained using a polarization diagram of an active metal (Figure 1.1). In the absence of the inhibitor, the metal corrodes in the active state corresponding to point A and as the corrosion inhibitor concentration is increased the metal moves from an active region to a more passive region. The point B represents the critical corrosion rate or concentration where the passive layer begins to develop. At point C the corrosion rate decreases due to the formation of a passive layer. In the presence of cathodic inhibitors, on a polarization plot, the slope of the cathodic branch is altered due to formation of precipitates at the cathode. Adsorption plays a very important role in corrosion control using inhibitors. Adsorption may occur as a result of electrostatic forces between the metal surface and the charge on the inhibitor molecules. The charge of a metal surface can be determined from the knowledge of corrosion potential (E_{corr}) and zero-charge potential (ZCP). If the difference (E_{corr} – ZCP) is negative then the metal surface is negatively charged and favors cation adsorption and if the difference is positive then anion adsorption is favored. The strength of the adsorption depends on the anchoring group and its ability to replace water molecules from the metal surface. At first the inhibitor interacts with the surface in a reversible low activation energy step. This process is called “physical adsorption”. Chemisorption takes place under more favorable conditions when physically adsorbed inhibitor molecules donate electrons and form an ionic bond. Chemisorption – type inhibitors usually contain Se, P, N, S or O atoms which have lone pair of electrons or loosely bound electrons. The inhibiting efficiency of such inhibitors depends on the nature of the heteroatom and the inherent electronegativity. Other types of inhibitors include scavengers that reduce the corrosivity of the metal by removing aggressive species present in the medium; vapor phase inhibitors that control corrosion by formation of a film at the metal environment interface after vaporizing and interacting with the metal.

Benzoic acid, Benzotriazole (BTA), Thiourea and their derivatives are good examples of organic inhibitors. Electronically conducting polymers such as pyrrole, thiophene and aniline are also good passivating corrosion inhibitors for metals. Chromate and nitrites are the best known oxidizers that passivate the metal surface. Benzoates, azelates and phosphates are non-oxidizing inhibitors that passivate the metal surface after adsorption. Zinc and magnesium salts are known to shut down cathodic reactions by the formation of hydroxides and depositing on the metal surface. Oxygen scavengers such as sodium sulfite limit the oxygen supply to facilitate cathodic reactions in neutral or basic conditions.

The performance of a corrosion inhibitor is evaluated by comparing the corrosion rate of a metal with and without the corrosion inhibitor and calculating the inhibitor efficiency given by,

$$\%I = \frac{i_0 - i}{i_0} \times 100 \tag{1.6}$$

where i_0 is the corrosion rate without the inhibitor and i is the corrosion rate with the inhibitor.

1.3.1. Chromates as Corrosion Inhibitors

No discussion about corrosion inhibition is complete without discussing the effectiveness of chromates as corrosion inhibitors. Chromates by far are the best known corrosion inhibitor for most commonly used metals such as steel, aluminum, zinc and magnesium.[14] Traditionally, chromates are applied as a pretreatment to passivate the metal surface and resist corrosion.[3] A typical chromate conversion coating for aluminum consists of soluble hexavalent chromium salts and chromic acids. This mixture upon interaction with aluminum precipitates as a continuous insoluble layer of trivalent chrome, which has excellent corrosion resistance, good paint adhesion, low cost and self-healing abilities.[15] The protection offered by this layer is so superior that they are used in areas where corrosion protection is of utmost importance such as in aerospace components.[11]

Chromates are both anodic and cathodic inhibitors due to their ability to form precipitates with metal ions at anodic sites and reduction to trivalent chromium at that cathodic sites.[16] In addition to being both a cathodic and anodic inhibitor, oxo-anion compounds of chromium have another unique ability to dissolve as stable compounds / complexes in water. Thus they are readily transported to localized sites where they get reduced to various stable inert compounds of Cr^{3+} .[17] Compounds of Cr^{3+} irreversibly adsorb at the metal surface to form a good hydrophobic barrier with good adhesion properties. When used in paint systems, oxo-anion compounds of chromates have limited solubility thereby not causing blistering of the paint but at the same time leaching at very low concentrations sufficient to act as an active corrosion inhibitor[3]. It has been reported in the literature that chromate conversion coatings not only act as reservoirs of hexavalent chromium but also release them upon attack by aggressive anions.[18, 19]In the presence of aggressive anions such as Cl^- or SO_4^{2-}, chromates competitively adsorb to the metal surface which is another major property of chromate conversion coatings[20]. In general, chromium conversion coatings function[17] as follows,

$$Cr^{6+} \rightarrow Cr^{3+} + 3H_2O \rightarrow Cr(OH)_3 + 3H^+ \rightarrow Cr_2O_3.3H_2O \tag{1.7}$$

In alkaline conditions[21],

$$CrO_4^{2-} + 4H_2O + 3e^- \rightarrow Cr(OH)_3 + 5OH^- \tag{1.8}$$

In case of iron corrosion in near neutral conditions[22],

$$6FeO + 2CrO_4^{2-} + 2H_2O \rightarrow Cr_2O_3 + 2Fe_2O_3 + 4OH^- \tag{1.9}$$

In an acidic environment, CrO_4^{2-} converts to $Cr_2O_7^{2-}$ which is a strong oxidant, and reacts with metal substrates as follows[23],

$$\frac{6}{n}M^0 + Cr_2O_7^{2-} + 7H^+ \rightarrow \frac{6}{n}M^{n+} + 2Cr^{3+} + 7H_2O \tag{1.10}$$

where M^0 can be Al, Fe or Zn.

The same reactivity of aqueous Cr^{6+} that imparts excellent corrosion resistance to metals can interfere with biochemical oxidation mediators in the body and make them highly toxic and carcinogenic.[16, 24] The harmful effects of chromates on humans have been well documented on human tissues. Dermatitis and skin cancer are have been reported among workers that handle components with chromium pretreatments.[25] Since chromates are highly water soluble they can easily pass through the cell membrane and form free radical intermediates that damage DNA.[26-28] The Environmental Protection Agency (EPA) reports that short exposure to > 0.1 ppm chromium can cause shortness of breath, coughing, wheezing and/or skin irritation, whereas, prolonged exposure can lead to damage to circulatory system and nervous tissues, stomach upsets, kidney and liver damage, bronchitis and potential death.[29] Owing to above mentioned ill effects due to the use of chromates, several agencies such as the World Health Organization (WHO), International Agency for Research on Cancer (IARC), EPA have declared chromates a human carcinogen.[30, 31] However strict the regulations are for the use and disposal of chromates, they still continued to be used because there exists no chemical in the market that offers the same degree corrosion protection as chromates.

1.3.2. Chromate Replacements

Due to rising environmental concerns and associated health impacts, several studies have been focused around replacing chromes as corrosion inhibitors. For an effective replacement of

Cr^{6+}, an inhibitor has to inhibit both oxygen reduction reaction as well as anodic dissolution reactions. The search to find a promising chromate replacement has increased the research and production of new materials and technologies in the academic, industrial and governmental sections.

Several barrier coatings have been developed or modified specifically to follow federal environmental regulations. Low temperature cationic plasma deposition is currently used to create ultra-thin hydrophobic barrier coatings with high crosslink densities and virtually defect free matrices.[32] Plasma coatings have two important properties, commendable corrosion resistance due to high crosslink densities and excellent adhesion to substrates. The polymerization method produces a highly cross-linked polymer film that is covalently bonded to the metal surface enabling the material to display excellent chemical resistance and adhesion. Low temperature plasma coatings display the best performance to corrosion protection for steel substrates immersed in simulated seawater.[33] Another most commonly used method for depositing thin oxide films is by the use of sol-gels. Upon deposition, the coating undergoes hydrolysis and condensation to form a continuous hydrophobic 3-D matrix. Even though sol-gel films provide excellent corrosion resistance, they offer limited use due to poor adhesion, shrinkage and oxidation of the substrate[34]. It has been found that one of the major characteristics controlling corrosion protection is the film thickness.[35, 36] The thinner the coating film, the better the barrier property. The use of conducting polymers such as polyaniline and polypyrrole as corrosion inhibitors has emerged in the past decade.[37] The mechanism for corrosion protection is not by increasing the barrier properties but by aiding the passive layer formation at the metal surface.[38, 39] Despite their excellent corrosion protection abilities the conducting polymers thus far reported, cannot be processed as thin films. Their application process involves either electropolymerization in acid media or casting non-conductive films and converting it to its conducting state. A polymer referred to as PAN/polyE, designed with both polyaniline (PAN) and polyelectrolyte (polyE) segment, was compared with traditional chromates using Electrochemical Impedence Spectroscopy and polarization measurements[40]. It was noted that the PAN/polyE system performed very similar to that of the chromates. Salt spray immersion also revealed that the polyaniline system showed negligible disbondment and no corrosion in the scribe.

Another approach to increased corrosion protection is the use of surface modification techniques to create a conversion layer. Conversion layers modify a surface to promote better adhesion, create a surface free of contaminants or incorporate active corrosion inhibitors. A conversion layer can be created by several methods such as electrochemical anodization, plasma abalation, vapor deposition, cathodic magnetron sputtering etc.

Molybdates, vanadates, permanganates and tungstates were the first candidates that evaluated as potential replacements for chromates since they are oxidants and have chemical elements from the VI and VII groups similar to chromates.

One of the earliest reports of using molybdates as corrosion inhibitors dates back to 1976. Molybdate conversion coatings can obtained by simple immersion or by electrochemical methods. The nature of the acids used and the pH of the bath have been reported to affect the quality of the deposited layer. Depending on the nature of the acid used, the pH of the bath can vary from 1-6. Other factors such as temperature, additives, concentration and immersion time have shown to affect the corrosion performance of molybdate conversion coatings. Due to their oxidizing power and ability to form stable reduction products which form a passivating layer molybdates are considered as close replacement to chromates. Molybdates do not offer superior corrosion protection as chromates because the oxidizing potential of MoO_4^{2-} was not as strong as dichromates and the molybdate species were too large to accumulate at flaws or defects.[41] The effectiveness of molybdates as inhibitors was also largely found to be dictated by the presence of chlorine ions and the concentration of the molybdate containing solution.[42] Among the most promising candidates being investigated as active inhibitors are cerium compounds, molybdates, vanadates and phosphates. What seems like the closest replacement to chromium (VI), its less toxic equivalent chromium (III) is not as effective as hexavalent chrome. In the presence of an oxidizing agent such as dissolved oxygen the metal undergoes oxidation generating hydroxyl ions that combine with the chromium (III) to form a conversion coating composed of mixed oxides and hydroxides of the substrate and chromium (III).

Zinc phosphates were initial replacement pigments for zinc chromates. They display no toxic effect and provide corrosion protection by forming a layer of $Zn_3(PO_4)_2.4H_2O$.[11] In a research article, EIS was used to determine the corrosion resistance of several commonly used phosphates for AA2024-T3. They determined that even though phosphates performed appreciably, chromates provided better protection to the substrate.[43]

In an attempt to evaluate possible alternatives for chromes Taylor and Chambers[44, 45] used a high throughput screening method to experimentally determine the best possible inhibitors to replace chromates in coatings. In this study 10 compounds and 44 binary combinations were tested for the corrosion inhibition on AA 2024 using DC polarization, copper redeposition and fluorometric methods. They found that the use of molydate anions and rare earth (cations) salts resulted in significant reduction in corrosion.

Organic corrosion inhibitors have also been studied alongside inorganic ones as possible chromate replacements. Most organic inhibitors come in the form of weak acids that interact with the metal surface and deposit as insoluble salts. Chelating agents are a class of organic inhibitors that complex and form a thin passive layer by bonding with the metal surface. Solution of sodium sebacate is known to form a thick white precipitate which was found to inhibit both pit nucleation and pit growth. Among the other organic corrosion inhibitors sodium benzoate, sodium acetate and thioglycolic acid have also been found to decrease pit initiation.

1.3.3. Lanthanide Compounds as Environmentally-friendly Corrosion Inhibitors

It is well known that lanthanide ions form insoluble hydroxides [46]which enable them to be used as cathodic inhibitors. Owing to their low toxicity, the ingestion or inhalation of these inhibitors or their complex oxides/hydroxides not considered harmful.[47] From an economic standpoint too, the use of these elements would be inexpensive[48] due to their relative abundance in nature.[48, 49] Considering these factors, it is reasonable to develop of corrosion protection methods using the lanthanide series of elements from the periodic table. Initially, the lanthanide elements were used for high temperature corrosion protection. The surface films that were generated by the use of these rare earth metals improved both high temperature oxidation and aqueous corrosion[50]. The earliest application of lanthanides as corrosion inhibitors were stimulated by the need to replace chromates imposed by the new international environmental standards. Lanthanides have been used as corrosion inhibitors for several metal alloys of zinc[51, 52], nickel[53, 54], copper[55], mild steel[56-58] and stainless steel.[59, 60]

Hinton et al. [61-65] extensively studied the corrosion protection offered by lanthanides on several aluminum alloys. The effect of $CeCl_3$ concentrations on both pitting and uniform corrosion of AA 7075 was studied using weight loss and linear polarization measurements. It was determined that the uniform corrosion rate decreased steeply in solutions containing up to 100 ppm of cerium chloride after which a steep increase in corrosion rate was noted in the concentration range of 100 to 1000 ppm. The inhibition behavior of other lanthanides such as YCl_3, $LaCl_3$, $PrCl_3$ and $NdCl_3$ has also been extensively studied by several authors.[60, 65, 66] In summary, it was determined that chloride salts of cerium provided the highest degree of corrosion inhibition in 3.5% NaCl solution on AA7075 (Figure 1.2) All the more, the degree of inhibition provided by optimum concentration of cerium chloride was determined to be on par with chromate, showing that lanthanide salts could be considered as an efficient and ecological alternative to chromates.

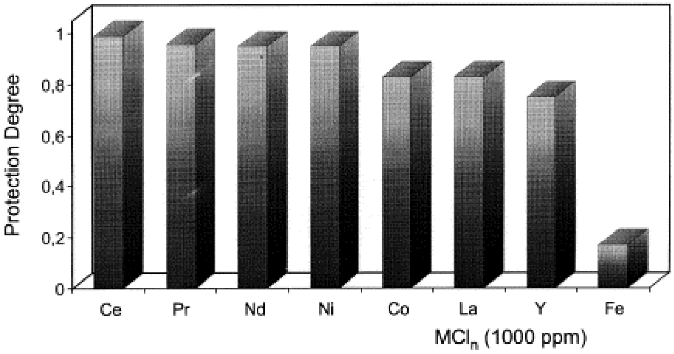

Figure 1.2. Degree of protection against uniform corrosion of AA 7075 in presence of 1000 ppm of different metallic chlorides in 3.5% NaCl solutions.(Reprinted from reference 67 Corrosion Science, 40 (11), Bethencourt, M.; Botana, F. J.; Calvino, J. J.; Marcos, M.; RodrÍguez-Chacón, M. A., Lanthanide compounds as environmentally-friendly corrosion inhibitors of aluminium alloys: a review, 1803-1819,1998, with permission from Elsevier.)

Cerium is the only lanthanide element that exhibits a tetravalent oxidation state that is stable in a complex aqueous solution. Ce^{4+} behaves somewhat like Cr^{6+}. However, the reduction product Ce^{3+} is not as stable as Cr^{3+}. Cerium salts inhibit corrosion cathodically as demonstrated by Isaac et al. [68], using galvanic coupling experiments where a cerium rich layer was found to deposit over copper (cathode) on AA 2024 surface as confirmed by Scanning Electron Microscopy (SEM) with elemental analysis. The corrosion inhibition using cerium salts was studied further by Bethencourt et al.[67] who confirmed its cathodic behavior using EDS on AA 5083 by monitoring the copper cathodic sites for cerium-island like deposits. The hydroxyl ions generated as a result of the cathodic corrosion reaction were found to react with the cerium ions resulting in the formation of cerium islands that decreased the available cathodic current and hence reduce the overall corrosion.

Based on this ability of lanthanides especially cerium to form protective films, different pretreatments have been proposed similar to that of chromes. The earliest attempt to obtain lanthanide conversion coatings by immersion was made by Hinton et al. where they immersed AA7075 in 1000 ppm of $CeCl_3$ until a minimum corrosion rate was observed. Scanning Electron Microscopy images of the alloy after 90 hours revealed that a cerium containing film was formed on the entire surface of the immersed metal. In order to evaluate the corrosion inhibition of these films, Electrochemical Impedance Spectroscopy (EIS) was employed.[69-72] It was determined from EIS that the cerium conversion coatings not only showed good performance against corrosion but also improved the adhesion of epoxy layers deposited on the metallic surfaces. The protective nature of these conversion coatings however, was determined to vary from alloy to alloy. One such example was observed in AA 2090 and AA 8090 where the protective nature of conversion coating film was limited for a short duration.[73] Hinton and Wilson[74] developed a new and a rapid film deposition method called “Cerating” which were successfully applied to a wide range of metal alloys. Cerate coating reported in the literature was basically obtained by fully immersing a metallic alloy in an aqueous solution of cerium chloride with 0.3% hydrogen peroxide for 10 minutes at 316 K and a pH of 1.9.[75] A prior surface cleaning and deoxidizing treatment was also applied followed by a silicate solution seal. In case of AA 2024, it was observed that the corrosion rate reduced by about 95% in sodium chloride solution after cerating. These cerate coatings shifted the corrosion potential by 200 mV cathodically and passed 336 hours in salt spray evaluation. However, the level of protection provided was found to be dependent on the pretreatment before the application of the cerium rich coating and the sealing after the coating.

Electrolytic activation has also been investigated by many authors as a method to deposit films of lanthanide elements on metallic surfaces. A galvanostatic treatment with a cathodic current of 0.1 $mAcm^{-2}$ and a 30 minute exposure to 1000 ppm $CeCl_3$ was determined to reduce corrosion rate by one order of magnitude which is significantly lesser in comparison to full immersion technique.[61] To improve the corrosion performance, cerium nitrate salts were used instead of cerium chloride and a cathodic potential of 90 V was applied for 150 seconds to AA7075. It was observed that pitting potential increased by 300 mV and this increase in pitting potential was attributed to the enriched layer of Ce^{3+}.

Another promising alternative to the use of single inhibitor species is that of using synergistic combinations of two or more compounds.[45] Synergy occurs when inhibition by the combinations exceeds the arithmetic sum of the inhibition by individual components. One of the earliest attempts in employing synergistic combinations of inhibitors was developed by Mansfeld et al. for AA 6061.[76] In this approach the alloy was immersed in hot dilute $CeCl_3$ and $Ce\ (NO)_3$ solutions in the pretreatment step followed by anodic polarization to 0.5 V (vs. SCE) in 0.1 M sodium molybdate. The resulting film on the metal surface was determined to be a highly stable oxide that inhibited oxygen reduction reaction. Baldwin et al.[77] studied the inhibitor efficiency by combining cerium and molybdate salts for several alloys employed in the aerospace industry with promising results.

1.4. Self-healing in coatings & composites

Another approach to providing corrosion protection to metal alloys is by the application of organic coatings to metal surfaces and thus limiting the interaction of the metal with its environment. Corrosion-resistant coatings are critical in the protection of metallic components that operate in aqueous environments. One of the limitations of currently used techniques for corrosion protection is the inability to provide protection when the barrier is damaged due to scratch/abrasion. To address this issue, researchers have examined the use of self-healing materials in coatings that heal a potential defect and restore the coating to its initial (virgin) state. . "Self-healing can be defined as the ability of a material to heal (recover) damages automatically and autonomously without external intervention".[78] One of the approaches used in self-healing coatings is microencapsulation. Microencapsulation, a process by which micron sized solid particles, liquids or gases are incorporated an inert shell enables the isolation and protection of the material from the environment.[79, 80] In the 1930s Barrett Green studied colloidal chemistry[81] and created the first gelatin microcapsules by coacervation technique which was later used to create a colorless dye based paper which upon application of mechanical pressure using a pen would release visible color.[82] The use of polymers as encapsulating materials came to existence in the early 1960s, when the need for materials to act as a rate controlling devices or containers began to gain importance.[83] Release technology is classified into various types depending on the kinetics and mode of release. The various types are (a) Erodible devices that disappear; (b) Membrane encapsulated reservoir devices; (c) Matrix devices; (d) Reservoir devices without a membrane.[83] Pharmaceutical industry has been the pioneer in the use of this technique to protect drugs from the acidic environment of the stomach to successfully target the drug to specific areas in the body, or provide sustained release of the same.[84-86] Encapsulation also finds applications in the food industry to encapsulate flavors, retain aroma, increase product shelf life and protect ingredients from oxidation.[87, 88]

Self-healing polymers and composites are classified into two types depending on the nature of the stimulus as (1) intrinsic and (2) extrinsic polymers. Intrinsic polymers exhibit self-healing without the assistance of any external stimulus whereas extrinsic ones require healants to be intentionally pre-embedded. The use of either types results in a full-scale or functionality restoration.

Intrinsic self-healing polymers and composites are based on specific molecular structures and interactions (physical, chemical and supramolecular) that enable crack recovery. Thermoplastic polymers have received significant interest in self-healing because of their ability to cover up damage by slight changes in temperature. Wool et al. [89, 90] highlighted that the self-healing process goes through five stages: (i) surface rearrangement,(ii) surface approach (iii) wetting (iv) diffusion and (v) randomization. The crack healing behavior of different molecular weights and compositions of poly (methyl methacrylate) and poly(methyl methacrylate co-methyl ethylacrylate) revealed 100% recovery in short term loading properties upon heating slightly above their glass transition temperature under slight pressure.[91] The recovery of fracture stress was also determined to be proportional to $t^{1/4}$ (t is the period of heat treatment).[92] Crack healing in thermoplastics only occurs at or above the glass transition temperature. For polymers with glass transition temperatures above the operating temperatures, effect of various solvents used to decrease the glass transition temperature has also been studied.[93-95] Elevated temperatures have shown better mechanical properties due to mechanical interlocking of the polymer chains and possible hydrogen bond formation between the solvent and the polymeric chains.[96] Mechanical recovery of several thermoplastics has also been investigated using not only global measurement techniques but also using localized measurement techniques such as atomic force microscopy.[97]

Unlike thermoplastics, heating induced healing in thermosets usually depends on crosslinking between unreacted functional groups. Healing of epoxies for example, has to proceed above the glass transition temperature[98] in order to facilitate the inter-diffusion of polymer molecules and cause the residual functional groups to react with one another. In such cases impact strength recoveries as much as 50% have been reported.[99] Furthermore, lower crosslink densities have shown to favor higher recovery.[100] In polyurethanes, by altering the [NCO] to [OH] ratio different crosslink densities were obtained, which at the proper ratio showed rapid recoveries (in cracks) at room temperature.[101] Higher percent recoveries were reported where high molecular weight pre-polymers were used.[102]In order to achieve repeatable self-healing, use of semi-interpenetrated network of thermo/thermoset plastics has also been explored. In such a system, a soluble linear polymer (thermoplastic polymer) was mixed into a thermosetting resin such as an epoxy.[103, 104] The mechanism by which these networks demonstrate self-healing is that upon heating the fractured resin system, the thermoplastic material would mobilize and diffuse through the thermoset resin with some chains bridging across the cracks, thus facilitating recovery. Such recovery has also been extended to composites to decrease delamination at the fiber-polymer interface. Besides simple heating induced healing, thermo-mechanical healing has also been investigated for ballistic applications.[105]

Another strategy used to heal micro-cracks and mechanical wear in polymers is by inversing reactions i.e. by recombination of broken bonds. One such compound that recovers by inverse reaction is poly-(phenylene ether) (PPE). In a PPE system a deterioration results in the generation of a radical that is subsequently is stabilized hydrogen ions. Copper (II), used as a catalyst in this system, aids the reaction and causes polymerization. Similar recovery was also observed in the cause of polycarbonate and poly (ether ketone).[106] Reversible polymers demonstrate reversibility in the polymerization process or in their crosslinking chemistries. One of the common chemistries in reversible polymerization is Diels-Alder (DA) reaction. At temperature above 120 °C, the inter-monomer linkages in multi-furan and multi-maleimide compounds disconnect, and reconnect upon cooling.[107] This fully reversible process can be used to restore fractured parts of polymers. In comparison, these reversible polymers were found to possess similar mechanical strength as commercial epoxy or unsaturated esters. Several multi – furan and multi-maleimide have been synthesized using epoxy precursors in order to incorporate the advantages of epoxy resins such as solvent and chemical resistance, thermal and electrical properties as well as good adhesion.[108] Click chemistry has also been utilized in synthesizing poly-methacrylate bearing reactive furfuryl functionality and crosslinked with bis-maleimide to form completely de-crosslinkable structure.[109] Several modifications have been done to DA type monomers to incorporate properties such as recyclability[110] and improved mechanical properties.[111-113]

The use of supramolecules for intrinsic self-healing has also been explored. In an attempt to make polymers with high performance properties with reversible crosslinking, effect of hydrogen bonding between different supramolecules was explored by Chino et al.[114] These molecules could be rearranged by heating and reformed upon cooling. A temperature dependent mechanical strength was also observed in case of these molecules with lower viscosities at higher temperatures. Initial adhesion due to physical contact was determined to be sufficient to hold the molecules together however, as long as 3 hours was required to restore the mechanical properties to its initial state.[115, 116] As much as 100 % recovery in mechanical properties with repetitive cycling has been reported using these large molecules.[116] This relatively fast recombination of high density groups is attributed to the grafting of hydrogen bonding moieties onto appropriate backbones. Harreld et al. synthesized self-healing non-covalently crosslinked organosiloxane-polypeptide block copolymer which not only provided toughness but also allowed for re-healing by reforming of the crosslinks.[117] π-π stacking interactions have also been utilized instead of hydrogen bonded self-healing using supramolecular chemistries. When low molecular weight polymers capable of adopting a chain-folded conformation, conform in a tweezer type conformation, they generate π – electron deficient receptors. The deficient sites in presence of a complimentary π – electron rich end groups were found to display autonomous healing at ambient temperatures self-repairing supramolecular polymer system.[118, 119] In a polydiimide-polysiloxane system, the thermo-reversible healing was reported to occur by the disruption of the π-π stacking crosslinks as the temperature increased followed by the flow due to low T_g of polysiloxane, resulting in the reestablishment of π-π stacking interactions.

The self-healing mechanism discussed thus far, are classified under intrinsic self-healing materials as the resin matrix display self-healing. The second class of materials widely used is extrinsic self-healing materials in which the resin matrix lacks the ability to self-heal. The healing agent is stored in some media and embedded into the resin during the application which provides the required self-healing capabilities. As soon as damage is inflicted upon this system the healing agent is released at the damage site and healing is achieved. Two types of containers are commonly used in self-healing, namely (i) healant loaded cylinders/pipes and (ii) healant loaded microcapsules.

Glass tubes and fibers commonly used in fiber reinforced composites might have been the inspiration to use as vehicles to carry healants in a continuous resin matrix. The core issue of this technique lies in filling the brittle walls of these vessels with polymerizable medium. One of the first attempts to use hollow glass tubes was proposed by Dry.[120-123] Initially attempts were made to incorporate hollow glass fibers that had a larger external diameter; owing to the large size (of the order of millimeters) these glass capillaries posed much serious problem to composite failure. In order to overcome this issue, the use of hollow fibers was proposed.[124] These tiny fibers were filled with healants using vacuum assisted capillary action. Using the vacuum assisted capillary technique three types of healing systems were developed: (i) single-part adhesive – hollow pipettes containing single component resin; (ii) two part adhesive : two component resin system both included in the hollow cylinders; (iii) two part adhesive : one component in microcapsules and other in hollow cylinders. The healing efficiency of these systems depend greatly on several factors such as the nature of the healing agent, characteristic parameters of hollow tubes, composite thickness and impact energy level.[125] Since the hollow glass fibers are similar in structure to that of the fiber reinforcements used in composites, self-healing hollow fibers were combined with glass fiber/epoxy to mitigate damage and restore mechanical strength. Using UV-fluorescent dyes healing agent release in composites was visualized, thus confirming this concept of self-healing.[126] It was also determined that by calculating optimum placement and orientation of the hollow tubes in a matrix, the percent recovery could be increased significantly.[127] The incorporation of shape memory alloys, which respond to localized compression or trigger closure forces, has also been attempted to recover mechanical damage in composites.[128] One of the major issues that one might encounter while using these hollow tubes in composites is the similarity in physical and chemical, properties of the hollow tubes and the matrix (or composites). For example, Zhao et al. showed that for epoxy/polyamide compounds with healing agent loaded into hollow plastic fibers did not show signs of rupture or release even when the matrix was completely broken due to the mismatch in the breaking/fracture point in the matrix and the tubes.[128] Another common issue is the flowability of the released healing agent. Properties such as the diffusivity and the internal pressure within the repair tubes must also be considered. It was determined that 95% of the crack planes showed recovery when the internal pressure exceeded 0.2 MPa.[128]

In conventional extrinsic self-healing systems, repeated healing is hard to achieve due to the consumption of a part of the healing agent after the first damage. In order to overcome this issue, a three-dimensional micro vascular network was proposed that would mimic the architecture similar to that of human skin.[129] Vascular self-healing sequesters the healing agent in a network of capillaries or channels, which may be interconnected until the damage occurs. Owing to the vascular nature of the supply system, repeated damage to the same area could be healed. The interconnected networks approach uses direct ink writing technique and subsequent infiltration with uncured polymer precursors and healing agent. In case of two and three dimensional networks, the healing chemistry most often used was the Ring – opening methathesis polymerization of dicyclopentadiene monomer in the presence of Grubbs' catalyst.[130] One of the drawbacks of this technique is the restricted availability of the catalyst in the crack despite the large network size. In order to overcome this issue two sets of independent vascular networks were included, one of them containing a two part epoxy amine and the other containing the catalyst.[131] Healing efficiencies as much as 60% were achieved for up to 16 intermittent healing cycles of a single crack.[132] Theoretical calculations were also made to optimize these interconnected vascular networks. For a fixed crack dimension and the total volume of the channels, it was determined that a grid configuration of the network provided faster response to crack healing. Studies also report the optimum size of the micro-channels and the effect of same on the crack recovery.[133] Several off shoots from this approach have also been reported in the literature by the use of different materials and different biomimetic approaches.

Even though some of these approaches seem too futuristic it is not too far in the future that these techniques would be commercialized.

Due to rapid development of encapsulation techniques and ease in mass production, the above mentioned hollow tubes are replaced by spherical containers know as micro or nano-capsules. Capsule-based self-healing materials sequester the healing agents in discrete capsules until damage triggers rupture and release of the capsule contents. A variety of encapsulation techniques exists for encapsulation of reactive materials. These techniques can be classified as interfacial, in situ, coacervation, meltable dispersion or physical based mechanism of wall formation. For self-healing materials, however, most common encapsulation techniques are in situ, interfacial and meltable dispersions. In situ and interfacial proceed by the reaction of urea-formaldehyde [134-137], melamine formaldehyde [138-140], acrylates[141], polyurethanes[142] and subsequent formation of polymer shells at the interface of the droplets in an oil-in-water emulsion. In case of meltable dispersion method, the core component is dispersed in a melted polymer. The melted polymer is dispersed with the help of surfactants and solidified by removing the solvent.[143] Several core-shell capsules have also been prepared using water in oil emulsions and used for self-healing applications.

The pioneers in the development of self-healing polymeric materials are the group of White et al. at the University of Illinois, Urbana-Champaign. At UIUC, this group investigates the use of ring-opening metathesis of encapsulated endo-isomer of dicyclopetadiene (DCPD). The stimulus used as a trigger for the healing to occur in their case is mechanical damage. The system consists of two types of microcapsules, one with DCPD and one with Grubbs' catalyst. Delamination[144, 145], low-velocity impact [146]and indentation induced cracks[147] were found to be successfully repaired by the healing agents incorporated in these capsules.

One of the most thoroughly studied systems is the dicyclopentadiene (DCPD)/Grubbs' catalyst system. Ring opening metathesis polymerization is initiated by the ruthenium (IV) catalyst which is responsible for the recovery of the damaged areas. White et al. designed such a system in 2001[130] which has been studied extensively. The system consists of DCPD incorporated in urea formaldehyde based microcapsules which are incorporated in a coating/ composite. When damage occurs, the crack propagates through the specimen and ruptures the microcapsules. Liquid healing agent then flows through the crack via capillary action and upon contact with the catalyst DCPD polymerizes and fill up the crack restoring the mechanical strength of the material. In this study, White et al. observed an increase in the load bearing capacity of neat epoxy. They also observed a 75% recovery of the virgin fracture load, evaluated using the tapered double cantilever beam (TDCB) experiment. In another study, the fracture recovery due to autonomous healing and self-injected healing was compared. It was noted that autonomic samples' performance was comparable to that of the samples that were manually injected with the healant.[148] Since the mechanism for recovery is based on the rupture of the microcapsules, the properties of the microcapsules such as wall thickness, mechanical properties and size were also important to achieve optimum damage recovery. Keller and Sottos determined the effect of the stiffness of the microcapsules and the stiffness of the surrounding medium and found that the stiffer the microcapsule walls higher the tendency of the crack to deflect away from the capsule.[149] It was also determined that more complaint shell wall tends to attract the crack towards the microcapsules. The size of the microcapsules also plays an important role in the performance of the system. It determines the amount of healing agent available and also the toughness of the system. The microcapsule size is primarily controlled by the rate of agitation during the encapsulation process. It has been reported that smaller the size of the microcapsules greater is the toughness of the system at lower concentrations.[150] However, the recovery efficiency was found to be proportional to the size of the microcapsules used due to volume of the healing agent delivered to the system.[151] Brown et al. determined that an optimum amount of healing agent was delivered at 10 wt. % of 386 µm sized microcapsules which translates to 4.5 mg of healing agent delivered per unit crack area healed.

Due to the high cost associated with Grubbs' catalyst, other chemistries have also been investigated for reconstructive healing. The use of poly(dimethyl siloxane) (PDMS) in self-healing materials was investigated by Cho et al.[142] Following this study, Keller et al.[152, 153] proposed a new matrix that consisted of the PDMS instead of epoxy-polyamide resin. With this system 75% healing efficiency was obtained with 10 wt. % resin and 5 wt. % initiator capsules. Interestingly, some samples showed an efficiency of 100% or greater because of the similarity between the resin matrix and the healing agent. Yin et al.[154] were the first to try the epoxy hardener system which contained an uncured epoxy resin and imidazole-metal hardener. However, the system was not fully autonomous because the imidazole metal hardener required a temperature range of 130°C to function/activate. Yaun et al.[137] on the other hand, designed a fully autonomous system with epoxy resin as the healing agent and mercaptan as the hardener. Recovery efficiencies over 100% were achieved because of the similarity in the resin system and the incorporated epoxy healing agent. Isocyanates were also added to the list of compounds to be encapsulated. The isocyanates encapsulated react when exposed to humid or wet environments to mimic healing. The healing due to encapsulated isophorone diisocyanate (IPDI) in many solvents [93,95,155,156] has also investigated by several authors. By dissolving the polymer in various solvents, the glass transition temperature was found to be lowered facilitating healing at lower temperatures. Caruso et al.[157] incorporated solvent capsules in a polymer matrix and determined that the healing efficiency was directly proportional to solvent polarity in the dielectric constant range of 32-47. It was also determined that the solvents were difficult to incorporate in the urea formaldehyde capsules however chlorobenzene was successfully incorporated and showed efficiencies of the order of 86% for 20 wt. % of the capsules.

1.4.1. Self-healing for Corrosion Inhibition

One of the newer areas where encapsulation technique currently finds applications is in the area of corrosion inhibition. The expectation from these coatings is the ability to protect the metallic substrates upon abrasion or corrosion due to water penetration. When a metal corrodes there are two reactions that occur simultaneously - oxidation and reduction. The oxidation site is where the electron is released and the reduction reaction takes places where the released electron is consumed. The site where the oxidation occurs is also referred to as an anode and the reduction site is called cathode. Referring to these sites in terms of pH we can say that the anode is acidic and the cathode is basic. The primary means of corrosion testing involves the exposure of a metallic test substrate to saline conditions of known concentrations and evaluating the properties of the metal.

As discussed earlier, the use of reflow and self-sealing type coatings have been researched extensively for applications in coatings to recover the barrier properties hence resulting in protection of the substrate from corrosion. Kumar et al.[158] examined urea-formaldehyde microcapsules containing various healing agents and evaluated their corrosion inhibition when incorporated into primer coatings for steel surfaces. The healing agents used in this study were either film forming or corrosion inhibiting compounds. It was concluded that the microcapsules exhibit long-term stability in dried paint films, retain their core materials and release them only when ruptured. After optically evaluating the corrosion performance of the experimental coatings by ASTM 5894 it was concluded that the microcapsules reduced the under-film corrosion significantly. Suryanarayana et al.[159] examined the effectiveness of linseed oil filled microcapsules in epoxy coatings for steel substrates. Using optical microscopy, it was observed that linseed oil films formed rapidly in the crack plane due to auto-oxidation. Scribed samples showed no signs of corrosion at the scribe up to 72 hours of exposure, whereas the control panels without microcapsules developed corrosion products at the scribe after 48 hours. The auto-oxidation of linseed oil was found to not only form films at the scribe but also prevent ingress of oxygen and moisture thus preventing corrosion. Epoxide based film forming particles were embedded into epoxy-amine coatings for steel under cathodic protection[160]. The ability of the coating to heal a crack was assessed by monitoring the evolution of current demand with time and Electrochemical Impedance Spectroscopy (EIS). In the series of experiments performed no significant changes in protection was observed. Self-healing films of 1, 2-bis (triethoxysilyl) ethane (BTESE) containing water glass and cerium (III) nitrate were prepared on a zinc electrode previously treated with 0.001 M cerium (III) nitrate solution. The self-healing abilities of scratched BTESE films were assessed by polarization measurements after immersion in 0.5 M NaCl for 4 - 72 hours. The protective efficiency of these films was found to decrease from 96.9% after 4 hours to 94 % after 72 hours. The release of cerium ions was postulated to reduce pitting. Corrosion performance of scratched sol-gel ceramic hybrid coatings containing a fluorinated resin was evaluated by Yabuki et al.[161] The corrosion resistance of the coating was found to increase after 100 hours. Elemental analysis of substrate showed a uniform fluorine layer which was attributed to the observed corrosion inhibition.

Polyelectrolyte assemblies have been employed as containers to store the corrosion inhibitor in protective coatings. The distinct advantages of using this technique is the isolation of the inhibitor and providing on-demand release of the inhibitor in response to changing environmental conditions. There also other more obvious disadvantages to this too, compatibility with the coating is one and the second is distribution within the coating. Change in local pH as a trigger is again preferred because corrosion reactions generally involve change in pH in the anodic and cathodic areas.[162] Zheludkevich et al.[163-165] demonstrated the use of SiO_2 particles coated with poly (ethylene imine)/poly(styrene sulfonate) (PEI/PSS) as nano-containers embedded in an epoxy functionalized ZrO_2/SiO_2 sol–gel coating. They also demonstrated the use of halloysite nanotubes with corrosion inhibitors. The corrosion performance of the synthesized PEI/PSS nanocontainers was evaluated visually and using Electrochemical Impedance Spectroscopy. Aluminum AA2024 samples coated with the sol-gel matrix with benzotriazole (corrosion inhibitor) dissolved directly in the sol–gel matrix and the benzotriazole loaded nanocontainers were compared in this study. It was observed that the coatings containing benzotriazole nanocontainers displayed better corrosion resistance against sodium chloride solutions of various concentrations up on immersed for 14 days. EIS results of aluminum AA2024 samples after 190 hours of immersion in 0.005 M NaCl showed that the undoped hybrid coatings with different concentrations of the nanocontainers show similar behavior beyond 0.1 Hz and the measured capacitance was found to be similar as well. The sample containing the highest concentration of the nanocontainers showed almost pure capacitive behavior at low frequencies and, hence appeared to demonstrate good corrosion protection even after long immersion times. The lower nano-container concentration coatings showed a good corrosion performance however, formation of resistances at low frequencies was demonstrated to be associated with active defect formation.

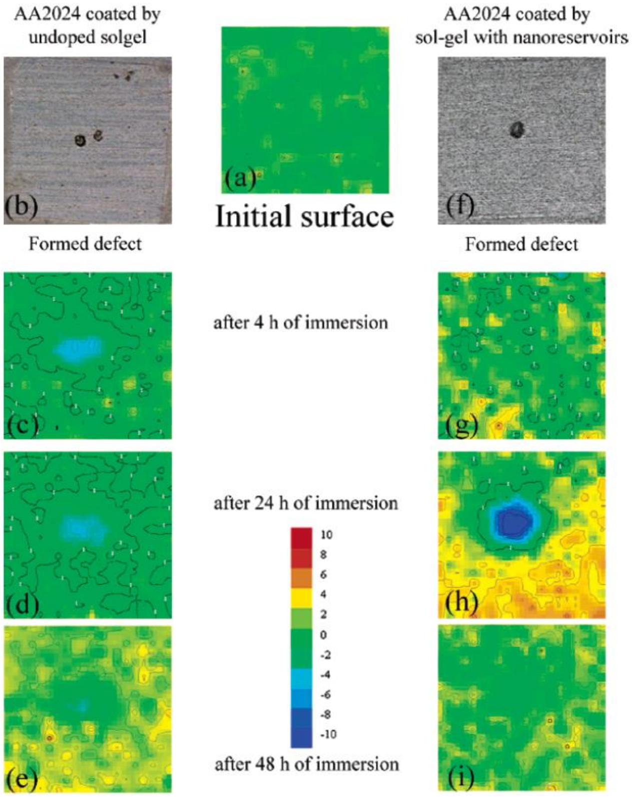

Figure 1.3. SVET maps of ionic currents measured above AA2024 panels with undoped sol- gel (a,c,d,e) and with pretreatments impregnated by nanocontainers (g-i). The maps were obtained before defect formation (a) and for 4 h (c,g), 24 h (d,h) and 48 h (e,i) after defect formation. Scanned area: 2 mm X 2 mm. (Reprinted from reference 163 with permission from "Zheludkevich, M. L.; Shchukin, D. G.; Yasakau, K. A.; Möhwald, H.; Ferreira, M. G. S., Anticorrosion Coatings with Self-Healing Effect Based on Nanocontainers Impregnated with Corrosion Inhibitor. Chemistry of Materials 2007, 19, (3), 402-411". ©2007 American Chemical Society.)

Scanning Vibrating Electrode Technique (SVET) measurements on the surface of undoped ZrO_X/SiO_X film and the ZrO_X/SiO_X film with embedded with benzotriazole nanocontainers are summarized in Figure 1.3. After 24 h of immersion in sodium chloride solution, an artificial defect (200 µm in diameter) was introduced on the coating to induce corrosion of the substrate. A well-defined cathode was observed in the area of the defect which was found to intensify with immersion time in case of the undoped ZrO_X/SiO_X film. However in case of the ZrO_X/SiO_X film doped with nano-containers no cathodic activity was observed by the authors after 4 h of the defect formation. However, 2 hours later the defect was found to have high intensity of cathodic current at the defect and after 48 hours no cathodic current was observed at the defect thus exhibiting the protection of the exposed metal by benzotriazole. As an extension to the above research Abdullayev et al.[166] designed end groups that acted like switches that turned the release of benzotriazole on or off thus tuning the release time from ten to hundreds of hours.

Multi-walled carbon nanotube (MWCNT) embedded poly(sodium- 4 –styrene sulfonate (PSS)/ poly(allylamine hydrochloride) (PAH) microcapsules have also been fabricated by LbL self-assembly technique and their electrochemical behavior evaluated.[167] The use of MWCNT is favorable due to its low cost compared to single walled carbon nanotubes. Cyclic voltammetry of (PSS)/(PAH) MWCNT on a glassy carbon (GC) electrode using a phosphate buffer at pH 6.86 at different scan rates showed well reversible voltammogram at -0.05 V. The redox response of polyelectrolyte/MWCNT was also found to be due to the redox process of the oxygen containing end groups. Since (PSS/PAH) at the GC electrode alone (used as a control) could not exhibit redox peaks, the observed peaks were attributed to the MWCNT. The change in the behavior of the MWCNT with changing pH was also studied and was understood that by increasing the pH the peak potential decreased due to the decrease in the concentration of protons at higher pH.

Thiourea corrosion inhibitors have been encapsulated in glutin and polyvinyl alcohol (PVA).[168] Polarization and EIS were performed on the steel samples after the addition of the microcapsules every 6 h. The release rate was measured using UV-vis spectroscopy. It was observed that the release time for microcapsules that were sealed once with glutin was 12 h, and 18 hours for the microcapsules sealed once with PVA. It was also observed that if these microcapsules were sealed for a second time the release time increased significant and could be used as a mechanism to protect the inhibitors for a longer duration of time. The EIS study and polarization experiments showed that the inhibitor that was released into the solution showed potential to protect the steel from corrosion.

1.5. Conclusions

Over the past decade, research on self-healing materials has increased significantly encompassing a wide range of damage modes and self-healing concepts. Although the vast majority of research of self-healing is in combating material failure due to fatigue or mechanical damage, other areas where similar self-healing technology can been applied is growing. One such area is corrosion inhibition of metal substrates. The most successful autonomous approach, realized so far, utilizes a layer-by-layer approach to release a corrosion inhibitor as a function of pH of the metal substrate. The limitation with this approach is the selectivity of the type of inhibitor that can be used, reduced concentration of corrosion inhibitor available over extended periods of time during the service life of the metal substrate in corrosive environments, compatibility (dispersion and pH sensitivity) in coatings and the associated cost with employing carbon nanotube based materials in coatings. The use of polymer encapsulation technique could potentially overcome the current limitations of autonomous materials in coatings for corrosion control. A pH responsive polymer shell designed to disintegrate with change in pH in conjunction with environmentally complaint corrosion inhibitors could be potentially used for hexavalent chrome replacement in coatings.

This work focuses on the use of polymer encapsulation as a viable route for the isolation and storage of highly water soluble corrosion inhibitor, namely cerium nitrate, which may be potential replacement for hexavalent chromes. In this dissertation, pH responsive microcapsules using disulfide linkages was synthesized containing water soluble cerium salts. These capsules were characterized using SEM, TEM, UV-vis spectroscopy, DMA, TGA and ICP-OES. The resultant capsules were employed in coatings on steel and aluminum alloys. The corrosion protection ability of the resulting coating was evaluated using EIS, polarization experiments, open circuit potential measurements, SECM and accelerated corrosion tests.

In chapter 3 of the dissertation, the synthesis of microcapsules containing a water core using internal phase separation is described. The structure and morphology of the synthesized capsules was studied. Core shell microcapsules with aqueous core were synthesized and confirmed using various characterization techniques.

In chapter 4, the effect of the synthesized microcapsules embedded in cured coatings on corrosion inhibition of aluminum and steel alloys was studied. Reduced corrosion was observed on steel and aluminum alloys in coatings containing the synthesized capsules due to the release of incorporated cerium within the microcapsules. Real time release of cerium was also monitored using SECM.

1.6. References

1. Terminology Relating to Corrosion and Corrosion Testing. In *American Society for Testing and Materials Designation*, 2000; Vol. G15-99b (revised).
2. Fontana, M. G., *Corrosion Engineering*. McGraw-Hill: New York, 1986.
3. Payer, J. H. V., Y.P.; Koch,G.H.; Brongers, M.P.H.; Thompson, N.G., Corrosion Costs and Preventive Strategies in the United States. In NACE International: 2002.
4. Revie, R. W., Economics of corrosion. In *Uhlig's Corrosion Handbook*, John Wiley & Sons: 2011; pp 21 - 30.
5. Zhang, J.; Klasky, M.; Letellier, B. C., The aluminum chemistry and corrosion in alkaline solutions. *Journal of Nuclear Materials* **2009,** 384, (2), 175-189.

6. Volk, C.; Dundore, E.; Schiermann, J.; LeChevallier, M., Practical evaluation of iron corrosion control in a drinking water distribution system. *Water Research* **2000,** 34, (6), 1967-1974.

7. Sarin, P.; Snoeyink, V. L.; Lytle, D. A.; Kriven, W. M., Iron Corrosion Scales: Model for Scale Growth, Iron Release, and Colored Water Formation. *Journal of Environmental Engineering* **2004,** 130, (4), 364-373.

8. Butler, G.; Mercer, A. D., Inhibitor Formulations for Engine Coolants. *British Corrosion Journal* **1977,** 12, (3), 171-174.

9. Krneger, R. H., Albertson, C.E., Miglin, B.P. Corrodable container for automatic addition of corrosion inhibitor to a coolant system. 1982.

10. Schmitt, G., Application of Inhibitors for Acid Media: Report prepared for the European Federation of Corrosion Working Party on Inhibitors. *British Corrosion Journal* **1984,** 19, (4), 165-176.

11. Twite, R. L.; Bierwagen, G. P., Review of alternatives to chromate for corrosion protection of aluminum aerospace alloys. *Progress in Organic Coatings* **1998,** 33, (2), 91-100.

12. Xingwen, Y.; Chunan, C.; Zhiming, Y.; Derui, Z.; Zhongda, Y., Study of double layer rare earth metal conversion coating on aluminum alloy LY12. *Corrosion Science* **2001,** 43, (7), 1283-1294.

13. Hackerman, N., Snavely, E.S., Corrosion Basics. In Delinder, L. S. V., Ed. NACE: Houston, TX, 1984; pp 127-146.

14. Harrop, D., *Chemical Inhibitors for Corrosion control*. Royal society of chemistry: Cambridge, 1991; Vol. 2.

15. U.S.Military, Chemical Conversion Materials for Coating Aluminum and Aluminum alloys. In *MIL-C-81706*.

16. Kending, M. W., Buchelt, R.G., Corrosion Inhibition of Aluminum and Aluminum Alloys by Soluble Chromates, Chromate Coatings, and Chromate-free Coatings. *Corrosion* **2003,** 59, 379-400.

17. Cotton, F., Wilkinson, G., *Advances Inogranic Chemistry*. 5 ed.; Wiley: New York, 1988.

18. Xia, L. A., Ejii; Frankel, Gerald; McCreery, Richard Storage and Release of Soluble Hexavalent Chromium from Chromate Conversion Coatings Equilibrium Aspects of CrVI Concentration. *Journal of Electrochemical Society* **2000,** 147, (2), 556.

19. Akiyama, E.; Markworth, A. J.; McCoy, J. K.; Frankel, G. S.; Xia, L.; McCreery, R. L., Storage and Release of Soluble Hexavalent Chromium from Chromate Conversion Coatings on Al Alloys: Kinetics of Release. *Journal of The Electrochemical Society* **2003,** 150, (2), B83-B91.

20. Kendig, M.; Jeanjaquet, S.; Addison, R.; Waldrop, J., Role of hexavalent chromium in the inhibition of corrosion of aluminum alloys. *Surface and Coatings Technology* **2001,** 140, (1), 58-66.

21. Cicek, V.; Al-Numan, B., *Corrosion Chemistry*. John Wiley & Sons.

22. Robert, C., *The Handbook of Chemistry and Physics*. CRC Press: Boca Raton,FL, 1997.

23. Weisberg, H. E., Chromate and Molybdate Pigments, Paint and Varnish Production. **1968**.

24. Sax, N. I., Lewis, R.J. Sr., *Dangerous properties of industrial materials*. 7 ed.; Van Nostrand Reinhold: New York, 1989; Vol. 2.

25. Becker, G. e. a., *Arch. Eisenhuettenwes.* **1969,** 40.

26. O'Brien, P. O., Kortenkamp, A., The generation of DNA single-strand breaks during the reduction of chromate by ascorbic acid and/or glutathione in vitro. *Transition Metal Chemistry* **1995,** 20.

27. Kortenkamp, A.; Oetken, G.; Beyersmann, D., The DNA cleavage induced by a chromium(V) complex and by chromate and glutathione is mediated by activated oxygen species. *Mutation Research/Fundamental and Molecular Mechanisms of Mutagenesis* **1990,** 232, (2), 155-161.

28. da Cruz Fresco, P.; Kortenkamp, A., The formation of DNA cleaving species during the reduction of chromate by ascorbate. *Carcinogenesis* **1994,** 15, (9), 1773-1778.

29. Intergrated Risk Information System (IRIS) on Chromium, VI. In Agency, U. S. E. P., Ed. Office of Research and Development: Washington, D.C., 1999.

30. "Code of Federal Regulations". In (OSHA), O. S. a. H. A., Ed. 1998; Vol. 29 CFR 1910.1000.

31. Organization, W. H., Environmental Health Criteria 61. In *Chromium*, Geneva, Switzerland, 1988.

32. Os, M. T. v., *Surface modification by plasma polymerization: Film deposition, tailoring of surface properties and biocompatibility*. Print Partners Ipskamp: Enschede, The Netherlands, 2000.

33. Schreiber, H. P.; Wertheimer, M. R.; Wrobel, A. M., Corrosion protection by plasma-polymerized coatings. *Thin Solid Films* **1980,** 72, (3), 487-494.

34. Metroke, T. L.; Parkhill, R. L.; Knobbe, E. T., Passivation of metal alloys using sol-gelderived materials - a review. *Progress in Organic Coatings* **2001,** 41, (4), 233-238.

35. Guglielmi, M.; Festa, D.; Innocenzi, P. C.; Colombo, P.; Gobbin, M., Borosilicate coatings on mild steel. *Journal of Non-Crystalline Solids* **1992,** 147â€“148, (0), 474-477.

36. Atik, M.; Aegerter, M. A., Corrosion resistant sol-gel ZrO2 coatings on stainless steel. *Journal of Non-Crystalline Solids* **1992,** 147â€“148, (0), 813-819.

37. Skotheim, T. A.; Elsenbaumer, R. L.; Reynolds, J. R., *Handbook of Conducting Polymers*. M. Dekker: 1998.

38. Sathiyanarayanan, S.; Dhawan, S. K.; Trivedi, D. C.; Balakrishnan, K., Soluble conducting poly ethoxy aniline as an inhibitor for iron in HCl. *Corrosion Science* **1992,** 33, (12), 1831-1841.

39. Mirmohseni, A.; Oladegaragoze, A., Anti-corrosive properties of polyaniline coating on iron. *Synthetic Metals* **2000,** 114, (2), 105-108.

40. R. J. Racicot; S. C. Yang; R. Brown In *Evidence of a Passive Layer Formation from a Conductive Polymer Coating on Aluminum Alloys*, MRS Fall Meeting, 1996; 1996; p 415.

41. Breslin, C. B.; Treacy, G.; Carroll, W. M., Studies on the passivation of aluminium in chromate and molybdate solutions. *Corrosion Science* **1994,** 36, (7), 1143-1154.

42. Shaw, B. A.; Davis, G. D.; Fritz, T. L.; Olver, K. A., A Molybdate Treatment for Enhancing the Passivity of Aluminum in Chloride-Containing Environments. *Journal of The Electrochemical Society* **1990,** 137, (1), 359-360.

43. MacQueen, R. C.; Miron, R. R.; Granata, R. D., Method for corrosion inhibitor mechanism studies in epoxy coated aluminium. *Journal of coatings technology* **1996,** 68, (857), 75-82.

44. Chambers, B. D.; Taylor, S. R., The high throughput assessment of aluminium alloy corrosion using fluorometric methods. Part I – Development of a fluorometric method to quantify aluminium ion concentration. *Corrosion Science* **2007,** 49, (3), 1584-1596.

45. Tayler, S. R.; Chambers, B. D. Synergistic Combinations of Chromate-Free Corrosion Inhibitors. US8088204, 2009.

46. Greenwood, N. N.; Earnshaw, A., *Chemistry of the elements*. Pergamon Press: Oxford, England, 1984.

47. Haley, T. J., *Journal of Pharmaceutical Sciences* **1965,** 54, (4).

48. Falconnet, P., The rare earth industry: a world of rapid change. *Journal of Alloys and Compounds* **1993,** 192, (1–2), 114-117.

49. Muecke, G. K.; Moller, P., The not-so-rare earths. *Scientific American* **1988,** 256, (1), 72-77.

50. Colson, J. C.; Buscail, H.; Bonnet, G.; Lachkar, M.; Larpin, J. P., The Effect of Deposited Rare Earth Oxide Films on High Temperature Corrosion Behaviour of Different Metals and Alloys. *Solid State Phenomena* **1995,** 41, 165-176.

51. Arenas, M. A.; Bethencourt, M.; Botana, F. J.; de Damborenea, J.; Marcos, M., Inhibition of 5083 aluminium alloy and galvanised steel by lanthanide salts. *Corrosion Science* **2001,** 43, (1), 157-170.

52. Arenas, M. A.; de Damborenea, J., Protection of Zn–Ti–Cu alloy by cerium trichloride as corrosion inhibitor. *Surface and Coatings Technology* **2005,** 200, (7), 2085-2091.

53. Czerwinski, F.; Smeltzer, W. W., The Early-Stage Oxidation Kinetics of CeO[sub 2] Sol-Coated Nickel. *Journal of The Electrochemical Society* **1993,** 140, (9), 2606-2615.

54. Czerwinski, F.; Smeltzer, W. W., The growth and structure of thin oxide films on ceria-sol-coated nickel. *Oxidation of Metals* **1993,** 40, (5), 503-527.

55. Rosalbino, F.; Carlini, R.; Soggia, F.; Zanicchi, G.; Scavino, G., Influence of rare earth metals addition on the corrosion behaviour of copper in alkaline environment. *Corrosion Science* **2012,** 58, (0), 139-144.

56. Blin, F.; Leary, S. G.; Wilson, K.; Deacon, G. B.; Junk, P. C.; Forsyth, M., Corrosion Mitigation of Mild Steel by New Rare Earth Cinnamate Compounds. *Journal of Applied Electrochemistry* **2004,** 34, (6), 591-599.

57. Blin, F.; Leary, S. G.; Deacon, G. B.; Junk, P. C.; Forsyth, M., The nature of the surface film on steel treated with cerium and lanthanum cinnamate based corrosion inhibitors. *Corrosion Science* **2006,** 48, (2), 404-419.

58. Suegama, P. H.; de Melo, H. G.; Benedetti, A. V.; Aoki, I. V., Influence of cerium (IV) ions on the mechanism of organosilane polymerization and on the improvement of its barrier properties. *Electrochimica Acta* **2009,** 54, (9), 2655-2662.

59. Pepe, A.; Aparicio, M.; Durán, A.; Ceré, S., Cerium hybrid silica coatings on stainless steel AISI 304 substrate. *Journal of Sol-Gel Science and Technology* **2006,** 39, (2), 131-138.

60. Bernal, S.; Botana, F. J.; Calvino, J. J.; Marcos, M.; Pérez-Omil, J. A.; Vidal, H., Lanthanide salts as alternative corrosion inhibitors. *Journal of Alloys and Compounds* **1995,** 225, (1–2), 638-641.

61. Hinton, B. R. W.; Arnott, D. R.; Ryan, N. E., Cerium Conversion Coatings for the Corrosion Protection of Aluminum *Materials Forum* **1986,** 9, (3), 162-173.

62. Arnott, D. R.; Ryan, N. E.; Hinton, B. R. W.; Sexton, B. A.; Hughes, A. E., Auger and XPS studies of cerium corrosion inhibition on 7075 aluminum alloy. *Applications of Surface Science* **1985,** 22–23, Part 1, (0), 236-251.

63. Hinton, B. R. W.; Wilson, L., The corrosion inhibition of zinc with cerous chloride. *Corrosion Science* **1989,** 29, (8), 967-985.

64. Hinton, B. R. W., Corrosion inhibition with rare earth metal salts. *Journal of Alloys and Compounds* **1992,** 180, (1–2), 15-25.

65. Arnott, D. R.; Hinton, B. R. W.; Ryan, N. E., Cationic film-forming inhibitors for the corrosion protection of AA 7075 aluminum alloy in chloride solutions. *Materials Performance* **1987,** 26, (8), 42-47.

66. Mishra, A. K.; Balasubramaniam, R., Corrosion inhibition of aluminium by rare earth chlorides. *Materials Chemistry and Physics* **2007,** 103, (2–3), 385-393.

67. Bethencourt, M.; Botana, F. J.; Calvino, J. J.; Marcos, M.; RodrÍguez-Chacón, M. A., Lanthanide compounds as environmentally-friendly corrosion inhibitors of aluminium alloys: a review. *Corrosion Science* **1998,** 40, (11), 1803-1819.

68. Aldykewicz, J. A. J.; Isaacs, H. S.; Davenport, A. J., The Investigation of Cerium as a Cathodic Inhibitor for Aluminum-Copper Alloys. *Journal of The Electrochemical Society* **1995,** 142, (10), 3342-3350.

69. Mansfeld, F.; Lin, S.; Kim, S.; Shih, H., Electrochemical impedance spectroscopy as a monitoring tool for passivation and localized Corrosion of aluminum alloys. *Materials and Corrosion* **1988,** 39, (11), 487-492.

70. Lin, S.; Shih, H.; Mansfeld, F., Corrosion protection of aluminum alloys and metal matrix composites by polymer coatings. *Corrosion Science* **1992,** 33, (9), 1331-1349.

71. Mansfeld, F.; Wang, Y.; Shih, H., The Ce・Mo process for the development of a stainless aluminum. *Electrochimica Acta* **1992,** 37, (12), 2277-2282.

72. Mansfeld, F., Electrochemical impedance spectroscopy (EIS) as a new tool for investigating methods of corrosion protection. *Electrochimica Acta* **1990,** 35, (10), 1533-1544.

73. W.N.Gerrard, Corrosion Behavior of Aluminum-Lithium Alloys. *Corrosion* **1994,** 50, (3), 215-226.

74. Wilson, L.; Hinton, B. R. W. A Method of Forming a Corrosion Resistant Coating. 1987.

75. Hinton, B. R. W.; Hughes, A.; Taylor, R.; Henderson, M.; Nelson, K.; Wilson, L., In *13th International Corrosion Conference*, Melbourne, Australia.

76. Mansfeld, F.; Wang, V.; Shih, H., Development of ``Stainless Aluminum". *Journal of The Electrochemical Society* **1991,** 138, (12), L74-L75.

77. Baldwin, K. R.; M.C., G.; Lane, P. L.; Smith, C. E. J. In Proceeding 7th European Symposium on Corrosion Inhibtiors, Ferrara, 1990; Ferrara, 1990; p 771.

78. Dr. Swapan Kumar, G., Self-Healing Materials: Fundamentals, Design Strategies, and Applications. *Self-Healing Materials* **2009**, 1-28.

79. Monique Seiller; Anne-Marie Orecchioni; Martini, M.-C., In *Microencapsulation:Methods and Industrial Applications*, Benita, S., Ed. Marcel Dekker: 1996; pp 707-745.

80. Park, S.-J.; Shin, Y.-S.; Lee, J.-R., Preparation and Characterization of Microcapsules Containing Lemon Oil. *Journal of Colloid and Interface Science* **2001,** 241, (2), 502-508.

81. Fanger, G. O., What good are microcapsules? *Chemtech* **1974,** 4, 397-405.

82. Bakan, J. A. Process for making capsules and method of making premix used therein. 3436355, April 1, 1969, 1969.

83. Paul D, R., Polymers in Controlled Release Technology. In *Controlled Release Polymeric Formulations*, AMERICAN CHEMICAL SOCIETY: 1976; Vol. 33, pp 1-14.

84. Tamber, H.; Johansen, P.; Merkle, H. P.; Gander, B., Formulation aspects of biodegradable polymeric microspheres for antigen delivery. *Advanced Drug Delivery Reviews* **2005,** 57, (3), 357-376.

85. Jae Hyung Park; Ye, M.; Park, K., Biodegradable Polymers for Microencapsulation of Drugs. *Molecules* **2005,** 10, 146-161.

86. Farahidah, M.; Christopher, F. v. d. W., Engineering biodegradable polyester particles with specific drug targeting and drug release properties. *Journal of Pharmaceutical Sciences* **2008,** 97, (1), 71-87.

87. Gharsallaoui, A.; Roudaut, G.; Chambin, O.; Voilley, A.; Saurel, R., Applications of spray-drying in microencapsulation of food ingredients: An overview. *Food Research International* **2007,** 40, (9), 1107-1121.

88. Sanguansri, P.; Augustin, M. A., Nanoscale materials development - a food industry perspective. *Trends in Food Science & Technology* **2006,** 17, (10), 547-556.

89. R. P. Wool; O'Connor, K. M., A theory crack healing in polymers. *Journal of Applied Physics* **1981,** 52, 5953 - 5964.

90. Wool, R. P.; Yuan, B. L.; McGarel, O. J., Welding of polymer interfaces. *Polymer Engineering & Science* **1989,** 29, (19), 1340-1367.

91. Jud, K.; Kausch, H. H., Load transfer through chain molecules after interpenetration at interfaces. *Polymer Bulletin* **1979,** 1, (10), 697-707.

92. Wool, R. P., Relations for Healing, Fracture, Self-Diffusion and Fatigue of Random Coil Polymers. *ACS Polymer Preprints* **1982,** 23, 62-63.

93. Lin, C. B.; Lee, S.; Liu, K. S., Methanol-Induced crack healing in poly(methyl methacrylate). *Polymer Engineering & Science* **1990,** 30, (21), 1399-1406.

94. Wang, P.-P.; Lee, S.; Harmon, J. P., Ethanol-induced crack healing in poly(methyl methacrylate). *Journal of Polymer Science Part B: Polymer Physics* **1994,** 32, (7), 1217-1227.

95. Wu, T.; Lee, S., Carbon tetrachloride-induced crack healing in polycarbonate. *Journal of Polymer Science Part B: Polymer Physics* **1994,** 32, (12), 2055-2064.

96. Liu, C. K.; Yang, T. J.; Shen, J. S.; Lee, S., Some recent results on crack healing of poly(methyl methacrylate). *Engineering Fracture Mechanics* **2008,** 75, (17), 4876-4885.

97. Yufa, N. A.; Li, J.; Sibener, S. J., Diblock copolymer healing. *Polymer* **2009,** 50, (12), 2630-2634.

98. Outwater, J. O.; Gerry, D. J., On the fracture energy, rehearing velocity and refracture energy of cast epoxy resin. *Journal of Adhesion* **1969,** 1, 290-298.

99. Wool, R. P., *Polymer interfaces: Structure and strength*. Hanser Publishers: Munich, 1994; p 463.

100. Raghavan, J.; Wool, R. P., Interfaces in repair, recycling, joining and manufacturing of polymers and polymer composites. *Journal of Applied Polymer Science* **1999,** 71, (5), 775-785.

101. Yamaguchi, M.; Ono, S.; Terano, M., Self-repairing property of polymer network with dangling chains. *Materials Letters* **2007,** 61, (6), 1396-1399.

102. Yamaguchi, M.; Ono, S.; Okamoto, K., Interdiffusion of dangling chains in weak gel and its application to self-repairing material. *Materials Science and Engineering: B* **2009,** 162, (3), 189-194.

103. Hayes, S. A.; Jones, F. R.; Marshiya, K.; Zhang, W., A self-healing thermosetting composite material. *Composites Part A: Applied Science and Manufacturing* **2007,** 38, (4), 1116-1120.

104. Hayes, S. A.; Zhang, W.; Branthwaite, M.; Jones, F. R., Self-healing of damage in fibre-reinforced polymer-matrix composites. *Journal of The Royal Society Interface* **2007,** 4, (13), 381-387.

105. Varley, R. J.; van der Zwaag, S., Towards an understanding of thermally activated self-healing of an ionomer system during ballistic penetration. *Acta Materialia* **2008,** 56, (19), 5737-5750.

106. Takeda, K.; Tanahashi, M.; Unno, H., Self-repairing mechanism of plastics. *Science and Technology of Advanced Materials* **2003,** 4, (5), 435-444.

107. Chen, X.; Wudl, F.; Mal, A. K.; Shen, H.; Nutt, S. R., New Thermally Remendable Highly Cross-Linked Polymeric Materials. *Macromolecules* **2003,** 36, (6), 1802-1807.

108. Liu, Y.-L.; Hsieh, C.-Y., Crosslinked epoxy materials exhibiting thermal remendablility and removability from multifunctional maleimide and furan compounds. *Journal of Polymer Science Part A: Polymer Chemistry* **2006,** 44, (2), 905-913.

109. Kavitha, A. A.; Singha, N. K., "Click chemistry" in tailor-made polymethacrylates bearing reactive furfuryl functionality: a new class of self-healing polymeric material. *ACS Applied Materials & Interfaces* **2009,** 7, 1427-1436.

110. Watanabe, M.; Yoshie, N., Synthesis and properties of readily recyclable polymers from bisfuranic terminated poly(ethylene adipate) and multi-maleimide linkers. *Polymer* **2006,** 47, (14), 4946-4952.

111. Murphy, E. B.; Bolanos, E.; Schaffner-Hamann, C.; Wudl, F.; Nutt, S. R.; Auad, M. L., Synthesis and Characterization of a Single-Component Thermally Remendable Polymer Network: Staudinger and Stille Revisited. *Macromolecules* **2008,** 41, (14), 5203-5209.

112. Wang, Y.; Bolanos, E.; Wudl, F.; Hahn, T.; Kwok, N. In *Self-healing polymers and composites based on thermal activation*, San Diego, California, USA, 2007; Dapino, M. J., Ed. SPIE: San Diego, California, USA, 2007; pp 65261I-12.

113. Jong Se Park; Takahashi, K.; Guo, Z.; Wang, Y.; Bolanos, E.; Hamann-Schaffner, C.; Murphy, E.; Wudl, F.; Hahn, H. T., Towards Development of a Self-Healing Composite using a Mendable Polymer and Resistive Heating. *Journal of Composite Materials* **2008,** 42, (26), 2869-2881.

114. Chino, K.; Ashiura, M., Themoreversible Cross-Linking Rubber Using Supramolecular Hydrogen-Bonding Networks. *Macromolecules* **2001,** 34, (26), 9201-9204.

115. Mynar, J. L.; Aida, T., Materials science: The gift of healing. *Nature* **2008,** 451, (7181), 895-896.

116. Cordier, P.; Tournilhac, F.; Soulie-Ziakovic, C.; Leibler, L., Self-healing and thermoreversible rubber from supramolecular assembly. *Nature* **2008,** 451, (7181), 977-980.

117. Harreld, J. H.; Wong, M. S.; Hansma, P. K.; Morse, D. E.; Stucky, G. D. Slef-healing organosiloxane materials containing reversible and energy-dispersive crosslinking domains. U.S. Patent 6783709, 2004.

118. Burattini, S.; Colquhoun, H. M.; Fox, J. D.; Friedmann, D.; Greenland, B. W.; Harris, P. J. F.; Hayes, W.; Mackay, M. E.; Rowan, S. J., A self-repairing, supramolecular polymer system: healability as a consequence of donor-acceptor [small pi]-[small pi] stacking interactions. *Chemical Communications* **2009**, (44), 6717-6719.

119. Burattini, S.; Cikquhoun, H. M.; Greenland, B. W.; Hayes, W., A novel self-healing supramolecular polymer system. *Faraday discussions* **2009,** 143, 251-263.

120. Dry, C., Passive tuneable fibers and matrices. *International Journal of Modern Physics B* **1992,** 6, (15-16), 2763-2771.

121. Dry, C., Procedures developed for self-repair of polymer matrix composite materials. *Composite Structures* **1996,** 35, (3), 263-269.

122. Carolyn, D., Matrix cracking repair and filling using active and passive modes for smart timed release of chemicals from fibers into cement matrices. *Smart Materials and Structures* **1994,** 3, (2), 118.

123. Carolyn, D.; William, M., Three-part methylmethacrylate adhesive system as an internal delivery system for smart responsive concrete. *Smart Materials and Structures* **1996,** 5, (3), 297.

124. Bleay, S. M.; Loader, C. B.; Hawyes, V. J.; Humberstone, L.; Curtis, P. T., A smart repair system for polymer matrix composites. *Composites Part A: Applied Science and Manufacturing* **2001,** 32, (12), 1767-1776.

125. Motuku, M.; Vaidya, U. K.; Janowski, G. M., Parametric studies on self-repairing approaches for resin infused composites subjected to low velocity impact. *Smart Materials and Structures* **1999,** 8, (5), 623.

126. Pang, J. W. C.; Bond, I. P., A hollow fibre reinforced polymer composite encompassing self-healing and enhanced damage visibility. *Composites Science and Technology* **2005,** 65, (11–12), 1791-1799.

127. Williams, G. J.; Bond, I. P.; Trask, R. S., Compression after impact assessment of self-healing CFRP. *Composites Part A: Applied Science and Manufacturing* **2009,** 40, (9), 1399-1406.

128. Zhang, M. Q.; Rong, M. Z., *Self-Healing Polymers and Polymer Composites*. John Wiley & Sons: 2011.

129. Toohey, K. S.; Sottos, N. R.; Lewis, J. A.; Moore, J. S.; White, S. R., Self-healing materials with microvascular networks. *Nat Mater* **2007,** 6, (8), 581-585.

130. White, S. R.; Sottos, N. R.; Geubelle, P. H.; Moore, J. S.; Kessler, M. R.; Sriram, S. R.; Brown, E. N.; Viswanathan, S., Autonomic healing of polymer composites. *Nature* **2001,** 409, (6822), 794-797.

131. Toohey, K. S.; Hansen, C. J.; Lewis, J. A.; White, S. R.; Sottos, N. R., Delivery of Two-Part Self-Healing Chemistry via Microvascular Networks. *Advanced Functional Materials* **2009,** 19, (9), 1399-1405.

132. Toohey, K.; Sottos, N.; White, S., Characterization of Microvascular-Based Self-healing Coatings. *Experimental Mechanics* **2009,** 49, (5), 707-717.

133. Bejan, A.; Lorente, S.; Wang, K. M., Networks of channels for self-healing composite materials. *Journal of Applied Physics* **2006,** 100, (3), 033528-6.

134. Brown, E. N.; Kessler, M. R.; Sottos, N. R.; White, S. R., In situ poly(urea-formaldehyde) microencapsulation of dicyclopentadiene. *Journal of Microencapsulation* **2003,** 20, (6), 719-730.

135. Blaiszik, B. J.; Sottos, N. R.; White, S. R., Nanocapsules for self-healing materials. *Composites Science and Technology* **2008,** 68, (3–4), 978-986.

136. Blaiszik, B. J.; Caruso, M. M.; McIlroy, D. A.; Moore, J. S.; White, S. R.; Sottos, N. R., Microcapsules filled with reactive solutions for self-healing materials. *Polymer* **2009,** 50, (4), 990-997.

137. Yuan, L.; Liang, G.; Xie, J.; Li, L.; Guo, J., Preparation and characterization of poly(urea-formaldehyde) microcapsules filled with epoxy resins. *Polymer* **2006,** 47, (15), 5338-5349.

138. Yuan, Y. C.; Rong, M. Z.; Zhang, M. Q.; Chen, J.; Yang, G. C.; Li, X. M., Self-Healing Polymeric Materials Using Epoxy/Mercaptan as the Healant. *Macromolecules* **2008,** 41, (14), 5197-5202.

139. Yuan, Y. C.; Rong, M. Z.; Zhang, M. Q., Preparation and characterization of microencapsulated polythiol. *Polymer* **2008,** 49, (10), 2531-2541.

140. Yuan, L.; Liang, G.-z.; Xie, J.-q.; He, S.-B., Synthesis and characterization of microencapsulated dicyclopentadiene with melamine–formaldehyde resins. *Colloid & Polymer Science* **2007,** 285, (7), 781-791.

141. Xiao, D. S.; Yuan, Y. C.; Rong, M. Z.; Zhang, M. Q., Hollow polymeric microcapsules: Preparation, characterization and application in holding boron trifluoride diethyl etherate. *Polymer* **2009,** 50, (2), 560-568.

142. Soo Hyoun Cho; Magnus Andersson; Scott R. White; Nancy R. Sottos; Braun, P. V., Polydimethylsiloxane- based self healing materials. *Advanced Materials* **2006,** 18, 997-1000.

143. Rule, J. D.; Brown, E. N.; Sottos, N. R.; White, S. R.; Moore, J. S., Wax-Protected Catalyst Microspheres for Efficient Self-Healing Materials. *Advanced Materials* **2005,** 17, (2), 205-208.

144. Kessler, M. R.; White, S. R., Self-activated healing of delamination damage in woven composites. *Composites Part A: Applied Science and Manufacturing* **2001,** 32, (5), 683-699.

145. Kessler, M. R.; Sottos, N. R.; White, S. R., Self-healing structural composite materials. *Composites Part A: Applied Science and Manufacturing* **2003,** 34, (8), 743-753.

146. Patel, A. J.; Sottos, N. R.; Wetzel, E. D.; White, S. R., Autonomic healing of low-velocity impact damage in fiber-reinforced composites. *Composites Part A: Applied Science and Manufacturing* **2010,** 41, (3), 360-368.

147. Moll, J. L.; White, S. R.; Sottos, N. R., A Self-sealing Fiber-reinforced Composite. *Journal of Composite Materials* **2010,** 44, (22), 2573-2585.

148. Kessler M R.; Sottos N R.; R., W. S., Self-healing structural composite materials. *Composites Part A : Applied science and manufacturing* **2003,** 34, 743-753.

149. Keller, M.; Sottos, N., Mechanical Properties of Microcapsules Used in a Self-Healing Polymer. *Experimental Mechanics* **2006,** 46, (6), 725-733.

150. Brown, E. N.; White, S. R.; Sottos, N. R., Microcapsule induced toughening in a self-healing polymer composite. *Journal of Materials Science* **2004,** 39, (5), 1703-1710.

151. Rule, J. D.; Sottos, N. R.; White, S. R., Effect of microcapsule size on the performance of self-healing polymers. *Polymer* **2007,** 48, (12), 3520-3529.

152. Keller M W.; White S R; Sottos N R., A self healing poly(dimethylsiloxane) elastomer. *Advanced Funtional Materials* **2007,** 17, 2399-2404.

153. Keller M W.; White S R.; N. R. Sottos, Torsion fatigue response of self-healing poly(dimethylsiloxane) elastomers. *Polymer* **2008,** 49, (3136-3145).

154. Yin, T.; Rong, M. Z.; Zhang, M. Q.; Yang, G. C., Self-healing epoxy composites - Preparation and effect of the healant consisting of microencapsulated epoxy and latent curing agent. *Composites Science and Technology* **2007,** 67, (2), 201-212.

155. Hsieh, H.-C.; Yang, T.-J.; Lee, S., Crack healing in poly(methyl methacrylate) induced by co-solvent of methanol and ethanol. *Polymer* **2001,** 42, (3), 1227-1241.

156. Wang, P. P.; Lee, S.; Harmon, J. P., Ethanol-induced crack healing in poly(methyl methacrylate). *Journal of Polymer Science Part B: Polymer Physics* **1994,** 32, (7), 1217-1227.

157. Caruso, M. M.; Delafuente, D. A.; Ho, V.; Sottos, N. R.; Moore, J. S.; White, S. R., Solvent-Promoted Self-Healing Epoxy Materials. *Macromolecules* **2007,** 40, (25), 8830-8832.

158. Kumar, A.; Stephenson, L. D.; Murray, J. N., Self-healing coatings for steel. *Progress in Organic Coatings* **2006,** 55, (3), 244-253.

159. Suryanarayana, C.; Rao, K. C.; Kumar, D., Preparation and characterization of microcapsules containing linseed oil and its use in self-healing coatings. *Progress in Organic Coatings* **2008,** 63, (1), 72-78.

160. Sauvant-Moynot, V.; Gonzalez, S.; Kittel, J., Self-healing coatings: An alternative route for anticorrosion protection. *Progress in Organic Coatings* **2008,** 63, (3), 307-315.

161. Yabuki, A.; Yamagami, H.; Noishiki, K., Barrier and self-healing abilities of corrosion protective polymer coatings and metal powders for aluminum alloys. *Materials and Corrosion* **2007,** 58, (7), 497-501.

162. Yasakau, K. A.; Zheludkevich, M. L.; Lamaka, S. V.; Ferreira, M. G. S., Mechanism of Corrosion Inhibition of AA2024 by Rare-Earth Compounds. *The Journal of Physical Chemistry B* **2006,** 110, (11), 5515-5528.

163. Zheludkevich, M. L.; Shchukin, D. G.; Yasakau, K. A.; Möhwald, H.; Ferreira, M. G. S., Anticorrosion Coatings with Self-Healing Effect Based on Nanocontainers Impregnated with Corrosion Inhibitor. *Chemistry of Materials* **2007,** 19, (3), 402-411.

164. Shchukin, D.; Zheludkevich, M.; Yasakau, K.; Lamaka, S.; Ferreira, M.; Möhwald, H., Layer-by-Layer Assembled Nanocontainers for Self-Healing Corrosion Protection. *Advanced Materials* **2006,** 18, (13), 1672-1678.

165. Shchukin, D. G.; Lamaka, S. V.; Yasakau, K. A.; Zheludkevich, M. L.; Ferreira, M. G. S.; Mohwald, H., Active Anticorrosion Coatings with Halloysite Nanocontainers. *The Journal of Physical Chemistry C* **2008,** 112, (4), 958-964.

166. Abdullayev, E.; Lvov, Y., Clay nanotubes for corrosion inhibitor encapsulation: release control with end stoppers. *Journal of Materials Chemistry* **2010,** 20, (32), 6681-6687.

167. Cui, J.; Liu, Y.; Hao, J., Multiwalled Carbon-Nanotube-Embedded Microcapsules and Their Electrochemical Behavior. *The Journal of Physical Chemistry C* **2009,** 113, (10), 3967-3972.

168. Kuang, F.; Shi, T.; Wang, J.; Jia, F., Microencapsulation technology for thiourea corrosion inhibitor. *Journal of Solid State Electrochemistry* **2009,** 13, (11), 1729-1735.

CHAPTER 2. EXPERIMENTAL METHODS

This chapter summarizes the experimental procedures and instrumentation used in the synthesis and characterization of pH responsive capsules in epoxy coating system.

2.1. Microcapsule synthesis

All reagents were used without further purification unless otherwise noted. Cymel® U80, a highly butylated urea formaldehyde resin, was used as received from Cytec Corporation. Pentaerythritol tetra (3 – mercaptopropionate) was used as received from VWR (manufactured by TCI chemicals). Acetone was used as a low boiling co-solvent whereas, 18 MΩ Millipore ® water was used to dissolve cerium nitrate to be incorporated inside the microcapsules. Heavy mineral oil (purchased from VWR) was used as received as a dispersion medium. Tween® 20 (purchased from VWR) and Span® 85 (purchased from Sigma Aldrich) were used as received to stabilizing surfactants. Hydrogen peroxide (30% solution, ACS grade; purchased from VWR) was used as an oxidizer.

The microcapsules were synthesized by internal phase separation polymerization method. Like any emulsion polymerization reaction, the ingredients were separated into two phases as shown in Table 2.1. Phase 1 (dispersion medium) consisted of the mineral oil, Span ® 85 and Tween ® 20. Phase 2 (dispersed phase) consisted of highly butylated urea formaldehyde resin, thiol crosslinker, acetone, water, cerium nitrate and hydrogen peroxide. Phase 1 was transferred into a resin kettle and subjected to a high shear at 2000 RPM using an angle tooth blade. Phase 2 was added at the rate of 1mL/min into the reactor. The mixture was allowed to emulsify for 30 minutes at the same high shear and was sonicated using Qsonica® S-4000 Liquid Processor for 10 minutes (amplitude – 50; ON duration - 10 s; OFF duration -10 s) to reduce the particle size further. The formed emulsion was then transferred to a rotatory evaporator (IKA® RV- 10 control) where it was polymerized at 50°C at 200 RPM and 750 mbar of pressure. After 3 hours, the formed microcapsules were vacuum filtered, triple washed with Millipore® water and centrifuged to remove any residual mineral oil. Table 2.1 summarizes the base formulation used for the synthesis. Care was taken while handling and disposing the microcapsules, resin and related formulations due to the carcinogenic nature of the Cymel ® U80 resin.

Table 2.1. Base formulation for the synthesis of microcapsules

Chemical Name	***Weight (g)***
Phase 1	
Mineral oil	100
Span® 85	6
Tween® 20	1.5
Phase 2	
Cymel ® U80	2
Pentaerythritoltetra–(3–mercaptopropionate)	2
Hydrogen peroxide	2
Cerium nitrate	0.3
Acetone	15
Water	1

2.2. Polymer characterization

2.2.1. Thermo-Gravimetric Analysis

Thermal degradation of samples was determined using Thermo-Gravimetric Analysis (TGA) using a TA Instruments Q 500 (New Castle, DE). Samples were heated in a nitrogen atmosphere from room temperature to 800°C at 10°C/min. The obtained results were analyzed using Universal Analysis 2000 software. Samples included microcapsules, films of the shell walls and cured coatings containing various percentages of microcapsules.

2.2.2. Dynamic Mechanical Analysis

Dynamic Mechanical properties were tested using TA Instruments Q800 Dynamic Mechanical Analyzer in multi frequency strain mode and ramping the temperature. Free films of the microcapsules shell walls were synthesized, typically of the dimensions of ~20 mm in length, 5 mm in width and 0.061-0.075 mm thickness were characterized using 1 Hz frequency, preload force of 0.015 – 0.02 N and a constant strain percent of 0.02 %, heating rate of 5°C/min over a temperature range of – 75°C to 300°C. The obtained data was analyzed using Universal Analysis 2000 software.

2.2.3. Raman Spectroscopy

Raman spectra of the resin and the crosslinker were, measured using a Nicolet NXR 9650 FT-Raman spectrometer (West Palm Beach, FL) equipped with a Nd:YAG laser, emitting at 1064 nm, and a germanium detector cooled with liquid nitrogen. In case of films and microcapsules synthesized, Raman spectra were recorded using a Horiba-Jobin Yvon LabRAM ARAMIS Raman spectrometer at room temperature with a 50 mW YAG laser at 532 nm on aluminum substrate. The appearance of disulfide bonds was monitored at 500 cm^{-1} and the disappearance of thiol bonds were monitored at 2570 cm^{-1}.

2.3. Microcapsule characterization

2.3.1. Particle Size Analysis

The particle size of the synthesized microcapsules was determined using single particle optical sizing technique using water as the solvent. AccuSizer 780 AD (Particle Sizing Systems, Port Richey FL) was used to determine the mean diameter of the particles. Mean diameter and standard deviation from data sets of at least 250 measurements.

2.3.2. Scanning Electron Microscopy/ Energy Dispersive Spectroscopy

Dried microcapsules were applied to a carbon adhesive tab on a cylindrical aluminum mount, and excess material blown off with a jet of dry nitrogen gas. Uncoated specimens were observed and photographed in a JEOL JSM-6490LV scanning electron microscope (JEOL USA Inc., Peabody MA).

Dried microcapsules were mixed into G1 epoxy with hardener (GATAN Inc., Pleasanton CA, USA) in silicone molds, covered with Aclar film (Ted Pella, Redding CA, USA), and polymerized on a 130°C hot plate. Blocks were removed from the molds and cross sectional polished using an argon ion beam (IB-09010CP Cross Section Polisher, JEOL USA Inc., Peabody MA). Cross-sectioned surfaces were observed and photographed in a JEOL JSM-6490LV scanning electron microscope (JEOL USA Inc., Peabody MA).

2.3.3. Transmission Electron Microscopy

Suspensions were dropped onto formvar-coated 300-mesh copper TEM grids and immediately wicked off with filter paper. Grids were allowed to air dry, then observed and photographed using a JEOL JEM-100CX II transmission electron microscope (JEOL USA Inc., Peabody MA) running at 80 keV.

Samples containing microcapsules were suspended in 50% acetone, then centrifuged (Eppendorf 5415 C microcentrifuge, Brinkmann Instruments, Inc., Westbury NY USA) at 5000 RPM for five minutes. This procedure was repeated in 90% acetone, then three times in 100% acetone. After a final centrifugation, microcapsules were mixed into Epon-Araldite embedding plastic (Tousimis Corp., Rockville MD USA), placed into BEEM capsules or flat silicone molds, and polymerized in an oven at 60°C for 24 hours. The resulting blocks were sectioned at 70-80 µm thickness with an ultramicrotome (PowerTome XL, RMC Products, Boeckeler Instruments, Inc., Tucson AZ USA). Sections were observed and photographed using a JEOL JEM-100CX II transmission electron microscope (JEOL USA Inc., Peabody MA) running at 80 keV.

2.3.4. UV-Vis Spectroscopy

The release of cerium nitrate was monitored using Varian Cary 5000 UV-Vis-NIR spectrophotometer by monitoring the absorbance at 252 nm for Ce^{3+} and 298 nm for Ce^{4+} ions. Scans were performed in the wavelength range between 500 nm to 200 nm. Typically, for the release experiments, a known quantity of the capsules was exposed to different pH solutions and the absorbance was measured. On certain occasions, microcapsules were ground using a mortar and pestle and solutions containing the ground capsules were measured.

2.3.5. Inductively Coupled Plasma

0.2 g of synthesized microcapsules was added to 100 mL of 0.1M sodium hydroxide. 5 mL samples were drawn every hour for eight hours and Spectro-Genesis® Inductively Coupled Plasma Optical Emission Spectrometer (ICP-OES) with Cross-flow nebulizer was used to detect the amount of cerium released from these microcapsules. A mean concentration from 3 replicate measurements was recorded. In order to ensure quality control and to verify the consistency of results, a control check verification standard (WW-IPC-1, Inorganic Ventures) was measured after every ten samples. The deviation of these standards was typically within 5 %. A 5-point calibration was used to standardize the measurements.

2.4. Coatings evaluation

2.4.1 Sample Preparation

Cold rolled steel panels (R-36) were ordered from Q-panel® in bulk to reduce minute differences in alloy composition. The panels were sand blasted at 40 PSI with 220 mesh grit (McMaster Carr) until uniform grey surface was obtained. After sand blasting, the panels were degreased with hexane to clean the surface before coating it. Panels were wiped with Kimwipes ® to remove any black residue as a result of sand blasting.

A water reducible 2K epoxy system was used as a vehicle to study the effect of microcapsules in coatings. BECKOPOX ® VEP 2381w/55WA water reducible epoxy resin (EEW = 980 g/equiv; Cytec Industries, Inc.) and BECKOPOX ® EH 623 w/80WA (AHEW = 200 g/equiv; Cytec Industries, Inc.) were mixed together with an epoxy to amine ratio of 1:1. Water was used to adjust the viscosity as needed. Coatings containing different percentages (by weight) of microcapsules were applied to sand blasted steel substrates using a draw down bar and allowed to ambient cure for at least 2 days before subjecting them to any type of testing.

2.4.2. König Pendulum Hardness

König pendulum hardness of the coatings was measured following ASTM D 4366. The hardness test results were reported in seconds (s).

2.4.3. Impact Resistance

Reverse impact strength of the coatings was determined following ASTM D 2794 using a Gardener impact tester. A drop weight of 4 lb (1.814 kg) was used. The maximum height achievable in the impact tester was 43 inches (1.09 m). Max height with no loss of adhesion or crazing was noted and the corresponding inch-pounds (in-lb) were reported.

2.4.4. Gloss Measurement

Gloss measurements were recorded at 20°, 60°, 85° using micro-TRI-gloss gloss meter according to ASTM D523-89.

2.4.5. MEK Double Rubs

MEK double rubs were carried out according to ASTM D 5402 to assess the solvent resistance of the coatings. Three layers of cheese cloth wrapped around a 26-oz (737 g) hammer soaked in MEK. The hammer head was rewet with MEK after ~50 double rubs. The number of double rubs was noted once the metal surface of the panel was visible due to removal of the coating layer during the test.

2.4.6. Adhesion Measurements

Cross hatch adhesion of the coatings was evaluated using a Gardco® cross hatch adhesion instrument according to ASTM D 3359.

2.5 Corrosion testing

2.5.1. Open Circuit Potential

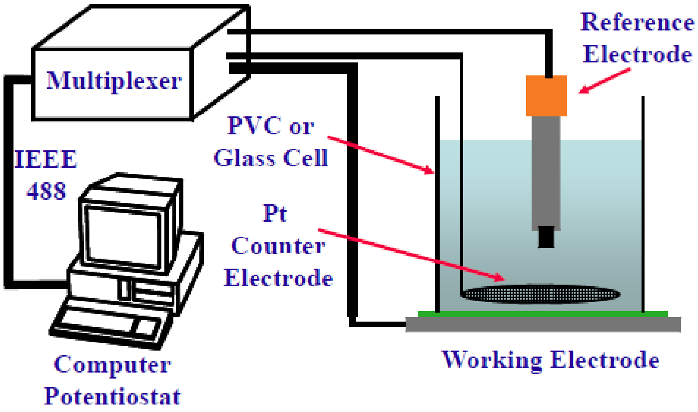

Figure 2.1. Typical electrochemical cell setup used in corrosion studies of coated metal substrates. Tallman, D.E. (2010). *Impedance spectroscopy* [PowerPoint slides]. Retrieved from Lecture Notes.

The corrosion potential (E_{corr}) was measured using a Gamry ® PC-4/FAS 1 potentiostat. A three electrode setup was used as shown in Figure 2.1 with Saturated Calomel Electrode (SCE) as the reference, platinum clad niobium as the counter and the sample as the working electrode. The sample consisted of an unscribed cured microcapsule containing epoxy coating. The corrosion potential was monitored for 24 hours.

2.5.2. Potentiodynamic Experiment

Potentiodynamic experiments were performed using a Gamry ® PC4/FAS1instrument**.** The electrochemical setup used was similar to that used to determine the open circuit potential

(Figure 2.1). A scribe approximately 2.5 cm in length and 1 mm in width was made through the coating. 5 % by weight solution of sodium chloride degassed with nitrogen for 10 minutes and 5% by weight aerated solution of sodium chloride were used as the electrolytes to evaluate the effect of oxygen on the inhibition of corrosion using cerium salts. Potentiodynamic scans were conducted from an initial voltage of -0.5 V to 1.0 V at 5 mV/s with an initial delay of 300 sec.

2.5.3. Cyclic Voltammetry

Pine Instruments' Rotating Disc Electrode setup was used for the cyclic voltammetry experiments using a three electrode set up consisting of an Ag/AgCl reference electrode, a platinum disc electrode/ glassy carbon as the working electrode and platinum disc electrode as the counter electrode. 0.25 g of cerium containing capsules was mixed into a cell containing 50 mL of 0.1 M sulfuric acid. The glassy-carbon working electrode was stirred at 1600 RPM and potential scans were performed at the rate of 50 mV/s in the potential range of 500 mV -1600 mV (vs. Ag/AgCl). Due to the precipitation of cerium salts in basic conditions, 0.1 M sulfuric acid was used as an electrolyte.

2.5.4. Electrochemical Impedance Spectroscopy

In order to study the corrosion inhibition due to the encapsulated inhibitor and the effect of the addition of capsules into coatings, EIS experiments were conducted. All the EIS measurements were carried out with a PC-4/FAS1 Femtostat (Gamry Instruments, Warminster, PA). A 10 mV (RMS) AC perturbation was applied to the sample relative to the open circuit potential. The frequency range monitored ranged from 100000 Hz to 0.01 Hz at 10 points per decade. The electrochemical cell was setup as shown in the Figure 2.1. Saturated Calomel Electrode (SCE) was used as the reference electrode, platinum clad niobium expanded mesh was used as the counter electrode and the sample was made the working electrode. 5 % sodium chloride was used as an electrolyte. The area of the electrochemical cell used in this arrangement was 7.1 $cm^{2.}$ Three replicate measurements were recorded per coating system.

2.5.5. Scanning Electrochemical Microscopy

Cerium release and deposition at the cathodic sites were monitored using 920D Scanning Electrochemical Microscope (CH Instruments, Austin, TX). All solutions were prepared from reagent grade chemicals as received from VWR and Sigma Aldrich, USA without further purification. 18 MΩ Millipore ® water was used in all aqueous solutions and during rinsing. Measurements were made in a three and four electrode configuration. The 3 electrode configuration requires the use of 10 µm diameter platinum tip ultra-microelectrode as the working electrode (E1), an Ag/AgCl reference electrode (R) and a platinum mesh as a counter electrode (C). In the 4 electrode configuration, the metal substrate could also be polarized at working electrode (E2). In 3 electrode configuration, measurements were made with the sample at open circuit potential (E2 = OFF). Coated metal samples were press fitted into a home-built electrochemical cell with a bottom orifice fixed with an O-ring. The electrochemical cell was mounted on the three-axis translation stage of the SECM. The tip potential was controlled by a bipotentiostat (CH Instruments, Austin, TX USA) and a CCD camera mounted above the cell helped position of the tip over the sample area to be studied.

Calibrating approach curves were obtained in 1 mM ferrocene–methanol in 0.1 M potassium chloride. The tip was placed at a suitable distance from the sample (typically 10–15 µm), and line scans and SECM images were recorded.

2.6. References

1. Luz M.Calle & Li, W. Coatings and methods for corrosion detection and/or reduction. United States patent 7790225 (2010).

2. Atkin, R., Davies, P., Hardy, J. & Vincent, B. Preparation of Aqueous Core/Polymer Shell Microcapsules by Internal Phase Separation. *Macromolecules* **37**, 7979-7985, doi:10.1021/ma048902y (2004).

CHAPTER 3. pH RESPONSIVE CAPSULES –SYNTHESIS & CHARACTERIZATION

3.1. Introduction

pH responsive capsules were synthesized as described in chapter 2. This chapter discusses the synthesis and characterization of pH responsive capsules. The capsules were characterized using various techniques to better understand structure & morphology, incorporation & release of the cerium based corrosion inhibitor. This chapter is divided into three sections. The sections 3.2 – 3.3, discusses the use of internal phase separated polymerization as a viable method for the synthesis of core - shell pH responsive capsules and the crosslinking reactions resulting in capsule shell. In the sections 3.4- 3.5, thermal and spectroscopic evaluation of the shell walls formed as a result of oxidative polymerization of the thiol is discussed. In the sections 3.6-3.9, the structure, morphology and incorporation of water soluble cerium salt within the capsules is discussed.

3.2. Principles of wall formation due to internal phase separated polymerization

Internal phase separation has been popularized by Vincent et al. for the synthesis of polymeric microcapsules with both aqueous and oil core. [1-3] The basics of internal phase separation are that water in oil emulsions are prepared with shell polymer dissolved in the aqueous phase by adding a low boiling co-solvent. Subsequently, the evaporation of this co-solvent leads to the phase separation of the polymer and depending on the spreading conditions leads to the formation of the shell around the aqueous core. The spreading coefficient (S_i) of each phase plays a very important role in the formation of the capsules. The spreading coefficient for any phase is given by the equation below.

$$S_i = \gamma_{jk}-(\gamma_{ij}+ \gamma_{ik}) \tag{3.1}$$

In a system consisting of three immiscible liquids (phase 1 -water, phase 2 - mineral oil & phase

3 - polymer), when two immiscible liquids, phase 1 and 3, are brought in contact with another immiscible liquid, phase 2, various equilibrium morphologies depends on the interfacial tensions between the phases (γ_{12}, γ_{23} and γ_{13}). For phase 1, if $\gamma_{12} > \gamma_{13}$ then $S_1 < 0$ and three possible combinations of S_i exist:

$$S_1<0;\ S_2<0;\ S_3>0 \tag{3.2}$$

$$S_1<0;\ S_2<0;\ S_3<0 \tag{3.3}$$

$$S_1<0;\ S_2>0;\ S_3<0 \tag{3.4}$$

Core shell particles are formed when condition 3.2 was satisfied with phase 1 appearing as the core within the shell of phase 3. When condition 3.3 is satisfied then "acorn" shaped particles are formed. Satisfaction of condition 3.4 led to the formation of separate droplets.[4, 5]

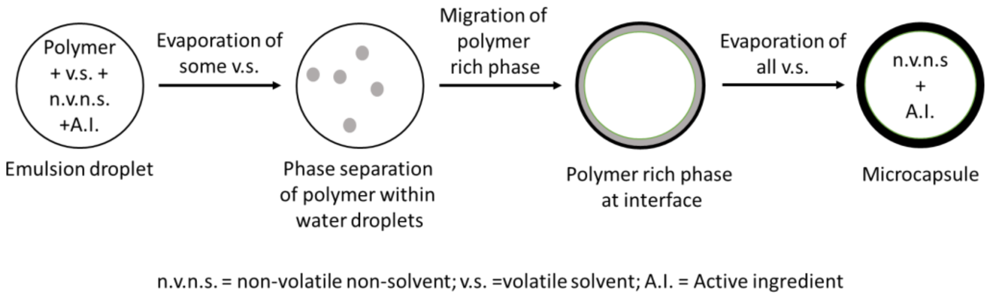

Figure 3.1. Schematic representation of the formation of microcapsules by internal phase separation.[1] Reproduced with permission from reference 1 from "Dowding, P. J.; Atkin, R.; Vincent, B.; Bouillot, P., Oil Core−Polymer Shell Microcapsules Prepared by Internal Phase Separation from Emulsion Droplets. I. Characterization and Release Rates for Microcapsules with Polystyrene Shells. Langmuir 2004, 20, (26), 11374-11379. Copyright 2004 American Chemical Society."

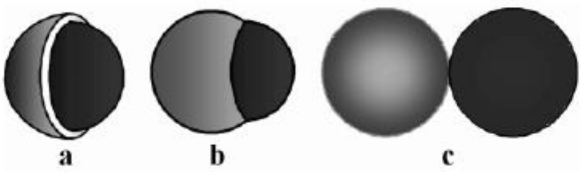

Figure 3.2. Schematic of three particle morphologies (a) core-shell (b) acorn (c) two separate particles.[2] Reprinted with permission from "Dowding, P. J.; Atkin, R.; Vincent, B.; Bouillot, P., Oil Core−Polymer Shell Microcapsules Prepared by Internal Phase Separation from Emulsion Droplets. I. Characterization and Release Rates for Microcapsules with Polystyrene Shells. Langmuir 2004, 20, (26), 11374-11379. Copyright 2004 American Chemical Society."

The concept of internal phase separated polymerization technique discussed by Vincent et al. was employed in designing a water in oil emulsion to incorporate water soluble corrosion inhibitors in core shell capsules. Vincent et al. report the synthesis of core shell capsules using an oil in oil emulsion for the encapsulation of organic non-polar solvent using internal phase separation. The technique was extended to incorporate interfacial crosslinking reaction between a thiol functional resin and an amino resin to incorporate pH sensitivity. In the synthesis, mineral oil was chosen as the dispersion medium in which polymer containing water phase was emulsified using a high speed disperser. Due to the immiscibility of the polymeric resins (amino resin and thiol resin) and water (non-volatile non solvent), acetone (b.p. 55 °C) was chosen, as the low surface activity water-miscible solvent with a boiling point significantly lower than that of water (b.p. 100 °C), for the dissolution of the monomers. Therefore, in place of typical water in oil (W/O) emulsion what we have is an acetone in oil (A/O) emulsion. Another reason for using water as the nonvolatile non-solvent was due to the high water solubility of the active ingredient (A.I), cerium nitrate hexahydrate, in this case. When acetone was removed gradually by evaporation, water (nonvolatile phase) was encapsulated by a cross-linked polymeric shell formed around the surfactant stabilized emulsion droplet. The pH sensitivity was incorporated into the capsules by the use of disulfide chemistry in the walls of the capsules. Disulfide bonds were formed as a result of the oxidation of pentaerythritol tetra kis (3-mercaptopropionate) (PEMP) in the presence of hydrogen peroxide. In addition to the phase separation described earlier, the crosslinking reaction also takes place by the oxidation of PEMP at the boiling point of acetone.

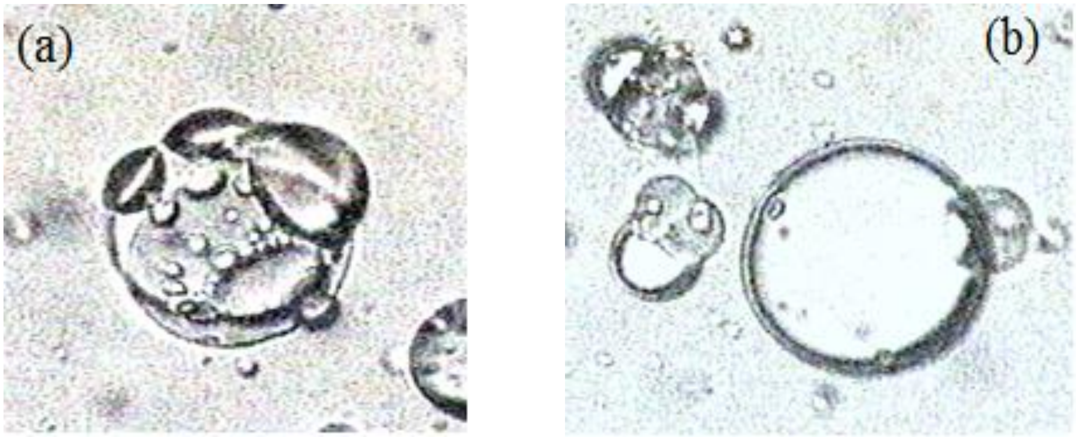

Figure 3.3. Formation of core-shell type capsules synthesized using internal phase separation observed using optical microscope at 20X (a) emulsion droplet showing internal phase separation with nucleation of polymer rich phases (b) emulsion droplet with a distinct polymer shell formed around water.

The synthesis of the capsules relies on the subtle balance that exists between all the components of the emulsion. A solvent to polymer ratio of approximately 4:1 was used to synthesize core shell particles. Such large ratio of solvent to polymer helps to keep the monomers/polymerized product solvated to facilitate the migration of the polymer to the oil-droplet interface. A slight excess of acetone also helps account for the losses due solvent evaporation during the emulsification process (evaporation during mixing and heating around the sonicator horn) and handling. A combination of two non-ionic surfactants were used to stabilize the acetone/water/resin emulsion in oil. A low HLB value surfactant and a high HLB value non-ionic surfactant was used adjust the HLB to form stable emulsions of the acetone/water/resin in mineral oil. Weight ratios of Span ® 85 (HLB = 1.85) and Tween ® 20 (HLB=16.7) were adjusted experimentally to a HLB value to form stable emulsion of acetone/water/resin phase in mineral oil. The actual process of microcapsule formation was followed using optical microscopy. Optical microscopy images revealed that the emulsion formed consisted of emulsion droplets of varying diameters. Subsequent acetone removal resulted in the appearance of polymer rich domains within the emulsion droplet (Figure 3.3 (a)). Upon further decrease in the solubility of the polymer, some droplet nucleation was observed followed by the migration of the polymer rich phase to the oil-droplet interface and resulting in the encapsulation of the aqueous phase. Figure 3.3 shows microcapsule walls are formed due to the evaporation of acetone. Evidence of the encapsulation of water and eventually cerium containing solution into the core capsule comes from the absence of water (from both hydrogen peroxide and added water) in the bottom of the reactor. In the early attempts of failed reactions however, a distinct layer of water was observed at the bottom of the reactor.

3.3. Proposed mechanism for crosslinking

The crosslinking reaction between highly butylated urea formaldehyde resin and a tetra functional thiol results in the formation of a cross-linked shell wall. Three major reactions may lead to the formation of the cross-linked shell wall namely: (a) the oxidation of thiols to produce disulfide bonds (Figure 3.5) (b) self-condensation of the amino resin (Figure 3.7) and (c) amino resin – thiol crosslinking reaction (Figure 3.6). The oxidation of the tetra functional thiol, pentaerythritol 3-mercaptopropionate by hydrogen peroxide produces disulfide linkages with decrease in pH.[6, 7] Amino resins form cross-linked networks with nucleophiles in the presence of an acid. N-butylated urea resins readily undergo self-condensation as well. The acidity of the thiol resin oxidation sufficiently catalyzes the self-condensation reaction of the butylated urea-formaldehyde resin as well as the nucleophilic substitution reaction between the cross-linked thiol pre-polymer and the amino resin.[8] The self-condensation of amino resin to form methylene ether or methylene linkages resulting in dimers, trimers etc. also contribute to the crosslinking of the shell wall.[8] This results in a crosslinking network which is pH responsive.

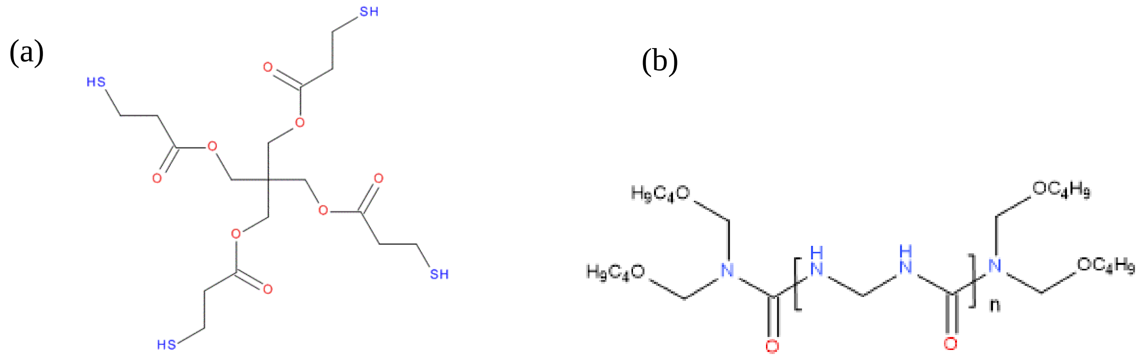

Figure 3.4. Schematic of (A) Pentaerythritol 3-(Mercaptopropionate) (PEMP) (B) Idealized Cymel ® U80 resin structure.

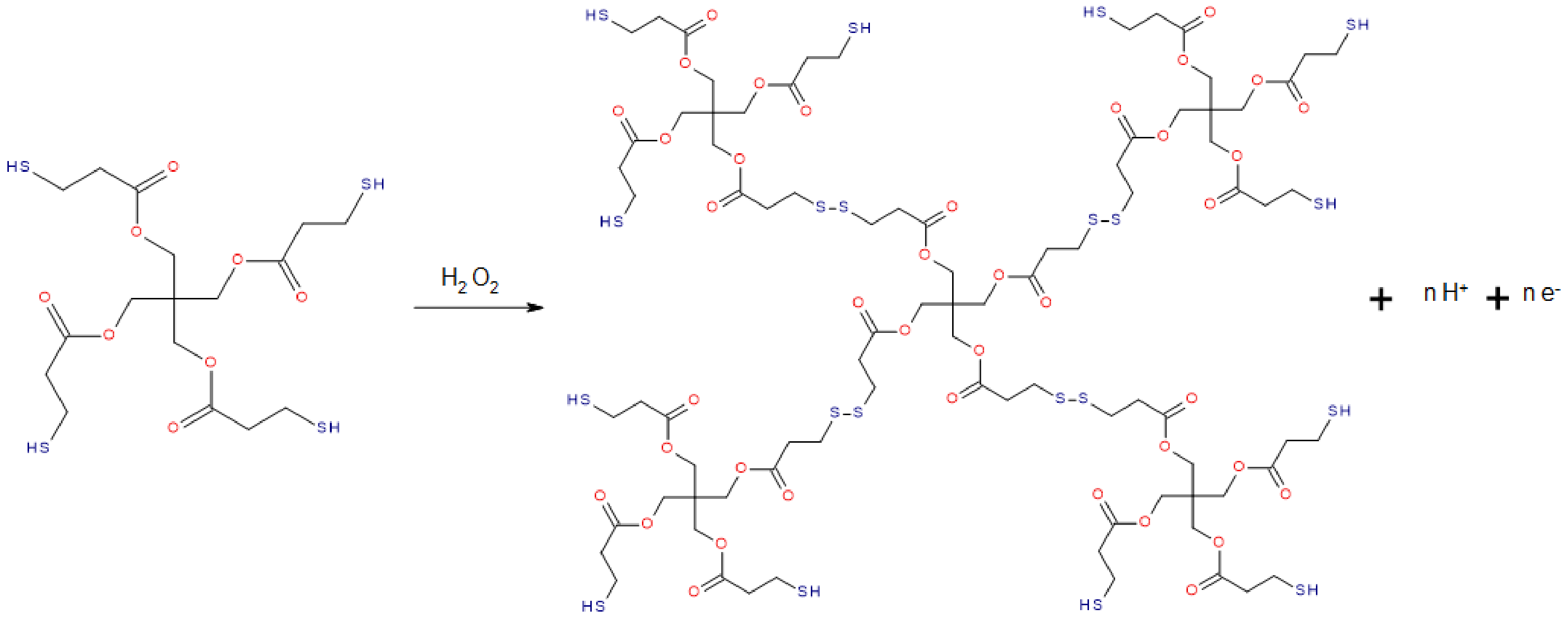

Figure 3.5. Oxidation of PEMP to form disulfide linkages.

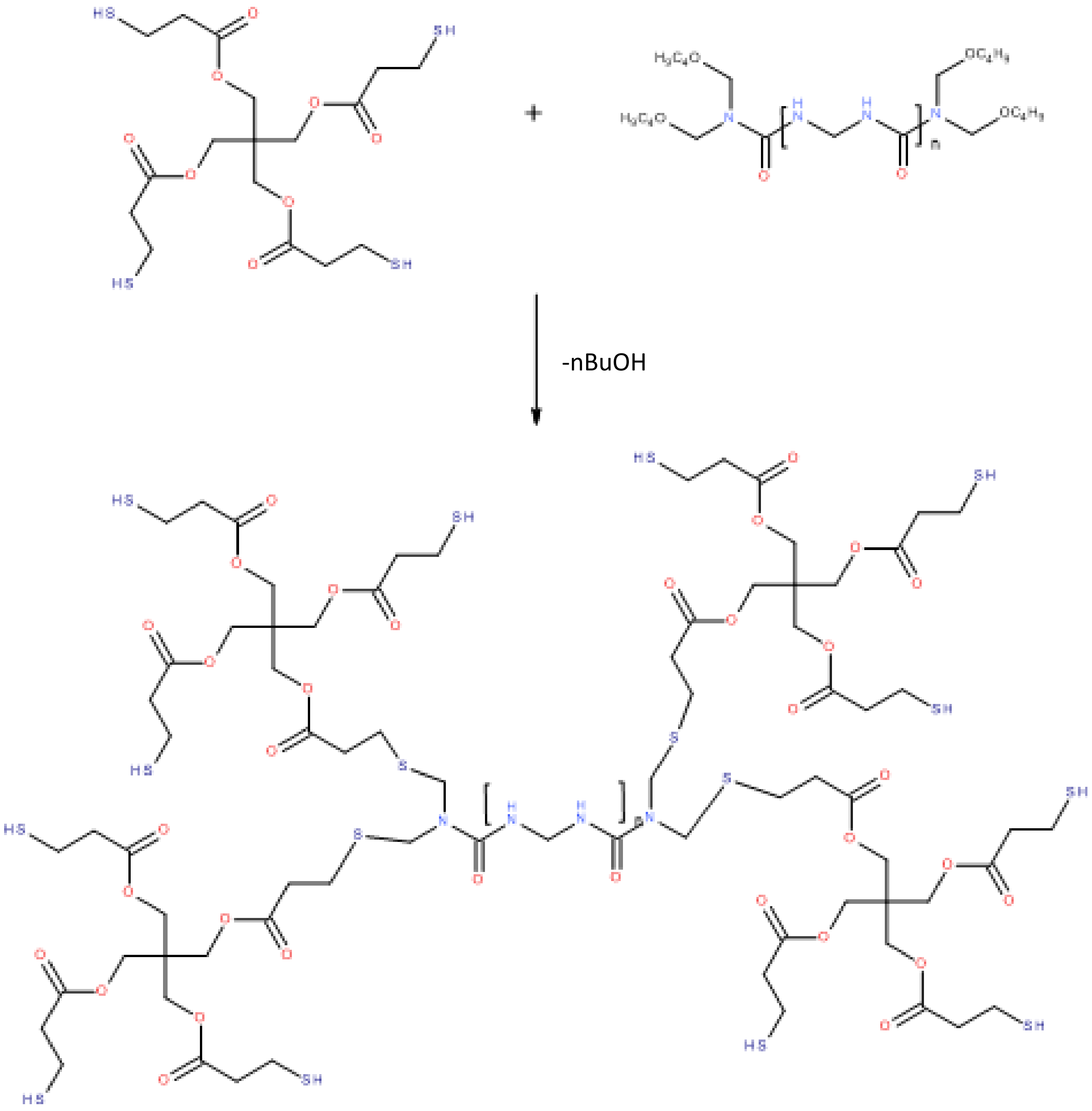

Figure 3.6. Crosslinking reaction of PEMP and Cymel® U80 resulting in microcapsules shell walls.

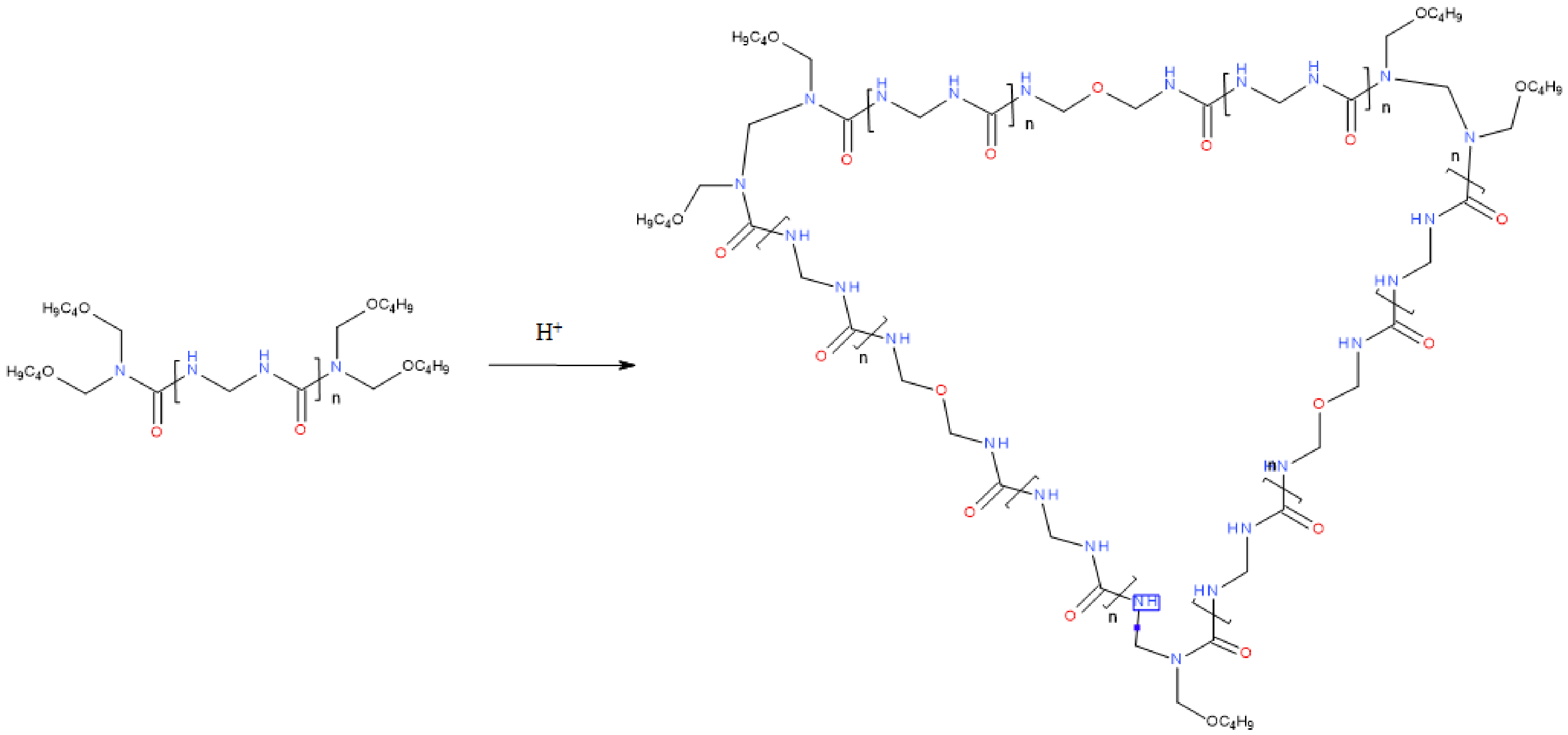

Figure 3.7. Self-condensation reactions of amino resin resulting the methylene and methylene ether linkages.

3.4. Spectroscopic analysis

In order to better understand the crosslinking reactions leading to the formation of the polymeric shell of the capsules, free films were cast on glass slides and analyzed using Fourier Transform Infra-Red spectroscopy and Raman Spectroscopy.

3.4.1. Fourier Transform Infra-Red Spectroscopy (FT-IR)

The chemical structures of Cymel® U80 and PEMP were obtained from the product data sheets of the manufacturer and summarized in Figure 3.4. Cymel ® U80 is a highly butylated urea formaldehyde (UF) resin which may readily self-condense in the presence of an acid catalyst. With the knowledge of the idealized structure of the UF resin, the peaks at 2873 cm^{-1}, 2933 cm^{-1} and 2958 cm^{-1} can be attributed to the symmetric and asymmetric C-H stretch from methyl (- CH_3) and methylene (-CH_2-) groups from the butyl groups. The methyl groups (in the butyl groups) also give rise to two bending vibrations, an asymmetric deformation band observed at 1465 cm^{-1} and a symmetric band at 1378 cm^{-1}. The bending vibration band of -CH_2- was also observed at 1479 cm^{-1}. Two broad peaks in the 3300 cm^{-1} region indicate the presence of secondary amine as they represent the symmetric and asymmetric N-H stretch which may be due to the presence of –$NHCH_2OH$ in the resin due to the methylolation of the –NH_2 groups in the UF resin. The decrease in the wavenumber of these peaks can be attributed to hydrogen bonding between the amine hydrogen and the carbonyl oxygen which results in a 150 cm^{-1} decrease in the wavenumber of the N-H stretch as observed in this case. A peak at 1529 cm^{-1} indicates the presence of both C-N bonds and secondary amine groups, as this peak is associated with the N-H bending vibration and a C-N stretch. The peak observed at 1276 cm^{-1} was due C-N (amide II) stretch of the amide. Another typical vibration observed in case of amides is the N-C-N stretch which was also observed at 1360cm^{-1} (asymmetric) and 1190 cm^{-1} (symmetric). In case of amides the C=O stretch was observed at 1668 cm^{-1}. The peak at 935 cm^{-1} was found to be due to the presence of para- formaldehyde which was present trace quantities in the resin.

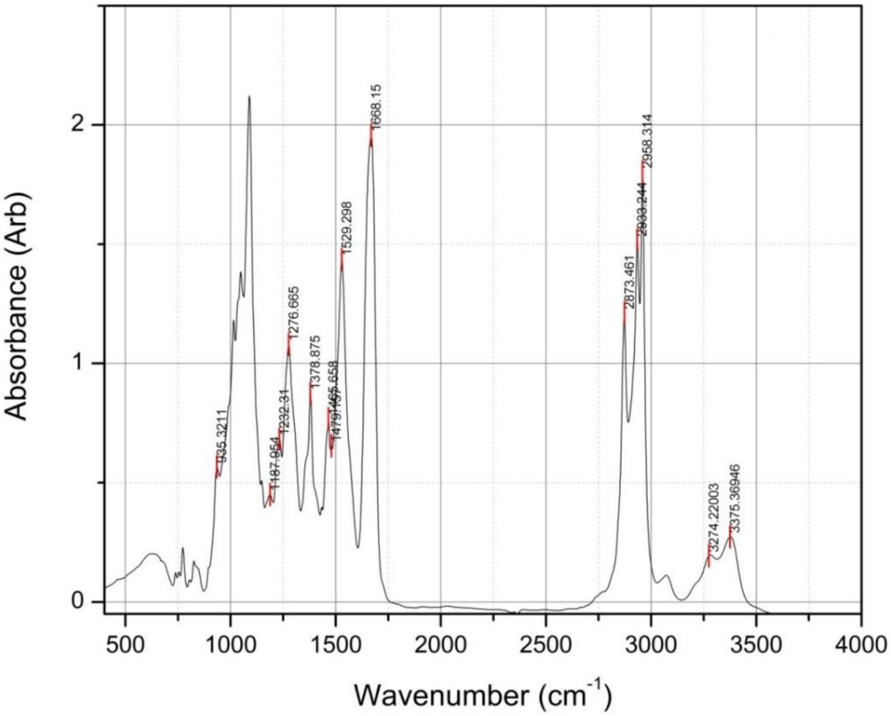

Figure 3.8. FT-IR spectra of Cymel ® U80 resin as received from Cytec Corporation.

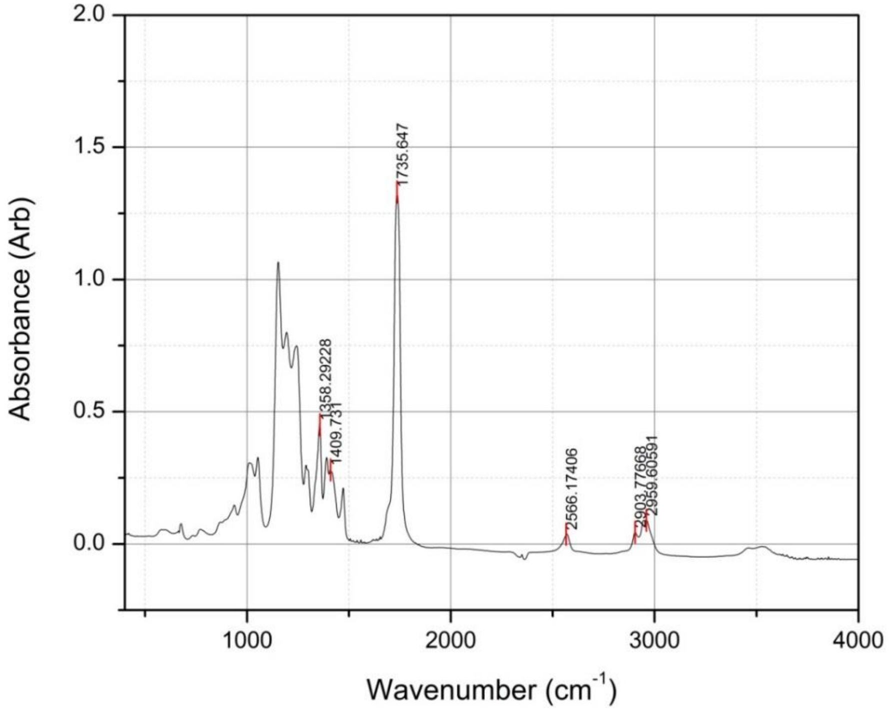

Figure 3.9. FT-IR spectra of Pentaerythritol 3-mercaptopropionate.

FT-IR spectra of PEMP was also recorded and analyzed. A sharp C=O stretch was observed at 1735 cm^{-1}. Being a thiol compound an S-H stretch was observed at 2566 cm^{-1}. The peaks at 2903 cm^{-1} and 2959 cm^{-1} are attributed to the symmetric and asymmetric vibrations of the methylene group.

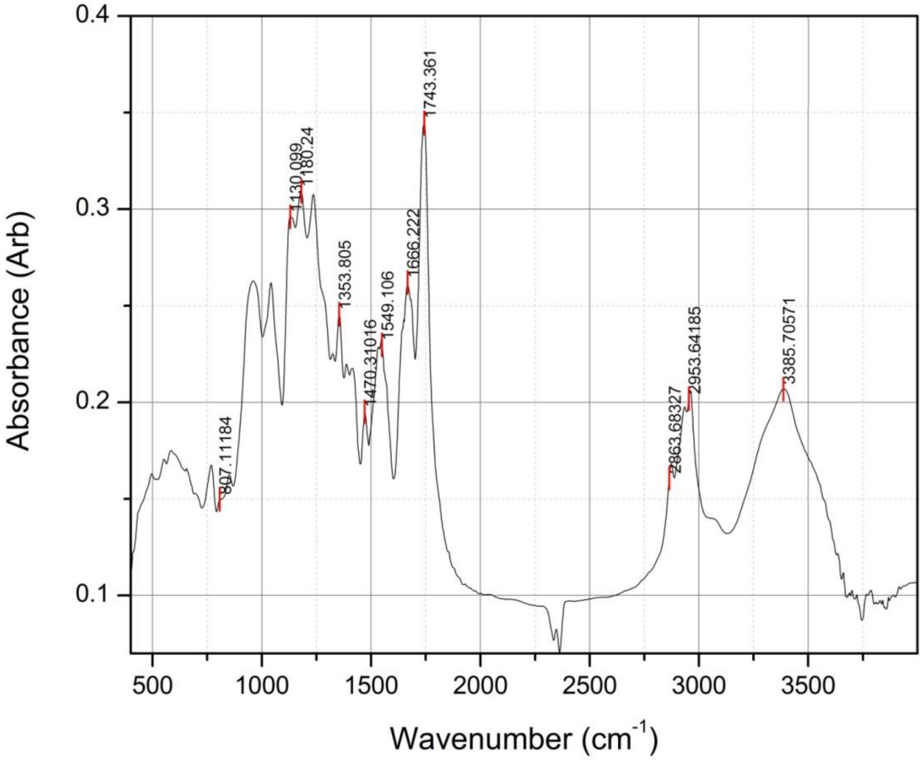

Figure 3.10. FT-IR spectra of the microcapsules wall cured film.

The FT-IR spectra of ground microcapsule films were recorded and analyzed. Characteristic broad band responsible for hydroxyl, imino and amino stretch were observed around 3388 cm^{-1}. Asymmetric and symmetric methylene stretches were observed at 2960 cm^{-1}and 2873 cm^{-1} respectively. The characteristic absorption of aliphatic C-N vibration appeared at 1180 cm^{-1}. C-O-C stretching due to the ether bridges was also noted at 1130 cm^{-1} which may be due to the methylene ether linkages formed as a result of the self-condensation reactions of the amino resin. Two characteristic C=O stretch were also observed. The stretch at 1666 cm^{-1} was due to the C=O stretch from Cymel® U80 and the peak at 1743 cm^{-1} was due to the C=O stretch from the PEMP. In order to obtain information about the disulfide and C-S linkages formed as a result of the crosslinking, Raman spectroscopy was performed.

3.4.2. Raman Spectroscopy

Raman spectra of the cured shell wall film, the resin and the thiol crosslinker were recorded to study the formation of C-S linkages, thiol linkages and the disulfide bonds.

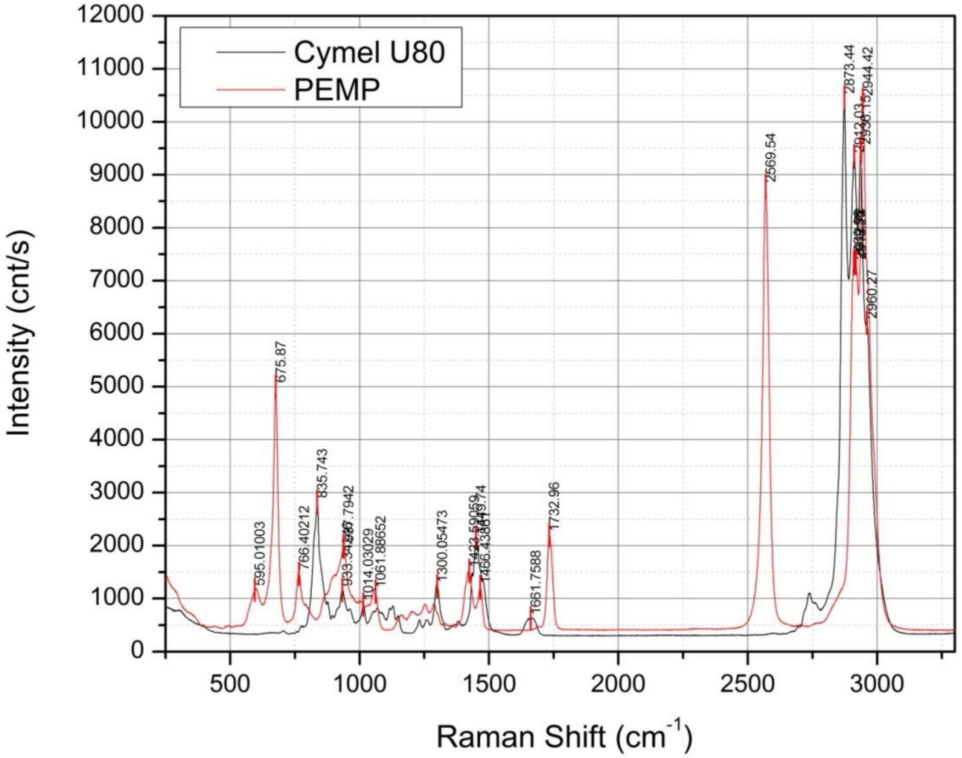

Figure 3.11. Raman Spectra of Pentaerythritol 3-mercaptopropionate and Cymel ® U80.

The Raman spectrum of PEMP shows a sharp peak at 2569 cm^{-1} due to the S-H stretch and a corresponding C-S stretch at 675 cm^{-1} due to the methylene group attached to the S-H group. In case of the cured microcapsule wall films, a strong peak at 506 cm^{-1} indicates the formation of disulfide bonds formed as a result of the oxidation of PEMP. The disappearance of thiol peak at 2569 cm^{-1} indicates the conversion of the thiols into disulfides. A sharp peak at 659 cm^{-1} indicates either a C-S stretch due to –CH_2-S- or a C-S-C (thioether) stretch. Since both the bands are in the same range it is difficult to resolve the both. The appearance of thioether stretch suggests that the amino resin (Cymel ® U80) may crosslink with the thiol groups from PEMP.

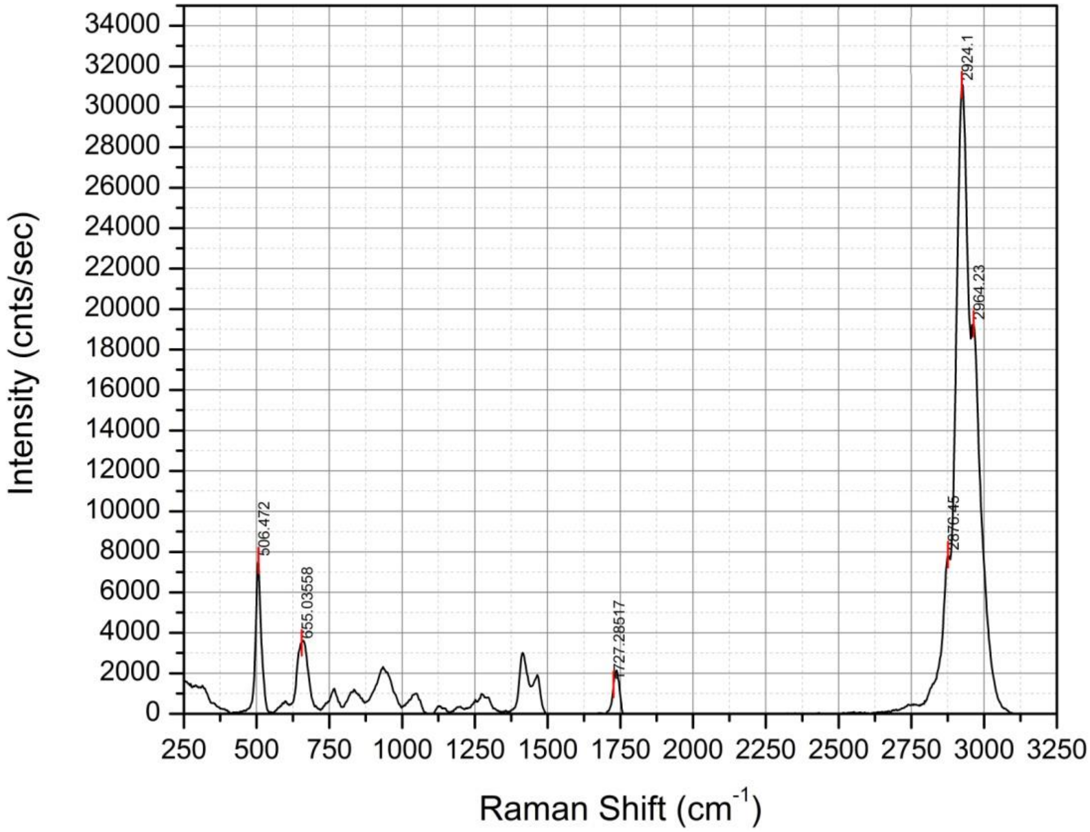

Figure 3.12. Raman spectra of cured microcapsule wall film.

3.5. Thermal analysis of microcapsules

The thermal stability of the microcapsules were determined by synthesizing water core (blank) and cerium containing microcapsules with different weight percentages of cerium nitrate. Thermo-gravimetric analysis was used to determine the incorporation of cerium into the capsules. Dynamic Mechanical Analysis was performed to determine the nature and glass transition temperature of the polymeric shell formed during the encapsulation process.

3.5.1. Thermo-Gravimetric Analysis (TGA)

The thermal stability of the synthesized capsules and the effect of cerium nitrate addition to the amount incorporated to the capsules were studied using Thermo-Gravimetric Analysis by comparing blank capsules to their cerium containing counterparts. Cerium containing capsules consisted of an organic polymer shell and an inorganic core, which decompose at different rates and at different temperatures. In an attempt to understand the decomposition of cerium containing capsules better, cerium (III) nitrate hexahydrate was allowed to decompose in the same temperature range at the same heating rate as that of cerium containing capsules. Up to 210°C cerium nitrate (III) hexahydrate was converted to its anhydrous form[9, 10]. The formed anhydrous salt was found to be thermally stable between 210°C - 220°C, after which the formed anhydrous salt was considered to undergo an oxidation reaction represented by:

$$Ce(NO_3)_3(s) \rightarrow CeO_2(s) + oxides\ of\ nitrogen$$

The decomposition of anhydrous cerium nitrate is considered to be a single irreversible step reaction which is evidenced a steady decrease in the slope after 210°C up to 300°C. Cerium oxide, the oxidized product, was found to be thermally stable up to 800°C.

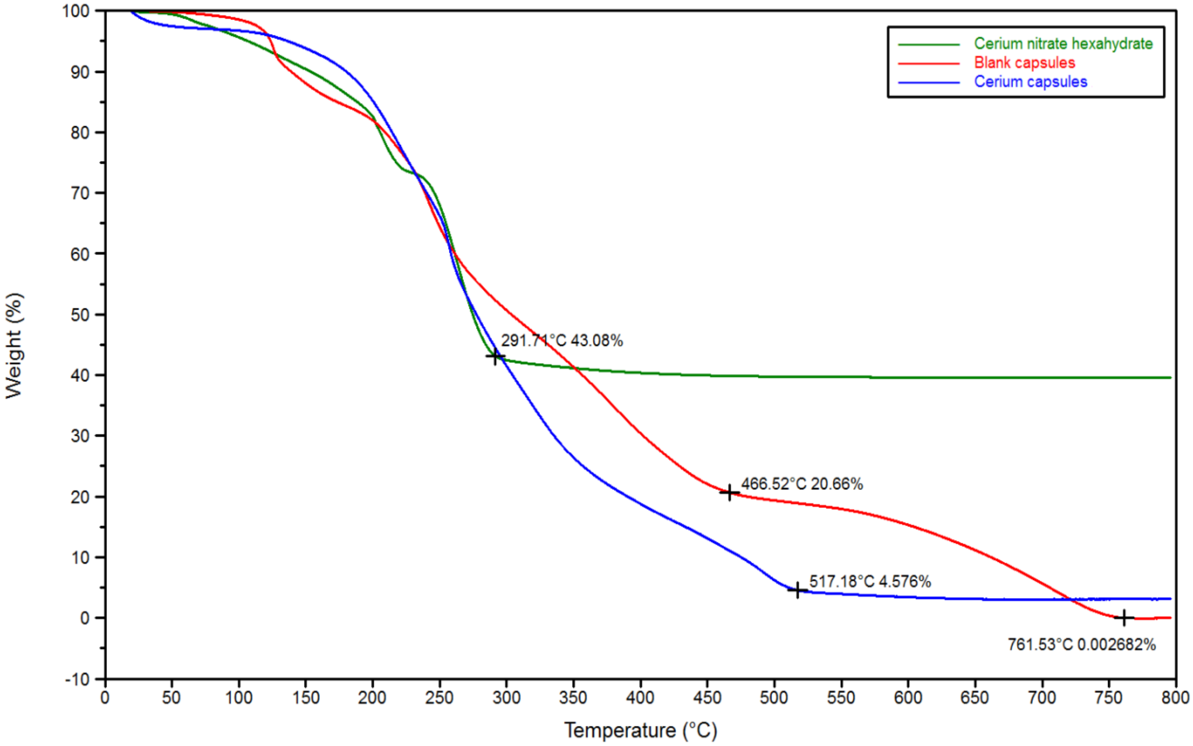

Figure 3.13. TGA plot showing the influence of cerium inclusion within the capsules.

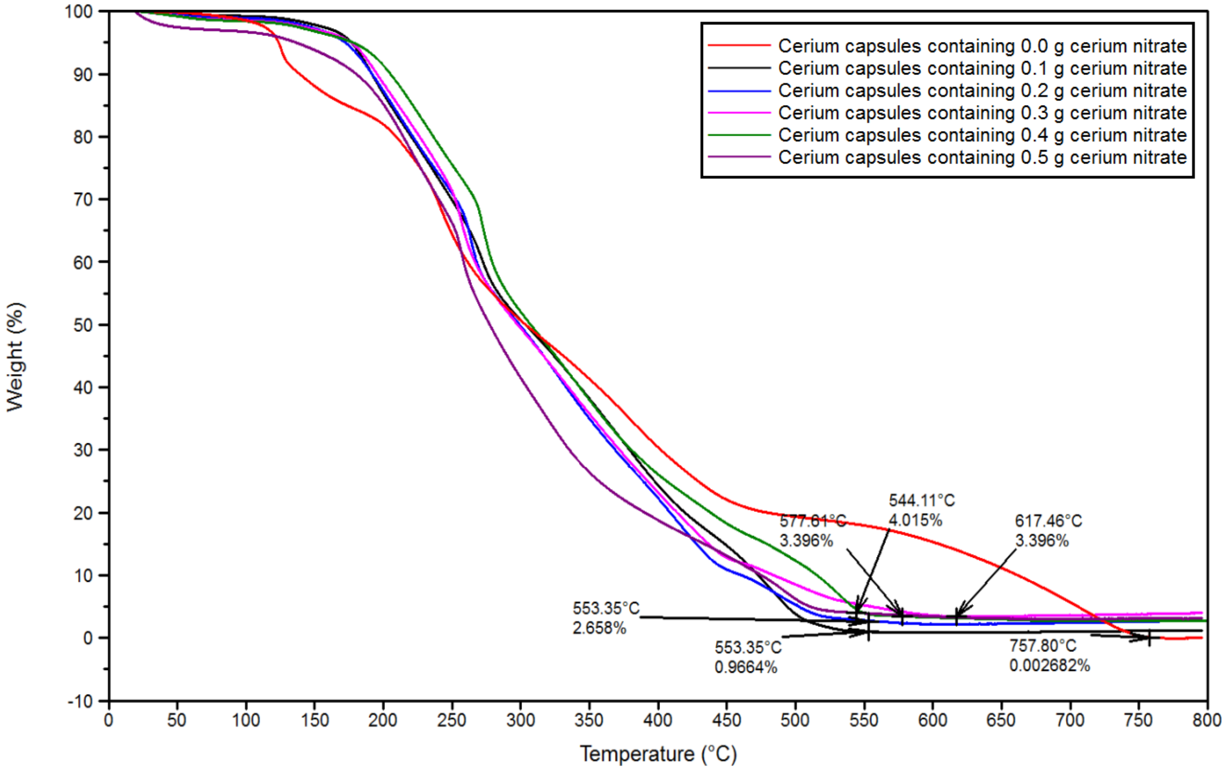

Figure 3.14. TGA plot of cerium containing capsules as a function of cerium nitrate added into the formulation.

The decomposition curves of both cerium containing capsules and blank capsules containing no cerium, showed a gradual change in mass loss initially which may be due to the loss of water of hydration followed by a rapid degradation of the polymer matrix. Blank capsules showed a complete degradation of polymer matrix at approximately 750°C whereas the cerium containing capsules showed the presence of residual mass on the TGA pan beyond decomposition temperature of blank capsules. The detection of residual mass in case of cerium containing capsules may indicate the formation of cerium oxide, which would be stable at high temperatures. To confirm the incorporation of cerium within the capsules, the weight percent of cerium was varied in the synthesis of the capsules. It was observed that by increasing the weight percent of cerium salts from 0.1 g – 0.5 g, the residual mass left in the pan varied from 0.97% to 4.015% respectively, thus confirming the incorporation of cerium salts at the core of the synthesized capsules. It also indicates that an increased quantity of cerium salts could be encapsulated within the core of the capsules by merely increasing the weight of cerium in the synthesis process.

3.5.2. Dynamic Mechanical Analysis (DMA)

Dynamic Mechanical Analysis (DMA) was performed on free films to determine the glass transition temperature of the shell walls by drawing down films (at 8 mils wet film thickness) with the same composition of the resins as that of the capsules and letting the films cure overnight in ambient conditions. To determine the T_g, the peak value of the tan δ curve was recorded. The effect of stoichiometry (ratio of PEMP to Cymel U80) the glass transition temperature was also studied by varying the weight of PEMP.

DMA results of the polymerized films revealed two values of T_g for the synthesized films that appeared to be more prominent at higher weight percentages of PEMP. The appearance of two T_g peaks could be due to the formation of two different molecular weights of the cross-linked polymer. Such a phenomena of two glass transition temperatures were also reported in cases where the formation of two polymer domains incompatible with each other when large enough have their own glass transition temperatures.[11] In this case, the appearance of two glass transition temperature may be attributed to the formation of two domains, one rich in PEMP (by oxidation of PEMP) and other rich in self-condensed Cymel ® U80 (due to the decrease in pH by oxidation of PEMP), which may show individual transition temperatures. However, in the case of lower amounts of PEMP, such a phenomena was not found to be dominant because of the smaller size of the domains and a higher compatibility of the two domains. [11] This may have resulted in the appearance of a broader tan delta curve in films at lower weight percentages. However, upon closer observation of the tan δ curve of 2g PEMP containing film (red trace in

Figure 3.15) a slight shoulder was observed at the around 20°C. The glass transition temperature was found to play a very important role in the morphology of the capsules. Vincent et al. suggest that higher glass transition temperatures of polymers result in a more polynuclear (with several cores) internal structures of the synthesized capsules.[1] This is because the higher the glass transition temperature, the tendency of the polymer to spread along the oil – capsule interface may be lower thus resulting particles with more than one water core within the droplet. In this case, however, mononuclear core shell type capsules were synthesized as confirmed by optical microscopy images and TEM. Thus, it can be said that the polymer rich phases consist of unpolymerized or partially polymerized segments which have lower T_g than that of the reaction temperature. Also, the excess of acetone added to dissolve the resin and the crosslinker keeps the polymer solvated until the polymer migrates to the interface. Thus, it can be said that polymerization of the shell takes place at the oil-capsule interface.

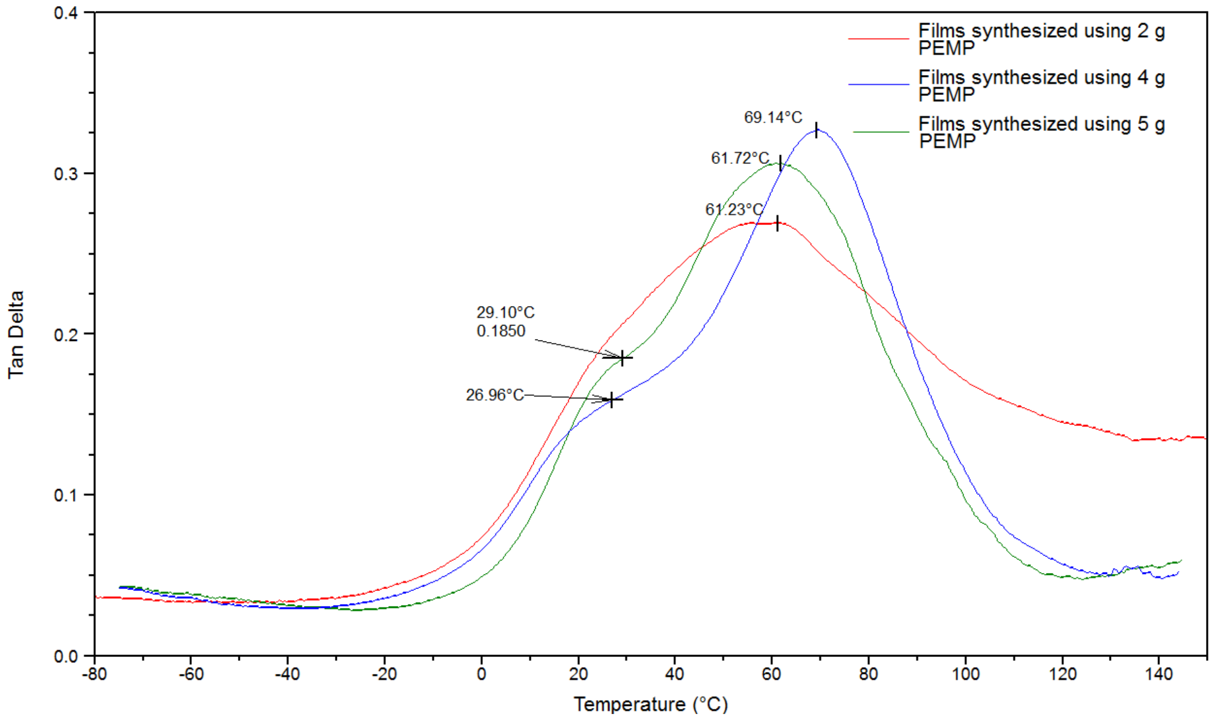

Figure 3.15. Tan delta plots of microcapsule wall films synthesizes using different weights of PEMP

3.6 Microscopic analysis

3.6.1. Scanning Electron Microscopy (SEM)

Scanning Electron Microscopy images of synthesized capsules were recorded to understand the structure and morphology of the synthesized capsules after the polymerization, as described in Chapter 2. Scanning Electron Microscopy images revealed that spherical particles with a wide size distribution with continuous smooth shell walls were synthesized. It was not unusual to observe particles with an oblong or an elliptical shape in SEM images similar to the optical microscopy images recorded before the polymerization of the shells (reported in Figure 3.3). This difference in shape was attributed due to the association of smaller droplets to form a larger droplet and subsequent polymerization of the particles. Even though most particles had a smooth surface, some particles showed circular “scar” formation on their surface. The scars may be associated to residual polymer left behind during the separation of two (or more) agglomerated particles by the force applied to spread the capsules on carbon tape. Drying and breaking of clumps of capsules also may have also resulted in the appearance of scars on the capsule surface. Some capsules were also observed with small spherical attachments on their surface. These surface defects were found to be small capsule particles attached to the larger capsules. In some cases, a large amount of residue of polymerize product was found around capsules, which may be due to the breakage of capsules as a result of handling and drying of the capsules.

The effect of cerium nitrate incorporation in the core of the capsules, on the structure and surface morphology of the synthesized capsules was also analyzed using SEM (Figure 3.17). Even though blank microcapsules were spherical in shape the analysis of the surface revealed slightly rough and flaky surface with polymer layers deposited on the surface. The particle size of the blank capsules was also observed to be approximately at 10 μm. The addition of 0.1 g of cerium nitrate in the microcapsule formulation showed a sharp decrease in the average particle size. Large agglomerates of smaller spherical particles were also observed upon addition of cerium nitrate. With increase in the cerium nitrate added into the microcapsule formulation, the small particles that were observed earlier were found to gradually increase in size. It was also observed that with increase in cerium concentration, more discrete capsules where formed. In the capsules with 0.4 and 0.5 g of added cerium nitrate, the scar formation along the exterior shell of the capsules, due to capsule-capsule association was not observed also indicating that an increase in cerium nitrate concentration results in discrete individual particles.

At lower concentration of cerium nitrate, large clusters of smaller spherical particles were observed which may be due to the formation of nano-sized ceria particles, due to oxidation of cerium nitrate by hydrogen peroxide, acting as sites for the deposition of the cross-linked polymer. The increase in the size of the particles with increase in the amount of cerium nitrate could be due to the additional surface area added by the nano-ceria particles. The smaller size polymeric particles could also be a consequence of low pH with results in large scale self-condensation of the amino resin.[12] This type of self-condensation may be lower for higher weight percentage of the cerium nitrate, since a part of the hydrogen peroxide may be utilized for the oxidation of cerium nitrate thus reducing the amount of PEMP oxidized, in turn resulting in lesser acid available to catalyze the self-condensation.

The effect of PEMP concentration was also studied because it was assumed that higher weight percentages of PEMP results greater number of oxidized disulfide linkages thus resulting in a higher sensitivity to pH. With increase in PEMP concentration, the capsules were found to agglomerate and fused to each other through polymer bridges. This fusion of the capsules becomes more predominant in capsules containing higher weight percentages of PEMP which might be because the viscosity of the polymeric phase may be modified due to the addition of the lower viscosity PEMP causing more capsule association.

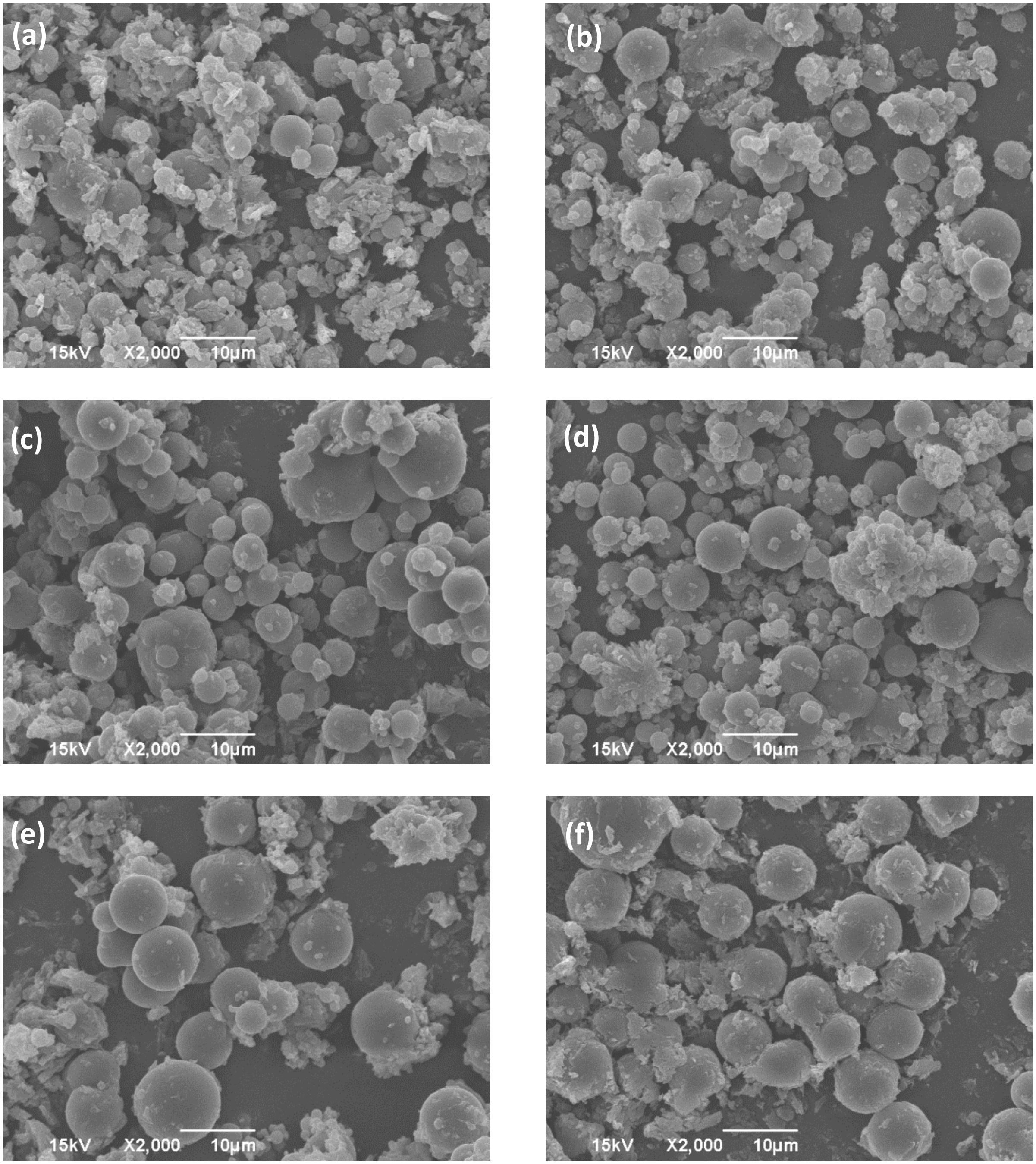

Figure 3.16. SEM images of microcapsules consisting of various weights cerium nitrate (a) 0.1 g, (b) 0.2 g, (b) 0.3 g, (d) 0.4 g, (e) 0.5 g & (f) blank.

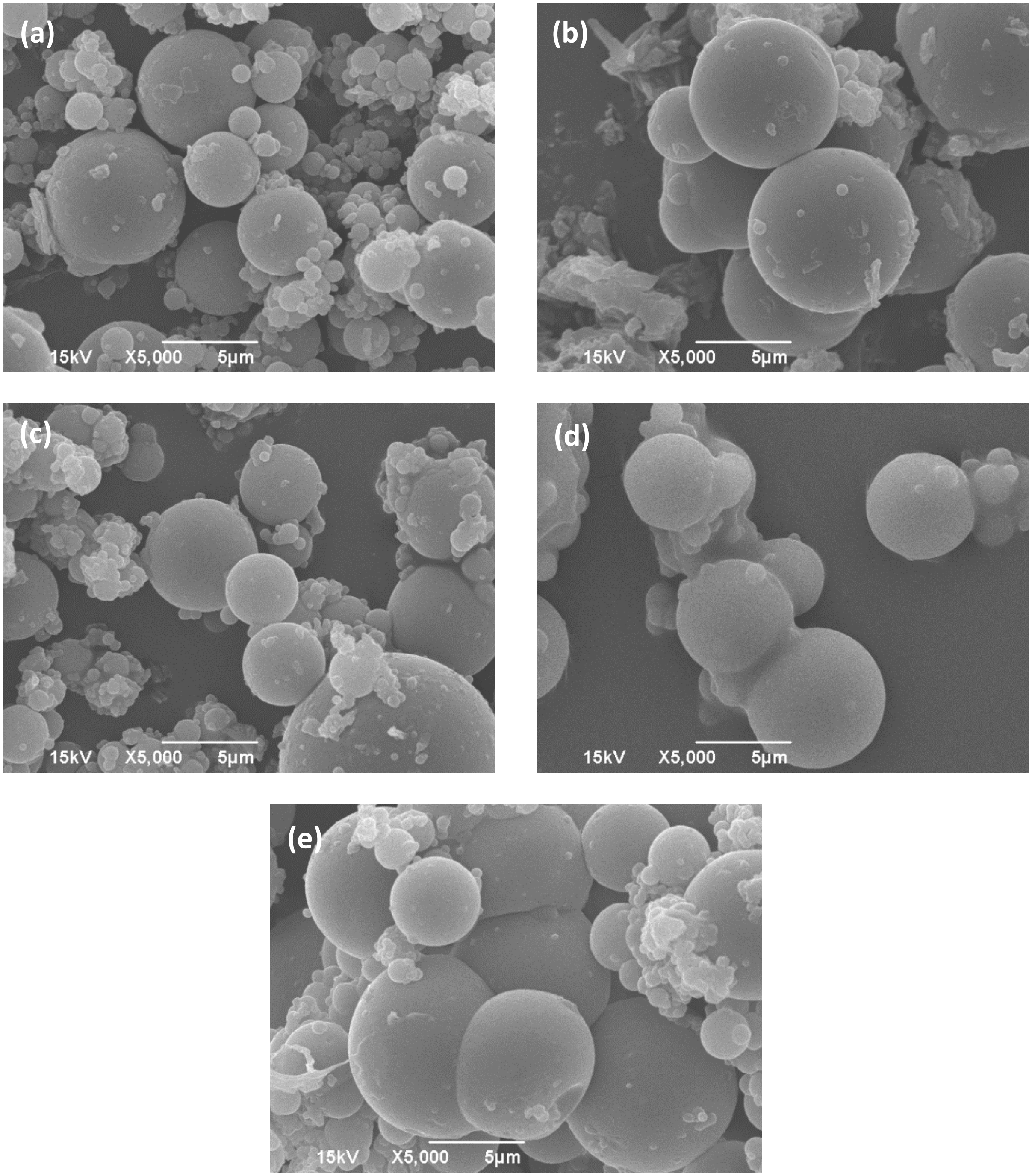

Figure 3.17. SEM images of microcapsules consisting of various weights of PEMP (a) 1 g, (b) 2 g, (b) 3 g, (d) 4 g, (e) 5 g.

3.6.2. Energy Dispersive Spectroscopy (EDS)

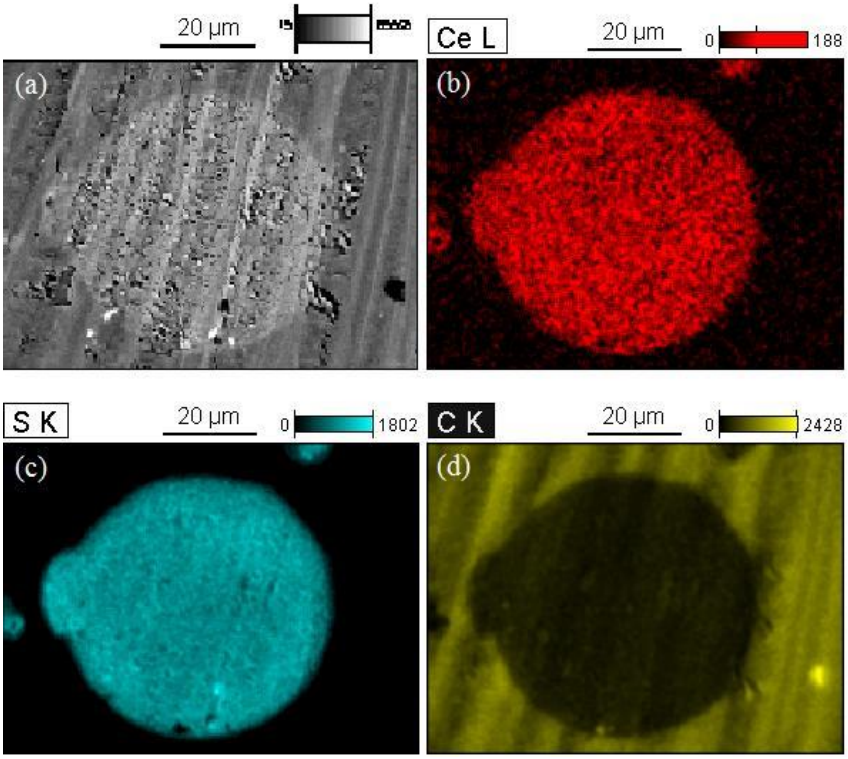

Figure 3.18. Cross-sectional Energy Dispersive X-ray Spectra of cerium containing microcapsules (a) cross-sectional SEM (b) cerium map (c) sulfur map (d) carbon map.

Energy Dispersive X-ray Spectroscopy (EDS) was performed using the Scanning Electron Microscope to detect the incorporation of cerium in the core of the synthesized capsules. Cross-section EDS maps of dried microcapsules embedded in cured epoxy resin revealed high concentration of cerium within these capsules (Figure 3.18). The highest concentration of cerium was observed throughout the interior of the capsules indicating that cerium was incorporated within the shell of the capsules. A closer observation of the cerium EDS map (Figure 3.18 (b)) revealed trace quantities of cerium outside the microcapsules shell which may be due to the rubbing action of the microtome on the capsules embedded in cured epoxy resin. A sulfur map of the cross section shows a uniform distribution of sulfur on the surface of the microcapsules which may indicate the uniform distribution of disulfide bonds (as no residual

S-H stretch was observed in Raman spectroscopy). A carbon map of the same cross section shows a darker, carbon lean region within the microcapsules which indicate the presence of an inorganic compound within the capsules. Since the only inorganic (carbon free) compound included in this synthesis of microcapsule reaction is cerium nitrate, the carbon map suggests the possible incorporation of cerium in the microcapsules.

3.6.3. Transmission Electron Microcopy (TEM)

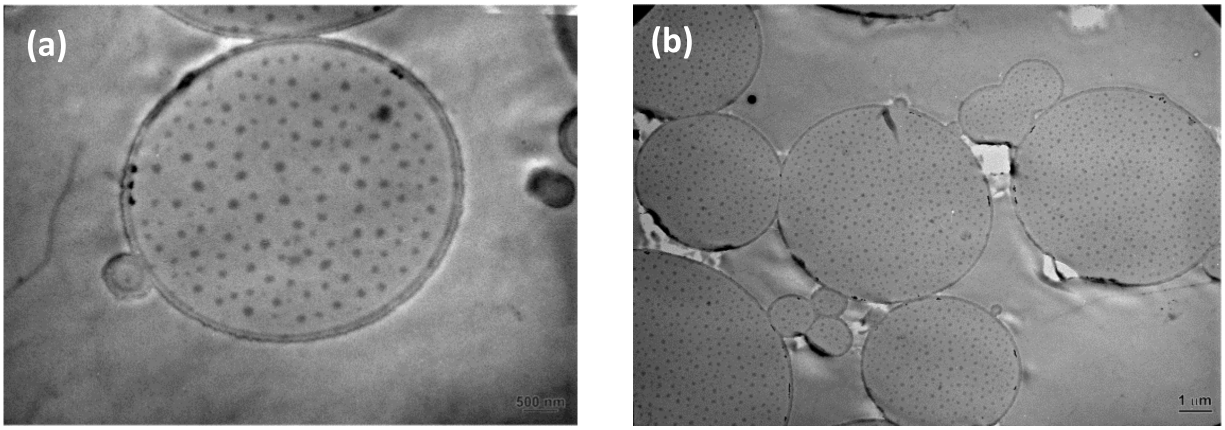

Figure 3.19. Cross-sectional Transmission Electron Microscopy images of cerium containing microcapsules embedded in an epoxy.

To obtain information about the internal structure of the microcapsules, cerium containing capsules were embedded in cured epoxy resin matrix and micro-tomed into thin slices (70-80 μm) and analyzed using Transmission Electron Microscope. It was observed that the capsules were hollow and the polymer formed a shell-like structure along the oil/ capsule interface of capsules. A continuous 100 nm wall was also observed around the capsules. Small circular structures were also observed with in the microcapsule which may be crystals of cerium oxide or a hydrated cerium oxide formed as a result of the oxidation of cerium nitrate.[13] Upon comparing the smaller capsule adjacent to the large capsule in Figure 3.19 (a) it can be said that irrespective of the size of the microcapsules, the thickness of the walls of the capsules remained the same. The formation of core shell type morphology indicates that the polymerization takes place after resin phase separation occurs in the emulsified droplet. If the polymerization were to take place before the spreading of the unpolymerized resins at the water – oil interface, core shell microcapsules would not be observed. The core-shell morphology also confirms the polymerization of the monomers after their migrating to the oil-droplet interface, as polymerization at the interior of the droplet leads to a more poly-nuclear morphology.[1]

3.7. Particle size analysis

An auto diluter setup with a magnetic stirrer was used to feed the microcapsules into the particle size analyzer conduct the particle measurement. The average particle size of the synthesized capsules typically in the ranged of 5 - 15 microns (number average). The addition of cerium nitrate caused a sharp decrease in the particle size with a large number of particles in the 1.5 micron range (Figure 3.20(a)). This observation was similar to that made with the SEM images discussed earlier. The particle size distribution of the synthesized capsules consisted of a bimodal distribution with a consistent peak at 50-60 microns. This may be because of the agglomeration due to the addition of dry capsules to water (which was used as the dispersion medium for particle size measurement). Since similar peak was observed at 50-60 microns with successive additions of cerium nitrate in the formulations, the appearance of a peak at the 60 micron range may be attributed to an agglomeration phenomena. The effect of varying the weight of PEMP in the microcapsule formulation revealed that with increase in the PEMP weight percentage, the average particle size was found to increase suggesting formation of agglomerates. This was also confirmed using the SEM that the particles begin to agglomerate with increase in the PEMP weight which may lead to the observed increase in the average particle size. The only exception to this trend of increasing particle size was observed in the case of the formulation with 4 g of PEMP (figure 3.21(d)). It was observed that even though the particle size distribution was similar to the other formulations, the tendency to agglomerate was significantly reduced (absence of the peak in the 60 micron range). Polymer bridge formation between the particles at higher mass of PEMP may have resulted increased mean particle size.

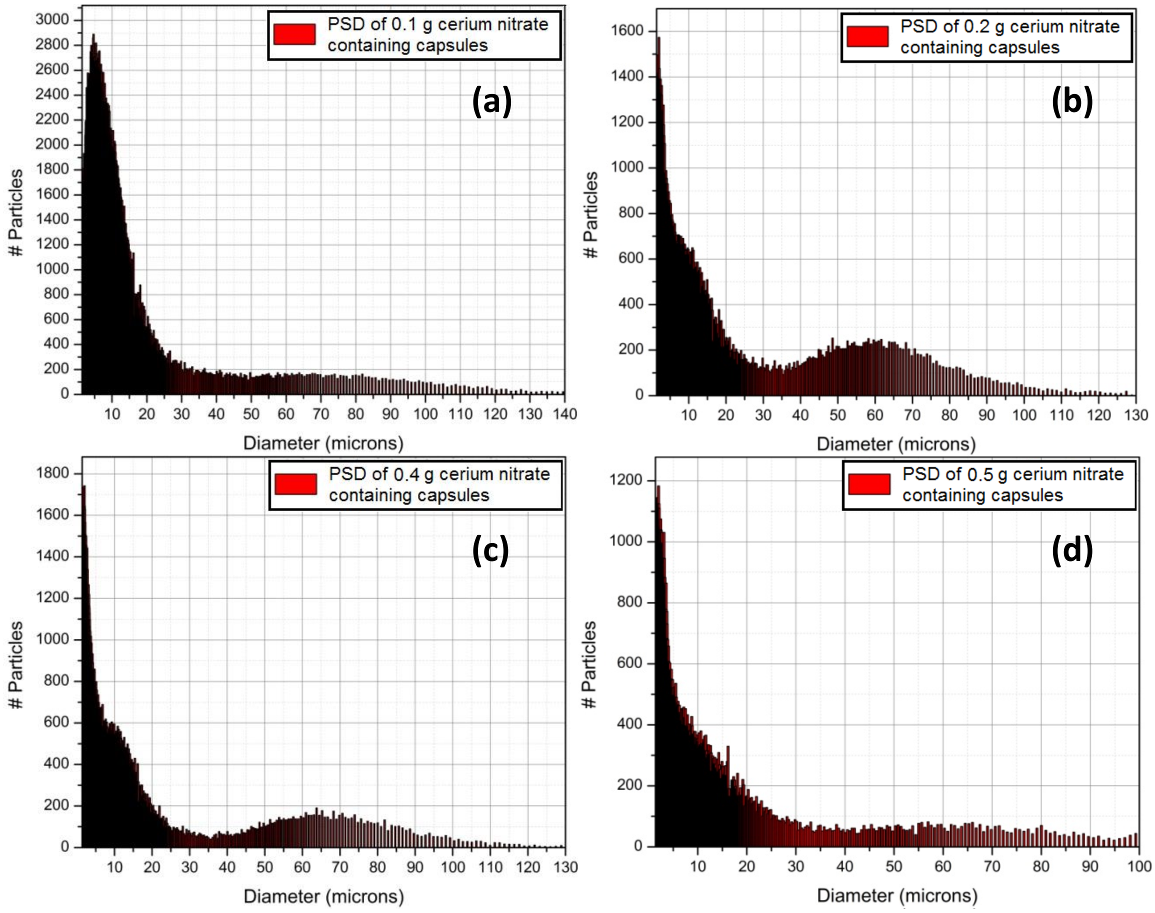

Figure 3.20. Particle size measurements of capsules containing cerium nitrate at (a) 0.1g; (b) 0.2g; (c)0.4g; (d) 0.5g.

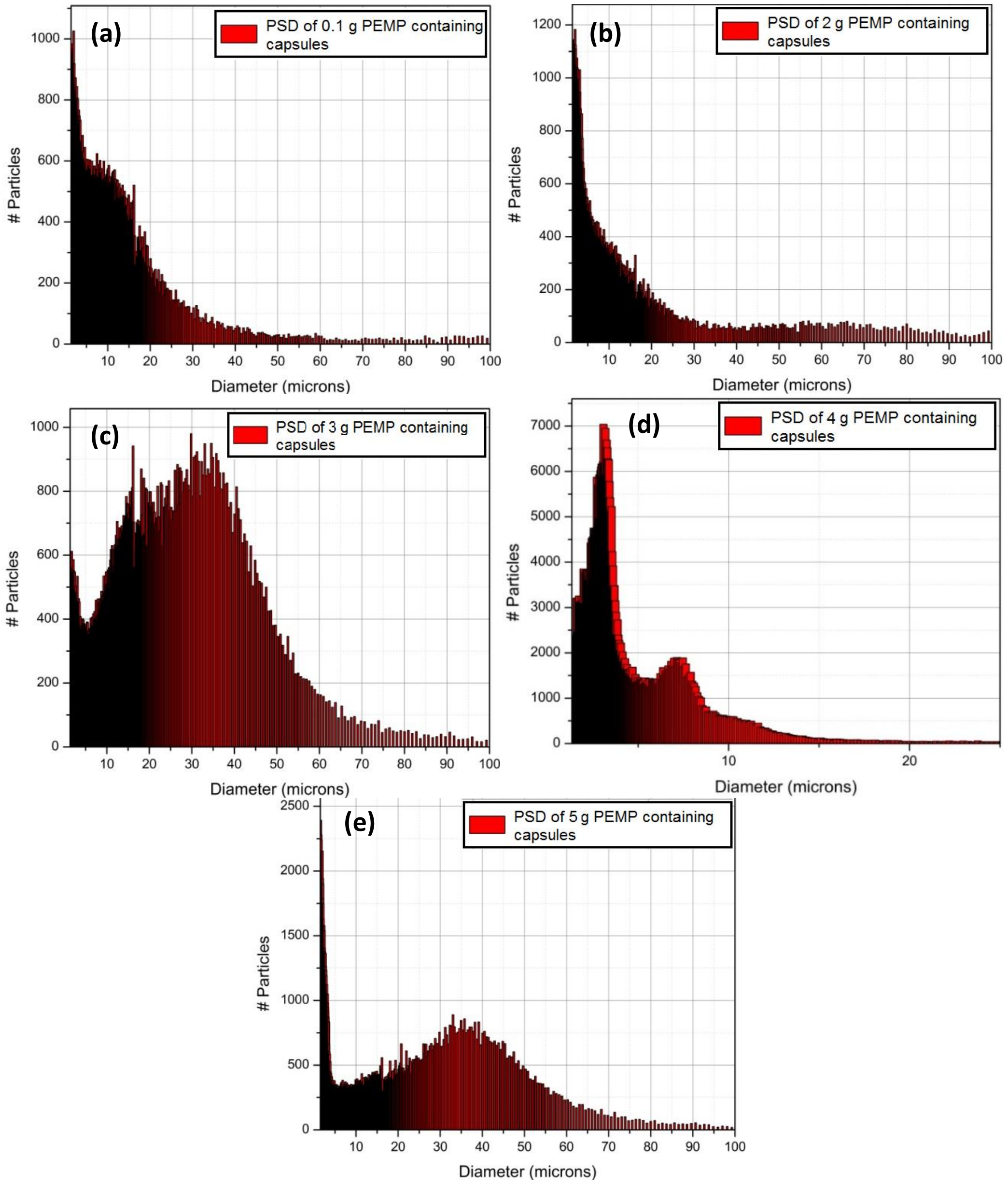

Figure 3.21. Particle size measurements of capsules containing various weights of PEMP (a)1g;(b) 2g; (c)3 g;(d) 4g; (e) 5g.

3.7.1. Effect of Stirring Rate on the Particle Size of Synthesized Capsules

In order to determine the effect of stirring rate on the particle size, the stirring rate of 200 – 2000 RPM was chosen for this study. Due to the limitations of the particle size analyzer, only capsules synthesized at 800 RPM and greater could be measured. The particle sizes measured have been summarized in Table 3.1. It was observed that with increase in the stirring rate, the number average particle size increase steadily. However, the standard deviation increased significantly with the stirring rate as well indicating a wide distribution in the particle size of the synthesized capsules. The wide distribution in particle size may be due to the creation of higher surface area at higher RPMs resulting in less stable particles which may either polymerize immediately or agglomerate and then polymerize resulting in particles of various sizes. It can also be inferred that irrespective of the stirring rate, the particle collision dictates the particle size.

Table 3.1. Particle size of microcapsules synthesized at different stirring rates

RPM	Mean (microns)	Std. Dev
1000	4.19	3.12 µm (74.4%)
1200	5.44	3.83 µm (70.4%)
1400	5.55	9.66 µm (163.3%)
1600	6.66	6.71µm (100.7%)
1800	7.8	9.52 µm (122.51%)

3.8. pH responsive degradation of wall materials

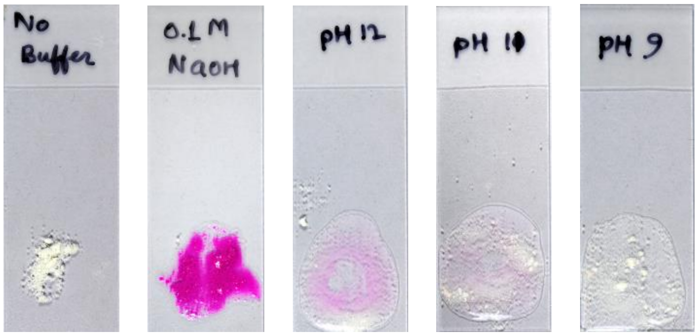

Figure 3.22. Photographs of pH responsiveness of the capsules as a function of pH.

pH responsiveness of the capsules was demonstrated by incorporating phenolphthalein solution into the capsules and exposing it to various pH buffers. Photographs of the capsules were taken before and after the addition of the pH buffers and compared for the appearance of pink color change. It was observed that capsules were pH responsive and showed a gradual increase in the intensity of the color demonstrating that the capsule walls degrade gradually. It can be argued that the change in color may be due to residual phenolphthalein present around the capsules. This influence was minimized by triple washing and immediate drying of these capsules to remove any residual phenolphthalein. Attempts to incorporate universal indicator was unsuccessful so the release of the core contents due to leaching or diffusion could not be detected in acidic and neutral conditions.

3.9. Encapsulation & release of cerium

3.9.1. Inductively Coupled Plasma

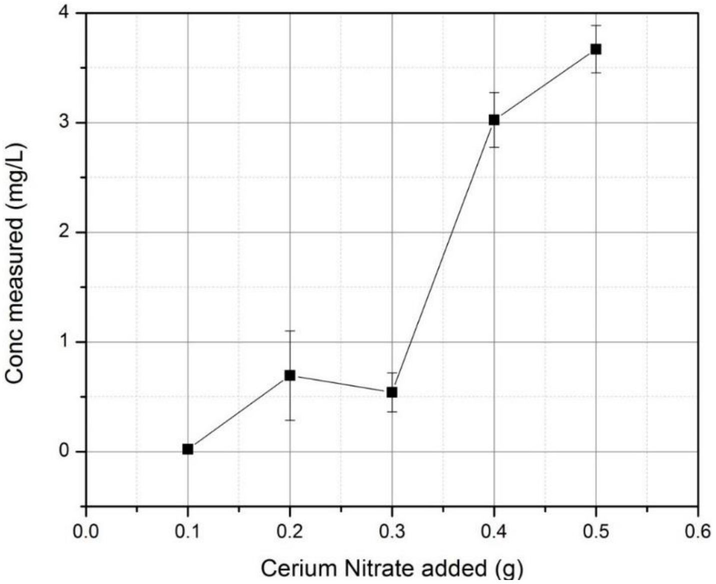

Figure 3.23. Effect of cerium incorporation into microcapsules as a function of cerium nitrate added into the formulation.

Inductively Coupled Plasma – Optical Emission Spectroscopy (ICP – OES) was used as a method to determine the concentration of cerium incorporated within the capsules. For the measurement of concentration of cerium, microcapsules containing cerium were ground using mortar and pestle and diluted with 18MΩ Millipore ® water. The supernatant liquid used to determine the concentration of cerium. The effect of including higher weight percentages of cerium nitrate in the synthesis of the capsules was also studied.

The incorporation of cerium in the capsules using the internal phase separation method was confirmed using ICP- OES. The measured concentration of cerium varied as a function of weight of cerium nitrate added into the microcapsule formulation. Even though a linear increase in the concentration with increase in cerium added into the formulation was not observed, a more general increasing trend was noted. Even though very low concentrations were recorded, however, the solution was diluted to 100 mL in order to report an average concentration between 3 measurements and to avoid polymeric debris from being pulled into the tubing of the ICP auto-sampler.

3.9.2. UV-Vis Spectroscopy

Another method used to demonstrate the incorporation of cerium within the synthesized capsules was UV –Vis spectroscopy. To begin with, a reference spectrum of a known concentration cerium (III) nitrate solution was recorded. Two peaks appeared one at 298 nm and the other at 252 nm. The peak at 298 nm was determined to be absorbance due the presence of Ce^{4+} ions and the peak at 252 nm was due to the absorbance by Ce^{3+} ions in the solution. It was also observed that with increase in concentration of cerium nitrate solution, the peak at 252 nm showed slight bathochromic shift. Since no shift in the peak at 298 nm was observed, the shift at 252 nm may be due to the sensitivity of the instrument’s detector at higher values of measured absorbance.

Next, the spectra of ground microcapsules in 18M ohm Millipore® water was recorded. The spectrum of ground microcapsules showed the presence of Ce^{3+} ions due the appearance of an absorbance peak at 252 nm. Even though the initial appearance of microcapsules were slightly yellow, a characteristic color of cerium (IV) oxide (CeO_2) due to the oxidation from Ce^{3+} to Ce^{4+} by hydrogen peroxide, acidic conditions due to the oxidation of thiols to form disulfides may result in the reduced pH in the solution which favor surface reduction of Ce^{4+} to Ce^{3+}. This surface reduction phenomena was found to be a function of ageing time. The spectrum of ground microcapsules shows a characteristic UV absorption at 252 nm from Ce^{3+}. The absence of 298 nm peak as in the case of the reference cerium nitrate solution indicates that cerium incorporated into the capsules was in the reduced Ce^{3+} form.

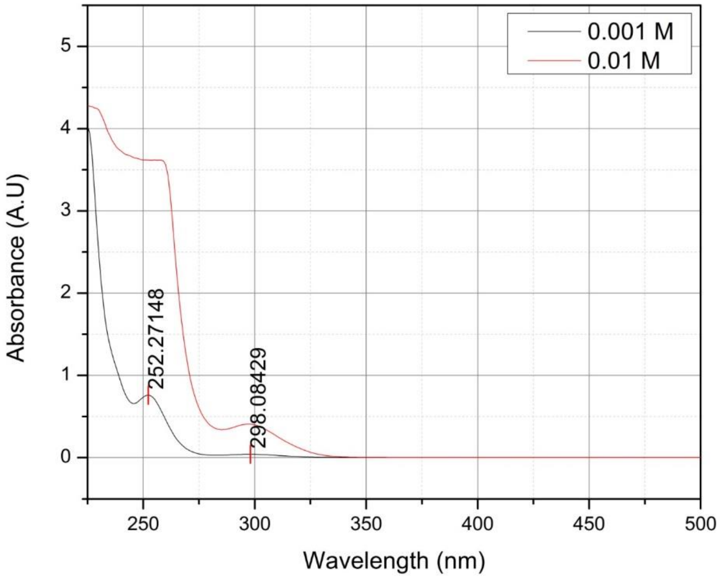

Figure 3.24. UV-Vis spectra of cerium nitrate solution showing Ce^{3+} and Ce^{4+} absorbance peaks.

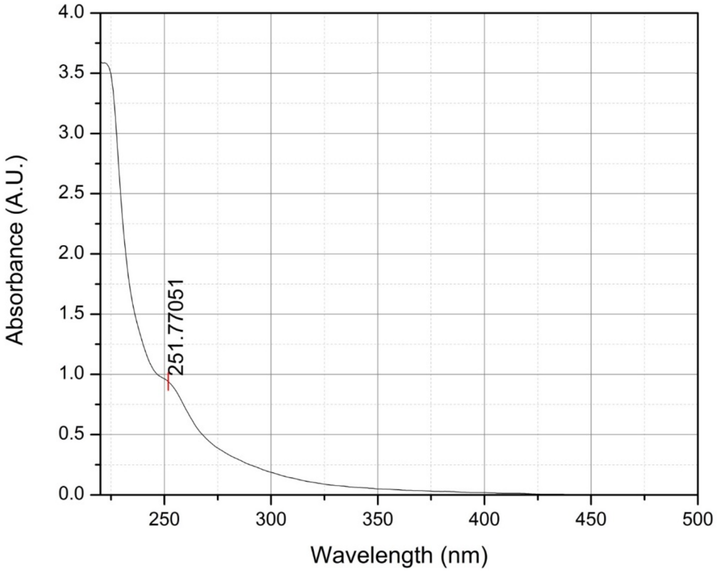

Figure 3.25. UV-Vis spectrum of crushed cerium containing microcapsules.

3.9.3. Incorporation of Cerium into Capsules

From the EDX experiments discussed previously high concentrations of cerium were detected in the core of the synthesized capsules. However, to better estimate the concentration of cerium within the capsules, ICP-OES and UV- Vis Spectroscopy techniques were employed. To determine the concentration of cerium within the capsules, a known mass of the capsules was crushed (broken) using a mortar and pestle and solutions of known volumes were made in 18 MΩ Millipore® water. The solutions were filtered using Whatman #1 filter paper before running further experiments. As discussed in section 3.9, the incorporation of cerium within the capsules was verified using ICP and UV-Vis measurements. It was also noted that cerium incorporated within the capsules was in the 3+ oxidation state using UV Vis spectroscopy due to the detection of 250 nm peak in the UV-Vis spectra of crushed capsules (Figure 3.25).

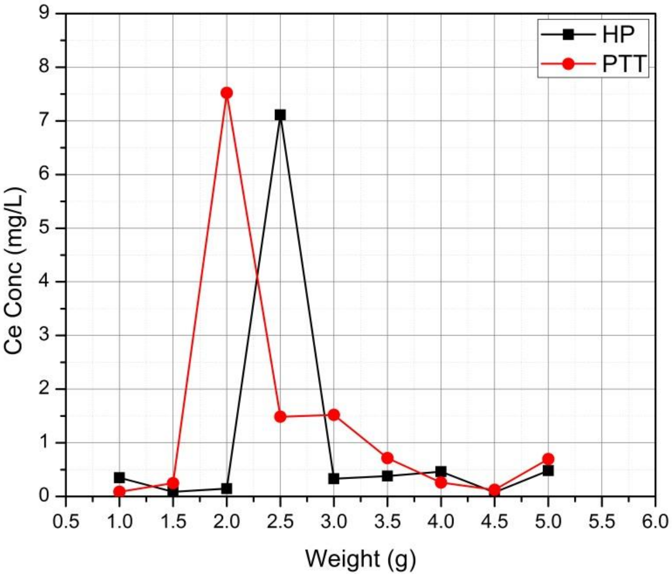

Figure 3.26. Effect of hydrogen peroxide (HP) and pentaerythritol 3-mercaptopropionate (PTT) on the incorporation of cerium in the capsules.

To determine the optimum microcapsule formulation to incorporate highest concentration of cerium within the capsules, pentaerythritol 3-mercaptopropionate (PEMP) and hydrogen peroxide (HP) weights in the formulation were varied and the concentrations of cerium incorporated within the polymer shell was measured using ICP- OES. With constant weight of cerium nitrate (0.5 g) and pentaerythritol 3-mercaptopropionate (PEMP) (2 g) in the formulation, the hydrogen peroxide weight was increased. It was observed that at 2.5 g of hydrogen peroxide in the formulation, highest concentration of cerium was detected. Similarly, with a constant weight of hydrogen peroxide and cerium nitrate in the formulation, PEMP was increased. At 2 g of PEMP, highest concentration of cerium was detected in the capsules.

3.9.4. Stability in Acidic/Neutral Solutions

The ability of capsules to retain cerium within the capsule shell was important because of two reasons: (a) to understand if the release of cerium was pH triggered event and (b) if the capsules would leach the contained cerium upon exposure to neutral solutions during the synthesis and purification of the capsules. To study the release of cerium from the capsules, UV-Vis spectroscopy, Cyclic Voltammetry (CV) and Inductively Coupled Plasma (ICP) measurements were employed.

Initially the capsules incorporated into coatings did not show any corrosion inhibition upon exposure to corrosion testing (ASTM B117). However, a significantly higher corrosion resistance was observed in case of capsules that were stored in neutral pH water for over a month. It has been reported that the oxidation of cerium using hydrogen peroxide results in the formation of ceria (cerium oxide particles) that is orange in color.[14-16] Due to a similar color change (colorless to orange) observed during the synthesis of the capsules, it was assumed that cerium oxide was formed and may be incorporated within the capsules. However, in several reports[17-19] an interesting observation has been made regarding the change in oxidation state of cerium from Ce^{4+} to Ce^{3+} upon exposure (soaking) in acidic solutions. This change in oxidation state has been studied by several authors and has been attributed to the oxygen vacancies in the crystalline structure.[19-22] It was also determined that cerium (IV) oxide nanoparticles layer possessed a 2 nm layer of Ce^{3+} upon exposure to acidic conditions.[23] This observation is interesting to this research because, the layer of Ce^{3+} on the surface of cerium (IV) oxide may be available to form cerium hydroxide and inhibit the cathodic reaction.

It was observed that soaking the capsules in neutral pH water for approximately 7 days resulted in the disappearance of the yellowish orange color. The disappearance of the orange color indicated that cerium oxide present within the capsules may have been reduced to 3+ state. Since the capsules were immersed in solution for a week, the knowledge of cerium leaching from the capsules was important. Rotating disc electrode experiments were performed in 0.1 M sulfuric acid solutions exposed to uncrushed capsules. Sulfuric acid was used as the acidic medium due to the high reactivity of Ce^{3+} with hydroxyl ions.

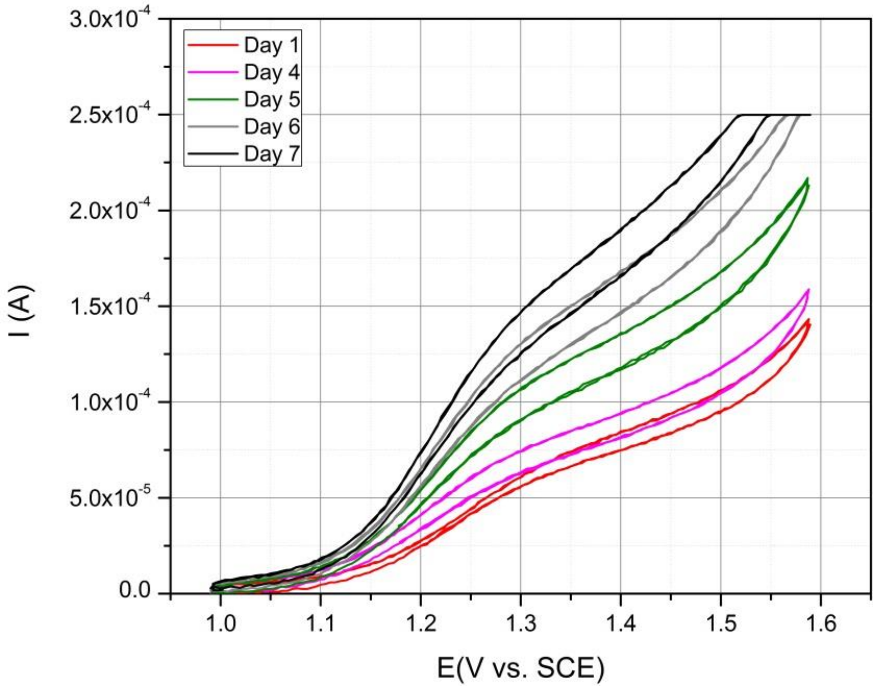

Figure 3.27. Cyclic Voltammetry plot of cerium capsule immersed in 0.1 M sulfuric acid measured using Rotating Disc Electrode (RDE) set at 1600 RPM.

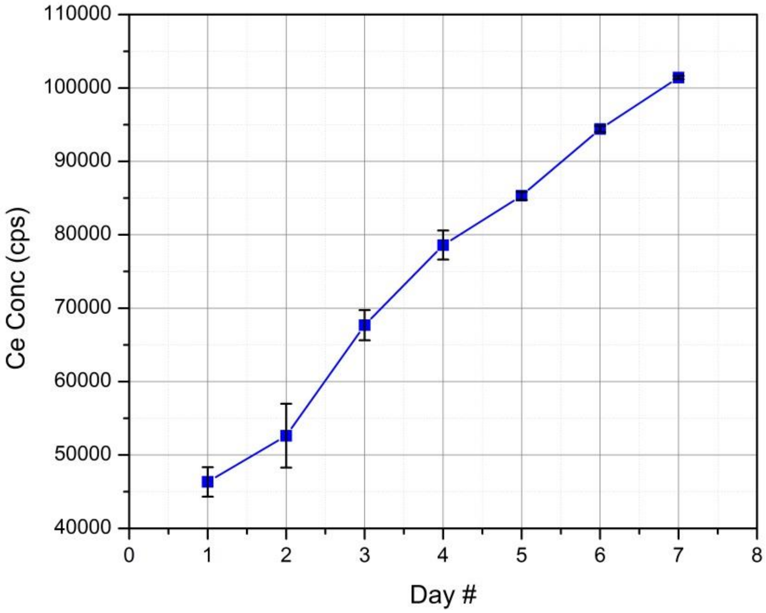

Figure 3.28. Cerium release from capsules upon exposure to 0.1 M sulfuric acid using ICP-OES.

Cyclic voltammetry was performed using 0.1 M sulfuric acid solutions with capsules immersed in exposed to using the Rotating Disc Electrode setup. The rotating electrode was set to 1600 RPM and the scans were recorded as described in chapter 2. Since cerium salts are redox active[24], an oxidation and reduction peak was observed in the solution used to immerse cerium containing capsules. It was observed that oxidation current of Ce^{3+} (1.3V vs. Ag/AgCl) increased with increase in the exposure time. This indicated that cerium ions from the capsules were released upon exposure to solution. One possible reason could be the swelling of the polymeric shell upon exposure to aqueous medium resulting in the release of cerium from the core of the capsules. A linear increase in concentration of cerium was detected using ICP OES measurements upon exposure to 0.1 M sulfuric acid.

3.9.5. pH Dependent Release of Cerium from Capsules

The pH responsive release of cerium from the capsules was also studied by exposing cerium containing microcapsules to various pH buffer solutions. The released cerium in solution was monitored using UV Vis spectroscopy and ICP- OES. UV Vis spectra of cerium nitrate control solutions revealed two distinct peaks, one at 252 nm and other at 298 nm. The peak at 252 nm was determined to be associated with Ce^{3+} and 298 nm was associated with Ce^{4+} ions in the solution[25]. 0.25 g of cerium containing capsules were immersed in various pH buffers from acidic to basic , solutions were drawn at regular intervals and analyzed for cerium ions released in the solution.

Figure 3.29 summarizes the absorption of Ce^{3+} in different buffer solutions. In acidic solutions, a gradual increase in cerium concentration was observed which may be due to the leaching of cerium from the core of the capsules as observed and discussed earlier. As the pH of the solution was increased (pH 7), an increase in the concentration of the cerium was observed.

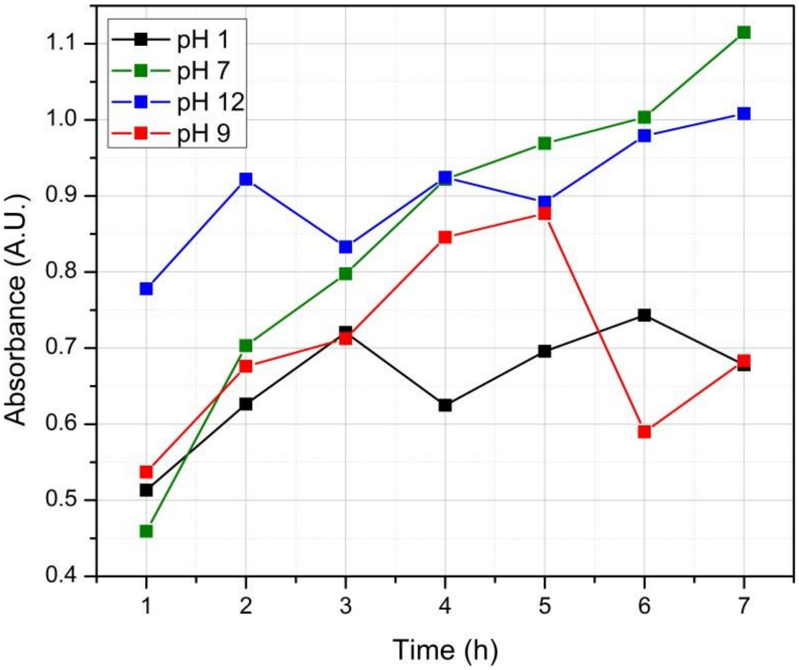

Figure 3.29. pH dependent release of cerium from the capsules monitored at 250 nm using UV Vis spectroscopy.

However, at higher pHs (pH 9 and 12) the concentration of cerium measured was lower than some of lower pH buffer solutions. As observed in figure 3.29, pH 7 shows almost a linear increase in the concentration of cerium with time, as compared to pH 12 solution that levels off with time. This can be explained by the interaction of cerium 3+ with the hydroxyl groups available in the solution and precipitation of cerium hydroxide. It was interesting to note that the initial absorbance of cerium capsules in pH greater than 7 was higher than that of the other pH buffer solutions indicating higher concentration of was cerium released at such pHs which decrease due to the precipitation of cerium hydroxide/oxide. The absorbance of cerium 3+ ions at other pHs were not reported due to the interference of potassium hydrogen phosphate in the same absorption range as that of cerium 3+ ions.[26]

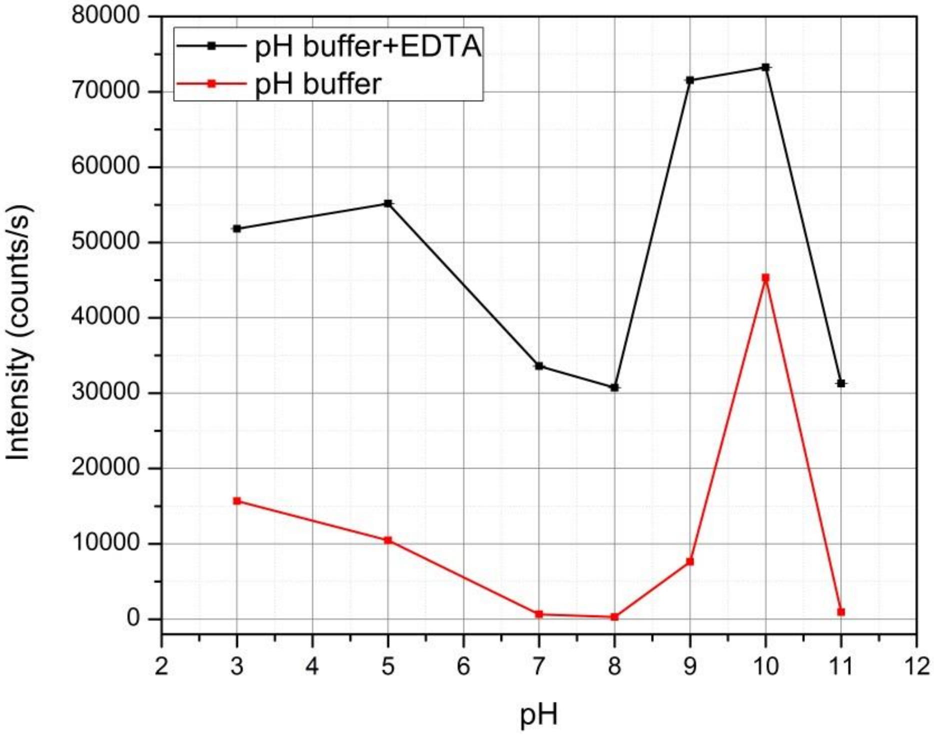

Figure 3.30. ICP plot of cerium concentration released from mechanically crushed microcapsules exposed to various pH buffer in the presence (black) and absence (red) of EDTA.

To understand the decrease in concentration of cerium due to precipitation of cerium in pH buffer solutions, 0.25 g of cerium containing capsules was exposed to various pH buffer solutions and the concentration of cerium was measured using ICP. The pH buffer solutions were compared to EDTA containing buffer solutions to understand the effect of basic conditions on released cerium. With increase in pH, a steady decrease in the concentration was observed up to a pH of 8, after which an increase in the measured concentration of cerium was noted. In case of the EDTA containing buffer solutions, a higher concentration of cerium was recorded at all pHs. This can be explained by the formation of cerium EDTA complex which prevents the precipitation of cerium as its hydroxide upon interacting with the pH buffer.[24] The decrease in cerium concentration up to a pH of 8 and then an increase can be explained by carefully examining the contents of the pH buffers used. In lower pH buffer solutions, the released cerium may react with potassium hydrogen phosphate and precipitate as a cerium phosphate resulting in the decrease in the concentration of cerium detected. Thus explaining the anomaly observed in the data.

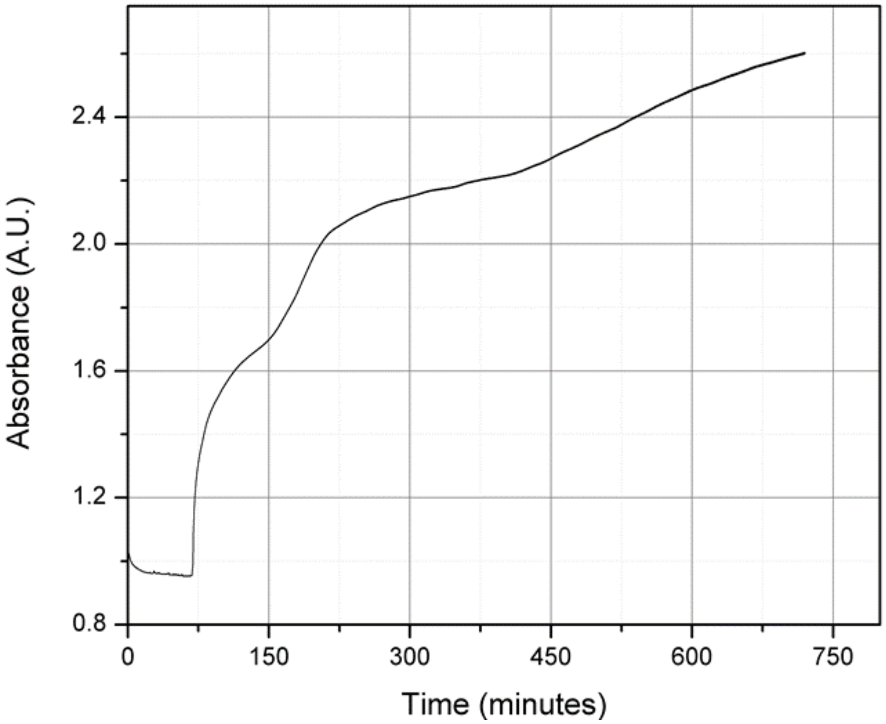

Figure 3.31. Cerium release from capsules upon addition of a strong base. Absorbance recorded at 252 nm.

In order to demonstrate the pH dependent release of cerium from the capsules, a kinetic study was performed by setting the UV-Vis spectrophotometer to 252 nm (to detect Ce^{3+}) and spiking the solution with a couple of drops of 0.1 M sodium hydroxide. The system was let to equilibrate for about 90 minutes prior to eliminate the effect of scattering and 2 drops of 0.1 M sodium hydroxide was added to the cell. Immediately after the addition, an increase in absorption was noted which may be due to the cerium ions released from the core of the capsules. This demonstrated that cerium was released from the capsules at high pH immediately and would be available for corrosion inhibition.

3.10. Conclusions

pH responsive capsules were synthesized using internally phase separated emulsion polymerization. pH responsiveness was incorporated into the capsule shells by the utilizing disulfide bonds formed by the oxidative polymerization of pentraerythritol 3-mercaptopropionate. The formation of disulfides by the oxidation of thiols was confirmed by the appearance of the disulfide peak at 500 cm^{-1} in the Raman spectra of the cured shell walls. Spherical microcapsules with smooth surface morphology were synthesized using this technique. The capsules have core-shell morphology with a thin polymer membrane of the order of ~100 nm encapsulating a water core. The shell wall thickness however, was found to be independent of the capsule size indicating a higher loading of the capsules with increase in the particle size. The microcapsules had a wide size distribution ranging from 5 – 100 microns depending on the stirring rate. The incorporation of cerium into the capsules was demonstrates using several techniques. Thermo-gravimetric analysis showed that cerium salts were incorporated into the capsules and with increase in the percentage of cerium nitrate in the capsules, higher amount of cerium salts were incorporated into the capsules. Similar result was observed in case of

Inductively Coupled Plasma. Transmission Electron Microscopy reveals the formation of nano-sized crystals which may be nanoceria formed due to the oxidation of cerium nitrate. Cross-sectional EDS mapping also reveals that cerium was incorporated in shell of the capsules and was found to be uniformly distributed inside the capsules. UV-Vis spectrum of cerium containing capsules reveal that cerium in its 3+ oxidation state was encapsulated within the capsules. The pH dependent release was observed as a function of pH in case of phenolphthalein solution containing capsules. The release of cerium in solution was also evaluated and a steady increase in the concentration of cerium in the solution was observed indicating that the synthesized capsules did not have completely cross-linked shells that are impervious to water penetration. This release was confirmed using RDE, UV Vis and ICP measurements. pH responsiveness of these capsules was also verified however, due to the high reactivity of cerium a very clear distinction between various pHs was noted. However, spiking the microcapsule containing solution with sodium hydroxide showed an immediate increase in cerium concentration indicating the high concentration cerium was released as the pH increased. By the use of EDTA as a complexing agent it was made clear that the released cerium reacted with either the hydroxyl groups or the phosphate groups and precipitated resulting in the decreased concentration observed in the ICP and UV Vis measurements.

3.11. References

1. Atkin, R.; Davies, P.; Hardy, J.; Vincent, B., Preparation of Aqueous Core/Polymer Shell Microcapsules by Internal Phase Separation. *Macromolecules* **2004,** 37, (21), 7979-7985.
2. Dowding, P. J.; Atkin, R.; Vincent, B.; Bouillot, P., Oil Core−Polymer Shell Microcapsules Prepared by Internal Phase Separation from Emulsion Droplets. I.

Characterization and Release Rates for Microcapsules with Polystyrene Shells. *Langmuir* **2004,** 20, (26), 11374-11379.

3. Dowding, P. J.; Atkin, R.; Vincent, B.; Bouillot, P., Oil Core/Polymer Shell Microcapsules by Internal Phase Separation from Emulsion Droplets. II: Controlling the Release Profile of Active Molecules. *Langmuir* **2005,** 21, (12), 5278-5284.
4. Torza, S.; Mason, S. G., Three-phase interactions in shear and electrical fields. *Journal of Colloid and Interface Science* **1970,** 33, (1), 67-83.
5. Landfester, K., Encapsulation through (mini)emulsion polymerization. In *Functional Coatings: by Polymer Microencapsulation*, Ghosh, S. K., Ed. John Wiley & Sons: 2006; pp 29-66.
6. Zelikin, A. N.; Li, Q.; Caruso, F., Disulfide-Stabilized Poly(methacrylic acid) Capsules: Formation, Cross-Linking, and Degradation Behavior. *Chemistry of Materials* **2008,** 20, (8), 2655-2661.
7. Roy, D.; Cambre, J. N.; Sumerlin, B. S., Future perspectives and recent advances in stimuli-responsive materials. *Progress in Polymer Science* **2010,** 35, (1–2), 278-301.
8. Zeno W. Wicks, J.; Jones, F. N.; Pappas, S. P.; Wicks, D. A., *Organic Coatings: Science and Technology*. John Wiley & Sons: 2007.
9. Vratny, F.; Kern, S.; Gugliotta, F., The thermal decomposition of cerium (III) nitrate hydrate. *Journal of Inorganic and Nuclear Chemistry* **1961,** 17, (34), 281-285.
10. Strydom, C. A.; Vuuren, C. P. J., The thermal decomposition of cerium(III) nitrate. *Journal of thermal analysis* **1987,** 32, (1), 157-160.
11. Rotter, G.; Ishida, H., Dynamic mechanical analysis of the glass transition: curve resolving applied to polymers. *Macromolecules* **1992,** 25, (8), 2170-2176.

12. Salaün, F.; Vroman, I., Influence of core materials on thermal properties of melamine–formaldehyde microcapsules. *European Polymer Journal* **2008,** 44, (3), 849-860.

13. Chen, H.-I.; Chang, H.-Y., Synthesis of nanocrystalline cerium oxide particles by the precipitation method. *Ceramics International* **2005,** 31, (6), 795-802.

14. Scholes, F. H.; Soste, C.; Hughes, A. E.; Hardin, S. G.; Curtis, P. R., The role of hydrogen peroxide in the deposition of cerium-based conversion coatings. *Applied Surface Science* **2006,** 253, (4), 1770-1780.

15. Djuričić, B.; Pickering, S., Nanostructured cerium oxide: preparation and properties of weakly-agglomerated powders. *Journal of the European Ceramic Society* **1999,** 19, (11), 1925-1934.

16. Decroly, A.; Petitjean, J.-P., Study of the deposition of cerium oxide by conversion on to aluminium alloys. *Surface and Coatings Technology* **2005,** 194, (1), 1-9.

17. Lord, M. S.; Jung, M.; Teoh, W. Y.; Gunawan, C.; Vassie, J. A.; Amal, R.; Whitelock, J. M., Cellular uptake and reactive oxygen species modulation of cerium oxide nanoparticles in human monocyte cell line U937. *Biomaterials* 33, (31), 7915-7924.

18. Celardo, I.; De Nicola, M.; Mandoli, C.; Pedersen, J. Z.; Traversa, E.; Ghibelli, L., Ce3+ Ions Determine Redox-Dependent Anti-apoptotic Effect of Cerium Oxide Nanoparticles. *ACS Nano* 5, (6), 4537-4549.

19. Dutta, P.; Pal, S.; Seehra, M. S.; Shi, Y.; Eyring, E. M.; Ernst, R. D., Concentration of Ce3+ and Oxygen Vacancies in Cerium Oxide Nanoparticles. *Chemistry of Materials* **2006,** 18, (21), 5144-5146.

20. Zhang, F.; Chan, S.-W.; Spanier, J. E.; Apak, E.; Jin, Q.; Robinson, R. D.; Herman, I. P., Cerium oxide nanoparticles: Size-selective formation and structure analysis. *Applied Physics Letters* **2002,** 80, (1), 127-129.

21. Celardo, I.; De Nicola, M.; Mandoli, C.; Pedersen, J. Z.; Traversa, E.; Ghibelli, L., Ce3+ Ions Determine Redox-Dependent Anti-apoptotic Effect of Cerium Oxide Nanoparticles. *ACS Nano* **2011,** 5, (6), 4537-4549.

22. Sayle, T. X. T.; Molinari, M.; Das, S.; Bhatta, U. M.; Mobus, G.; Parker, S. C.; Seal, S.; Sayle, D. C., Environment-mediated structure, surface redox activity and reactivity of ceria nanoparticles. *Nanoscale* 5, (13), 6063-6073.

23. Turner, S.; Lazar, S.; Freitag, B.; Egoavil, R.; Verbeeck, J.; Put, S.; Strauven, Y.; Van Tendeloo, G., High resolution mapping of surface reduction in ceria nanoparticles. *Nanoscale* **2011,** 3, (8), 3385-3390.

24. Abbaspour, A.; Mehrgardi, M. A., Electrocatalytic activity of Ce(III)-EDTA complex toward the oxidation of nitrite ion. *Talanta* **2005,** 67, (3), 579-584.

25. Pepe, A.; Aparicio, M.; Cere, S.; Duran, A., Preparation and characterization of cerium doped silica sol-gel coatings on glass and aluminum substrates. *Journal of Non-Crystalline Solids* **2004,** 348, (0), 162-171.

26. Akthar, F.; Podder, J., A study on structural,optical,electrical and etching characteristics of pure and L-alanine doped potassium dihydrogen phospahte crystals. *Journal of crystallization process and technology* **2011,** 1, (1), 55-62.

CHAPTER 4. CORROSION INHIBITION USING pH RESPONSIVE CAPSULES

4.1. Introduction

In this chapter, assessment of cerium containing capsules as corrosion inhibiting pigments in coatings using various corrosion evaluation techniques is presented. This chapter begins with a summary of the mechanism of corrosion inhibition by the use of cerium salts as reported by several authors. Next, the results of the corrosion evaluation experiments on cold rolled steel (CRS) and aluminum alloy 2024 T-3 (AA2024 T-3) substrates are summarized. The experimental results include open circuit potential (OCP) measurements, potentiodynamic experiments and electrochemical impedance spectroscopy (EIS) experiments. Results from scanning electrochemical microscopy (SECM) experiments, a localized electrochemical technique, are also presented in this chapter.

4.2. Mechanism of corrosion inhibition by cerium salts

The mechanism of corrosion inhibition by the use of cerium salts on steel and aluminum substrates has been investigated extensively by several authors.[1-6] Cerium was determined to inhibit corrosion by forming an insoluble film at the cathodic sides blocking the oxygen reduction reaction. The result is a decrease in the consumption of electrons supplied by the anodic reaction thereby a reduction in metallic dissolution. To understand the inhibition mechanism better, it is important to understand the interaction of cerium with corrosion reactions at the cathode of a metal resulting in the reduced corrosion current. The possible cathodic reactions occurring on the surface of the metal surface are as follows:

$$O_2 + 2H_2O + 4e^- \rightarrow 4OH^- \tag{4.1}$$

$$O_2 + 2H_2O + 2e^- \rightarrow 2OH^- + H_2O_2 \tag{4.2}$$

The hydroxyl ions produced as a result of these cathodic reactions result in increase in the local pH at the cathodic sites. The mechanism suggested by Yasakau et al. was that free Ce^{3+} present in the (neutral) solution reacts with the OH^- to produce several cerium hydroxo complexes depending on the local pH. Several cerium hydroxo complexes exist in a solution depending on the pH of the solution[3] (Figure 4.1). Summarized below are some of the possible hydroxo-complexes of Ce^{3+}.

$$Ce^{3+} + OH^- \rightarrow Ce(OH)^+; \log K = 5.57 \tag{4.3}$$

$$Ce^{3+} + 2OH^- \rightarrow Ce(OH)_2{}^+; \log K = 10.4 \tag{4.4}$$

$$Ce^{3+} + 3OH^- \rightarrow Ce(OH)_3 \downarrow; \log K = 14.71 \tag{4.5}$$

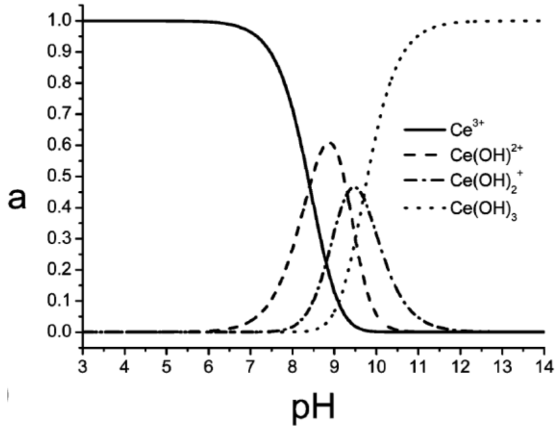

Figure 4.1. Fractions of various cerium hydroxo complexes in the solution depending on pH.[3] Reprinted with permission from “Yasakau, K.A.;Zheludkevich, M.L.; Lamaka,S.V.; Ferreira, M.G.S, Mechanism of corrosion inhibition of AA2024 by rare-earth compounds. The Journal of Physical Chemistry B 2006, 110, (11), 5515-5528. Copyright © 2006 American Chemical Society."

According to Figure 4.1 an increase in the pH greater than 9 causes the formation of cerium hydroxide. The cerium hydroxide is deposited immediately at the cathodic sites since much higher pH cannot be achieved far from the source of the hydroxyl ions as fast diffusion processes equalize the concentration of OH^- in the bulk solution. By the precipitation of this layer, the diffusion of oxygen towards the cathodic sites is greatly reduced resulting in the decreased kinetics of cathodic reactions. Cerium (III) also reacts with residual oxygen and water to form stable compounds of cerium (IV) hydroxide or cerium (IV) oxide. The relative ease in the formation of cerium hydroxide in basic conditions can also be further understood by looking at formation constants for Ce^{4+} and hydroxyl ions.

$$Ce^{4+} + OH^{-} \rightarrow Ce(OH)^{3+}; \log K = 14.76 \tag{4.6}$$

$$Ce^{4+} + 2OH^{-} \rightarrow Ce(OH)_2{}^{2+}; \log K = 28.04 \tag{4.7}$$

$$Ce^{4+} + 3OH^{-} \rightarrow Ce(OH)_3{}^{+}; \log K = 40.53 \tag{4.8}$$

$$Ce^{4+} + 4OH^{-} \rightarrow Ce(OH)_4 \downarrow; \log K = 51.86 \tag{4.9}$$

Microcapsules synthesized, as described in chapter 3, was incorporated into 2K waterborne coatings and applied over CRS and aluminum 2024 T-3 before performing electrochemical evaluation. The coating properties of such coatings are summarized in appendix B.

4.3. Open circuit potential

Open circuit potential measurements were performed on epoxy coated on metal substrate with cerium containing capsules (thickness measurements in Appendix B). An artificial defect about 0.5 cm in length was introduced in the coated samples using an engraver and the open circuit potential was monitored over a period of 12 hours in 5% sodium chloride solution using a potentiostat under freely corroding conditions. For this study CRS and AA2024 T-3 metal substrates were investigated.

4.3.1. OCP Measurement of Cold Rolled Steel

Corrosion potential measurements of cerium containing capsules revealed that corrosion behavior of cerium was different depending on the substrate. OCP measurement of epoxy coated

CRS without cerium containing capsules was determined to stabilize at ~ -0.75V (vs. SCE) over a period of 12 hours. In the case of scribed CRS samples containing cerium capsules, an anodic shift in the measured value of OCP was recorded. This anodic shift in potential may be due to the deposition of iron/cerium compound at the metal surface or a carbonate salt of cerium upon reaction with residual CO_2 or HCO_3^- in the solution.[7] The oxide/hydroxide of ceria available at the exposed CRS surface may have resulted in the ennoblement of the scribe resulting an anodic shift in the recorded corrosion potential. The presence of ceria nanoparticles has also been reported to shift the corrosion potential of mild steel to nobler potentials up to 0.1 V (vs Ag/AgCl) in 0.1 M NaCl solutions, which was consistent with the results that were recorded in this measurement.[8]

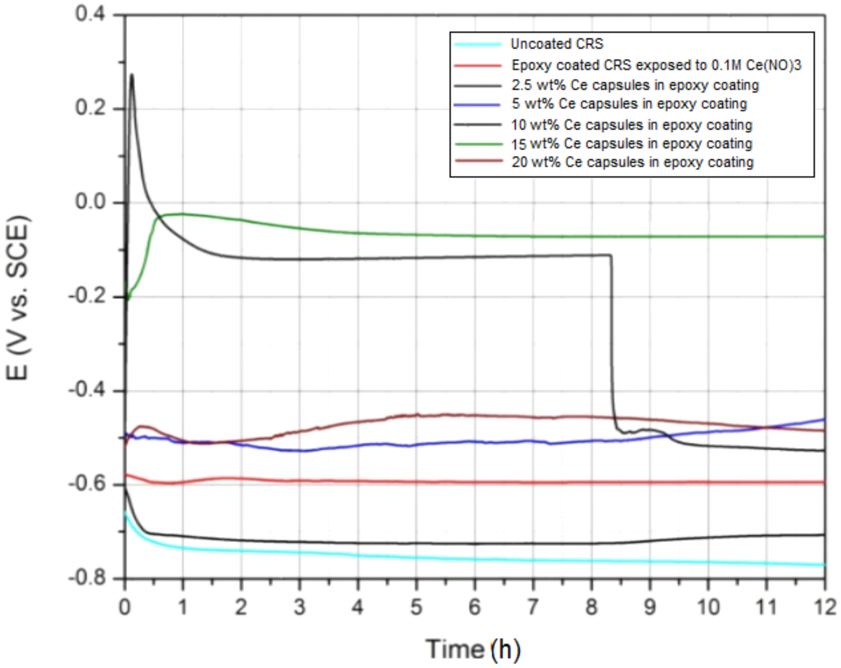

Figure 4.2. Open Circuit Potential (OCP) of cerium containing capsules on CRS.

Coatings containing cerium capsules showed an anodic shift in the OCP when compared to the coatings without capsules. As a control, OCP measurements were recorded on coated steel sample with a similar scribe with 0.1 M cerium nitrate as the electrolyte. Similar anodic shift in the potential was observed indicating that cerium behaves as an anodic inhibitor on steel. The concentration of cerium nitrate has been demonstrated to show an anodic shift in the potential on steel surfaces which may also be responsible for the anodic shift observed in the recorded OCP measurements.[9] However, the OCP results reinforced the anodic shift in the corrosion potential observed in case of the potentiodynamic curves. Even after 12 hours of exposure, a steady anodic shift was observed in the capsule containing samples indicating a sustained protection over time.

4.3.2. OCP Measurements on AA 2024 T-3

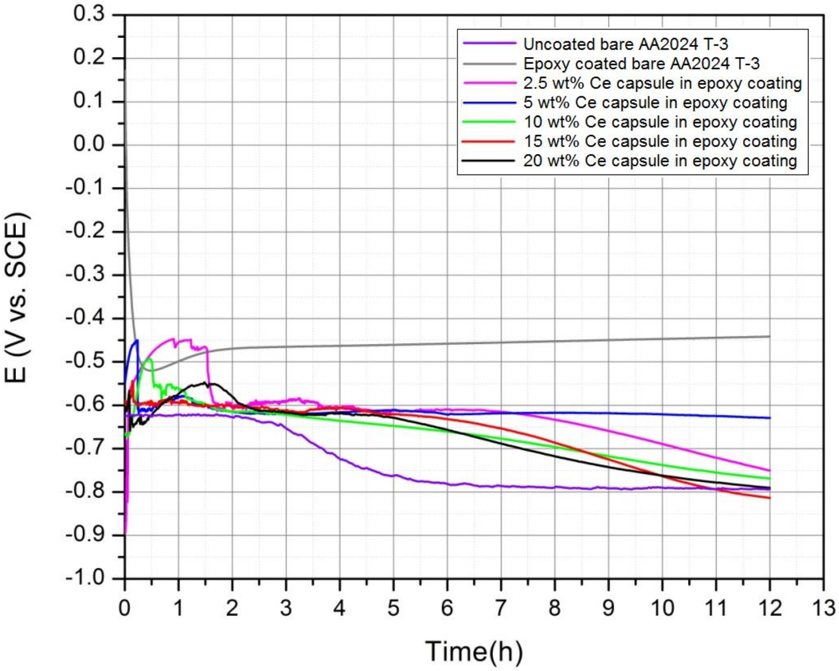

Figure 4.3. Open Circuit Potential (OCP) of cerium containing capsules on AA 2024-T3.

In case of AA 2024-T3, the general trend in OCP of the inhibited system containing cerium showed a cathodic shift in the potential when compared to coated scribed aluminum samples. In some measurements fluctuations in the potential were noted in the first two hours followed by a steady decrease in the corrosion potential to a stable potential. This potential change with time is attributed to oxide layer formation upon the immersion of the sample in the corrosive medium and the simultaneous attack by the chloride ions in the solution.[10] The open circuit potential of coated AA2024 T-3 containing cerium capsules was in all cases lower than non-capsule containing coatings on AA2024 in 5% NaCl solution and were observed to decrease with increase in immersion time. The decrease in OCP is indicative of the cathodic inhibition mechanism as reported by Hinton et al.[5, 11, 12]

4.4. Potentiodynamic scans

To determine the effect of cerium containing capsules in coatings, on the corrosion behavior of an exposed corroding substrate, potentiodynamic experiments were performed. A defect of 0.5 cm was introduced in the metal substrates coated with coatings containing various weight percentages of cerium containing capsules. Measurements were also performed in both aerated and de-aerated solutions in order to understand the role of oxygen in the corrosion inhibition using cerium containing capsules.

Figures 4.4 (a) and (b) presents the polarization curves of cerium capsule containing coatings on steel substrate immersed in an aerated and de-aerated 5% sodium chloride solution respectively. As it can be observed, the addition of cerium containing capsules to coatings does not affect the oxygen reduction reaction significantly as reported by Lu et al., however, an anodic shift in the corrosion potential was observed.[13] This shift in the corrosion potential may be attributed to the release of cerium from the capsules, resulting in the deposition of cerium hydroxide/oxide on the metal surface. Mansfeld et al. report that the efficiency in formation of cerium hydroxide/oxide layer and its adhesion to the substrate was greatly responsible for the modification of cathodic branch of the polarization curve.[14] In this case, the released cerium from the capsules may be not depositing on the exposed surface of the scribe efficiently, detaching from the surface which might be a reason why the cathodic branch may not be altered significantly. The anodic shift in the corrosion potential also observed by the addition of cerium containing capsules to steel substrates may be a concentration effect. Amadeh et al. observed a similar phenomenon when corrosion potential decreased with increase in cerium nitrate concentration up to 500 ppm.[15] For concentrations greater than 500 ppm, an anodic shift in the corrosion potential was observed accompanied by decreased current densities. Calculation of cerium nitrate concentration per batch of capsules suggests a very high concentration of cerium nitrate in the capsules (~ 20625.5 ppm per g of resin solids), which may be responsible for the anodic shift in the corrosion potential. However, a linear increase in the corrosion potential with increase in weight percent of capsules in coatings was not observed which may be because of the variation in size of the capsules and the concentration differences that might exist within each coating formulation. This increased concentration of cerium nitrate may cause it to behave as a mixed inhibitor instead of a cathodic inhibitor. Another factor affecting the corrosion potential and current of metal surfaces exposed to cerium nitrate solution is the time of exposure. It was observed that shorter exposure time (t = 10s) resulted in more uniform layer of cerium hydroxide/oxide on the metal surface which reduced the corrosion current and increased the corrosion potential.[16] The anodic shift in the corrosion potential from the base metal alloy in capsule containing coatings can also be explained by a similar phenomenon where cerium released from the capsules deposit at the cathodic sites at short exposure times, resulting in an anodic shift in the corrosion potential. No significant effect was observed in the polarized steel substrate with no dissolved oxygen in the polarization curves. Due to the application of a strong cathodic potential during the polarization, the metal substrate was lowered to pseudo corrosion potential of ~ -1.1 V (vs. SCE). A similar phenomena was reported by Garcia et al. for AA2024

T-3 where pH>9 at the working electrode resulted a cathodic shift in the corrosion potential.[17] Thus, cerium on cold rolled steel was determined to behave as an anodic inhibitor. The results from the potentiodynamic curves were in agreement with the OCP measurements as well.

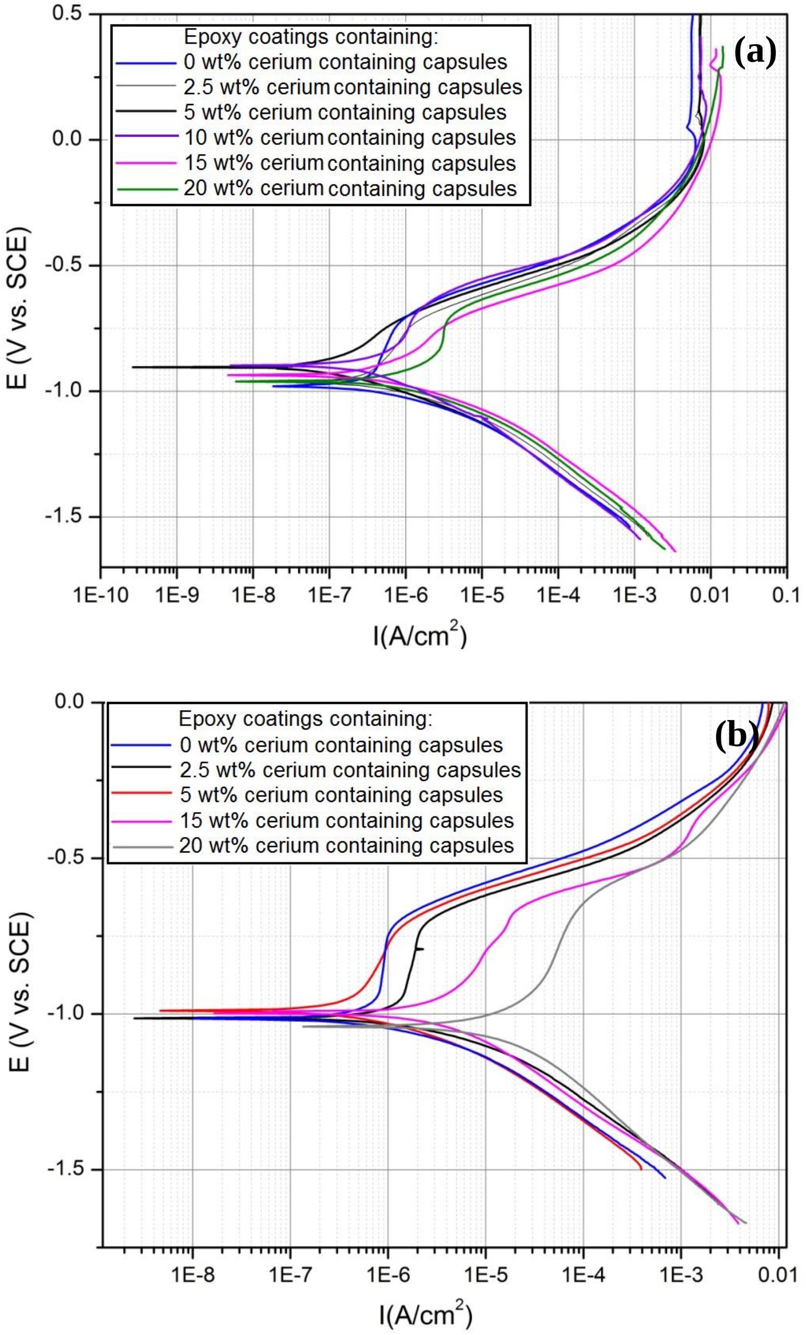

Figure 4.4. Potentiodynamic curves of different weight percentages of cerium capsule containing coatings on Cold Rolled Steel in (a) aerated (b) de-aerated 5% NaCl solution.

The electrochemical behavior of AA2024-T3 alloy coated with capsule-containing coatings was studied using polarization curves. All the samples containing cerium capsules presented less noble OCPs than the control (0% capsules) indicating a high cathodic activity of the inhibitor. In deoxygenated environment, no significant decrease in the cathodic current was observed by the addition of cerium containing capsules. It can be explained by understanding the mechanism of corrosion inhibition using cerium salts. The mechanism of protection proceeds via precipitation of $Ce\ (OH)_3$ on the cathodic sites upon reacting with OH^- ions generated by the oxygen reduction reaction. Thus, the absence of dissolved oxygen affects the precipitation and corrosion inhibition using cerium salts. However, a reduction in the corrosion current and a cathodic shift in the corrosion potential was observed in coated samples exposed to deaerated electrolyte solution as well. On the contrary, aerated solution, a cathodic shift in the corrosion potential was observed accompanied by a decrease in the corrosion current which was in agreement with the results obtained by other authors for aluminum alloys[9, 11, 18-22]. The cathodic curve, for all the coatings containing cerium capsules, corresponding to the reduction of dissolved oxygen was shifted to the left, indicating a slowing down of the cathodic reaction kinetics. The decrease in corrosion current and potential may be due to the precipitation of cerium oxide/hydroxide and the suppression of the oxygen reduction reaction.[23] The increase in the passive region of the cerium capsule containing coatings also indicates that the cerium oxide layer reduces metal dissolution in a chloride environment. The analysis of the anodic branch in aerated coatings containing cerium capsules revealed a higher passivating region than that of bare aluminum, indicating the formation of a passive layer, which may be that of cerium hydroxide/oxide.

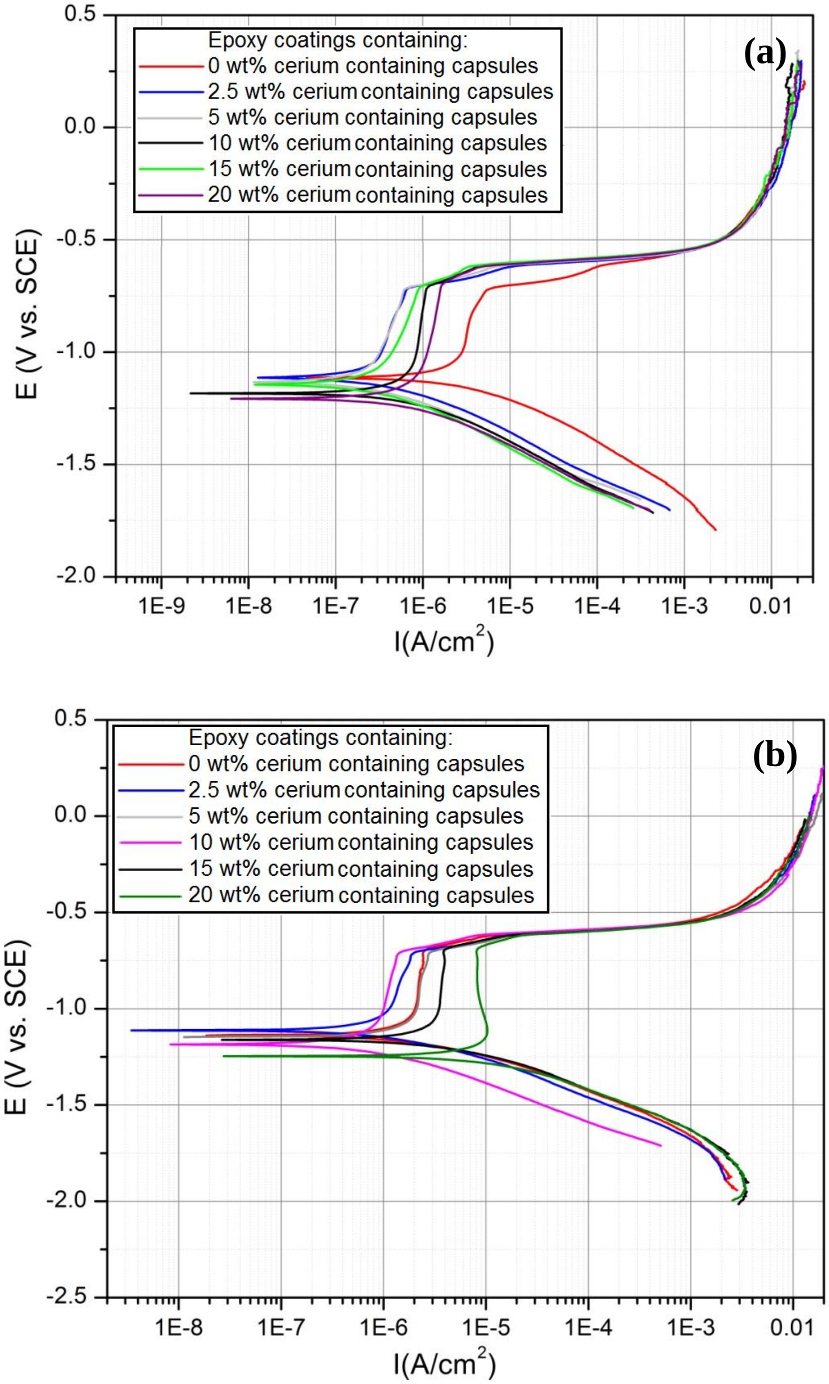

Figure 4.5. (a) Potentiodynamic curves of different weight percentages of cerium capsule containing coatings on AA 2024- T3 in aerated 5% NaCl solution (b) Potentiodynamic curves of different weight percentages of cerium capsule containing coatings on AA 2024- T3 in deaerated 5% NaCl solution.

The concentration of cerium released / present at the scribe and the localized pH were determined to play an important in the inhibition of corrosion. The superficial oxide layer formed as a result of the cathodic reaction may dissolve due to localized pH changes to acidic conditions. This phenomena was reported in cases where the concentration of cerium was larger and the pH was lower[24]. In areas with higher pHs and lower concentrations of cerium ions the superficial layer formed remains relatively undisturbed resulting in lower values of cathodic current densities. The effect of concentration on the measured corrosion potential and cathodic current measurement can thus be explained by the formation of a stable undisturbed superficial layer of cerium oxide/hydroxide. The passive region formed on the anodic branch may be because of the presence of the nitrate ions which inhibit the anodic partial reaction by increasing the formation of the oxide film on the anodic zones.[25] Thus, the cerium salts act as mixed inhibitor for the corrosion of AA2024 in chloride environment.

4.5. Cyclic voltammetry

The redox activity of the incorporated cerium salt and the oxidation state of the incorporated cerium into the capsules was assessed using rotating disk electrode (RDE). Low concentrations of cerium were detected in acidic solutions using a glassy carbon electrode.[26] It was determined that microcapsules containing cerium were redox active as shown in Figure 4.6 by the appearance of the redox peaks in the voltammogram. A standard solution of 1mM cerium (III) nitrate hexahydrate used as a control revealed that the oxidation of Ce^{3+} to Ce^{4+} takes place at 1.3 V (vs.Ag/AgCl) and the reduction from Ce^{4+} to Ce^{3+} at 1.15 V (vs. Ag/AgCl). It was found that the measured redox potential was in good agreement with literature data.[26] A voltammogram of a mixture of cerium (IV) and cerium (III) nitrates showed an increased oxidation and reduction current.

Next, cerium containing capsules were crushed and made up in 50 mL of 0.1 M sulfuric acid and the voltammogram from the crushed capsule containing solution was recorded. Weak oxidation and reduction peaks were observed at 1.3 V and 1.15 V (vs.Ag/AgCl) respectively similar to that of cerium nitrate control solutions. This indicates that cerium was incorporated into the capsules. It was also observed that the reduction current was closer to zero indicating that the available cerium in the capsules was in the +3 oxidation state. A similar observation was made in case of the uncrushed capsules indicating that the cerium in the capsules diffuse through the capsule shell upon exposure to the electrolyte. This indicates that cerium was available in the +3 oxidation state within the capsules.

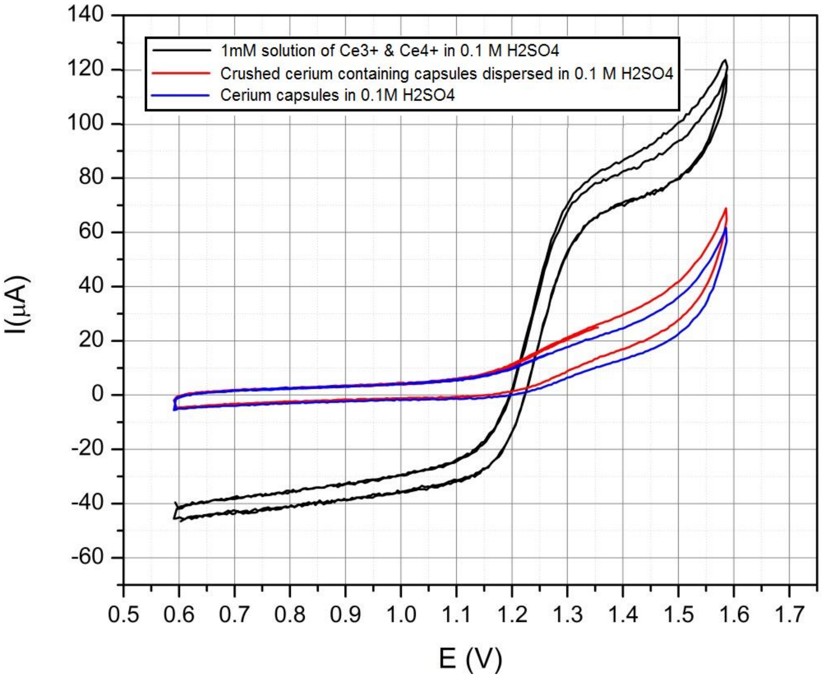

Figure 4.6. Cyclic Voltammetry of cerium containing capsules in 0.1 M sulfuric acid on glass carbon electrode at 1600 RPM and 50 mV/s.

4.6. Electrochemical impedance spectroscopy

Electrochemical impedance spectroscopy (EIS) of epoxy-amine coating containing different weight percentages of microcapsule was measured using the electrochemical setup described previously in Chapter 2. Equivalent circuit modeling was used to understand the behavior of the coating upon exposure to 5% NaCl solution. The circuit modeling is presented in Appendix A of the dissertation.

Constant immersion studies were performed on epoxy coatings containing cerium containing capsules applied over CRS and AA 2024 T-3 (AA2024 T-3) substrates to study the corrosion inhibition of cerium nitrate (containing capsules) on these substrates. Coatings were formulated containing different weight percentages ranging from 5 – 20 wt. % of capsules to study the effect of capsule concentration (cerium nitrate) on the impedance of the coating and corrosion inhibition.

4.6.1. Immersion Studies on Cold Rolled Steel Substrate

Electrochemical impedance spectroscopy was performed on cold rolled steel substrates coated with 2K epoxy coating containing with various weight percentages of microcapsules, exposed to 5% sodium chloride solution. Equivalent circuit models of the recorded spectra (summarized in Appendix A) were used to understand the changes at the coating/substrate interface and the subsequent corrosion inhibition by the introduction of pH responsive capsules in the virgin 2K epoxy coatings. The plot of the low frequency (0.01 Hz) impedance with immersion time was used to measure the resistance of the coating to electrolyte. At the very beginning of immersion, all the coatings exhibited high values of coating resistance (R_C) greater than 10^9 **Ω** in the low frequency (0.01 Hz) regime and were highly capacitive. With increase in exposure time, the coating resistance (Rc) of 0 wt. % capsule containing epoxy coating began to decrease as a result of the diffusion of the electrolyte into the coating. This decreased impedance at low frequency was also accompanied by a corresponding increase in the coating capacitance (C_C), which indicates the penetration of electrolyte into the epoxy coating. The resistance of the 0wt. % capsule containing epoxy coating drastically decreased in the first 12 hours following which a steady value of resistance was observed as shown in Figure 4.8.This steady state value in the coating resistance may be because of the saturation of the coating with electrolyte. The increase in the capacitance of the coating can also be explained similarly as the diffusion of the electrolyte causes an increase in the dielectric constant of the coating resulting in the increase value of coating capacitance that was observed as a function of time. In the model, a diffusion element was included in the first 12 hours to indicate the diffusion of an electro-active (electrolyte) species into the coating. After 12 hours, once the coating was saturated with the electrolyte a new second RC couple was observed which can be attributed to the coating- metal interface or better known as the double layer capacitance (C_{dl}) and the polarization resistance of the metal (R_p).[27, 28]

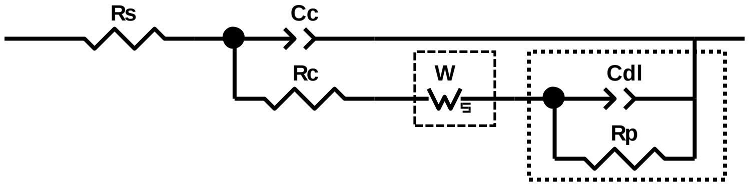

Figure 4.7. Equivalent circuit model used for modeling microcapsule containing coatings epoxy coatings.[29,30]

In case of the epoxy coating containing 5 wt. % cerium capsules, a higher initial value of the coating resistance was observed compared to the 0 wt. % epoxy coating. The model used to represent the 5 wt. % cerium capsule containing coating was similar to that shown in figure 4.7 but with no diffusion or a second RC couple. The decrease in coating resistance was observed with 5 wt. % coating up to 48 hours after which a steady state value was observed. The capacitance of the coating also increased as a function of immersion time in the electrolyte due to the diffusion of the electrolyte into the coating. Similar trend was observed in case of the 10 wt. %, 15 wt. % and 20 wt. % cerium capsules containing coating as well. Even though, the addition of capsules to the epoxy coating resulted in increased coating resistance compared to the virgin coating (coating with no capsules), a decrease in the coating resistance was observed with proportionate increase in capsule weight percentage. The swelling of the hollow capsules in the coating upon exposure to electrolyte and the associated porosity introduced due to the hollow core of the capsules in the exposed coatings upon rupture may be the reasons for observed decrease in the coating resistance in case of coatings containing capsules.

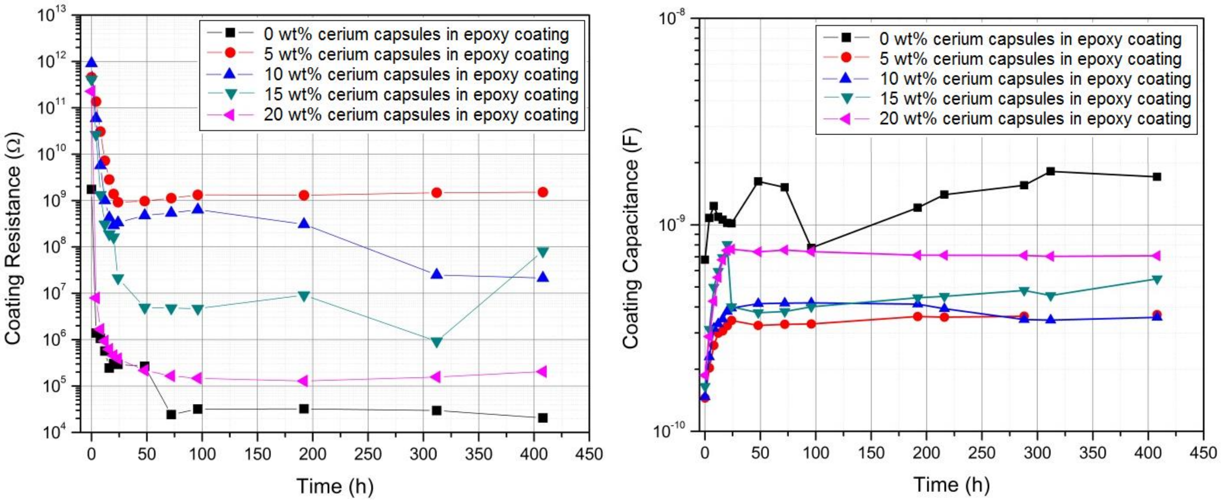

Figure 4.8. Coating resistance and capacitance of cerium capsule containing coatings on CRS.

The effect of cerium capsules in coatings has been discussed thus far; however, the corrosion inhibition due to cerium within the capsules can also be studied by monitoring the change in the polarization resistance of the metal using EIS.[31] Since the metal - coating interface was inaccessible to the electrolyte at lower weight percentages of capsules in coatings; the 20 wt. % capsule containing coating was a great candidate to study the effect of cerium on the polarization resistance of Cold Rolled Steel (CRS). The polarization resistances of 0 wt. % capsules containing epoxy coatings and 20 wt. % capsule containing coatings were compared to demonstrate the change in polarization resistance due to the release of cerium from the capsules. Rp values were calculated from the equivalent circuit models (shown in Appendix A).

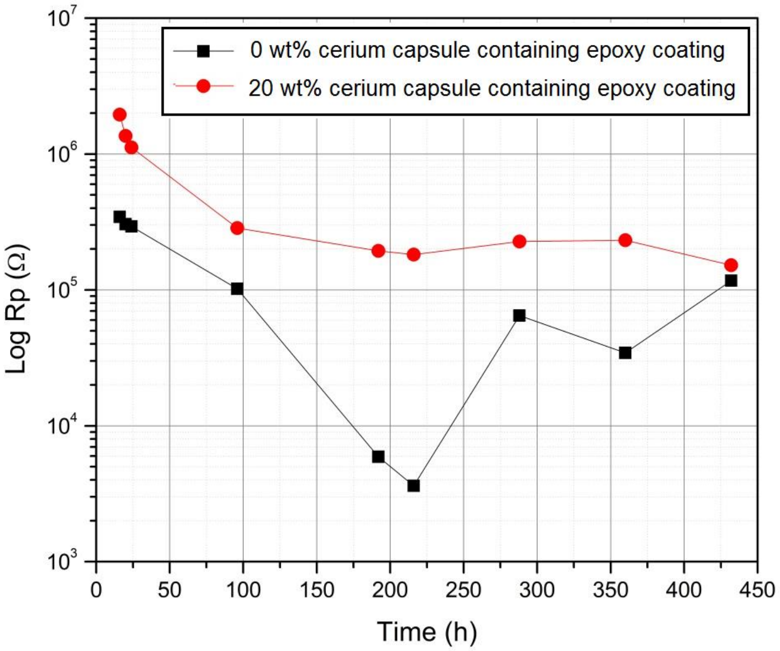

Figure 4.9. Comparison of the polarization resistance (R_P) between 20 wt. % cerium capsule containing and virgin epoxy coating on CRS substrate.

A 20 wt. % capsule containing coating demonstrated about 1 order of magnitude increase in the polarization resistance as compared to that of the virgin coating without any capsules. With the knowledge of corrosion inhibition mechanism of cerium salts, it can be said that the deposition of cerium hydroxide/oxides at the coating – metal interface may be why an increased polarization resistance of steel was observed. It is important to note that since the values of Rp were based on equivalent circuit models, only those values have been used in Figure 4.9. where Rp was observed in the model. In case of the virgin coating, Rp was not observed until 16 hours of immersion and hence an offset is observed between the virgin and 20 wt. % capsule containing coatings.

4.6.2. Immersion Studies on Aluminum Alloy 2024 T-3 (AA2024 T-3)

Epoxy coatings were formulated with various weight percentages of cerium capsules and applied over AA 2024 T-3. EIS experiments were carried out on various samples as described in chapter 2. In order to evaluate the barrier properties of the coatings during immersion as well as their active corrosion inhibition properties all the impedance spectra were fitted to appropriate equivalent circuits (Appendix A).

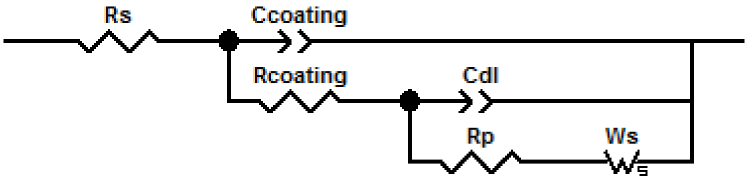

Figure 4.10. Typical equivalent plots obtained after prolonged immersion of microcapsule containing coatings.

A typical impedance spectra used for coated aluminum alloy showing three relaxation constants is presented in Figure 4.10. For the equivalent circuit represented below, R_s is the resistance of the electrolyte; $C_{coating}$ and $R_{coating}$ represent the capacitance and the resistance of the coating; C_{oxide} and R_{oxide} represent the capacitance and resistance of oxide film over the macroscopic alloy; C_{dl} is the capacitance of the electrochemical double layer at the metal-electrolyte interface and R_p is the polarization resistance of the corrosion process. In case processes with reduced number of relaxation constants the corresponding RC elements were removed from the models. In certain cases, a Warburg element was included in the equivalent circuit models where diffusion of the electrolyte was dominant at the low frequencies. Figure 4.11 shows the evolution of coating capacitance and resistance as a function of immersion time as observed at the low frequency (0.01 Hz) of the impedance spectra. The coating without microcapsules shows a drastic increase in the coating capacitance and a corresponding decrease in coating resistance, due to the ingress of the electrolyte into the coating. Upon addition of cerium capsule to virgin epoxy coating, the steady state coating resistance was found to be higher than virgin epoxy coatings with incremental weight percent increase of cerium capsules upto 15 wt. %. The capsule containing coatings (5 , 10 , 15 wt %) demostrated a very similar trend with in initial increase in the capacitance upto 16 hours of immersion before leveling to a contant value. This may be due to the inclusion of hollow core shell capsules in the coatings which increase the porosity of the coating upon breakage/swelling. It was interesting to note that resistance of the coating containing capsules was greater than that of the blank epoxy coating during the time that the coating was exposed to the electrolyte, which may be due to the tortuosity introduced by microcapsules in the coating. It was observed that highest coating resistance was observed in case of the 15 wt.% cerium capsule containing coatings.

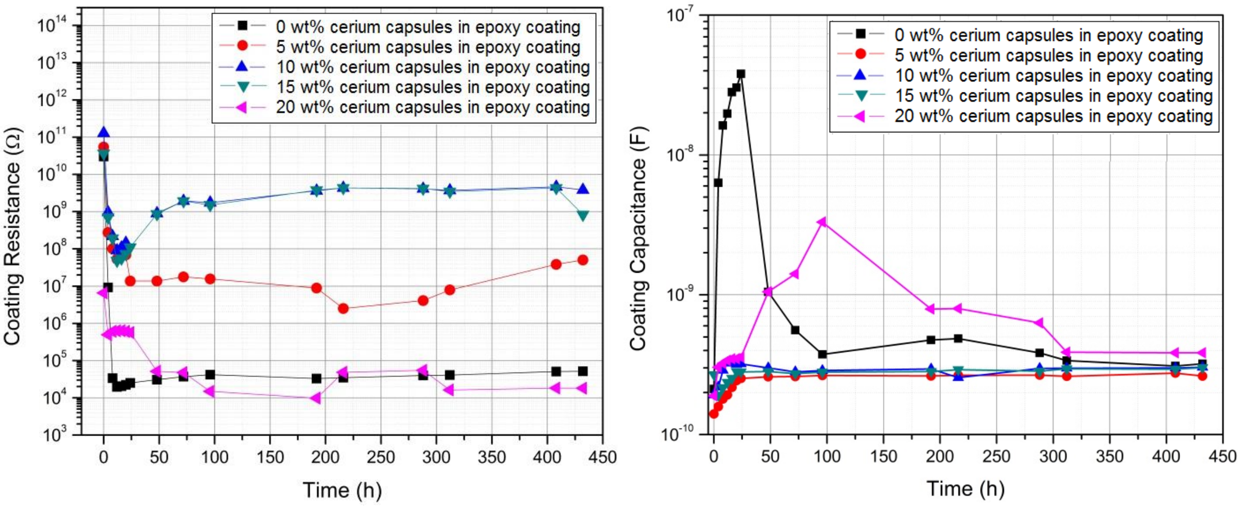

Figure 4.11. Coating resistance and capacitance of cerium capsule containing coatings on AA 2024 T-3.

However, this trend does not hold true for 20 wt. % cerium containing capsules. As it can be observed, 20 wt. % capsules containing coating shows a drastic decrease in the coating resistance with time and after about 24 hours have a resistances lower than that of the 0 wt. % epoxy coatings. This reduction in coating resistance can be explained by the understanding of the pigment volume concentration (PVC) of pigments in coatings. At PVCs greater that critical PVC (CPVC) pores are introduced in the coatings which facilitate the transportation of electrolyte and the dissolved species to the metal surface which result in the decrease of the coating resistance. At 20 wt. % the capsule concentration in the coating, the concentration of microcapsules may be just below CPVC of the coating system resulting in the very similar values of coating resistance as the virgin epoxy coating. The comparison of the polarization resistance was not possible in case of AA 2024 T-3 due to absence of the metal-electrolyte interface in the microcapsule containing coatings.

4.7. Salt spray – ASTM B117

Traditional salt spray was performed using the procedures stated in ASTM B117 on CRS and AA2024 T-3 substrates coated with water based epoxy coating with different weight percentages of cerium capsules. In spite of giving only qualitative information about the behavior of the coating system when exposed to an aggressive medium (5% NaCl at 35°C), the salt spray test is widely used for comparing the corrosion performance of coatings. CRS samples coated with different weight percent microcapsules were subjected to 500 h of salt spray. The samples were X-scribed in order to evaluate the undercut/ under coating corrosion. The coated substrates were removed from the salt spray cabinet and digital photographs were recorded to visually assess the under film corrosion from the scribe as a function of exposure time.

For steel samples, after 38 h of exposure to salt spray (Fig. 4.12.), the samples showed evidence of corrosion at the scribe. Even though the scribed area showed with an intense red color in all the cases, the underfilm corrosion was obvious in case of the blank epoxy coating which could be observed as the appearance of a bluish green line along the edge of the scribe. All the samples containing cerium capsules did not show any under film corrosion after 38 hours after exposure to salt spray. After 110 hours, it was observed that underfilm corrosion began to occur in all the samples but varied in the creep from the scribe decreasing in distance from the scribe with increase in the weight percentage of cerium capsules added to the coating. At 230 hours, the creep from the scribe increase further in case of the blank epoxy, 2.5 wt. % and 5 wt. % coatings but no increase in the creep was observed in case of 10, 15 and 20 wt. % coatings. Similarly, at 398 hours the creep distance increased in case of the blank coatings, however the capsule containing coatings did not show a significant increase distance from the scribe. At 500 hours, the blank epoxy coating began to delaminate from the substrate whereas the capsule containing coatings were determined to be adhered to the surface. Chipping of the coating along the scribe, however, was observed in case of the microcapsule containing coatings. Even at the end of 500 hours, the coatings containing 10 wt. % and greater show significantly greater corrosion inhibition at the scribe than blank coatings.

Since adhesion plays a very important role in the corrosion inhibition processes, pull-off adhesion measurements (Appendix B) were recorded to determine the adhesion of the coating to the substrate as a function of the weight percent of capsules incorporated into the coatings. It was observed with increase in the weight percent of the capsules in the coatings the force required to pull the dolly from the substrate decreased. This indicates that the incorporated cerium capsules in the coatings did not increase the adhesion of the coating to the substrate. The decrease in the creep observed from the scribe was the result of reduced corrosion product at the scribe which was a consequence of the addition of cerium in the coatings. In case AA 2024 T-3, blistering was observed unlike steel where visible signs of underfilm corrosion was noted. The addition of cerium capsules showed a decrease in the blisters formed around the edge of the scribe in capsule containing coatings as compared to the epoxy coatings in the first 24 hours. In the first 24 hours, a notable decrease in blister formation was noted at 15 and 20 wt. %, indicating that the increase in concentration reduced the blister formation in case of coated AA 2024 T-3.

As reported in the literature lanthanide ions for insoluble hydroxides and function as cathodic inhibitors. Thus, the blockage of the cathodic sites by cerium hydroxide/oxide decreases the available cathodic current for the liberation of hydrogen and hence the decrease in blistering.[32] After 120 hours of salt spray exposure, the blister density in all the samples was found to have increased. The blister formation was reduced with increase in the weight percent of capsules in the coatings. Even though no signs of under film were observed after 120 hours a slight delamination of the coatings at the scribe was observed in most cases. After 277 hours of salt spray exposure widespread penetration of electrolyte into the coating was observed resulting in the decreased adhesion of the coating around the scribe. With increase in the weight percent of the capsules a decrease in creep from the scribe was also noted. A similar trend was observed in salt spray exposed samples after 397 hours accompanied by the delamination of the coating at the intersection of the two scribe lines. However, with time a decrease in the number of blisters was observed due to coalescence of the formed blisters.

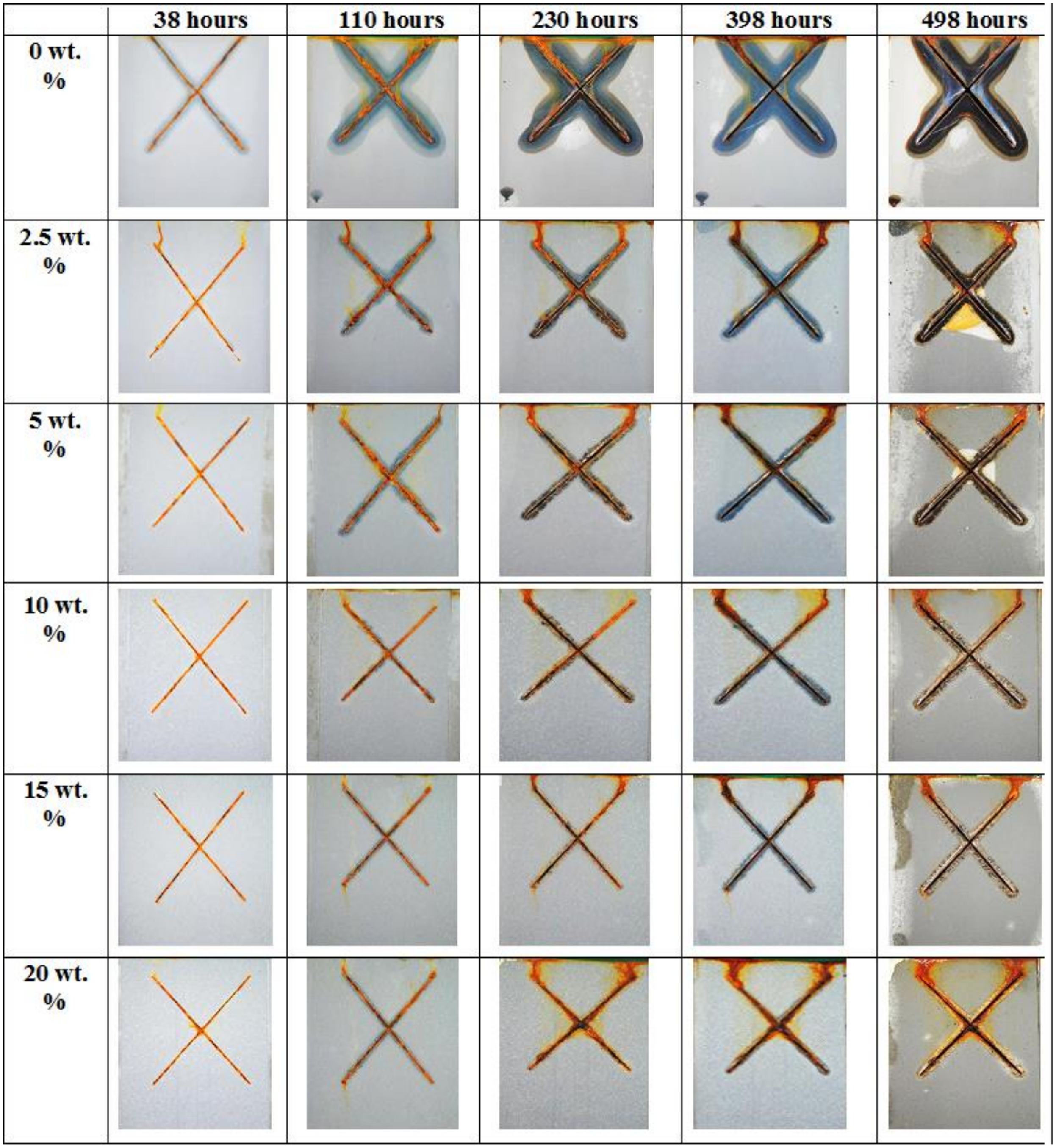

Figure 4.12. Photographic images of various microcapsule containing epoxy coatings on cold rolled steel substrate after neutral salt spray exposure in accordance to ASTM B117.

Figure 4.13. Photographic images of various microcapsule containing epoxy coatings on AA2024 T-3 substrate after neutral salt spray exposure in accordance to ASTM B117.

4.8. Scanning electrochemical microscopy (SECM)

Scanning Electrochemical Microscopy (SECM) was used to understand the processes taking place at the scribe. Samples were prepared by applying coatings containing microcapsules on metal substrates and a scribe was introduced in the sample to induce corrosion. The release and effect of cerium from the capsules was studied using Scanning Electrochemical Microscopy.

Scanning Electrochemical Microscopy system was used to perform line scans on scribed 20 wt. % cerium capsules containing coatings in aerated 0.2 M potassium chloride solution. The 10 µm diameter platinum SECM ultra-microelectrode (UME) was used for all the experiments. The probe was set to - 0.7 V (vs. Ag/AgCl) to reduce oxygen at the tip. At locations with a lower oxygen concentration, where oxygen is consumed by the cathodic reactions, the introduction of the UME introduces a competing reaction for the available dissolved oxygen in the solution resulting in a lower value of measured current. As discussed earlier in this chapter, it is known that cerium released from the capsules combine with the hydroxyl ions in the solution from the cathodic corrosion reaction and precipitates at the cathode as its hydroxide. This precipitation at the cathodic sites of the metal substrate would result in lower cathodic currents measured at the tip of the UME set to the reduction potential of dissolved oxygen, than a freely corroding sample. As a control experiment, scribed steel sample coated with epoxy coating was exposed to aerated 0.2M KCl solution and scanned for oxygen depletion by applying -0.7 V (vs. Ag/AgCl) to the UME. A well-defined oxygen depletion was observed at the scribe evidenced by the dip in current in the probe scan curve between 800 µm and 1200 µm which corresponded to the scribe. To verify the corrosion inhibition by cerium nitrate at the cathode, 0.2 M KCl solution was replaced by 0.1M cerium (III) nitrate and allowed to stand for 15 minutes. After the exposure the cerium (III) nitrate solution was replaced by aerated 0.2 M KCl and line scans were again recorded along on the same line path as before. An overall decrease in the measured value of current measured was observed and no dip in current at 800 – 1200 µm was recorded in the case of the samples exposed to cerium nitrate solution, indicating that cerium deposition at the scribe could be a possible reason for the decrease in the oxygen consumption at the cathodic sites.

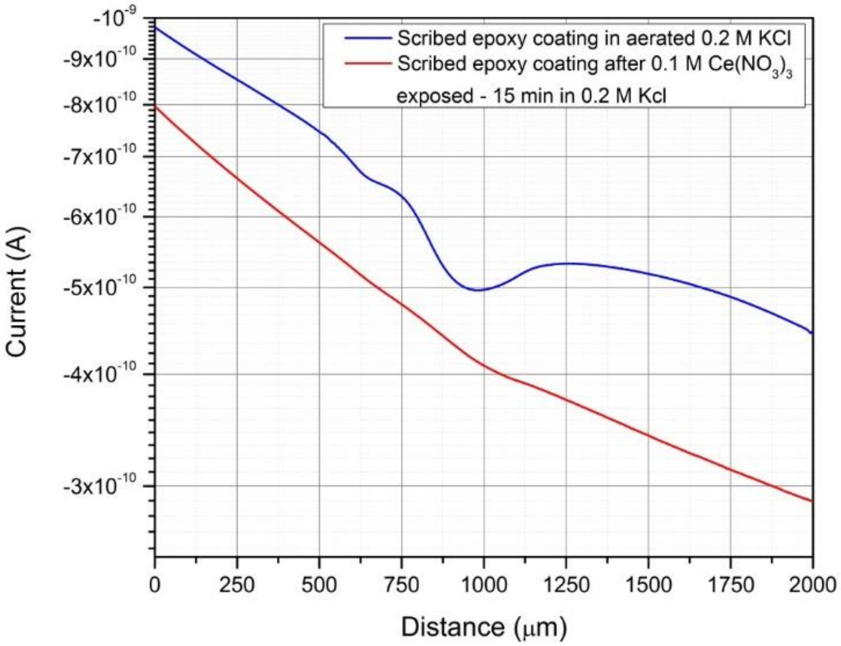

Figure 4.14. Probe scan curve of scribed epoxy coating over cold rolled steel substrate scanning for oxygen depletion (E_{probe} = -0.7 vs. Ag/ AgCl) before (blue) and after (red) exposure to 0.1 M cerium nitrate solution in 0.2 M KCl solution.

Thus, scanning for oxygen consumption at the scribe was determined to be a viable method for the detection of cerium assisted corrosion inhibition. Coated steel samples with 20 wt. % cerium capsules were then exposed to aerated 0.2 M KCl and scans were performed to detect oxygen depletion by setting the probe to -0.7 vs.Ag/AgCl reference electrode. Instantly, the first scan after exposure revealed a larger current at the scribe compared to the coated substrate. Assuming that peak in current to be a topographic feature, the probe was 100 µm drawn away from the surface and the scan was repeated. The same feature was observed indicating the formation of a precipitate. Since this observation of was made immediately after exposure to KCl the possibility of any corrosion product at the scribe can be ignored. Upon observing the scribe through the video camera no coating residue was observed at the location of the scan. From this observation, it can be said that the formation of a precipitate of cerium may have resulted in the feature to appear at the scribe.

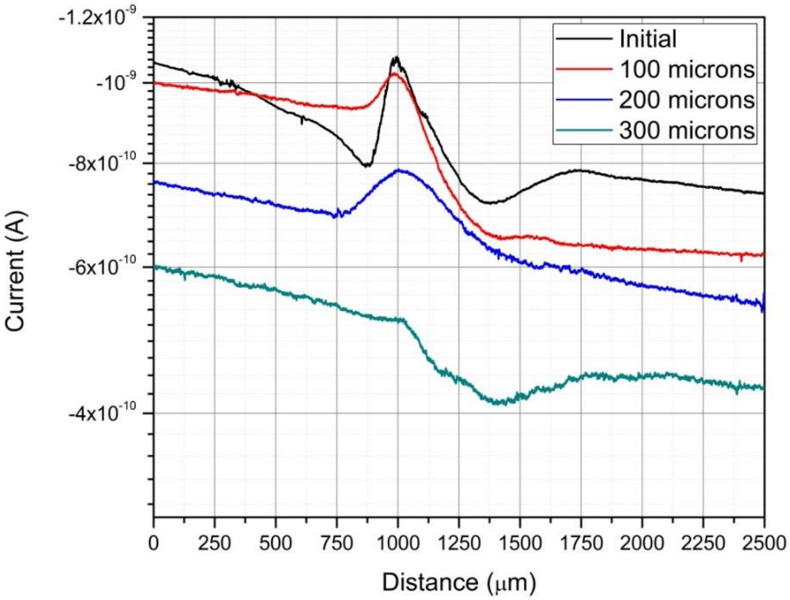

Figure 4.15. Probe scan curve of scribed epoxy coating containing 20 wt. % cerium capsules over steel substrate. Scanning for oxygen depletion (E_{probe} = -0.7 vs. Ag/ AgCl) in 0.2 M KCl solution as a function of tip distance from the substrate.

Since Ce^{3+} ions are highly reactive towards hydroxyl ions, Ethylenediaminetetraacetic acid (EDTA) was used as a complexing agent to capture the released cerium. The advantage of using cerium EDTA complex is that the complex is redox active. The cyclic voltammetry of the cerium EDTA (Ce-EDTA) complex is shown Figure 4.16. It was observed that the Ce-EDTA complex oxidized at 0.846 V (vs.Ag/AgCl) and reduced at 0.774 V (vs.Ag/AgCl). With this information, the probe tip was set to the oxidation potential of Ce-EDTA of 0.9 V (vs.Ag/AgCl) and scanning electrochemical microscopy scans were performed over a microcapsule embedded in the epoxy coating. The substrate was polarized cathodically at -0.8 V (vs. Ag/AgCl) to induce hydroxyl ion generation and in turn release cerium from the capsules. A higher probe response current was detected over the capsule surface indicating that the concentration of Ce-EDTA complex was higher in this region. This indicated that cerium was released from the capsules.

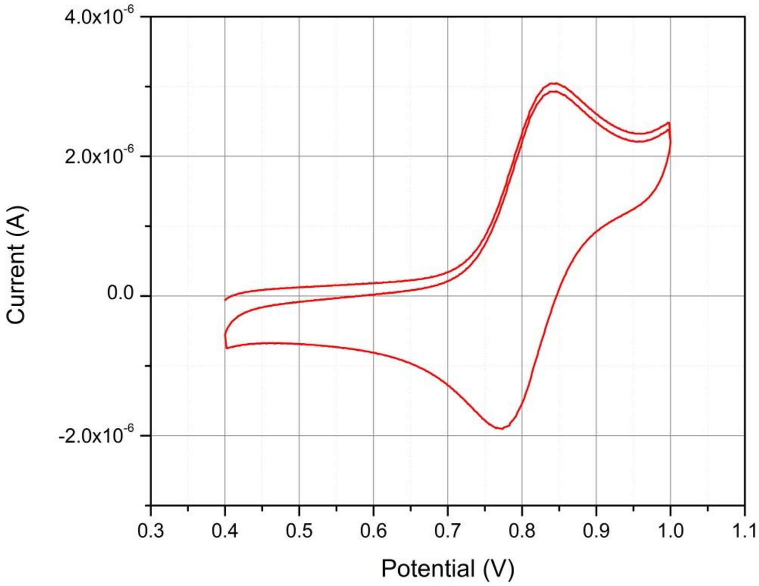

Figure 4.16. Cyclic Voltammetry of Cerium-EDTA complex. E_{ox} = 0.846 V (vs.Ag/AgCl) E_{red} = 0.774 V (vs.Ag/AgCl) performed using Pt disk electrode.

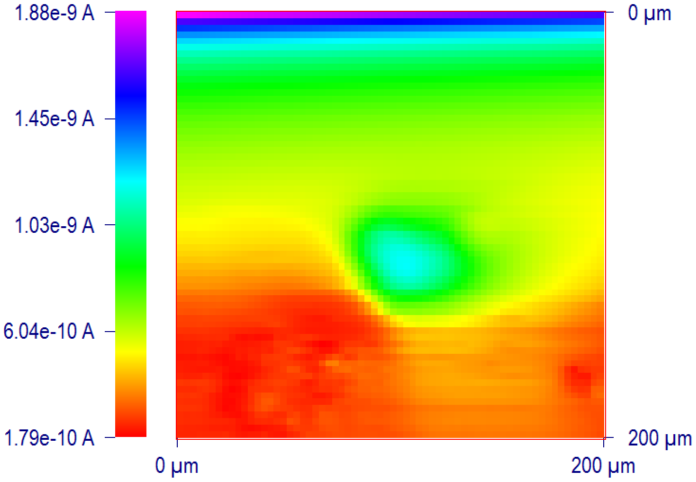

Figure 4.17. Scanning Electrochemical Microscopy image of cerium containing capsule in epoxy coating on cold rolled steel substrate. Release of cerium detected using 0.001 M EDTA as a complexing agent. E_{probe} = 0.9 V (vs.Ag/AgCl), Esubstrate = -0.8 V (vs.Ag/AgCl).

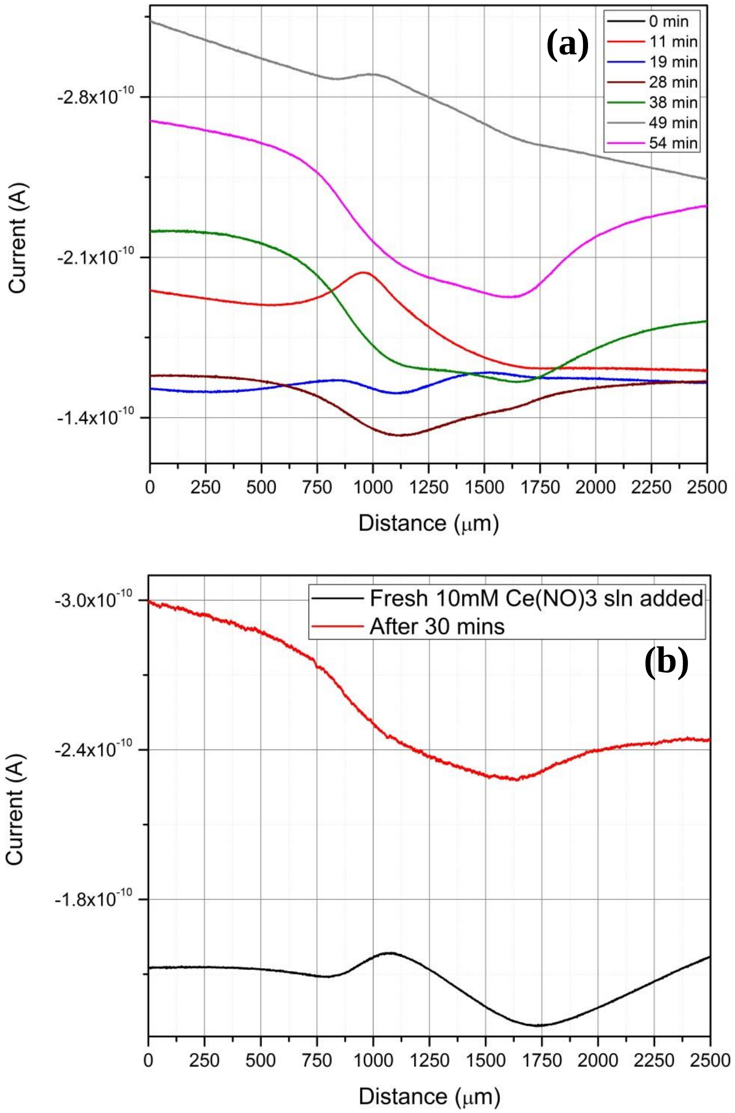

Figure 4.18.(a) Change in the scribe current as a function of time upon addition of 10 mM cerium nitrate solution observed using probe scan curves of scribed epoxy coating on AA 2024 T-3. (b) Probe scan curves of scribed epoxy coating on AA 2024 T-3 upon addition of fresh 10mM cerium nitrate solution.

Similar experiments were performed on AA 2024 T-3 substrates as well. As a control experiment, AA2024 T-3 coated with epoxy was scribed and a line scan for oxygen depletion was performed over the scribe with the potential at the probe at -0.7 V (vs.Ag/AgCl) in aerated 0.2 M KCl. After the first scan, the electrolyte was replaced with a 10 mM cerium nitrate solution and let to equilibrate for 6 minutes. The 0.2 M KCl electrolyte was reintroduced and probe scan curve was obtained as a function of time. It was interesting to observe that initially the scribe showed a high value current at the scribe, which began to decrease with the evolution of time. This phenomenon can be explained by the formation of cerium oxide/hydroxide layer that may not have been completely adhered to the surface of the metal. This phenomena was completely reversible upon repeating the exposure of the scribe to 10mM cerium nitrate solution confirming the formation of a non-adhered corrosion product to the surface. However it was interesting to note that the cathodic current of the native (initial) scribe (time t = 0) to the cathodic current after the exposure was slightly higher indicating the gradual deposition of cerium at the cathodic sites on the scribe.

After having observed this phenomenon on AA2024 T-3, 2500 X 400 microns SECM scans were recorded across the scribe to study the effect of cerium containing capsules on corrosion inhibition in the scribe. The ultra-microelectrode was set to -0.7 V (vs.Ag/AgCl) and SECM oxygen depletion plot was mapped. In Figure 4.19, it can be observed that the SECM oxygen maps concur with the topography observed using SEM. Interestingly, no oxygen depletion was observed at the scribe. After suspecting the disappearance of the oxygen depletion dip to the deposition of cerium at the scribe, a razor blade was used to introduce fresh underlying metal. After the fresh scribe was made, a probe scan curve for oxygen was measured across the scribe. Upon exposure of fresh substrate, the depletion of oxygen was observed again at the scribe once again. This indicates the formation of a passive layer that prevents further corrosion of aluminum. SEM images of the scribe after exposure to the electrolyte indicated the formation of a very smooth surface at the scribe. To understand the corrosion product formed at the scribe upon exposure to the electrolyte, EDX measurements were recorded at the scribe before and after exposure to the electrolyte. No traces of cerium were observed in the scribe before exposure to aerated 0.2 M KCl. However, the 20 wt. % cerium capsule containing coatings exposed to 0.2M KCl showed traces of cerium in the scribe indicating the cerium from the capsules migrated to the scribe where they were deposited. Thus, the decrease in the current measurements recorded in the line scans on scribed AA20204 T-3 may be due to the deposition of a thin layer of cerium based corrosion product which suppresses the cathodic reaction resulting in the overall reduction in corrosion. Even though several reports indicate the formation of cerium hydroxide at the scribe, XPS measurements at the scribe after exposure to electrolyte would help understand the oxidation state and type of cerium product formed at the scribe.

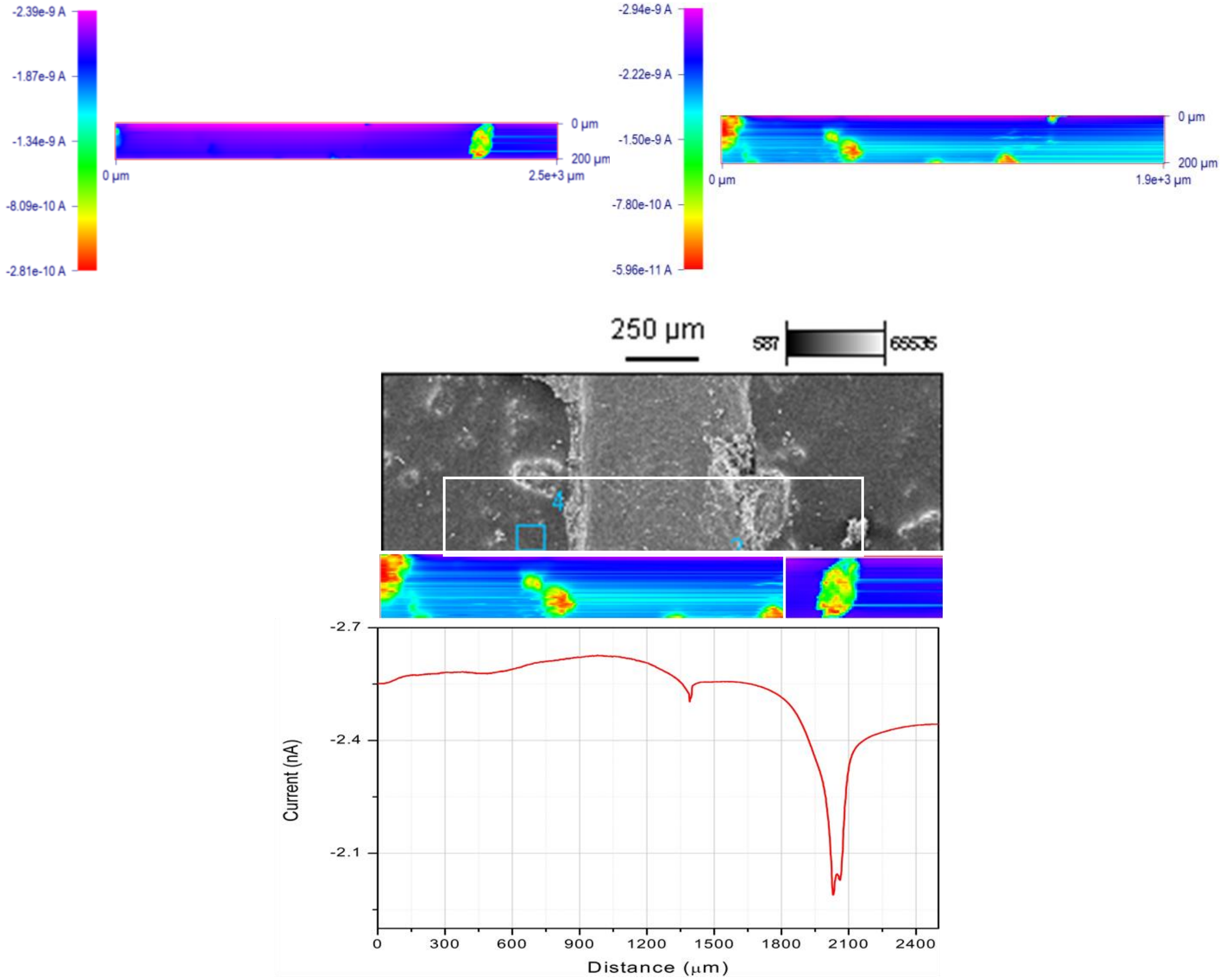

Figure 4.19. Stitched SECM image and a line scan of scribed cerium capsule containing coating with probe potential -0.7 V (vs.Ag/AgCl).

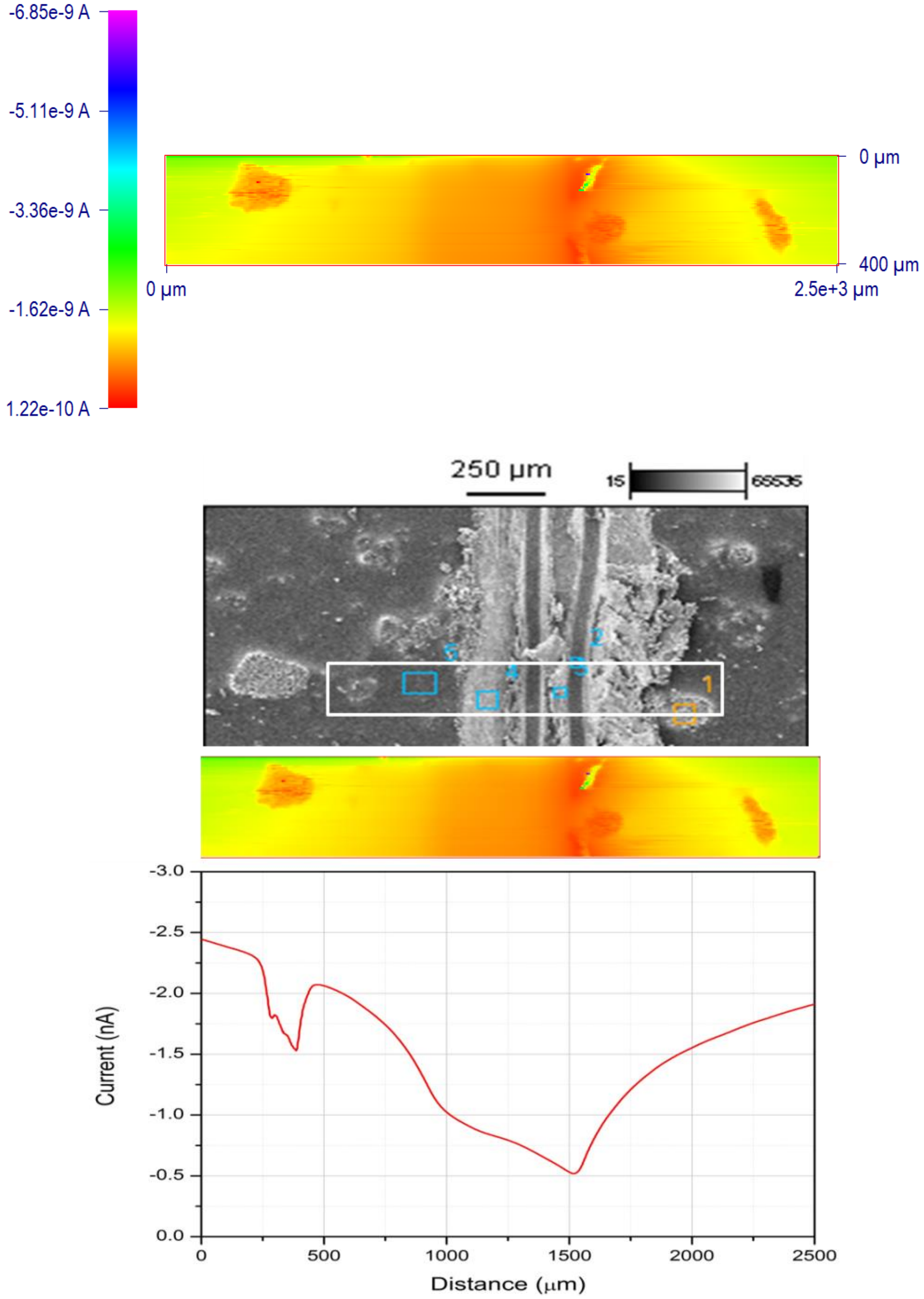

Figure 4.20. Stitched SECM image and a line scan of scribed cerium capsule containing coating with probe potential -0.7 V (vs.Ag/AgCl).

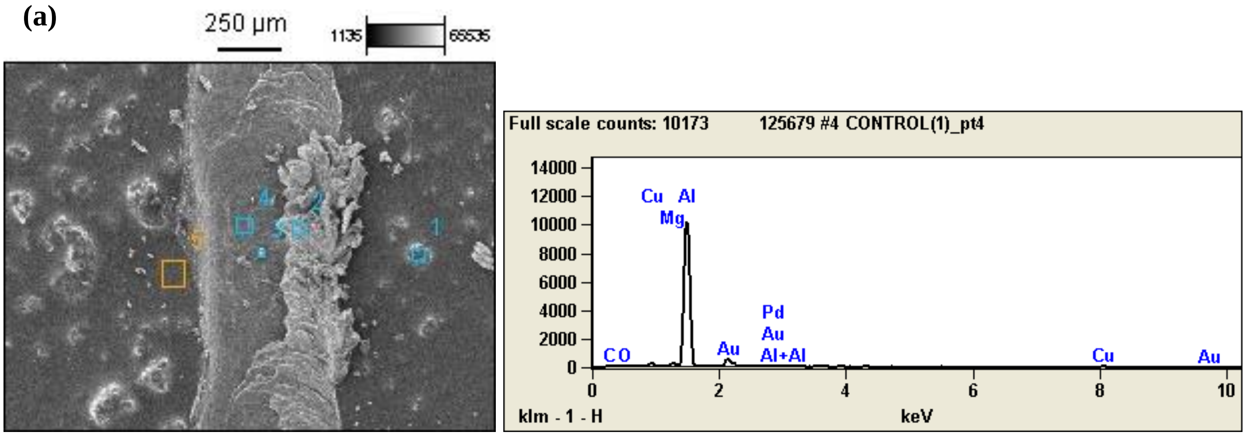

	C-K	O-K	Mg-K	Al-K	S-K	Mn-K	Cu-K	Pd-L	Ce-L
Point 1	10238	1593			2963			2770	72
Point 2	3239	678	895	95599			455	2605	
Point 3	214		196	34779		153	419		
Point 4	791	193	963	88767			463	1291	
Point 5	8672	802			222			1348	0

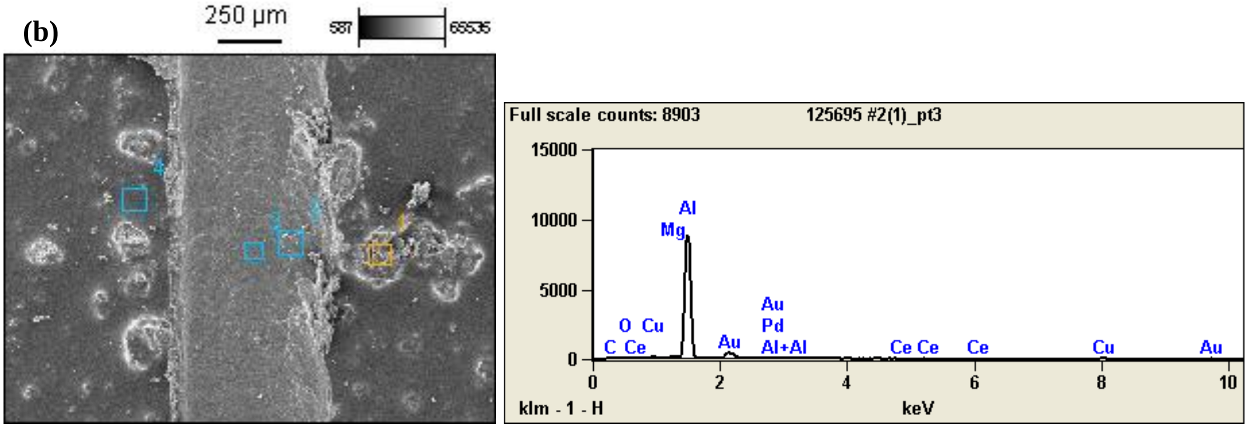

	C-K	N-K	O-K	Mg-K	Al-K	S-K	Mn-K	Cu-K	Pd-L	Ce-L
Point 1	20122		3342			10966			2857	450
Point 2	3624	321	1358	2422	251392		486	1188	4223	126
Point 3	854		217	774	77555			395	1412	16
Point 4	7433		799			146			1096	38

Figure 4.21. EDX measurements on the scribe in a 20 wt. % capsule containing coating (a) before and (b) after exposure to 0.2 M KCl.

4.9. Conclusions

Cerium containing microcapsules were formulated into traditional 2K waterborne epoxy coatings and applied to CRS and AA 2024 T-3 substrates to study the viability of these capsules as potential corrosion inhibiting pigment. It was determined that cerium containing compounds act as anodic inhibitors on the surface of cold rolled steel and as mixed inhibitor on the AA2024 T-3 as determined by OCP measurements and by potentiodynamic polarization measurements. CV measurements revealed that the released cerium corrosion inhibitor was found to be redox active and in the +3 oxidation state. EIS results revealed that the incorporation of the cerium containing capsules in epoxy coatings did not result in detrimental effect to the barrier properties of the coating. ASTM B117 measurements indicated that the inclusion of cerium containing capsules in the coating resulted in reduced creep from the scribe in both CRS and AA2024 T-3 substrates. A closer look at the scribe using SECM revealed that a layer of cerium containing compound may be as an oxide/hydroxide was deposited at the scribe which suppresses the cathodic reaction resulting in the overall reduction in corrosion.

4.10. References

1. Zhao, D.; Sun, J.; Zhang, L.; Tan, Y.; Li, J., Corrosion behavior of rare earth cerium based conversion coating on aluminum alloy. *Journal of Rare Earths* **2010,** 28, Supplement 1, (0), 371-374.
2. Aldykewicz, A. J.; Isaacs, H. S.; Davenport, A. J., The Investigation of Cerium as a Cathodic Inhibitor for Aluminum-Copper Alloys. *Journal of The Electrochemical Society* **1995,** 142, (10), 3342-3350.

3. Yasakau, K. A.; Zheludkevich, M. L.; Lamaka, S. V.; Ferreira, M. G. S., Mechanism of Corrosion Inhibition of AA2024 by Rare-Earth Compounds. *The Journal of Physical Chemistry B* **2006,** 110, (11), 5515-5528.

4. Allachi, H.; Chaouket, F.; Draoui, K., Corrosion inhibition of AA6060 aluminium alloy by lanthanide salts in chloride solution. *Journal of Alloys and Compounds* **2009,** 475, (1–2), 300-303.

5. Hinton, B. R. W., Corrosion inhibition with rare earth metal salts. *Journal of Alloys and Compounds* **1992,** 180, (1–2), 15-25.

6. Bethencourt, M.; Botana, F. J.; Calvino, J. J.; Marcos, M.; RodrÍguez-Chacón, M. A., Lanthanide compounds as environmentally-friendly corrosion inhibitors of aluminium alloys: a review. *Corrosion Science* **1998,** 40, (11), 1803-1819.

7. Forsyth, M.; Forsyth, C. M.; Wilson, K.; Behrsing, T.; Deacon, G. B., ATR characterisation of synergistic corrosion inhibition of mild steel surfaces by cerium salicylate. *Corrosion Science* **2002,** 44, (11), 2651-2656.

8. Fedel, M.; Ahniyaz, A.; Ecco, L. G.; Deflorian, F., Electrochemical investigation of the inhibition effect of CeO2 nanoparticles on the corrosion of mild steel. *Electrochimica Acta*, (0).

9. El-Taib Heakal, F.; Tantawy, N. S.; Shehata, O. S., Influence of cerium (III) ions on corrosion and hydrogen evolution of carbon steel in acid solutions. *International Journal of Hydrogen Energy* 37, (24), 19219-19230.

10. Machkova, M.; Matter, E. A.; Kozhukharov, S.; Kozhukharov, V., Effect of the anionic part of various Ce(III) salts on the corrosion inhibition efficiency of AA2024 aluminium alloy. *Corrosion Science* 69, (0), 396-405.

11. Hinton, B. R. W.; Arnott, D. R.; Ryan, N. E., Cerium Conversion Coatings for the Corrosion Protection of Aluminum *Materials Forum* **1986,** 9, (3), 162-173.
12. Wilson, L.; Hinton, B. R. W. A Method of Forming a Corrosion Resistant Coating. 1987.
13. Lu, Y. C.; Ives, M. B., Chemical treatment with cerium to improve the crevice corrosion resistance of austenitic stainless steels. *Corrosion Science* **1995,** 37, (1), 145-155.
14. Mansfeld, F.; Breslin, C. B.; Pardo, A.; Pérez, F. J., Surface modification of stainless steels: green technology for corrosion protection. *Surface and Coatings Technology* **1997,** 90, (3), 224-228.
15. Amadeh, A.; Allahkaram, S. R.; Hosseini, S. R.; Moradi, H.; Abdolhosseini, A., The use of rare earth cations as corrosion inhibitors for carbon steel in aerated NaCl solution. *Anti-Corrosion Methods and Materials* **2008,** 55, (3), 135-143.
16. Montemor, M. F.; Simões, A. M.; Ferreira, M. G. S., Composition and behaviour of cerium films on galvanised steel. *Progress in Organic Coatings* **2001,** 43, (4), 274-281.
17. García, S. J.; Muster, T. H.; Özkanat, Ö.; Sherman, N.; Hughes, A. E.; Terryn, H.; de Wit, J. H. W.; Mol, J. M. C., The influence of pH on corrosion inhibitor selection for 2024-T3 aluminium alloy assessed by high-throughput multielectrode and potentiodynamic testing. *Electrochimica Acta* **2010,** 55, (7), 2457-2465.
18. Aldykewicz, J. A. J.; Isaacs, H. S.; Davenport, A. J., The Investigation of Cerium as a Cathodic Inhibitor for Aluminum-Copper Alloys. *Journal of The Electrochemical Society* **1995,** 142, (10), 3342-3350.
19. Andreatta, F.; Druart, M. E.; Lanzutti, A.; Lekka, M.; Cossement, D.; Olivier, M. G.; Fedrizzi, L., Localized corrosion inhibition by cerium species on clad AA2024

aluminium alloy investigated by means of electrochemical micro-cell. *Corrosion Science* 65, (0), 376-386.

20. Arenas, M. A.; Bethencourt, M.; Botana, F. J.; de Damborenea, J.; Marcos, M., Inhibition of 5083 aluminium alloy and galvanised steel by lanthanide salts. *Corrosion Science* **2001,** 43, (1), 157-170.

21. Arnott, D. R.; Ryan, N. E.; Hinton, B. R. W.; Sexton, B. A.; Hughes, A. E., Auger and XPS studies of cerium corrosion inhibition on 7075 aluminum alloy. *Applications of Surface Science* **1985,** 22–23, Part 1, (0), 236-251.

22. Davenport, A. J.; Isaacs, H. S.; Kendig, M. W., XANES investigation of the role of cerium compounds as corrosion inhibitors for aluminum. *Corrosion Science* **1991,** 32, (5â€“6), 653-663.

23. Shi, H.; Han, E.-H.; Liu, F., Corrosion protection of aluminium alloy 2024-T3 in 0.05M NaCl by cerium cinnamate. *Corrosion Science* **2011,** 53, (7), 2374-2384.

24. Matter, E. A.; Kozhukharov, S.; Machkova, M.; Kozhukharov, V., Comparison between the inhibition efficiencies of Ce(III) and Ce(IV) ammonium nitrates against corrosion of AA2024 aluminum alloy in solutions of low chloride concentration. *Corrosion Science* 62, (0), 22-33.

25. Pyun, S.-I.; Moon, S.-M., The inhibition mechanism of pitting corrosion of pure aluminum by nitrate and sulfate ions in neutral chloride solution. *Journal of Solid State Electrochemistry* **1999,** 3, (6), 331-336.

26. Paulenova, A.; Creager, S. E.; Navratil, J. D.; Wei, Y., Redox potentials and kinetics of the Ce3+/Ce4+ redox reaction and solubility of cerium sulfates in sulfuric acid solutions. *Journal of Power Sources* **2002,** 109, (2), 431-438.

27. Jin-Tao, Z.; Ji-Ming, H.; Jian-Qing, Z.; Chu-Nan, C., Studies of water transport behavior and impedance models of epoxy-coated metals in NaCl solution by EIS. *Progress in Organic Coatings* **2004,** 51, (2), 145-151.

28. Mansfeld, F., Electrochemical impedance spectroscopy (EIS) as a new tool for investigating methods of corrosion protection. *Electrochimica Acta* **1990,** 35, (10), 1533-1544.

29. Zheludkevich, M. L.; Serra, R.; Montemor, M. F.; Yasakau, K. A.; Miranda Salvado, I. M.; Ferreira, M. G. S., Nanostructured sol–gel coatings doped with cerium nitrate as pre-treatments for AA2024-T3: Corrosion protection performance. *Electrochimica Acta* **2005,** 51, (2), 208-217.

30. Heming, W.; Robert, A., Encapsulated cerium nitrate inhibitors to provide high-performance anti-corrosion sol–gel coatings on mild steel. *Corrosion Science* **2008,** 50, (4), 1142-1148.

31. Trabelsi.W.; Cecilio, P.; Ferreira, M. G. S.; Montemor, M. F., Electrochemical assessment of the self healing properties of Ce-doped silane solutions for the pretreatment of galvanized steel substrates. *Progress in Organic Coatings* **2005,** 54, 276-284.

32. El-Taib Heakal, F.; Tantawy, N. S.; Shehata, O. S., Influence of cerium (III) ions on corrosion and hydrogen evolution of carbon steel in acid solutions. *International Journal of Hydrogen Energy* **2012,** 37, (24), 19219-19230.

CHAPTER 5. SUMMARY

Chromates have been widely and successfully used as corrosion inhibitors applied on a large number of metal alloys due to their high efficiency and low cost. However, hexavalent chromes present a very high toxicity leading to legislation that prohibits the use of such chemicals. The need for a new alternative and an environmentally friendly approach has led to the use of rare earth metals and their salts as corrosion inhibitors. Cerium salts were determined to reduce corrosion on metal alloys by inhibiting/reducing the kinetics of the cathodic reaction in a corrosion cell. However, most of the cerium salts are highly water soluble and difficult to incorporate in coatings as their individual salts. In order to reduce the solubility of such salts in coatings, an encapsulation approach was employed. To increase the efficiency of cathodic inhibition, a polymer with high sensitivity to hydroxyl ions was designed by incorporating disulfide bonds.

In the reported work, pH responsive capsules were synthesized using internally phase separated emulsion polymerization and coatings with the synthesized capsules were formulated for aluminum 2024 T-3 and cold rolled steel substrates. The incorporation, release and corrosion protection assessment provided by these coatings was carried out using various characterization techniques. The use of pH responsive capsules in coatings enables the use/incorporation of reactive or incompatible materials in coatings to improve the corrosion protection of metal substrates while making the system completely autonomous.

Spherical microcapsules with a core shell morphology containing a cerium core were synthesized as confirmed by SEM and TEM. The synthesized capsules exhibited pH depended release as observed using UV-vis spectroscopy, ICP and CV. The incorporated cerium within the capsules behaved as a cathodic inhibitor on the surface of aluminum alloy 2024 T-3 and as an anodic inhibitor on cold rolled steel substrate. The incorporation of capsules in the coatings not only increased the barrier properties of the coating but also was determined to inhibit corrosion by increasing the polarization resistance of the metal using EIS. The cerium capsule containing coatings exhibited reduced underscribe corrosion in both aluminum 20204 T-3 and cold rolled steel substrate. It was also revealed using SVET that the deposition of cerium hydroxide/oxide at the cathodic sites resulted in the reduced metallic dissolution of aluminum alloy. The combined use of SECM and SEM/EDS confirmed the deposition of released cerium from the capsules at the scribe reducing the corrosion.

In summary, in the reported research, new coating system containing pH responsive microcapsules for the corrosion protection of aluminum and steel alloys were developed as a replacement for hexavalent chromes. These new coating systems were characterized with global and local electrochemical techniques to assess the corrosion performance and the possible mechanism of corrosion inhibition using cerium salts.

CHAPTER 6. FUTURE STUDIES

pH responsive capsules synthesized using internal phase separation was determined to be a viable method for the synthesis of microcapsules containing water core/or water soluble corrosion inhibitors as potential replacement for hexavalent chromes. In the approach used presently, the oxidative polymerization of the UF resin and thiol crosslinker to generate disulfide bond containing polymer shell also oxidizes the corrosion inhibitor leading to a low efficiency of corrosion inhibition. As an alternative to thiol crosslinker PEMP used, a polymer adduct /pre-polymer containing disulfide bonds could be synthesized prior to the phase separated polymerization reaction in order to eliminate the use of hydrogen peroxide (or any other oxidizer) in the synthesis of the capsules. Some low molecular weight chemicals containing disulfide bonds such as 2-hydroxyethyl disulfide could also be used to crosslink the amino-resin to include disulfide linkages without oxidizing the corrosion inhibitor. One of the major issues faced during the formulation of coatings was the agglomeration and settling of the capsules. To improve this, several modifications could also be made on the polymer backbone to include dispersants in order to better disperse the capsules in coatings. Improvement by including certain functional groups on the shell is also suggested in order to increase the compatibility of the capsules in the coating system.

As a part of this work, it has been demonstrated that cerium nitrate could be used as a corrosion inhibitor for steel and aluminum alloy 2024 T-3. There is a plethora of water soluble corrosion inhibitors that can be encapsulated using the polymerization technique and their impact on corrosion inhibition can be investigated as a replacement for chromes. Another approach to effective corrosion inhibition may also be the inclusion of an anodic inhibitor and developing a coating that works synergistically to inhibit corrosion effectively. As a word of caution, preliminary investigation of the corrosion inhibitor with individual chemicals employed in the synthesis of the capsules is very important as it was found out early in the development of these capsules that sodium molybdate and hydrogen peroxide have an explosive interaction in solution.

Due to certain limitations in the availability of characterization techniques and funds, certain techniques were not employed to better investigate the synthesized capsules and their effect on corrosion processes. Even though it has already been investigated by several authors, the use of X-ray Photoelectron Spectroscopy (XPS) to characterize the corrosion product formed at the interface/scribe after exposure to a corrosive environment could be helpful to understand the release mechanism and the throw power of capsules in a coating. This data would enable one to determine the optimum concentration and distribution of capsules in the coating. Localized electrochemistry by the use of biological techniques such as the patch clamp technique could also be used to study an individual microcapsule to measure the local concentration of the corrosion inhibitor, the oxidation state and the electrochemical properties of the corrosion inhibitor within the capsule. Using scanning ion electrode technique (SIET) release of cerium ions as a function of pH change in solution could also be monitored.

APPENDIX A. CIRCUIT MODELS

A.1. Results and discussion

Electrochemical Impedance spectroscopy (EIS) data sets were circuit fitted using Scribner's Zview software (version 3.3a). Representative data sets are reported in this appendix. The aim of the experiment was to obtain interfacial information about the microcapsule containing coating as a consequence of the release of cerium from the microcapsules. Even though numerous reports of circuit modeling of electrochemical impedance spectroscopy are available for cerium pretreatments and cerium salts in the electrolyte solution, very few reports of cerium salts encapsulated in a coating exist in the literature.

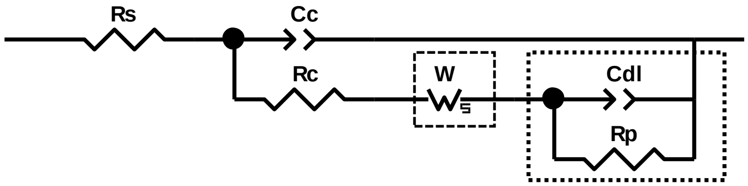

Figure A.1. Circuit model used to model a coated metal substrate.

The barrier properties and corrosion behavior of 2K epoxy coatings containing 0%, 5%, 10%, 15% and 20% weight percentages were studied using EIS applied on Cold Rolled Steel substrates and aluminum 2024 T-3 immersed in 5% NaCl solution. Figure A summarizes a typical equivalent circuit model for cerium containing coating system. The dotted boxes around elements indicate that the components evolve as a function of time of exposure to an electrolyte. In this model, Rs is the uncompensated resistance between the reference electrode and the working electrode in the electrolyte solution fixed at 10 Ω, Cc is the coating capacitance as a result of the dielectric nature of the coating system; W is the Warburg element associated with the diffusion of the active species; Cdl is the double layer capacitance at the metal coating interface; Rp is the polarization resistance of the metal due to corrosion process.

A.2. Circuit models for epoxy coatings containing cerium capsules on AA2024 T-3

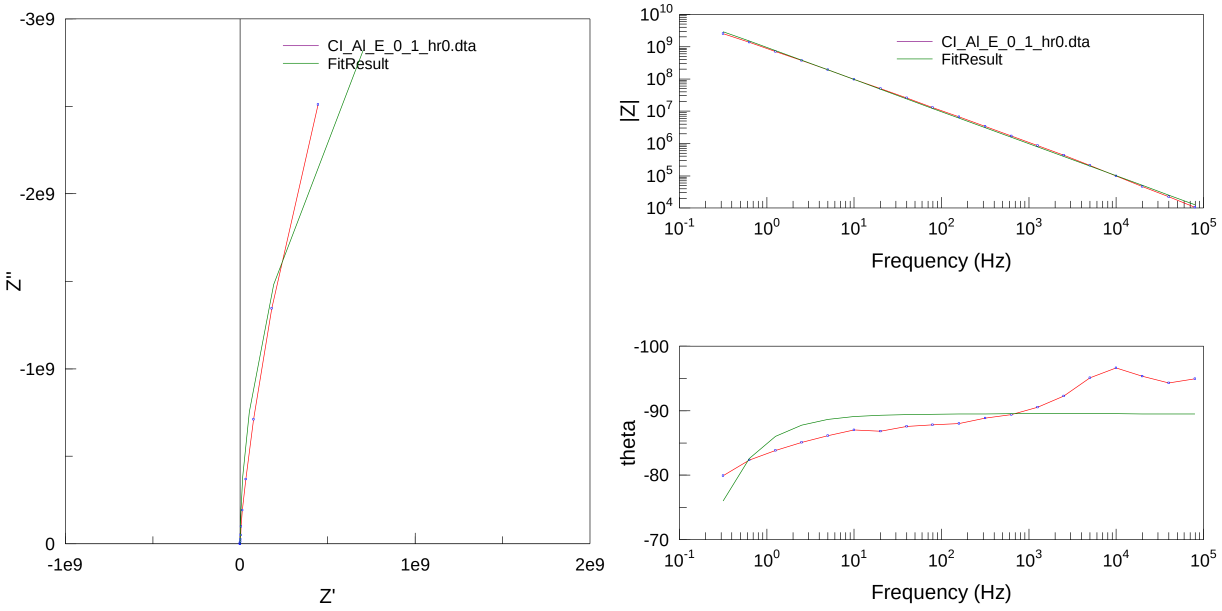

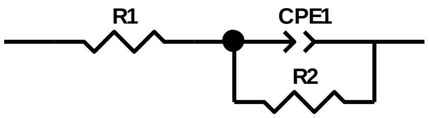

Element	Freedom	Value	Error	Error %
R1	Fixed(X)	10	N/A	N/A
CPE1-T	Free(±)	1.6869E-10	6.236E-12	3.6967
CPE1-P	Free(±)	0.99474	0.0047003	0.47252
R2	Free(±)	1.241E10	3.5018E09	28.218

Chi-Squared:	0.3648
Weighted Sum of Squares:	12.768
Data File:	C:\Users\Abhijit\Dropbox\EIS Models\AA2024\CI_Al_E_0_1_hr0.dta
Circuit Model File:	
Mode:	Run Fitting / All Data Points (1 - 19)
Maximum Iterations:	100
Optimization Iterations:	0
Type of Fitting:	Complex
Type of Weighting:	Calc-Modulus

Figure A.2. Equivalent Circuit Model for Epoxy coating on AA2024 with 0% cerium capsules after 0 hours of immersion in 5% NaCl solution.

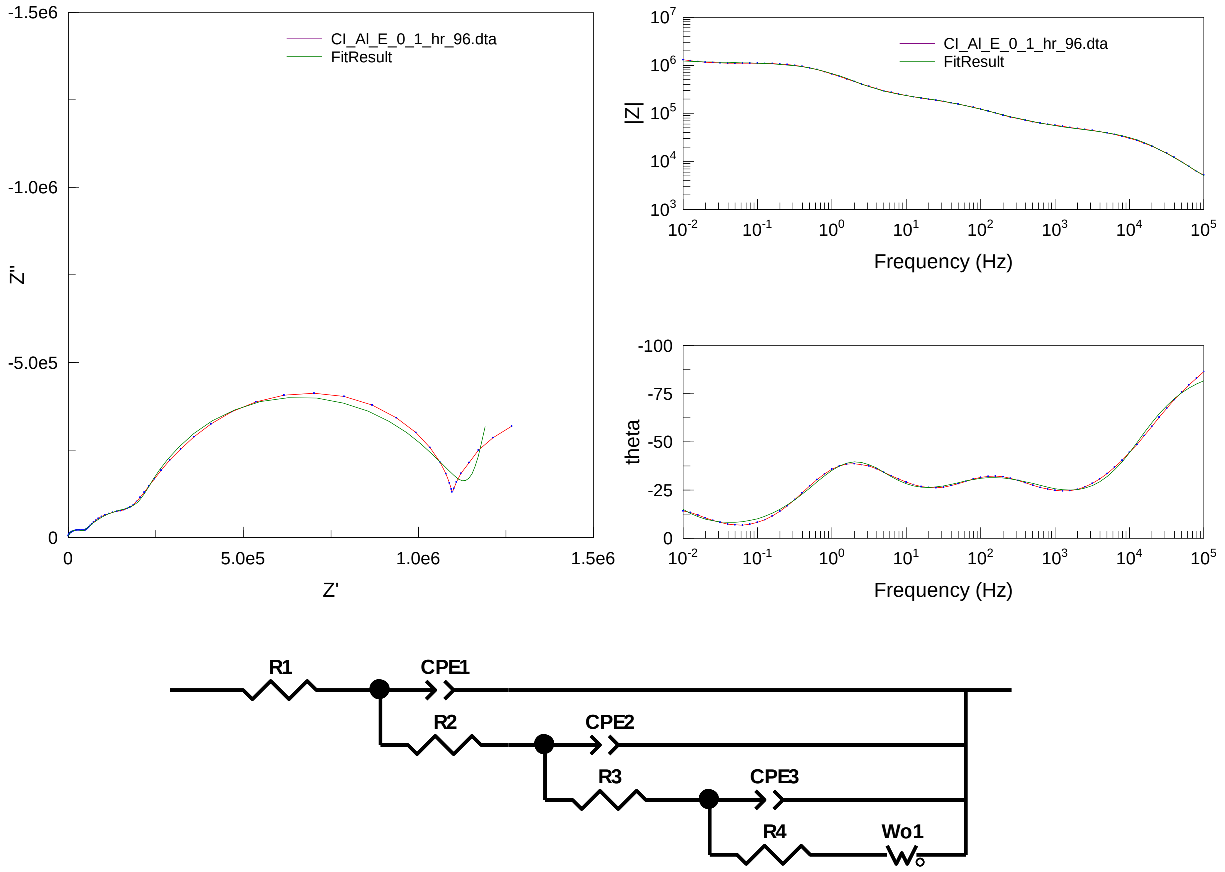

Element	Freedom	Value	Error	Error %
R1	Fixed(X)	10	N/A	N/A
CPE1-T	Free(+)	3.744E-10	2.9123E-11	7.7786
CPE1-P	Free(+)	0.98573	0.006133	0.62218
R2	Free(+)	41923	866.28	2.0664
CPE2-T	Free(+)	1.0875E-07	1.4027E-08	12.898
CPE2-P	Free(+)	0.67668	0.017527	2.5901
R3	Free(+)	2.4932E05	17262	6.9236
CPE3-T	Free(+)	1.8758E-07	3.984E-08	21.239
CPE3-P	Free(+)	0.9576	0.060252	6.292
R4	Free(+)	8.7059E05	2.1773E05	25.009
Wo1-R	Free(+)	24782	6.1344E05	2475.3
Wo1-T	Free(+)	0.98008	27.132	2768.3
Wo1-P	Free(+)	0.4471	0.023495	5.255

Chi-Squared:	0.0012089
Weighted Sum of Squares:	0.15716

Figure A.3. Equivalent Circuit Model for Epoxy coating on AA2024 with 0% cerium capsules after 96 hours of immersion in 5% NaCl solution.

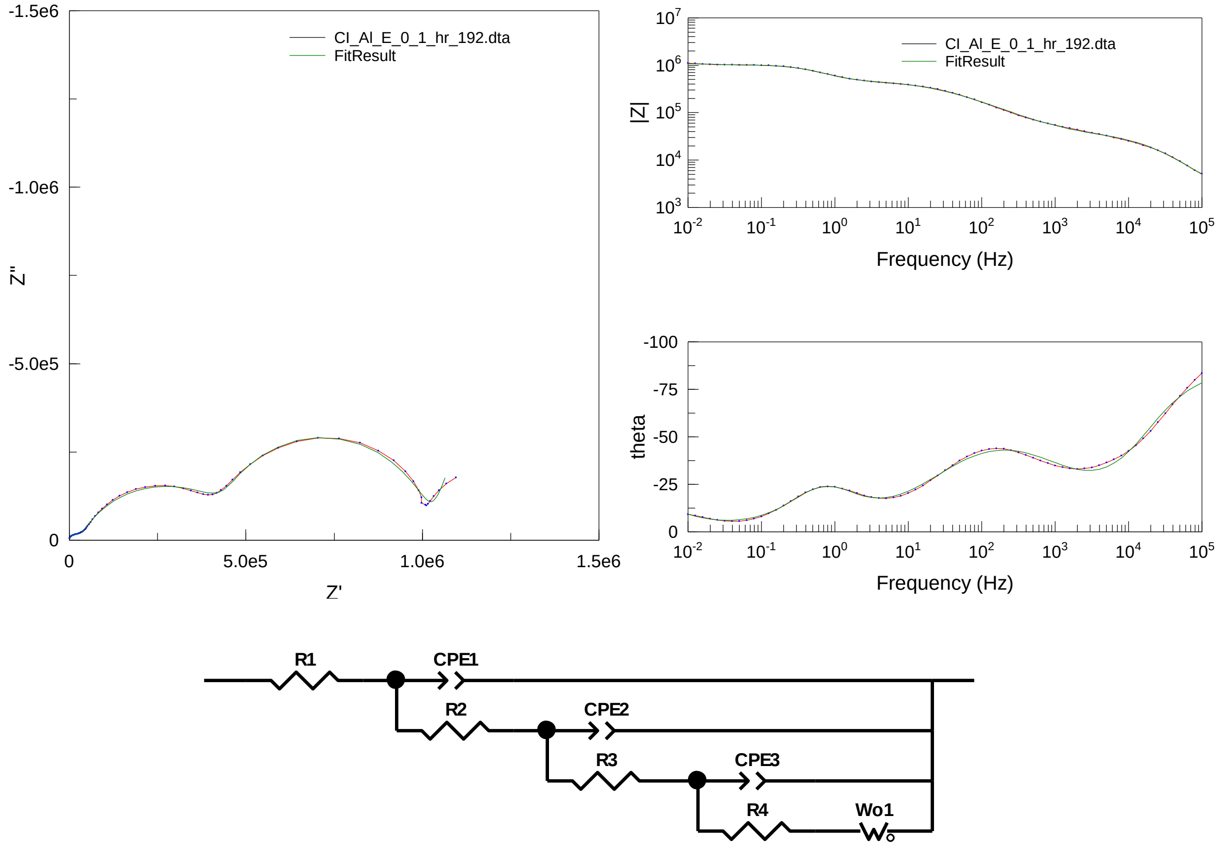

Element	Freedom	Value	Error	Error %
R1	Fixed(X)	10	N/A	N/A
CPE1-T	Free(+)	4.747E-10	4.136E-11	8.7129
CPE1-P	Free(+)	0.96841	0.0068329	0.70558
R2	Free(+)	33053	628.36	1.9011
CPE2-T	Free(+)	5.5319E-08	2.2877E-09	4.1355
CPE2-P	Free(+)	0.71416	0.0060234	0.84342
R3	Free(+)	4.7001E05	6029	1.2827
CPE3-T	Free(+)	5.8044E-07	1.8187E-08	3.1333
CPE3-P	Fixed(X)	1	N/A	N/A
R4	Free(+)	5.2553E05	3.2688E06	622
Wo1-R	Free(+)	72.05	9.8085E06	1.3613E07
Wo1-T	Free(+)	0.0011704	195.75	1.6725E07
Wo1-P	Free(+)	0.40697	0.037726	9.27

Chi-Squared:	0.0013499
Weighted Sum of Squares:	0.17684

Figure A.4. Equivalent Circuit Model for Epoxy coating on AA2024 with 0% cerium capsules after 192 hours of immersion in 5% NaCl solution.

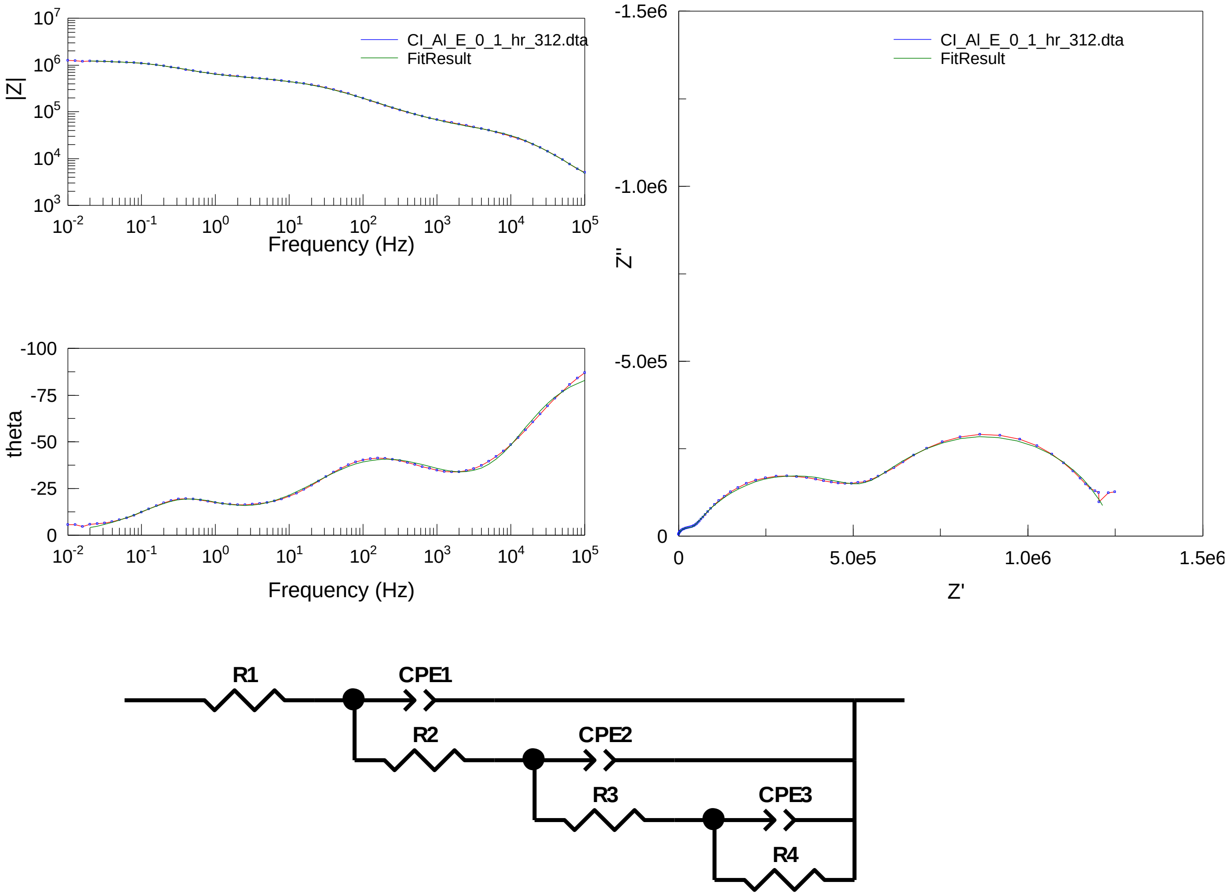

Element	Freedom	Value	Error	Error %
R1	Fixed(X)	10	N/A	N/A
CPE1-T	Free(+)	4.1758E-10	2.694E-11	6.4515
CPE1-P	Free(+)	0.9822	0.0054487	0.55474
R2	Free(+)	40874	758.26	1.8551
CPE2-T	Free(+)	5.9061E-08	2.4214E-09	4.0998
CPE2-P	Free(+)	0.68437	0.005911	0.86371
R3	Free(+)	5.6942E05	8846.8	1.5537
CPE3-T	Free(+)	1.0494E-06	2.9443E-08	2.8057
CPE3-P	Free(+)	0.87692	0.020086	2.2905
R4	Free(+)	6.1499E05	15545	2.5277

Chi-Squared: 0.00094873

Weighted Sum of Squares: 0.11859

Figure A.5. Equivalent Circuit Model for Epoxy coating on AA2024 with 0% cerium capsules after 312 hours of immersion in 5% NaCl solution.

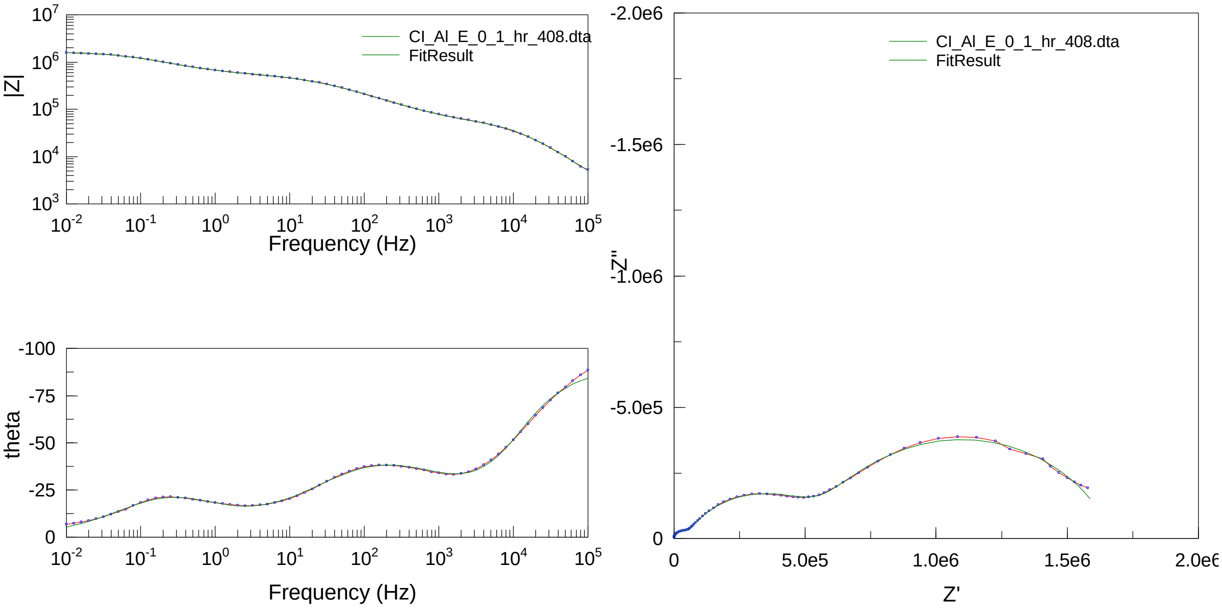

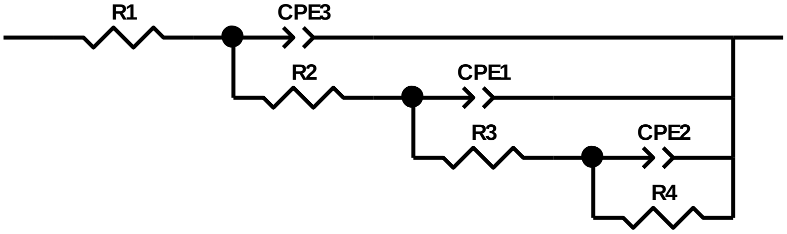

Element	Freedom	Value	Error	Error %
R1	Fixed(X)	10	N/A	N/A
CPE3-T	Free(+)	3.097E-10	1.2825E-12	0.41411
CPE3-P	Fixed(X)	1	N/A	N/A
R2	Free(+)	50873	427.97	0.84125
CPE1-T	Free(+)	5.8994E-08	1.8295E-09	3.1012
CPE1-P	Free(+)	0.67034	0.0044033	0.65688
R3	Free(+)	5.5363E05	6890.2	1.2445
CPE2-T	Free(+)	1.1238E-06	1.6963E-08	1.5094
CPE2-P	Free(+)	0.73841	0.010241	1.3869
R4	Free(+)	1.0794E06	15942	1.4769

Chi-Squared: 0.00047075
Weighted Sum of Squares: 0.063081

Figure A.6. Equivalent Circuit Model for Epoxy coating on AA2024 with 0% cerium capsules after 408 hours of immersion in 5% NaCl solution.

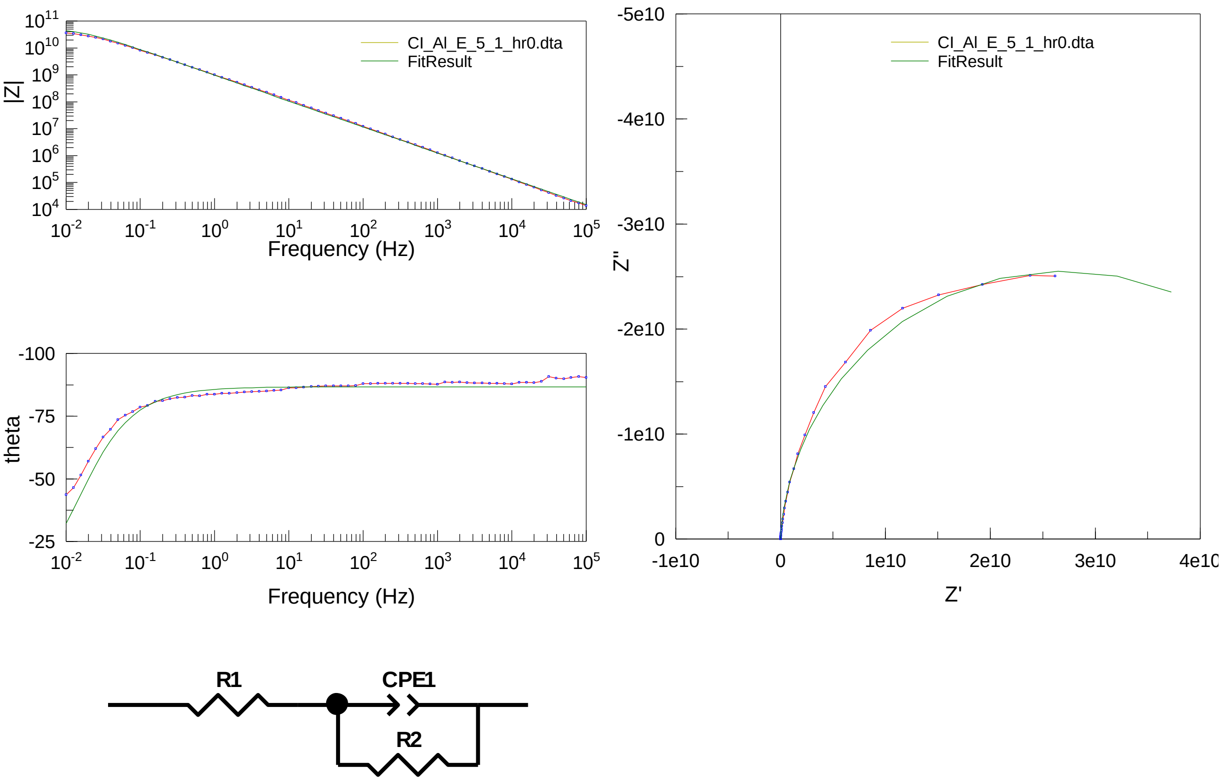

Element	Freedom	Value	Error	Error %
R1	Fixed(X)	10	N/A	N/A
CPE1-T	Free(+)	1.7451E-10	2.0696E-12	1.1859
CPE1-P	Free(+)	0.96355	0.0016485	0.17109
R2	Free(+)	5.4063E10	1.9781E09	3.6589

Chi-Squared: 0.044013

Weighted Sum of Squares: 6.1178

Figure A.7. Equivalent Circuit Model for Epoxy coating on AA2024 with 5% cerium capsules after 0 hours of immersion in 5% NaCl solution.

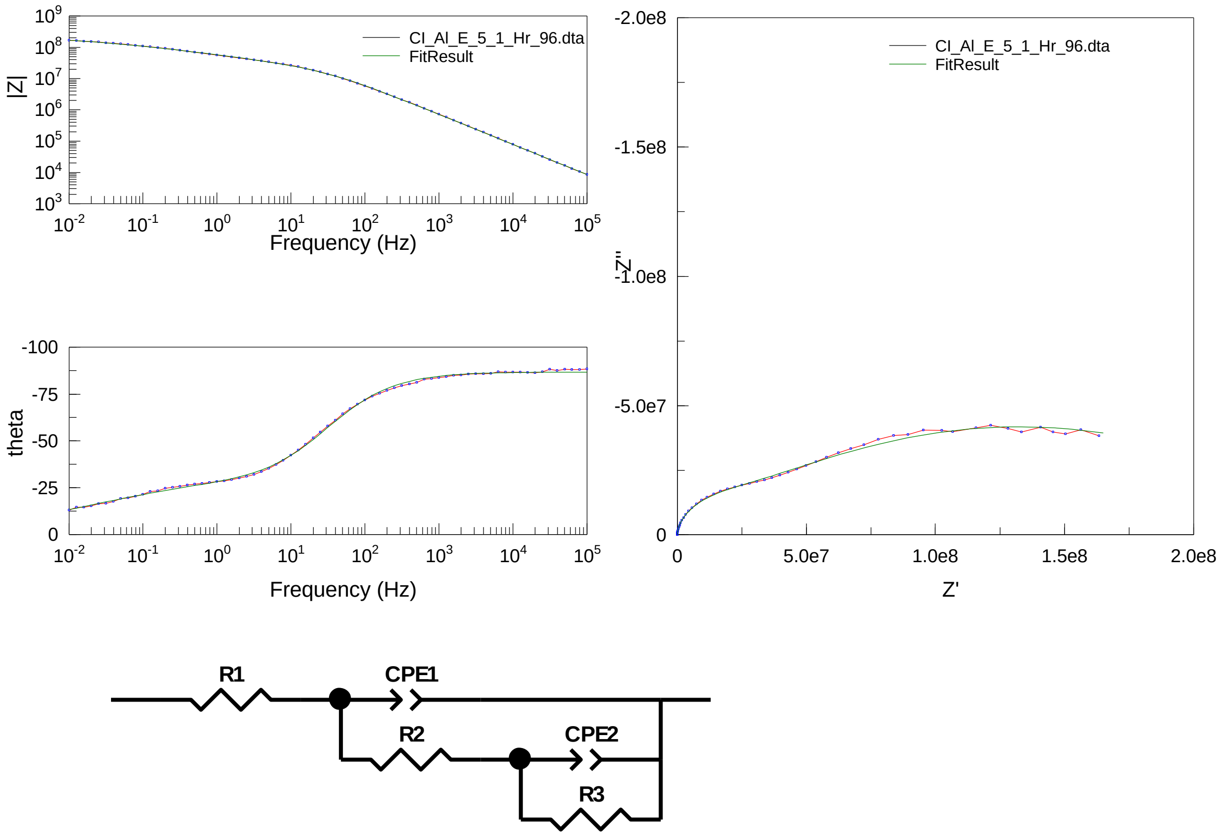

Element	Freedom	Value	Error	Error %
R1	Fixed(X)	10	N/A	N/A
CPE1-T	Free(+)	3.0203E-10	3.34E-12	1.1059
CPE1-P	Free(+)	0.96395	0.0010561	0.10956
R2	Free(+)	1.5658E07	6.1201E05	3.9086
CPE2-T	Free(+)	8.4337E-09	8.2686E-11	0.98042
CPE2-P	Free(+)	0.41374	0.0063494	1.5346
R3	Free(+)	2.4253E08	6.0371E06	2.4892

Chi-Squared:	0.00078982
Weighted Sum of Squares:	0.10741

Figure A.8. Equivalent Circuit Model for Epoxy coating on AA2024 with 5% cerium capsules after 96 hours of immersion in 5% NaCl solution.

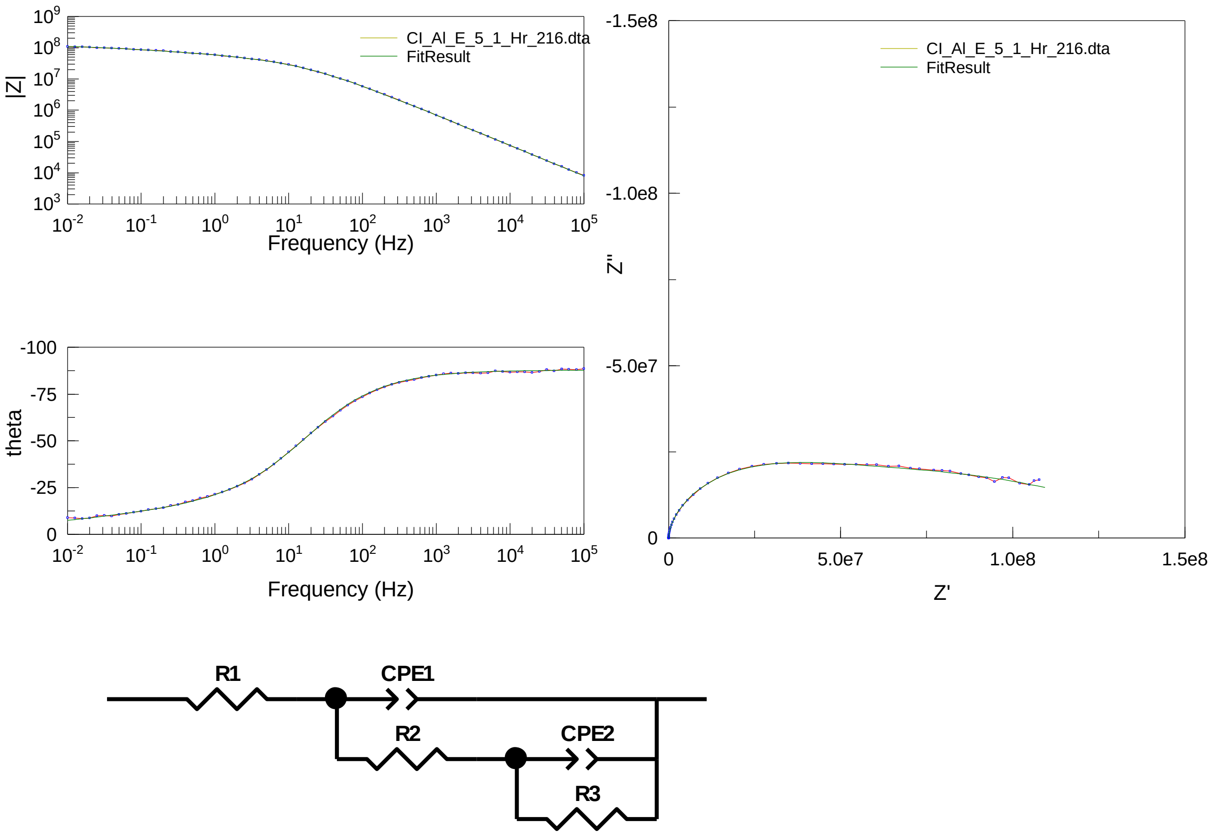

Element	Freedom	Value	Error	Error %
R1	Fixed(X)	10	N/A	N/A
CPE1-T	Free(+)	2.7455E-10	3.8166E-12	1.3901
CPE1-P	Free(+)	0.97645	0.0011552	0.11831
R2	Free(+)	2.5113E06	1.6767E06	66.766
CPE2-T	Free(+)	6.2735E-09	1.3128E-10	2.0926
CPE2-P	Free(+)	0.29925	0.0077205	2.5799
R3	Free(+)	1.4834E08	3.9547E06	2.666

Chi-Squared:	0.00033838
Weighted Sum of Squares:	0.046019

Figure A.9. Equivalent Circuit Model for Epoxy coating on AA2024 with 5% cerium capsules after 216 hours of immersion in 5% NaCl solution.

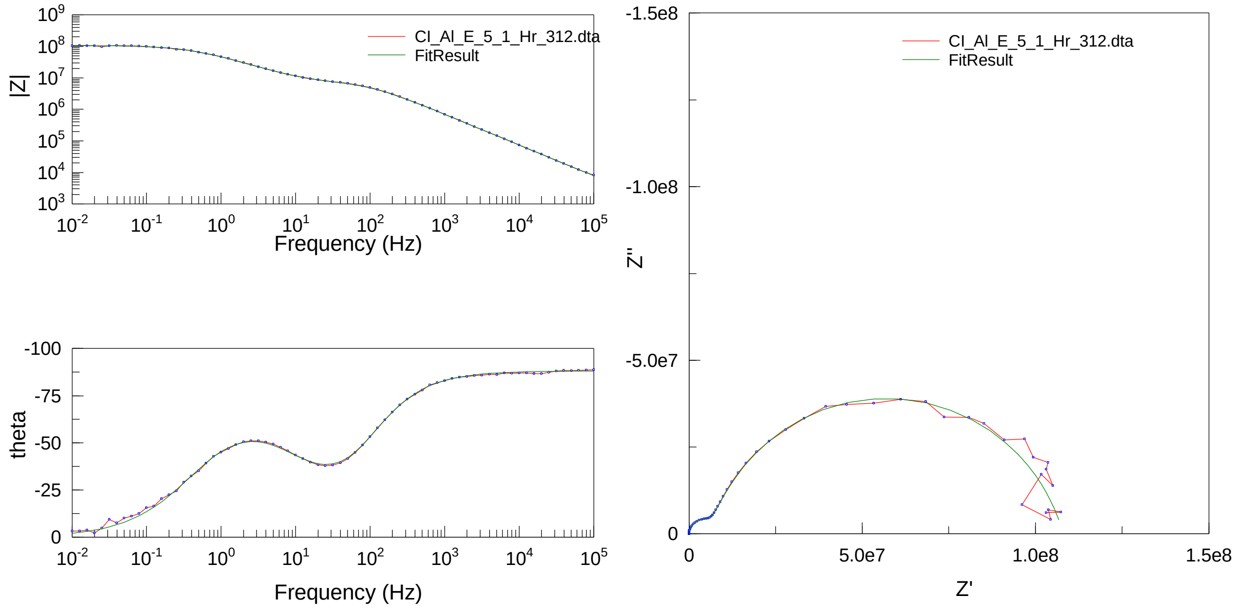

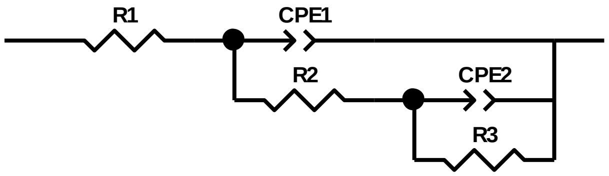

Element	Freedom	Value	Error	Error %
R1	Fixed(X)	10	N/A	N/A
CPE1-T	Free(+)	2.6992E-10	3.4776E-12	1.2884
CPE1-P	Free(+)	0.9792	0.0012397	0.1266
R2	Free(+)	7.911E06	75835	0.9586
CPE2-T	Free(+)	4.0026E-09	4.2335E-11	1.0577
CPE2-P	Free(+)	0.82213	0.0037847	0.46035
R3	Free(+)	1.0005E08	5.4242E05	0.54215

Chi-Squared:	0.0014616
Weighted Sum of Squares:	0.19878

Figure A.10. Equivalent Circuit Model for Epoxy coating on AA2024 with 5% cerium capsules after 312 hours of immersion in 5% NaCl solution.

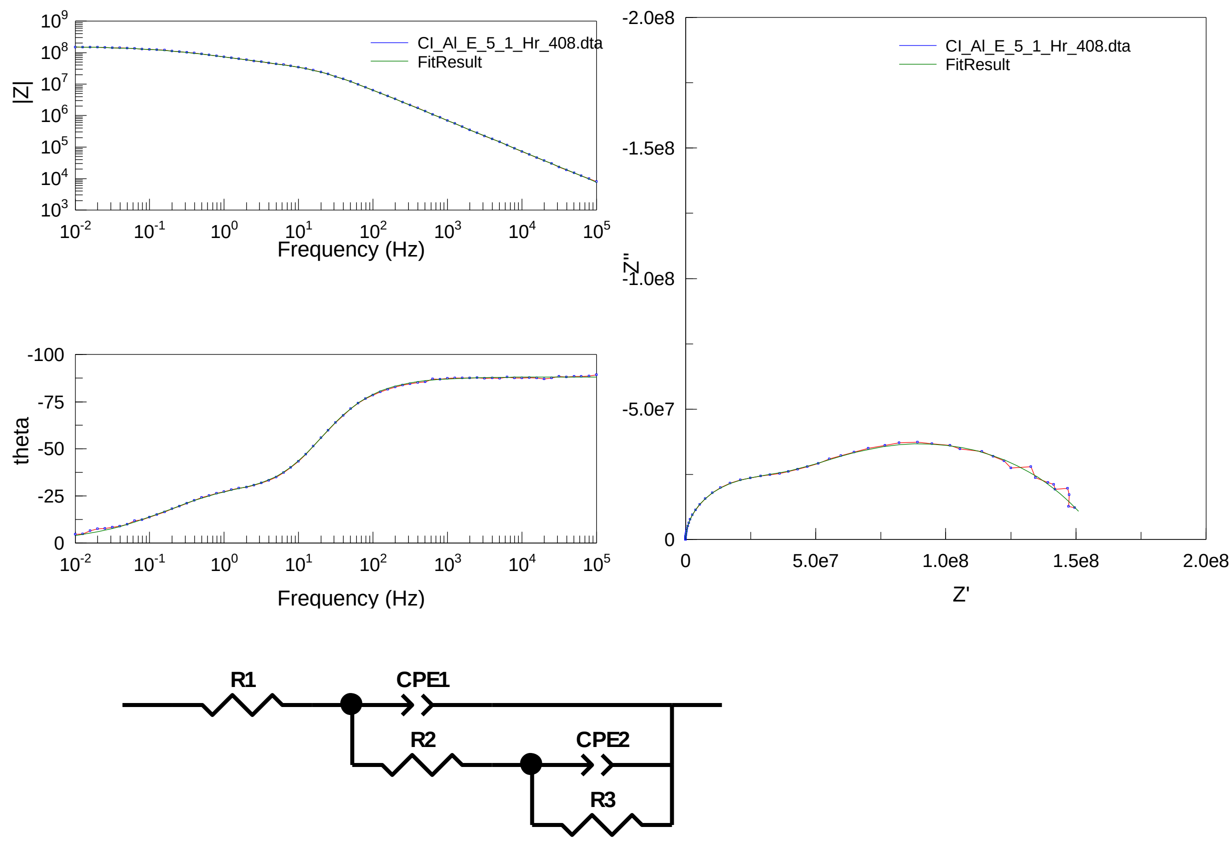

Element	Freedom	Value	Error	Error %
R1	Fixed(X)	10	N/A	N/A
CPE1-T	Free(+)	2.7405E-10	1.424E-12	0.51961
CPE1-P	Free(+)	0.97906	0.00052685	0.053812
R2	Free(+)	3.8293E07	3.5468E05	0.92623
CPE2-T	Free(+)	5.5118E-09	4.8155E-11	0.87367
CPE2-P	Free(+)	0.62558	0.0051117	0.81711
R3	Free(+)	1.2117E08	9.1697E05	0.75676

Chi-Squared:	0.00050455
Weighted Sum of Squares:	0.068618

Figure A.11. Equivalent Circuit Model for Epoxy coating on AA2024 with 5% cerium capsules after 408 hours of immersion in 5% NaCl solution.

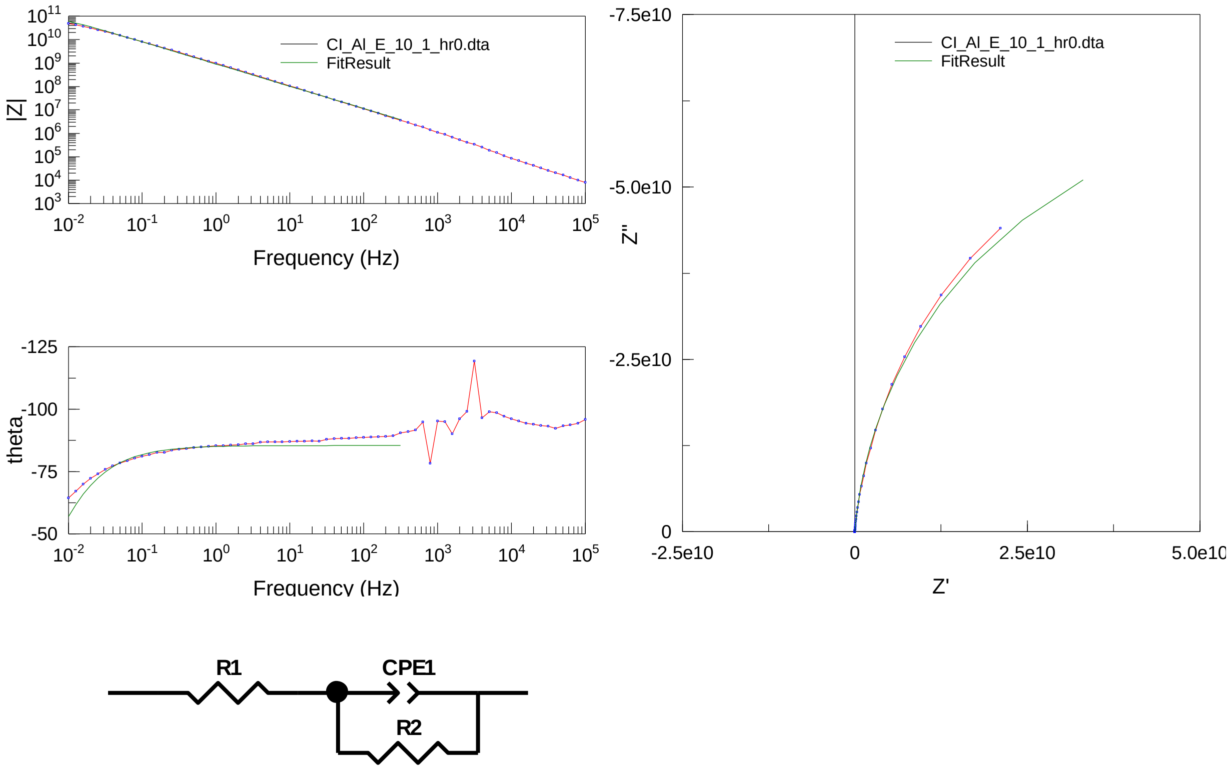

Element	Freedom	Value	Error	Error %
R1	Fixed(X)	10	N/A	N/A
CPE1-T	Free(+)	1.9172E-10	1.999E-12	1.0427
CPE1-P	Free(+)	0.94959	0.0025769	0.27137
R2	Free(+)	1.2736E11	8.3309E09	6.5412

Chi-Squared:	0.026589
Weighted Sum of Squares:	2.3664

Figure A.12. Equivalent Circuit Model for Epoxy coating on AA2024 with 10% cerium capsules after 0 hours of immersion in 5% NaCl solution.

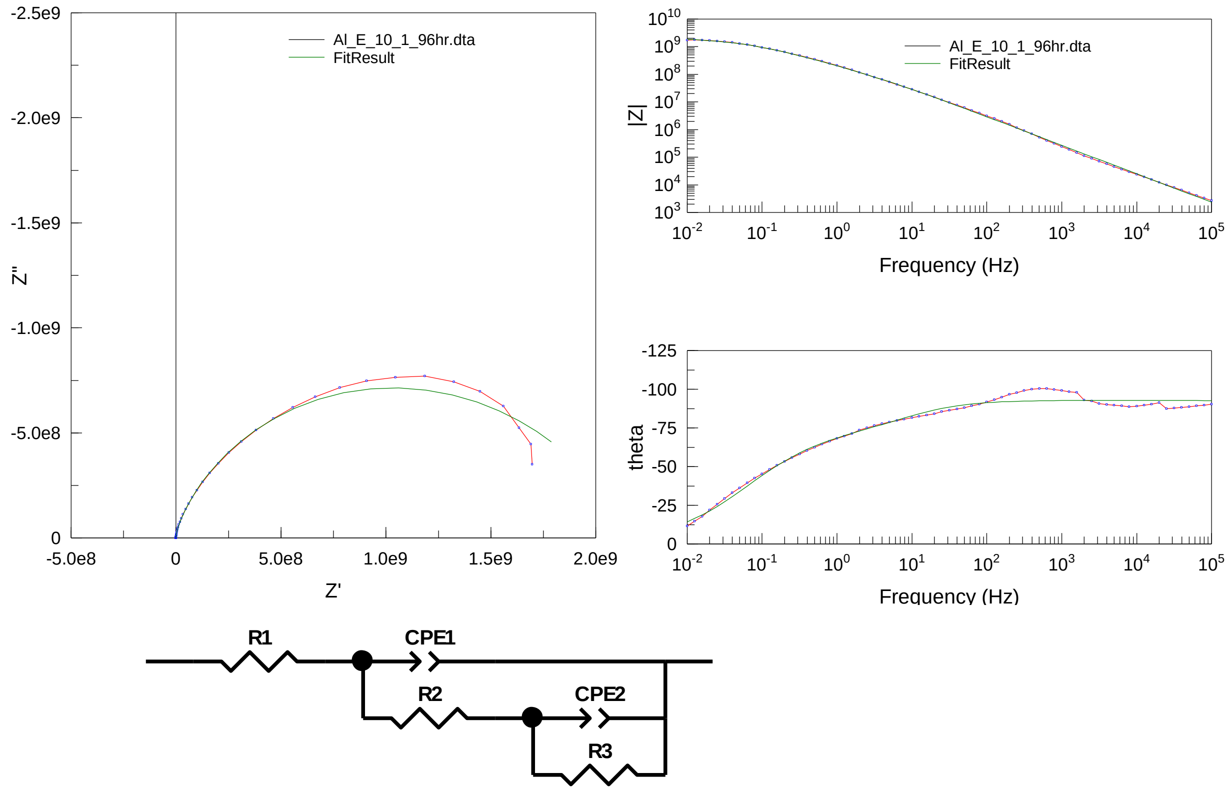

Element	Freedom	Value	Error	Error %
R1	Fixed(X)	10	N/A	N/A
CPE1-T	Free(±)	4.4477E-10	1.4918E-11	3.3541
CPE1-P	Free(±)	1.032	0.003451	0.3344
R2	Free(±)	9.4752E07	2.4771E07	26.143
CPE2-T	Free(±)	8.531E-10	3.4482E-11	4.042
CPE2-P	Free(±)	0.65165	0.027871	4.277
R3	Free(±)	2.0866E09	1.172E08	5.6168

Chi-Squared: 0.037883
Weighted Sum of Squares: 5.1521

Data File: C:\Users\Abhijit\Desktop\AA2024\Al_E_10_1_96hr.dta
Circuit Model File:
Mode: Run Fitting / All Data Points (1 - 71)
Maximum Iterations: 100
Optimization Iterations: 0
Type of Fitting: Complex
Type of Weighting: Calc-Modulus

Figure A.13. Equivalent Circuit Model for Epoxy coating on AA2024 with 10% cerium capsules after 96 hours of immersion in 5% NaCl solution.

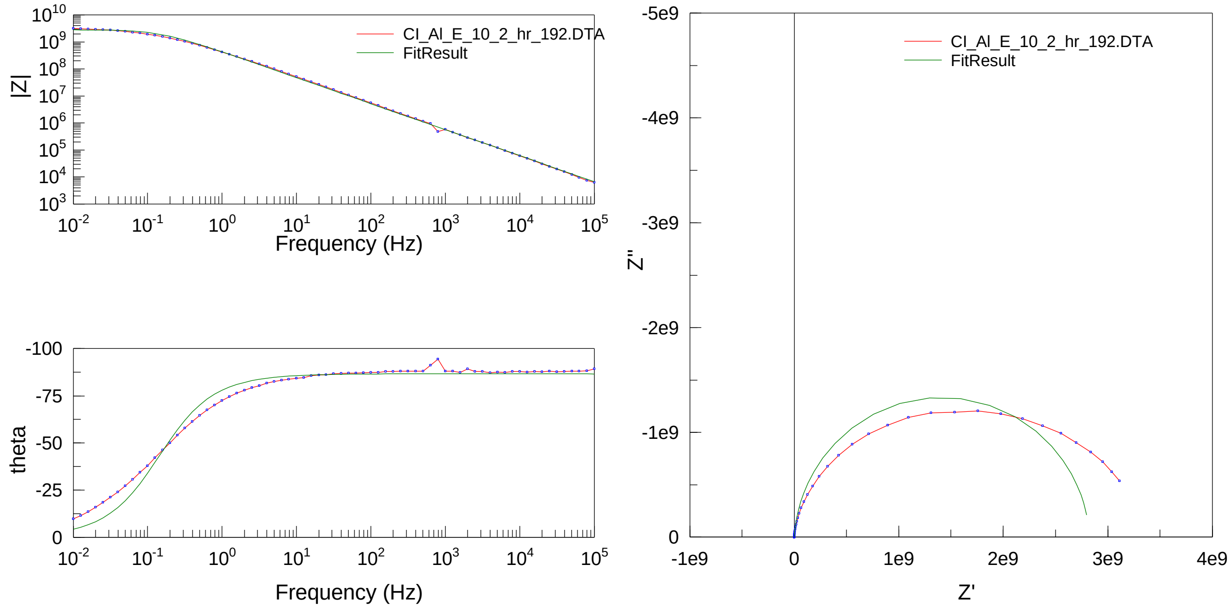

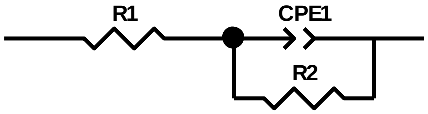

Element	Freedom	Value	Error	Error %
R1	Fixed(X)	10	N/A	N/A
CPE1-T	Free(+)	3.8826E-10	7.0788E-12	1.8232
CPE1-P	Free(+)	0.96301	0.0023632	0.2454
R2	Free(+)	2.827E09	5.928E07	2.0969

Chi-Squared:	0.053627
Weighted Sum of Squares:	7.4541

Figure A.14. Equivalent Circuit Model for Epoxy coating on AA2024 with 10% cerium capsules after 192 hours of immersion in 5% NaCl solution.

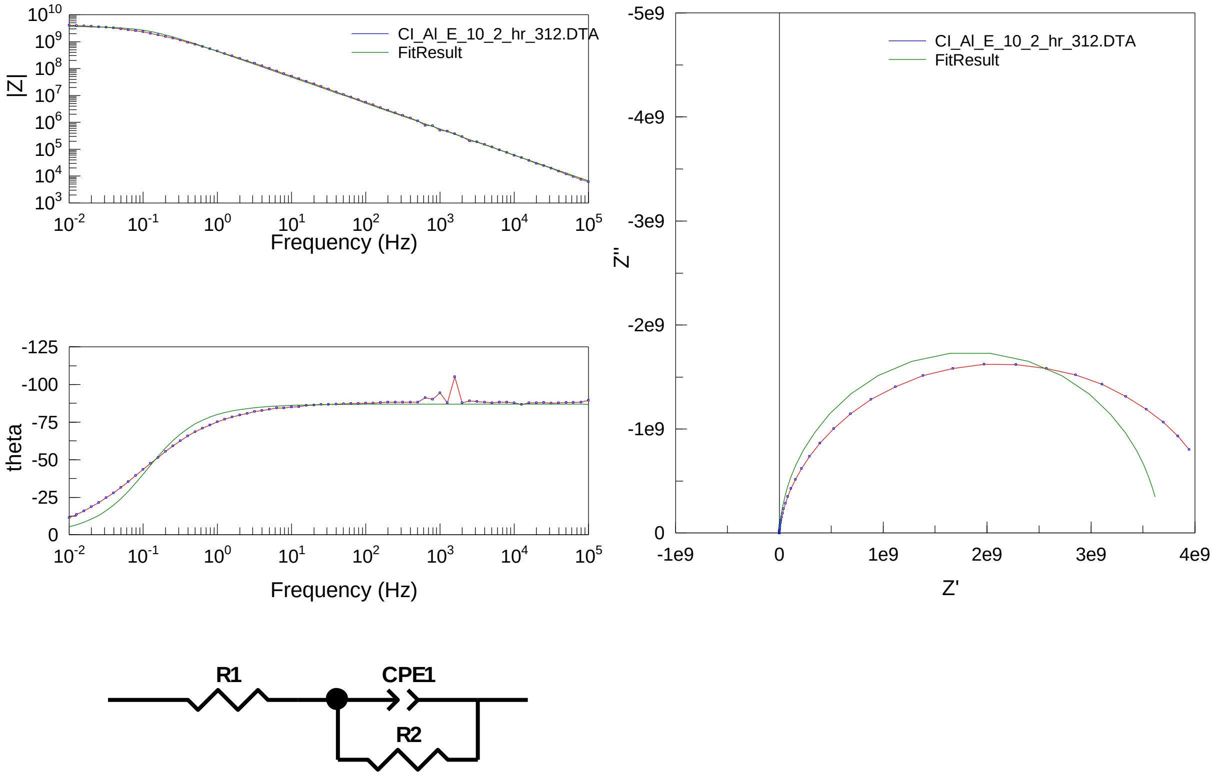

Element	Freedom	Value	Error	Error %
R1	Fixed(X)	10	N/A	N/A
CPE1-T	Free(+)	3.8153E-10	6.7262E-12	1.763
CPE1-P	Free(+)	0.96602	0.002306	0.23871
R2	Free(+)	3.6678E09	8.0604E07	2.1976

Chi-Squared: 0.056905

Weighted Sum of Squares: 7.9098

Figure A.15. Equivalent Circuit Model for Epoxy coating on AA2024 with 10% cerium capsules after 312 hours of immersion in 5% NaCl solution.

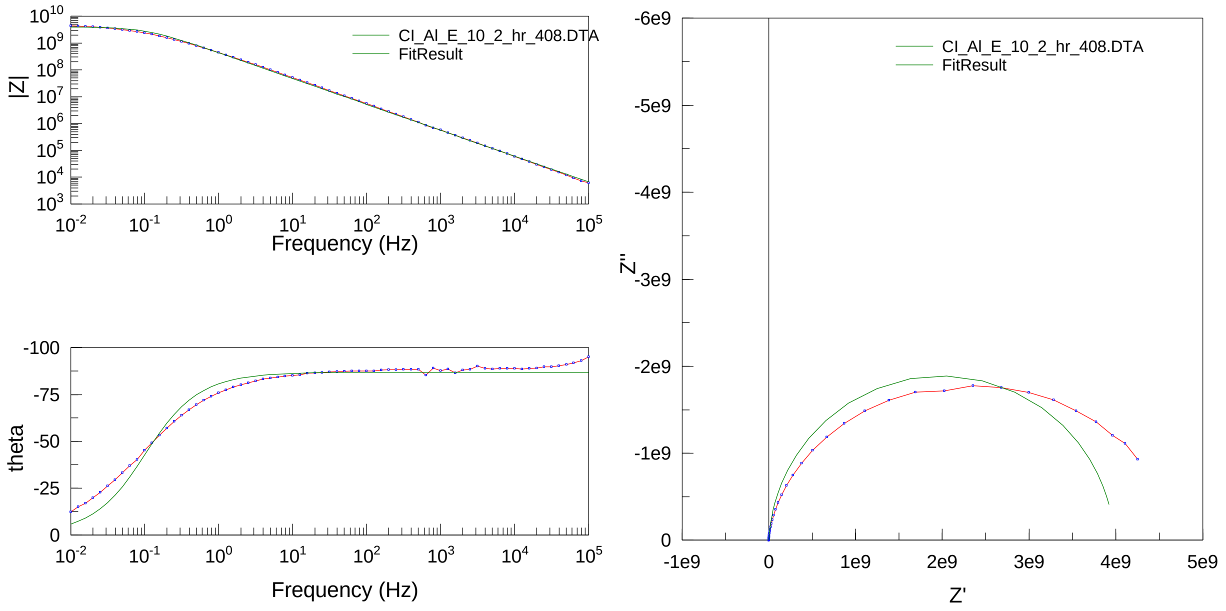

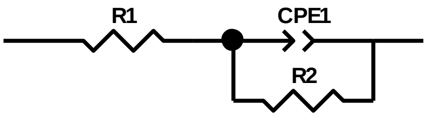

Element	Freedom	Value	Error	Error %
R1	Fixed(X)	10	N/A	N/A
CPE1-T	Free(+)	3.8138E-10	6.1366E-12	1.6091
CPE1-P	Free(+)	0.96609	0.0021146	0.21888
R2	Free(+)	3.9855E09	8.2048E07	2.0587

Chi-Squared:	0.048301
Weighted Sum of Squares:	6.7139

Figure A.16. Equivalent Circuit Model for Epoxy coating on AA2024 with 10% cerium capsules after 408 hours of immersion in 5% NaCl solution.

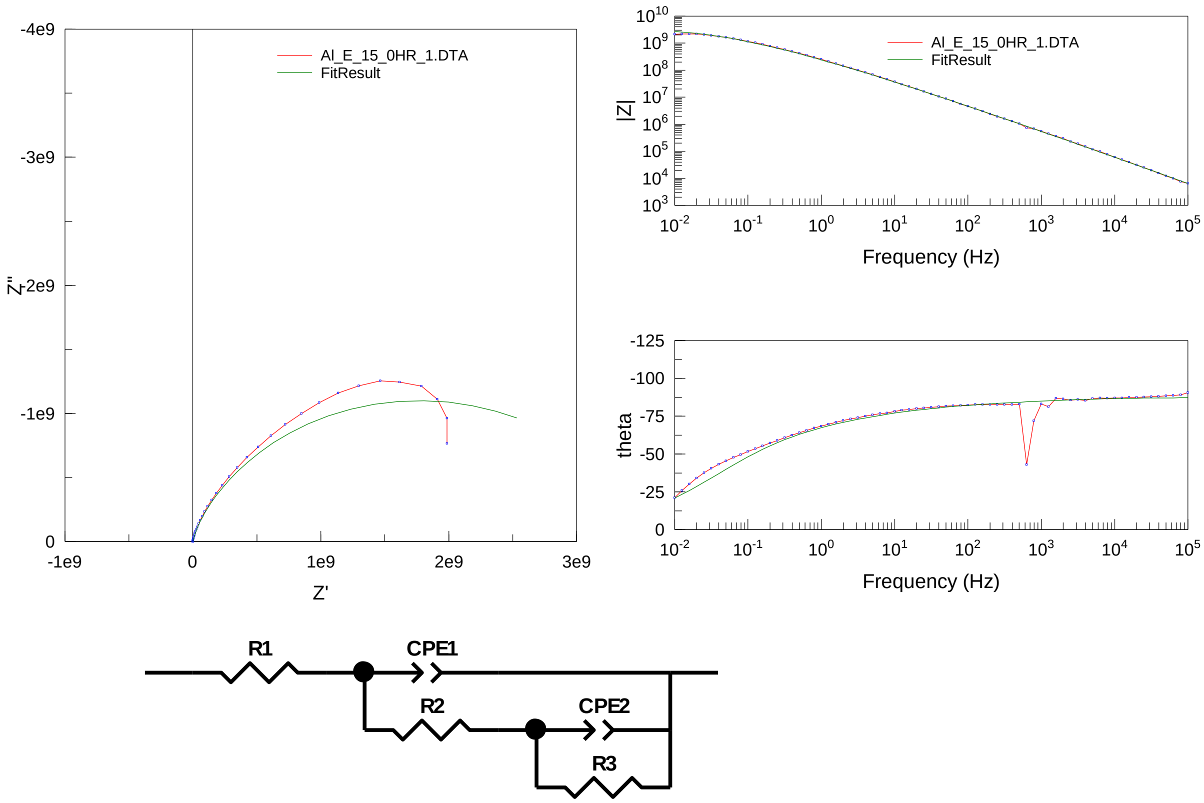

Element	Freedom	Value	Error	Error %
R1	Fixed(X)	10	N/A	N/A
CPE1-T	Free(±)	3.6572E-10	7.8795E-11	21.545
CPE1-P	Free(±)	0.96989	0.017106	1.7637
R2	Free(±)	3.5048E06	1.2489E07	356.34
CPE2-T	Free(±)	6.9452E-10	6.421E-11	9.2452
CPE2-P	Free(±)	0.59891	0.0452	7.547
R3	Free(±)	3.7592E09	2.9196E08	7.7665

Chi-Squared:	0.032579
Weighted Sum of Squares:	4.4307
Data File:	C:\Users\Abhijit\Desktop\AA2024\Al_E_15_0HR_1.DTA
Circuit Model File:	
Mode:	Run Fitting / All Data Points (1 - 71)
Maximum Iterations:	100
Optimization Iterations:	0
Type of Fitting:	Complex
Type of Weighting:	Calc-Modulus

Figure A.17. Equivalent Circuit Model for Epoxy coating on AA2024 with 10% cerium capsules after 0 hours of immersion in 5% NaCl solution.

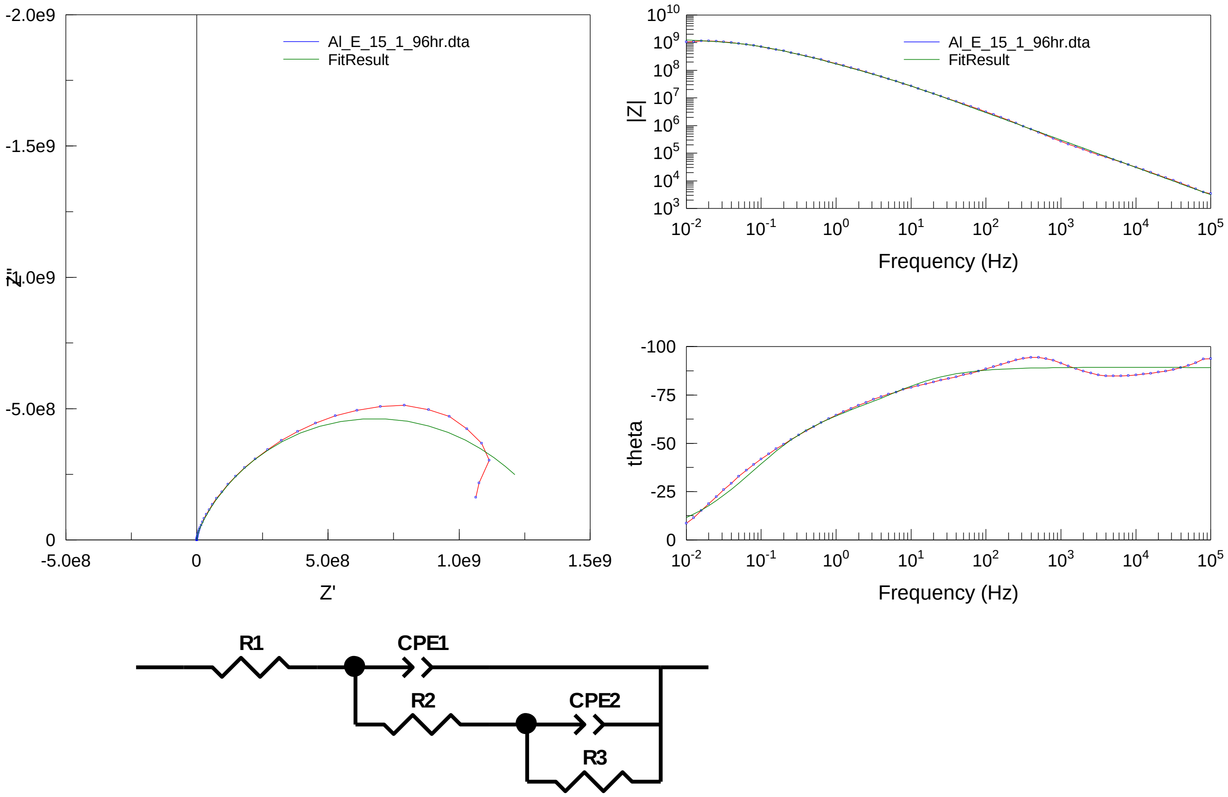

Element	Freedom	Value	Error	Error %
R1	Fixed(X)	10	N/A	N/A
CPE1-T	Free(±)	5.6626E-10	1.4299E-11	2.5252
CPE1-P	Free(±)	0.99184	0.002634	0.26557
R2	Free(±)	1.075E08	1.8276E07	17.001
CPE2-T	Free(±)	1.0819E-09	4.2937E-11	3.9687
CPE2-P	Free(±)	0.6578	0.026089	3.9661
R3	Free(±)	1.2947E09	5.8916E07	4.5506

Chi-Squared:	0.02836
Weighted Sum of Squares:	3.857
Data File:	C:\Users\Abhijit\Desktop\AA2024\Al_E_15_1_96hr.dta
Circuit Model File:	
Mode:	Run Fitting / All Data Points (1 - 71)
Maximum Iterations:	100
Optimization Iterations:	0
Type of Fitting:	Complex
Type of Weighting:	Calc-Modulus

Figure A.18. Equivalent Circuit Model for Epoxy coating on AA2024 with 15% cerium capsules after 96 hours of immersion in 5% NaCl solution.

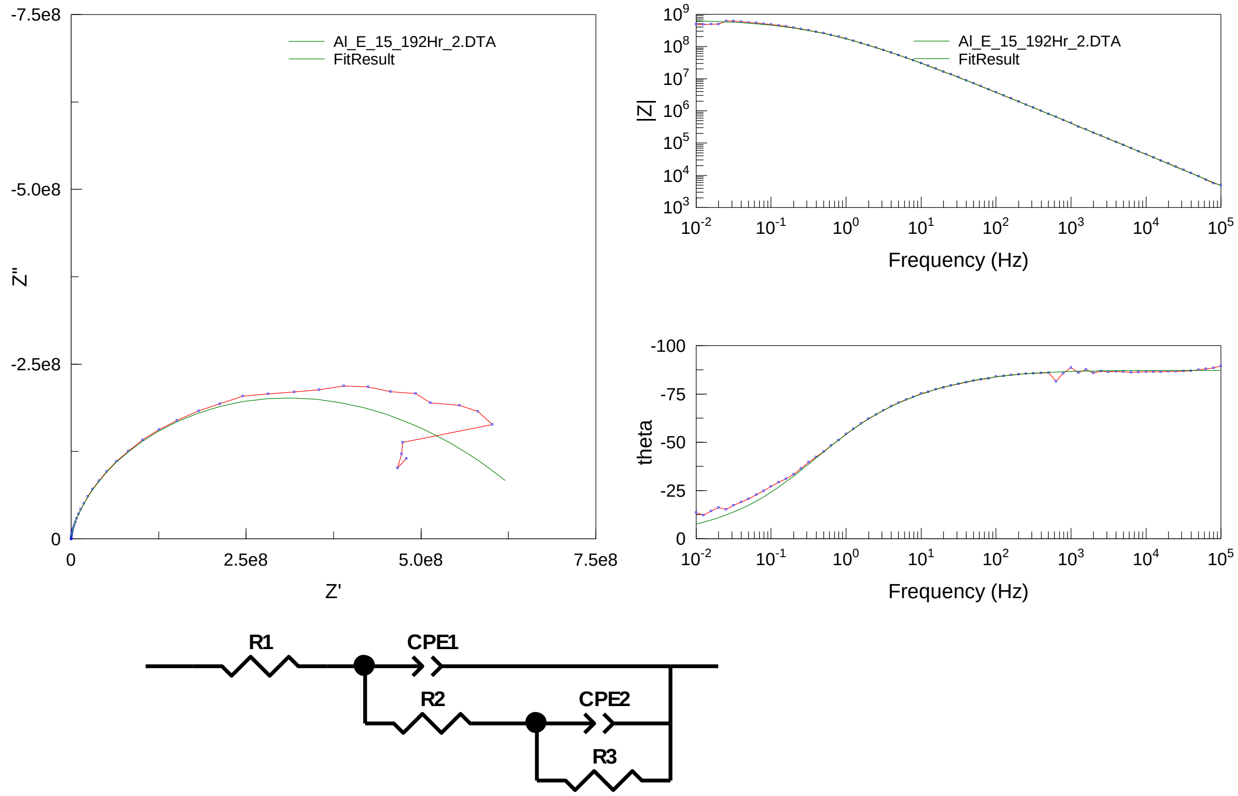

Element	Freedom	Value	Error	Error %
R1	Fixed(X)	10	N/A	N/A
CPE1-T	Free(±)	5.0112E-10	2.1899E-11	4.37
CPE1-P	Free(±)	0.96886	0.0040877	0.42191
R2	Free(±)	3.1833E07	1.9762E07	62.08
CPE2-T	Free(±)	1.146E-09	6.7992E-11	5.933
CPE2-P	Free(±)	0.51863	0.027102	5.2257
R3	Free(±)	6.7683E08	3.782E07	5.5878

Chi-Squared:	0.013511
Weighted Sum of Squares:	1.8375
Data File:	C:\Users\Abhijit\Desktop\AA2024\Al_E_15_ 192Hr_2.DTA
Circuit Model File:	
Mode:	Run Fitting / All Data Points (1 - 71)
Maximum Iterations:	100
Optimization Iterations:	0
Type of Fitting:	Complex
Type of Weighting:	Calc-Modulus

Figure A.19. Equivalent Circuit Model for Epoxy coating on AA2024 with 15% cerium capsules after 192 hours of immersion in 5% NaCl solution.

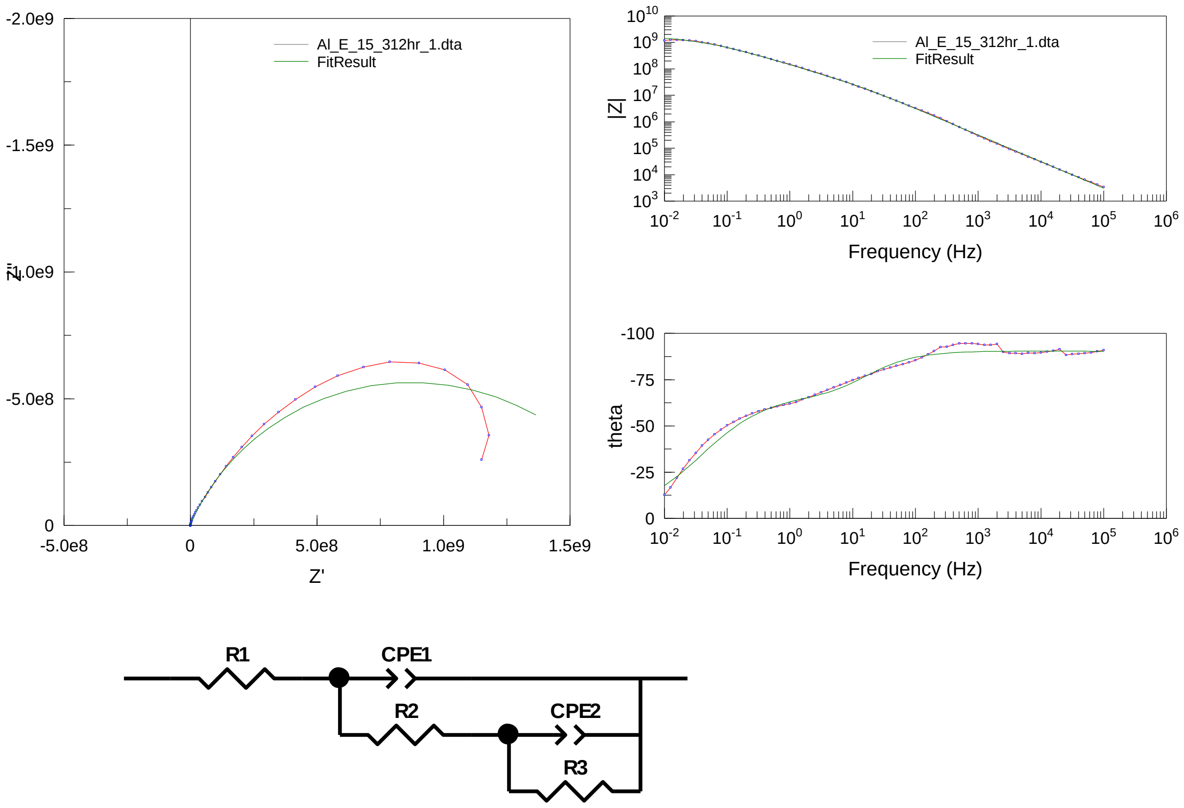

Element	Freedom	Value	Error	Error %
R1	Fixed(X)	10	N/A	N/A
CPE1-T	Free(±)	4.7749E-10	1.2686E-11	2.6568
CPE1-P	Free(±)	1.005	0.0027043	0.26908
R2	Free(±)	4.7381E07	5.4984E06	11.605
CPE2-T	Free(±)	1.4327E-09	2.9233E-11	2.0404
CPE2-P	Free(±)	0.66969	0.013546	2.0227
R3	Free(±)	1.7426E09	6.5983E07	3.7865

Chi-Squared: 0.032784
Weighted Sum of Squares: 4.4586

Data File: C:\Users\Abhijit\Desktop\AA2024\Al_E_15_312hr_1.dta
Circuit Model File:
Mode: Run Fitting / All Data Points (1 - 71)
Maximum Iterations: 100
Optimization Iterations: 0
Type of Fitting: Complex
Type of Weighting: Calc-Modulus

Figure A.20. Equivalent Circuit Model for Epoxy coating on AA2024 with 15% cerium capsules after 312 hours of immersion in 5% NaCl solution.

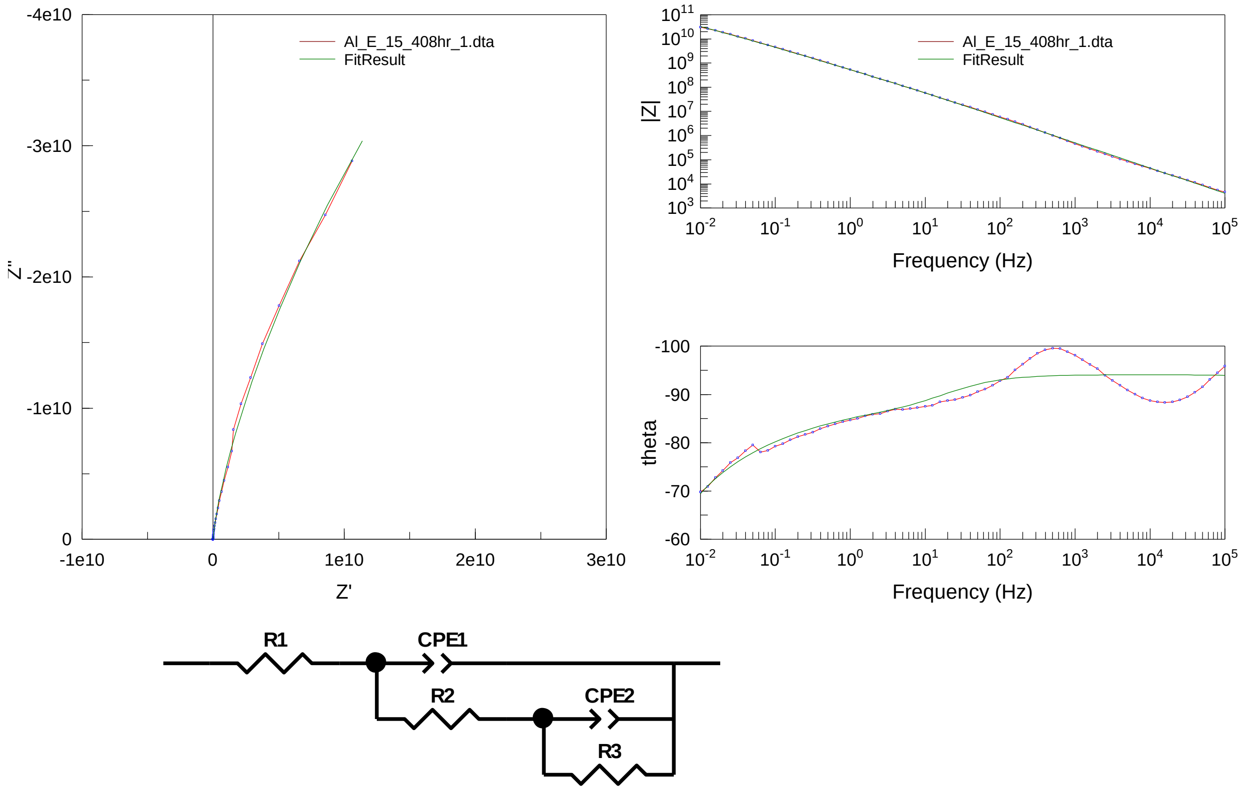

Element	Freedom	Value	Error	Error %
R1	Fixed(X)	10	N/A	N/A
CPE1-T	Free(±)	2.1263E-10	6.2546E-12	2.9415
CPE1-P	Free(±)	1.045	0.0029877	0.2859
R2	Free(±)	2.6166E08	1.0558E08	40.35
CPE2-T	Free(±)	1.4142E-10	6.1879E-12	4.3755
CPE2-P	Free(±)	0.72681	0.018229	2.5081
R3	Free(±)	2.6754E11	9.9722E10	37.274

Chi-Squared:	0.03387
Weighted Sum of Squares:	4.6063
Data File:	C:\Users\Abhijit\Desktop\AA2024\Al_E_15_408hr_1.dta
Circuit Model File:	
Mode:	Run Fitting / All Data Points (1 - 71)
Maximum Iterations:	100
Optimization Iterations:	0
Type of Fitting:	Complex
Type of Weighting:	Calc-Modulus

Figure A.21. Equivalent Circuit Model for Epoxy coating on AA2024 with 15% cerium capsules after 408 hours of immersion in 5% NaCl solution.

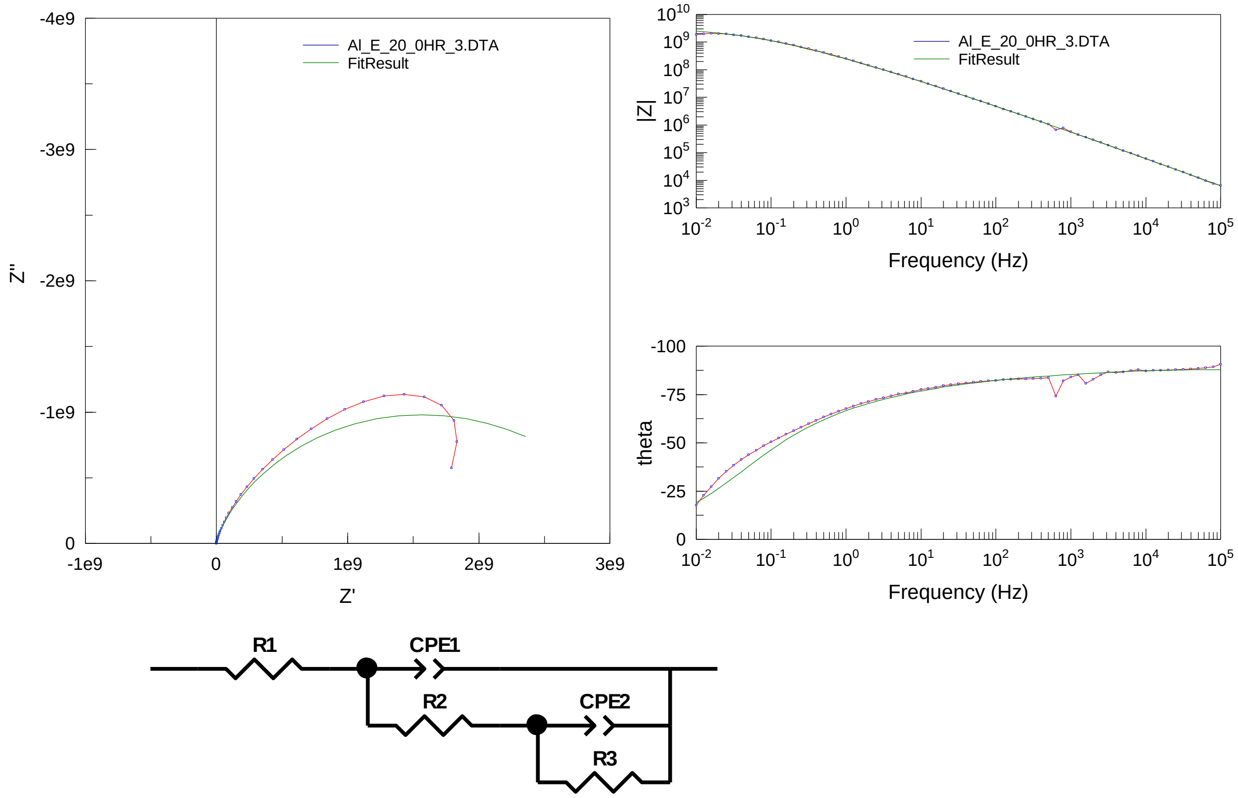

Element	Freedom	Value	Error	Error %
R1	Fixed(X)	10	N/A	N/A
CPE1-T	Free(±)	3.3256E-10	5.0226E-11	15.103
CPE1-P	Free(±)	0.97823	0.011889	1.2154
R2	Free(±)	2.7568E06	6.2411E06	226.39
CPE2-T	Free(±)	7.1854E-10	4.1197E-11	5.7334
CPE2-P	Free(±)	0.60797	0.029491	4.8507
R3	Free(±)	3.3148E09	1.5982E08	4.8214

Chi-Squared:	0.015777
Weighted Sum of Squares:	2.1457
Data File:	C:\Users\Abhijit\Desktop\AA2024\Al_E_20_0HR_3.DTA
Circuit Model File:	
Mode:	Run Fitting / All Data Points (1 - 71)
Maximum Iterations:	100
Optimization Iterations:	0
Type of Fitting:	Complex
Type of Weighting:	Calc-Modulus

Figure A.22. Equivalent Circuit Model for Epoxy coating on AA2024 with 20% cerium capsules after 0 hours of immersion in 5% NaCl solution.

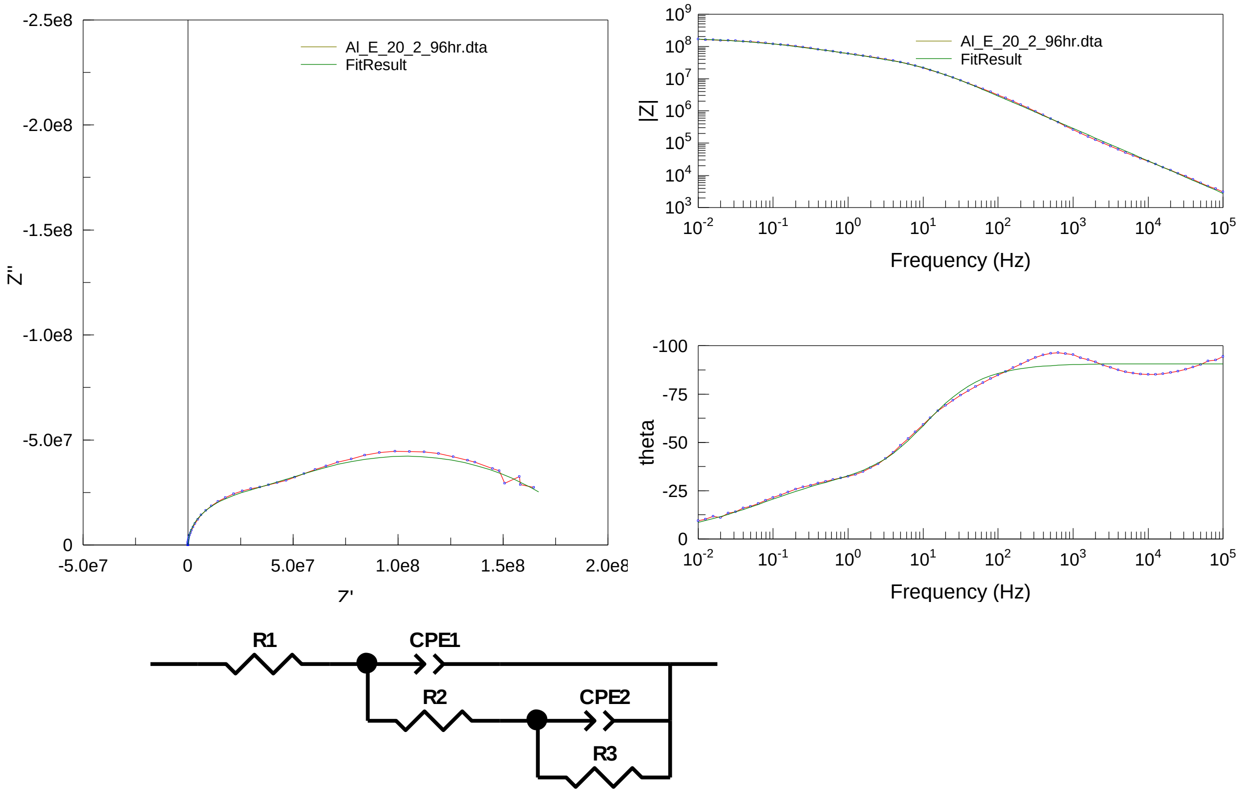

Element	Freedom	Value	Error	Error %
R1	Fixed(X)	10	N/A	N/A
CPE1-T	Free(±)	5.13E-10	1.4829E-11	2.8906
CPE1-P	Free(±)	1.008	0.0029657	0.29422
R2	Free(±)	3.0288E07	2.5936E06	8.5631
CPE2-T	Free(±)	7.6174E-09	3.5806E-10	4.7006
CPE2-P	Free(±)	0.55109	0.030684	5.5679
R3	Free(±)	1.665E08	1.0393E07	6.242

Chi-Squared: 0.035585
Weighted Sum of Squares: 4.8395

Data File: C:\Users\Abhijit\Desktop\AA2024\Al_E_20_2_96hr.dta
Circuit Model File:
Mode: Run Fitting / All Data Points (1 - 71)
Maximum Iterations: 100
Optimization Iterations: 0
Type of Fitting: Complex
Type of Weighting: Calc-Modulus

Figure A.23. Equivalent Circuit Model for Epoxy coating on AA2024 with 20% cerium capsules after 96 hours of immersion in 5% NaCl solution.

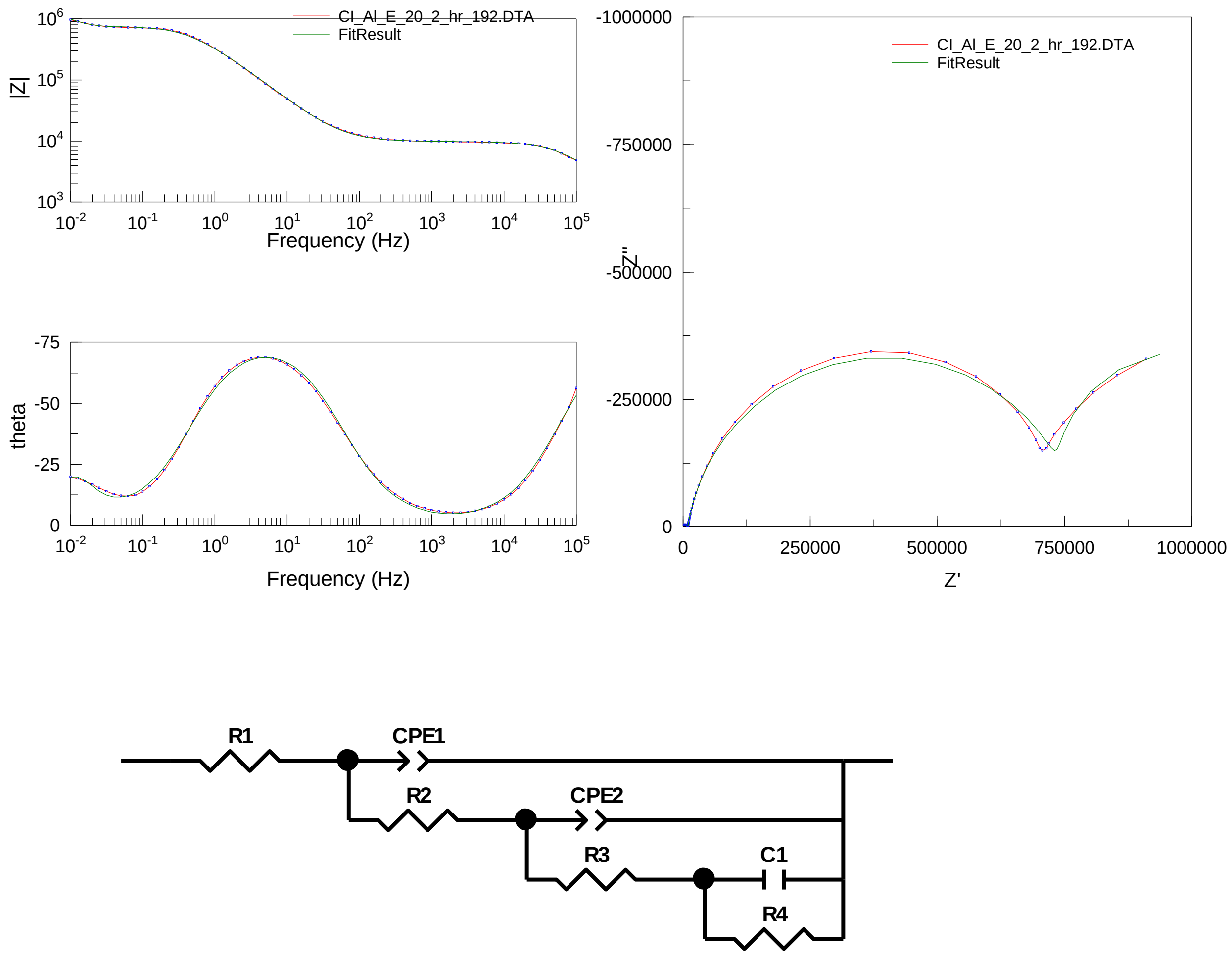

Element	Freedom	Value	Error	Error %
R1	Fixed(X)	10	N/A	N/A
CPE1-T	Free(+)	7.8831E-10	7.3327E-11	9.3018
CPE1-P	Free(+)	0.91842	0.0072557	0.79002
R2	Free(+)	9849	42.771	0.43427
CPE2-T	Free(+)	5.0063E-07	4.4074E-09	0.88037
CPE2-P	Free(+)	0.90558	0.0021515	0.23758
R3	Free(+)	7.6287E05	4881.4	0.63987
C1	Free(+)	4.1945E-05	1.3807E-06	3.2917
R4	Free(+)	8.1408E05	81307	9.9876

Chi-Squared:	0.00123
Weighted Sum of Squares:	0.16482

Figure A.24. Equivalent Circuit Model for Epoxy coating on AA2024 with 20% cerium capsules after 192 hours of immersion in 5% NaCl solution.

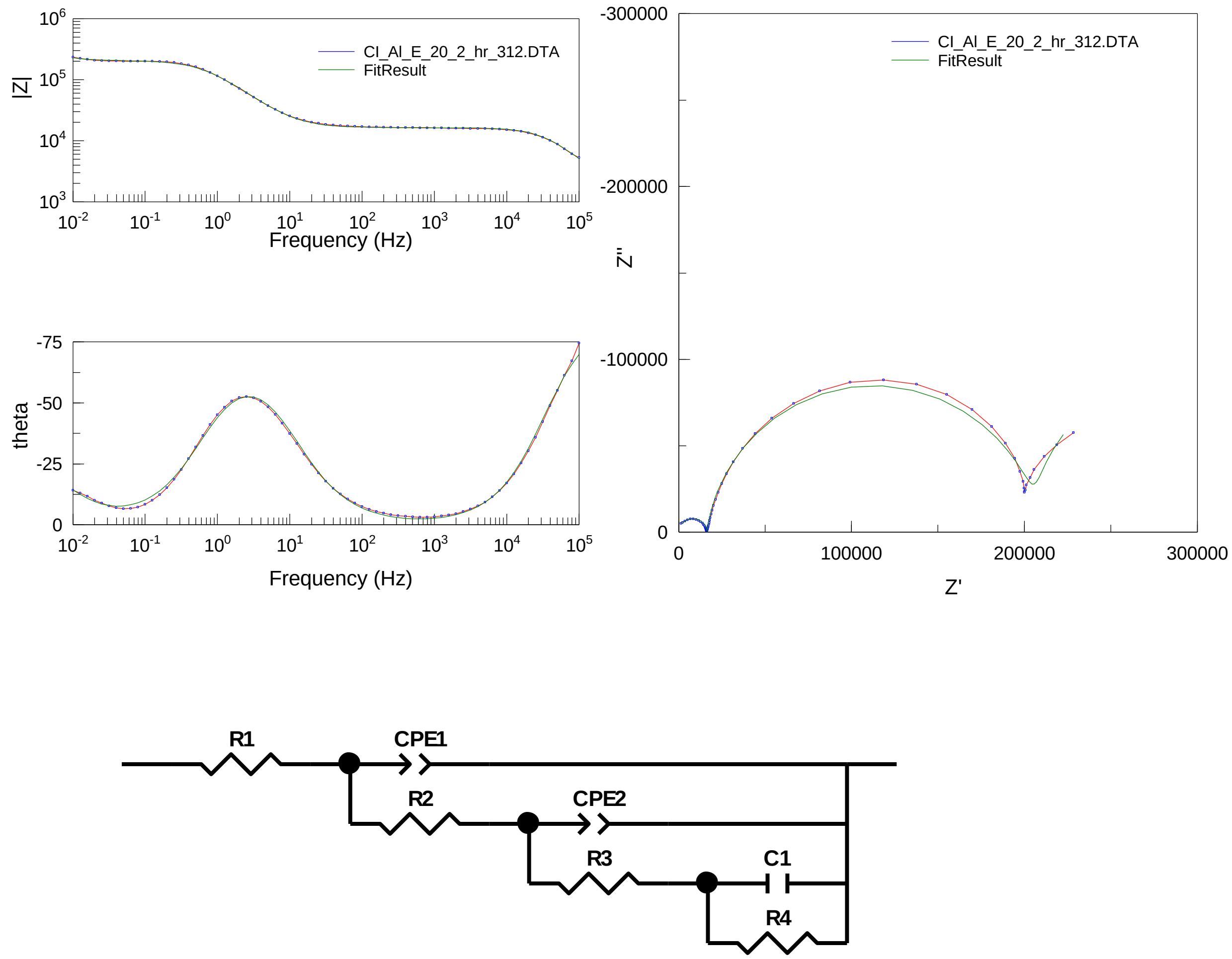

Element	Freedom	Value	Error	Error %
R1	Fixed(X)	10	N/A	N/A
CPE1-T	Free(+)	3.8952E-10	2.3808E-11	6.1121
CPE1-P	Free(+)	0.97904	0.0048373	0.49409
R2	Free(+)	16334	57.783	0.35376
CPE2-T	Free(+)	1.3737E-06	1.5846E-08	1.1535
CPE2-P	Free(+)	0.91722	0.0034613	0.37737
R3	Free(+)	1.9305E05	1189.2	0.61601
C1	Free(+)	0.00027653	1.2843E-05	4.6443
R4	Free(+)	1.8791E05	40645	21.63

Chi-Squared: 0.0014581
Weighted Sum of Squares: 0.19538

Figure A.25. Equivalent Circuit Model for Epoxy coating on AA2024 with 20% cerium capsules after 312 hours of immersion in 5% NaCl solution.

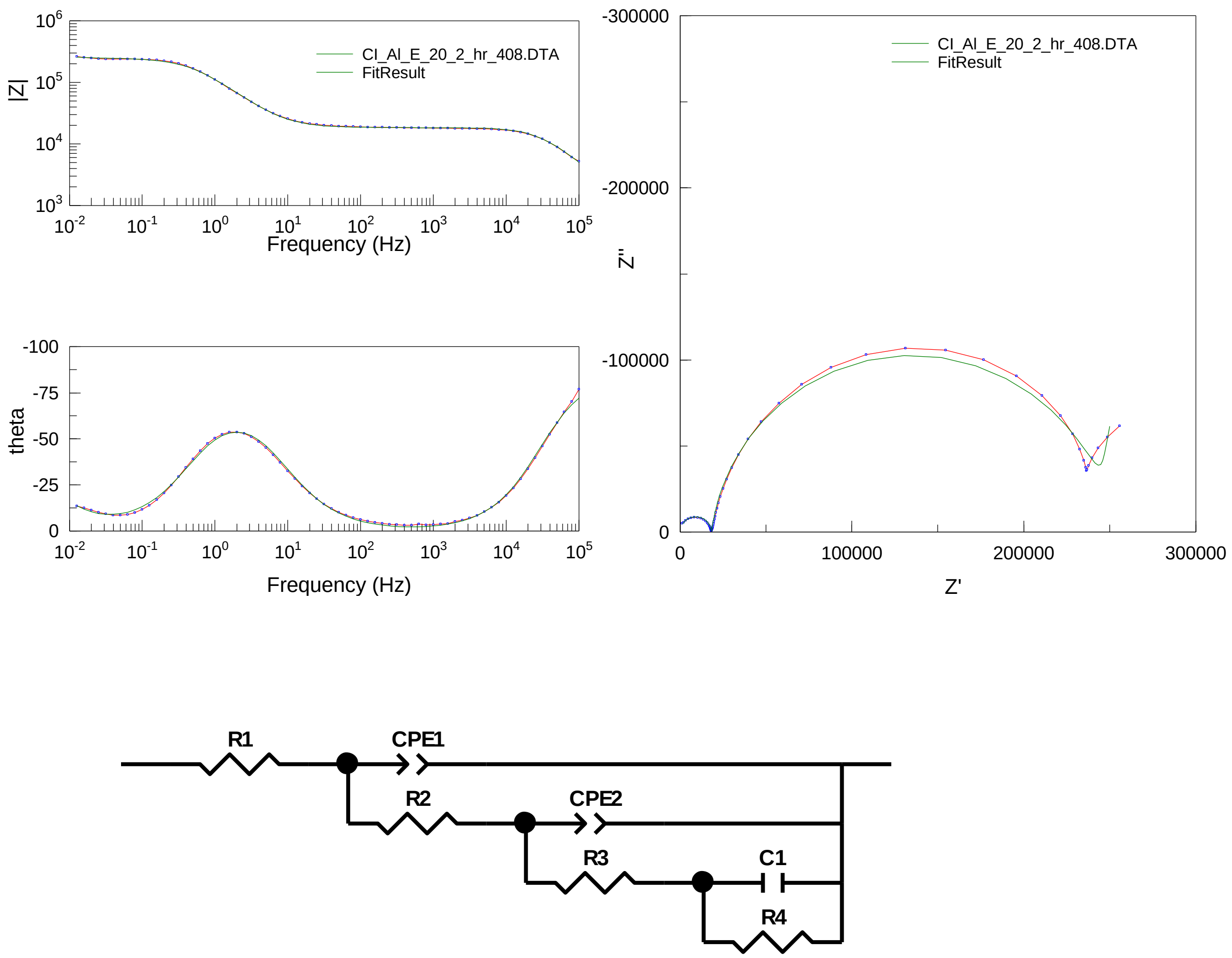

Element	Freedom	Value	Error	Error %
R1	Fixed(X)	10	N/A	N/A
CPE1-T	Free(+)	3.8641E-10	2.2302E-11	5.7716
CPE1-P	Free(+)	0.98117	0.0045844	0.46724
R2	Free(+)	18333	64.041	0.34932
CPE2-T	Free(+)	1.551E-06	1.649E-08	1.0632
CPE2-P	Free(+)	0.91918	0.0034497	0.3753
R3	Free(+)	2.3295E05	1585.4	0.68058
C1	Free(+)	0.00023137	1.2241E-05	5.2907
R4	Free(+)	7.9803E05	9.2363E05	115.74

Chi-Squared:	0.0014699
Weighted Sum of Squares:	0.19403

Figure A.26. Equivalent Circuit Model for Epoxy coating on AA2024 with 20% cerium capsules after 408 hours of immersion in 5% NaCl solution.

A.3. Circuit models of capsule containing epoxy coatings on cold rolled steel

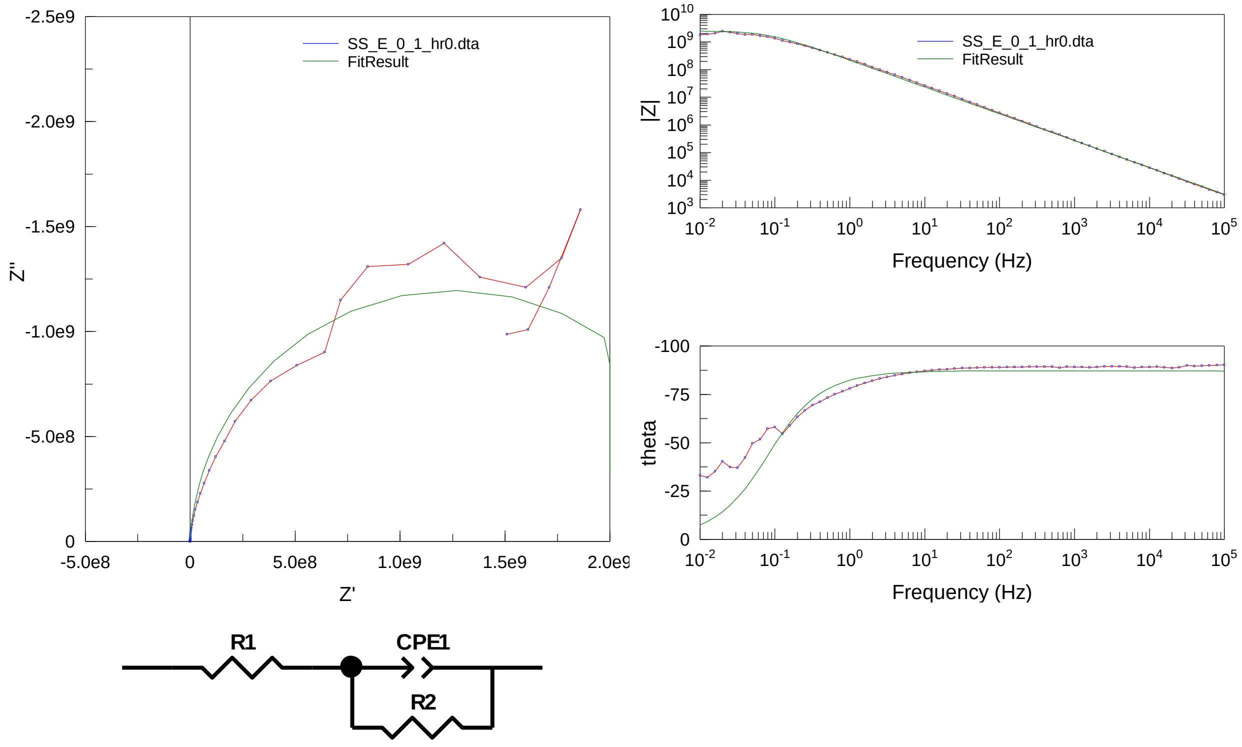

Element	Freedom	Value	Error	Error %
R1	Fixed(X)	10	N/A	N/A
CPE1-T	Free(±)	7.7063E-10	1.9907E-11	2.5832
CPE1-P	Free(±)	0.96908	0.0034498	0.35599
R2	Free(±)	2.5112E09	9.6681E07	3.85

Chi-Squared:	0.14809
Weighted Sum of Squares:	20.585
Data File:	C:\Users\Abhijit\Desktop\CRS\SS_E_0_1_hr0.dta
Circuit Model File:	
Mode:	Run Fitting / All Data Points (1 - 71)
Maximum Iterations:	100
Optimization Iterations:	0
Type of Fitting:	Complex
Type of Weighting:	Calc-Modulus

Figure A.27. Equivalent Circuit Model for Epoxy coating on Cold Rolled Steel with 0% cerium capsules after 0 hours of immersion in 5% NaCl solution.

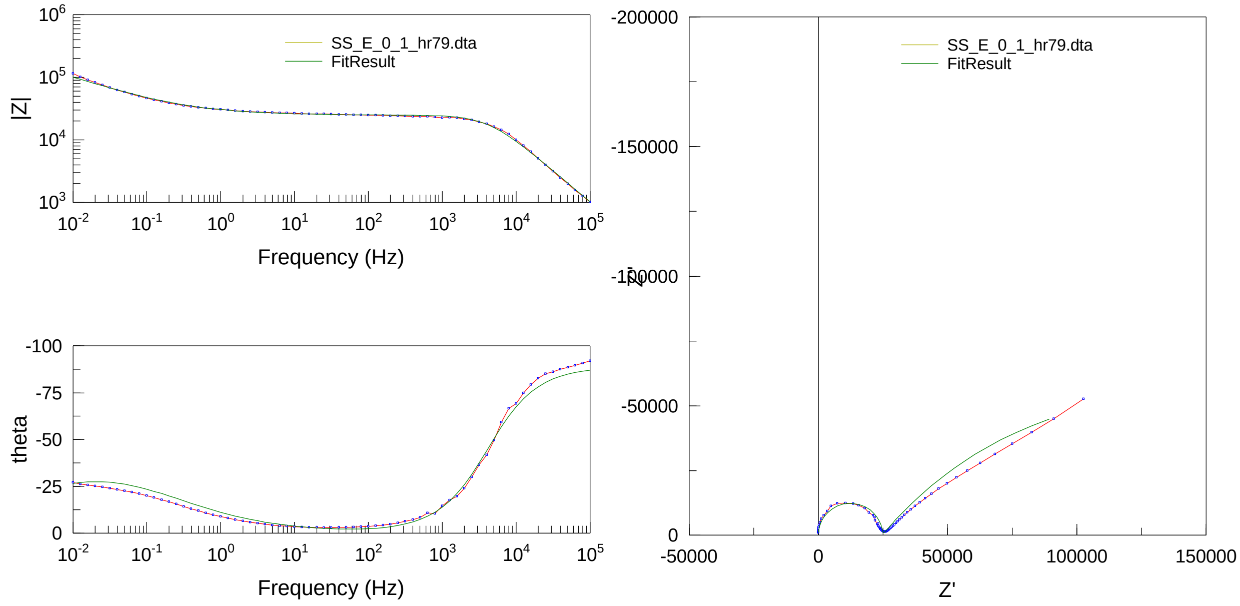

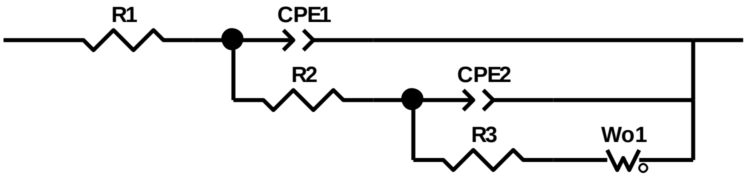

Element	Freedom	Value	Error	Error %
R1	Fixed(X)	10	N/A	N/A
CPE1-T	Free(+)	1.5583E-09	1.6477E-11	1.0574
CPE1-P	Fixed(X)	1	N/A	N/A
R2	Free(+)	24720	210.21	0.85036
CPE2-T	Free(+)	4.4215E-05	1.2537E-06	2.8355
CPE2-P	Free(+)	0.55866	0.01748	3.1289
R3	Free(+)	2.2636E05	45910	20.282
Wo1-R	Free(+)	8.5949E-05	44.331	5.1578E07
Wo1-T	Free(+)	0.00010871	22.435	2.0637E07
Wo1-P	Free(+)	0.15564	3.1695E05	2.0364E08

Chi-Squared: 0.0098766
Weighted Sum of Squares: 1.3235

Figure A.28. Equivalent Circuit Model for Epoxy coating on Cold Rolled Steel with 0% cerium capsules after 96 hours of immersion in 5% NaCl solution.

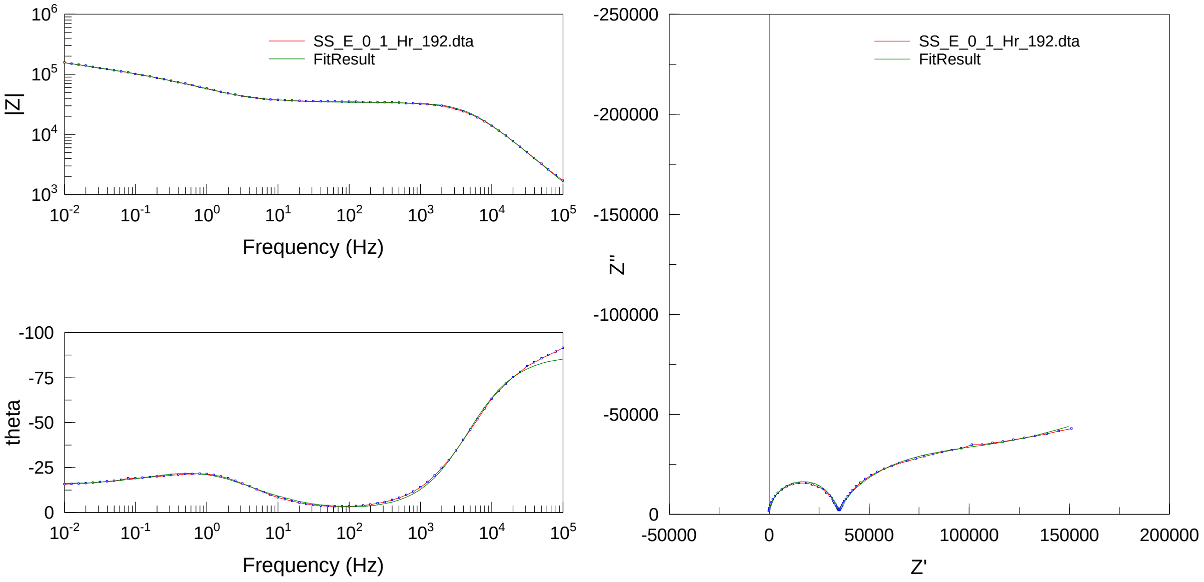

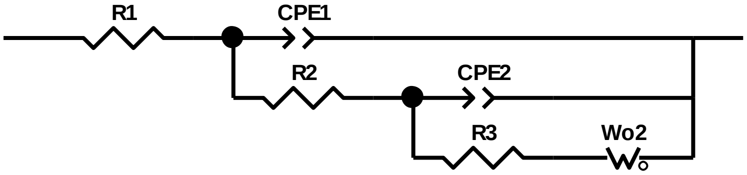

Element	Freedom	Value	Error	Error %
R1	Fixed(X)	10	N/A	N/A
CPE1-T	Free(+)	1.2238E-09	4.5794E-11	3.742
CPE1-P	Free(+)	0.98306	0.0031381	0.31922
R2	Free(+)	33775	229.71	0.68012
CPE2-T	Free(+)	6.6175E-06	5.3428E-06	80.737
CPE2-P	Free(+)	0.73042	0.12441	17.033
R3	Free(+)	46962	3.0963E06	6593.2
Wo2-R	Free(+)	7372	9.5157E06	1.2908E05
Wo2-T	Free(+)	0.002164	10.286	4.7532E05
Wo2-P	Free(+)	0.13882	0.077907	56.121

Chi-Squared:	0.0018695
Weighted Sum of Squares:	0.24864

Figure A.29. Equivalent Circuit Model for Epoxy coating on Cold Rolled Steel with 0% cerium capsules after 192 hours of immersion in 5% NaCl solution.

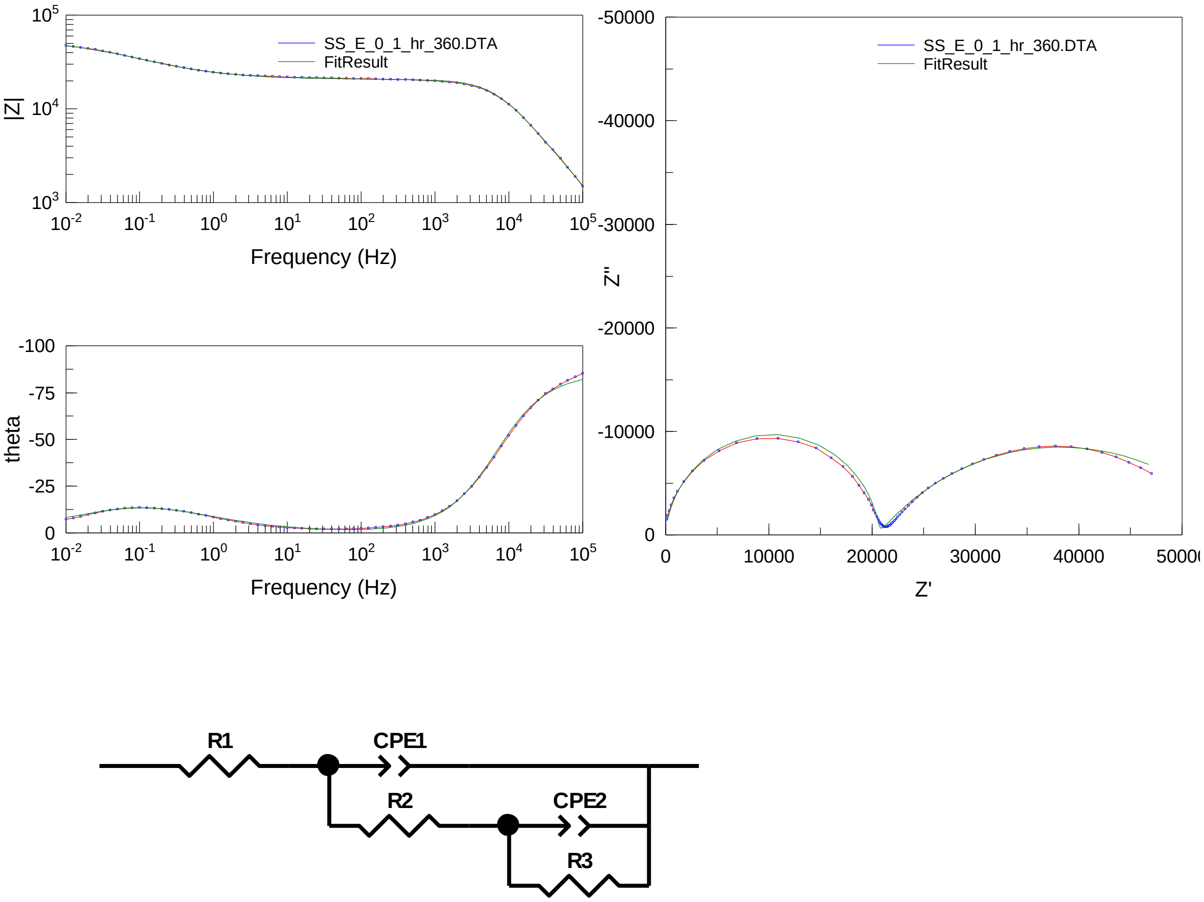

Element	Freedom	Value	Error	Error %
R1	Fixed(X)	10	N/A	N/A
CPE1-T	Free(+)	1.7219E-09	4.3585E-11	2.5312
CPE1-P	Free(+)	0.96231	0.0021012	0.21835
R2	Free(+)	20575	58.666	0.28513
CPE2-T	Free(+)	5.7966E-05	8.0285E-07	1.385
CPE2-P	Free(+)	0.57111	0.0086148	1.5084
R3	Free(+)	35277	785.66	2.2271

Chi-Squared:	0.0011756
Weighted Sum of Squares:	0.15989

Figure A.30. Equivalent Circuit Model for Epoxy coating on Cold Rolled Steel with 0% cerium capsules after 360 hours of immersion in 5% NaCl solution.

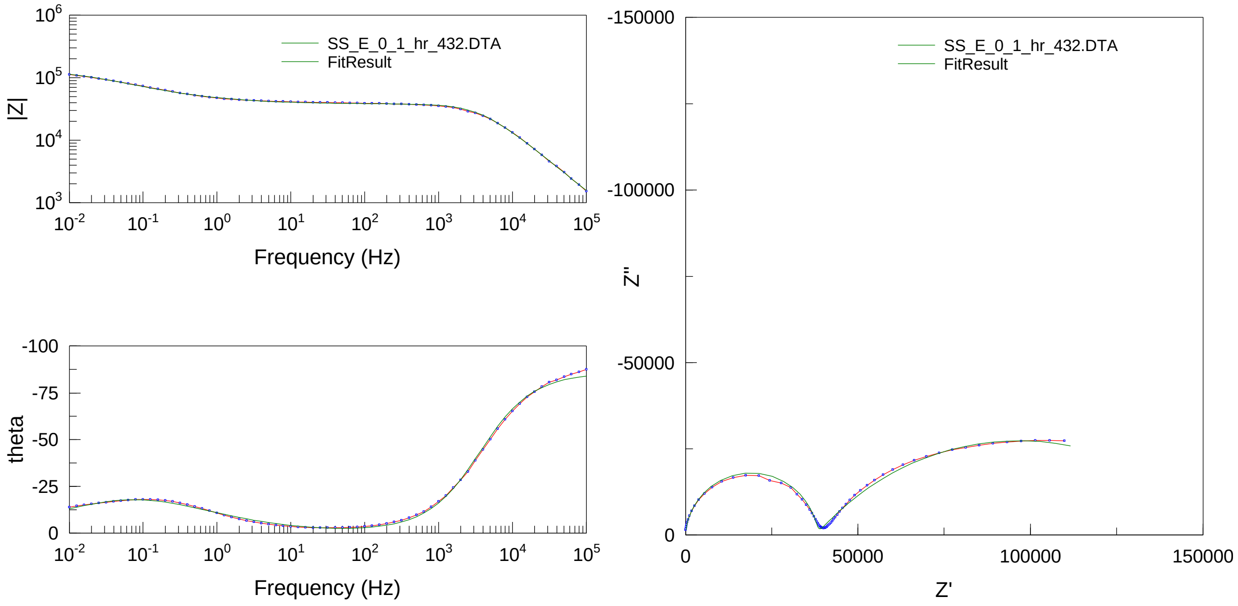

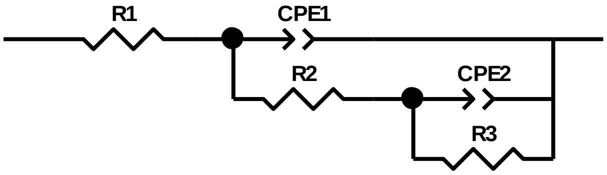

Element	Freedom	Value	Error	Error %
R1	Fixed(X)	10	N/A	N/A
CPE1-T	Free(+)	1.6571E-09	4.2884E-11	2.5879
CPE1-P	Free(+)	0.96362	0.0021955	0.22784
R2	Free(+)	38036	139.65	0.36715
CPE2-T	Free(+)	2.5852E-05	3.1555E-07	1.2206
CPE2-P	Free(+)	0.55533	0.0080766	1.4544
R3	Free(+)	1.1734E05	3393.1	2.8917

Chi-Squared:	0.0014004
Weighted Sum of Squares:	0.19046

Figure A.31. Equivalent Circuit Model for Epoxy coating on Cold Rolled Steel with 0% cerium capsules after 432 hours of immersion in 5% NaCl solution.

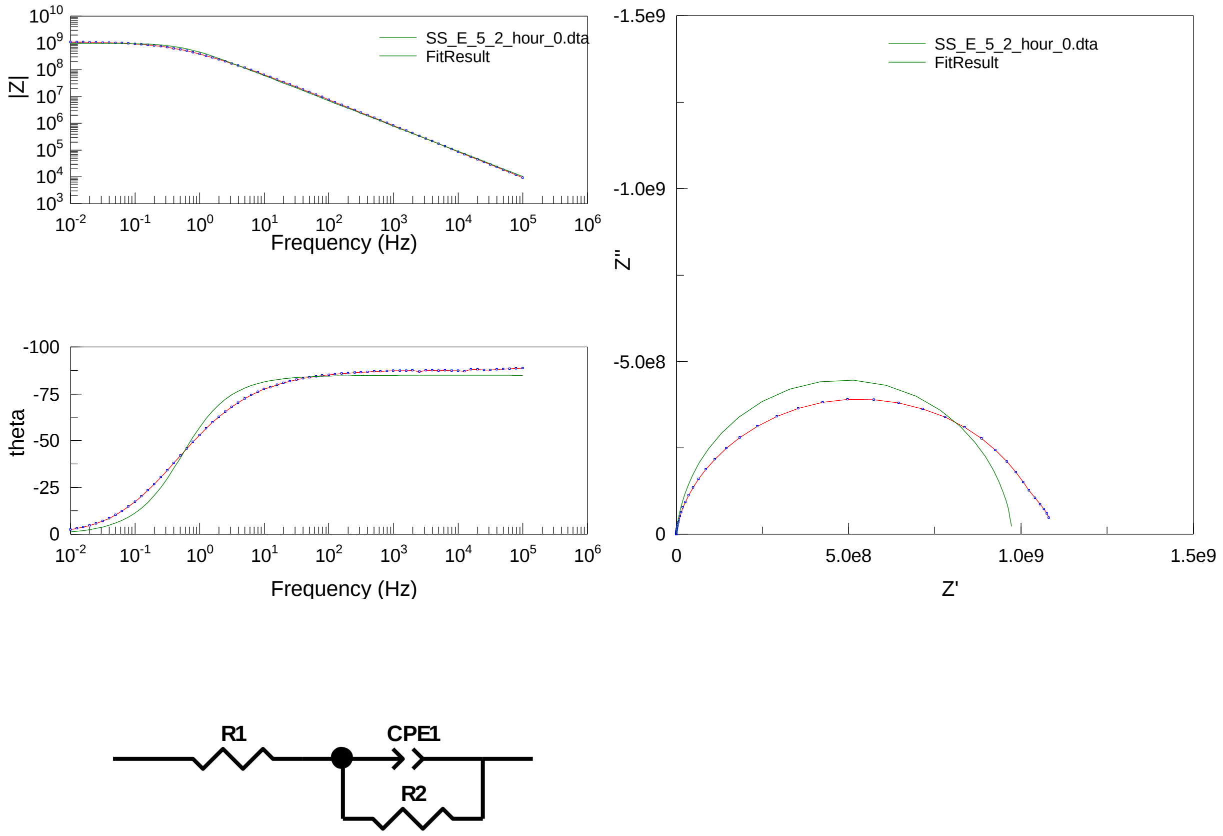

Element	Freedom	Value	Error	Error %
R1	Fixed(X)	10	N/A	N/A
CPE1-T	Free(+)	3.2578E-10	7.02E-12	2.1548
CPE1-P	Free(+)	0.94392	0.0026586	0.28166
R2	Free(+)	9.7475E08	1.6286E07	1.6708

Chi-Squared:	0.040454
Weighted Sum of Squares:	5.623

Figure A.32. Equivalent Circuit Model for Epoxy coating on Cold Rolled Steel with 5% cerium capsules after 0 hours of immersion in 5% NaCl solution.

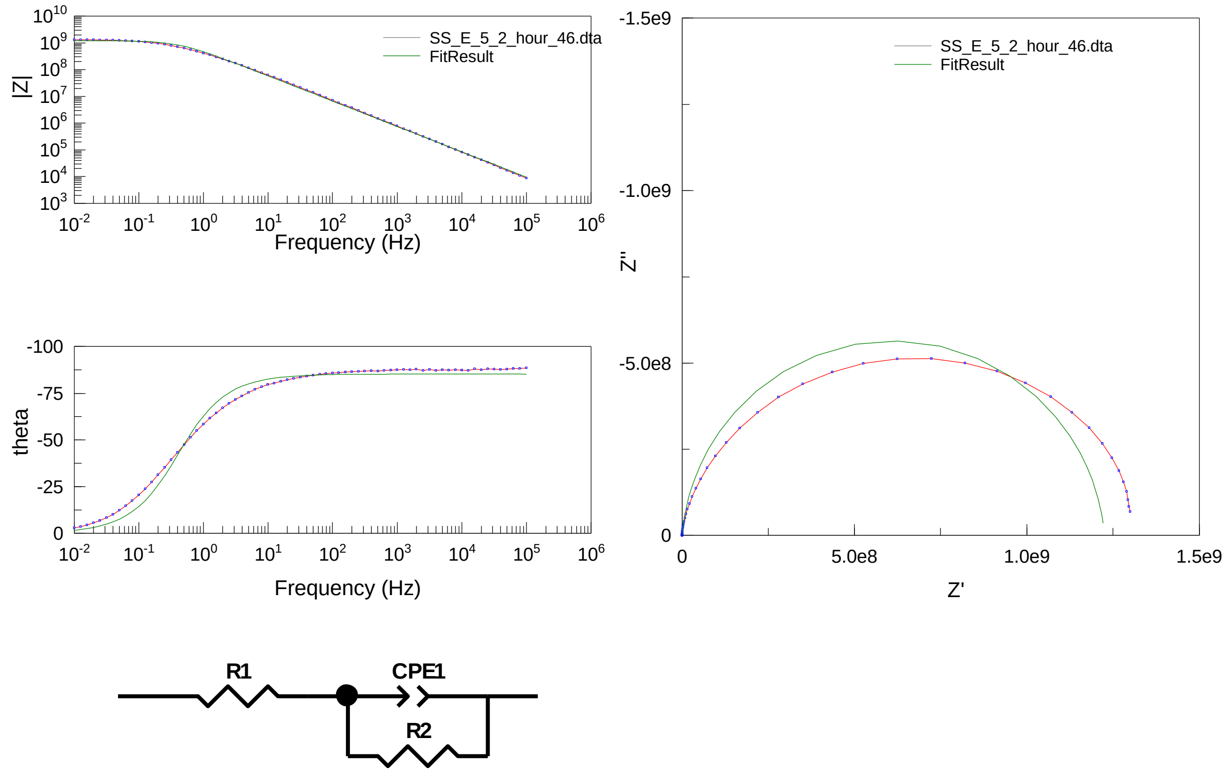

Element	Freedom	Value	Error	Error %
R1	Fixed(X)	10	N/A	N/A
CPE1-T	Free(+)	3.329E-10	6.0746E-12	1.8248
CPE1-P	Free(+)	0.94794	0.0022778	0.24029
R2	Free(+)	1.2248E09	1.8826E07	1.5371

Chi-Squared: 0.0327

Weighted Sum of Squares: 4.5453

Figure A.33. Equivalent Circuit Model for Epoxy coating on Cold Rolled Steel with 5% cerium capsules after 96 hours of immersion in 5% NaCl solution.

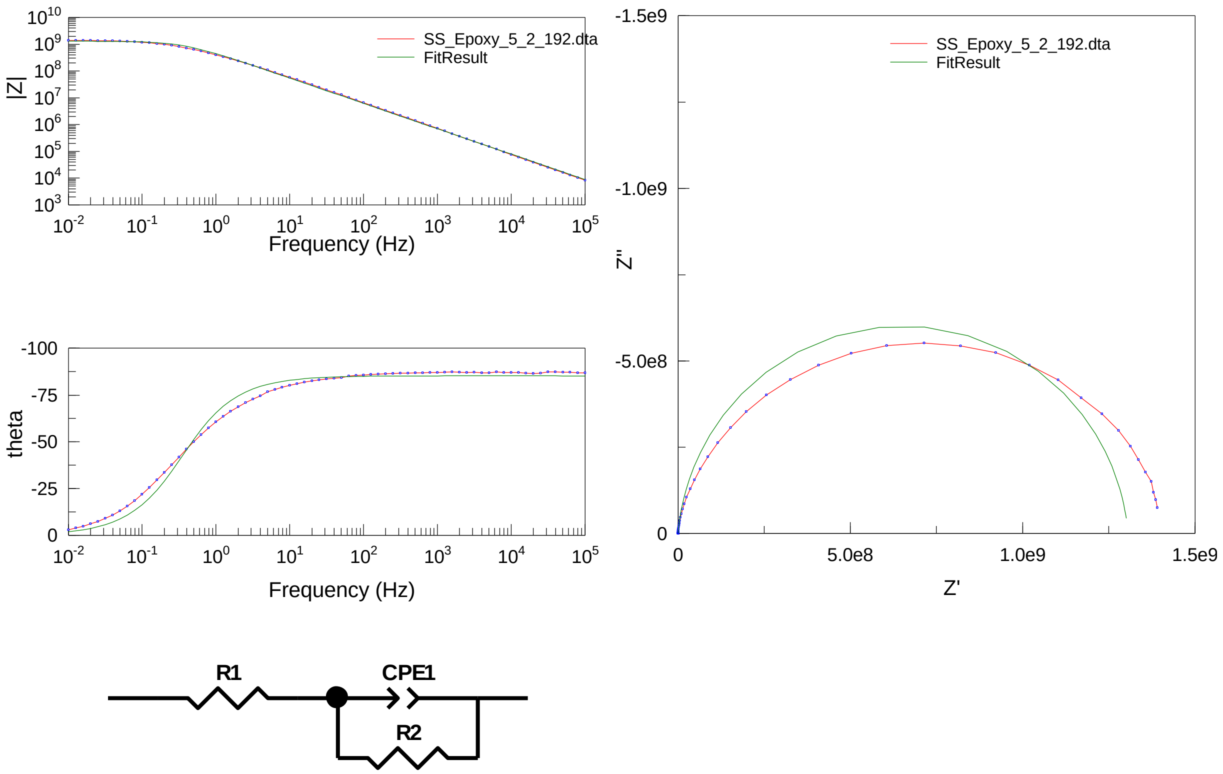

Element	Freedom	Value	Error	Error %
R1	Fixed(X)	10	N/A	N/A
CPE1-T	Free(+)	3.6009E-10	5.9401E-12	1.6496
CPE1-P	Free(+)	0.94774	0.002068	0.2182
R2	Free(+)	1.3055E09	1.8972E07	1.4532

Chi-Squared: 0.02773

Weighted Sum of Squares: 3.8544

Figure A.34. Equivalent Circuit Model for Epoxy coating on Cold Rolled Steel with 5% cerium capsules after 192 hours of immersion in 5% NaCl solution.

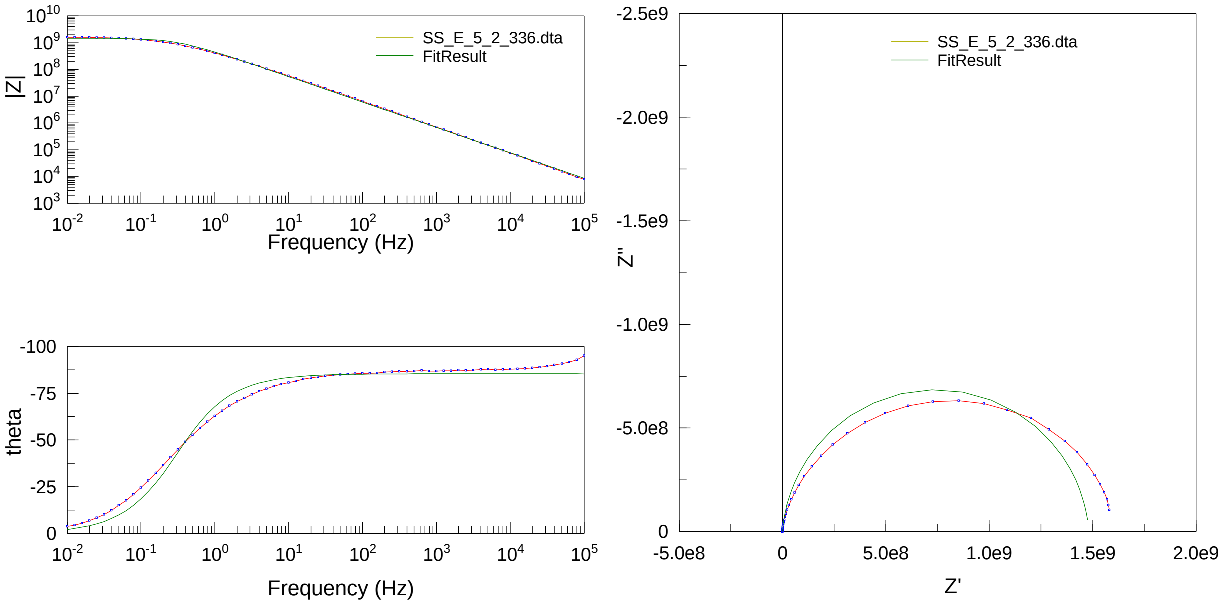

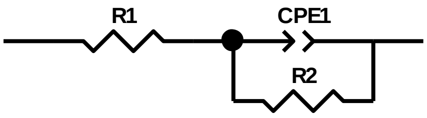

Element	Freedom	Value	Error	Error %
R1	Fixed(X)	10	N/A	N/A
CPE1-T	Free(+)	3.6132E-10	6.502E-12	1.7995
CPE1-P	Free(+)	0.94978	0.0022639	0.23836
R2	Free(+)	1.4824E09	2.4215E07	1.6335

Chi-Squared:	0.034055
Weighted Sum of Squares:	4.7336

Figure A.35. Equivalent Circuit Model for Epoxy coating on Cold Rolled Steel with 5% cerium capsules after 336 hours of immersion in 5% NaCl solution.

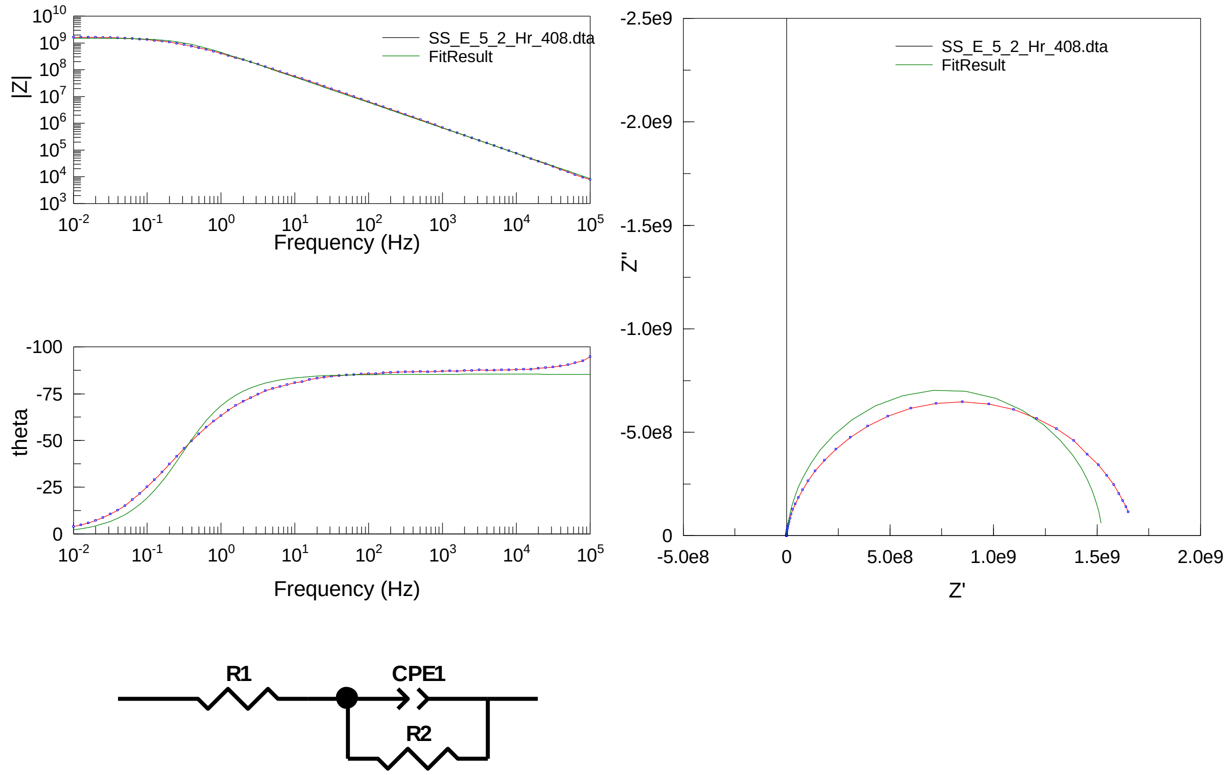

Element	Freedom	Value	Error	Error %
R1	Fixed(X)	10	N/A	N/A
CPE1-T	Free(+)	3.6763E-10	6.5733E-12	1.788
CPE1-P	Free(+)	0.94929	0.0022533	0.23737
R2	Free(+)	1.5263E09	2.5119E07	1.6457

Chi-Squared: 0.033815

Weighted Sum of Squares: 4.7003

Figure A.36. Equivalent Circuit Model for Epoxy coating on Cold Rolled Steel with 5% cerium capsules after 408 hours of immersion in 5% NaCl solution.

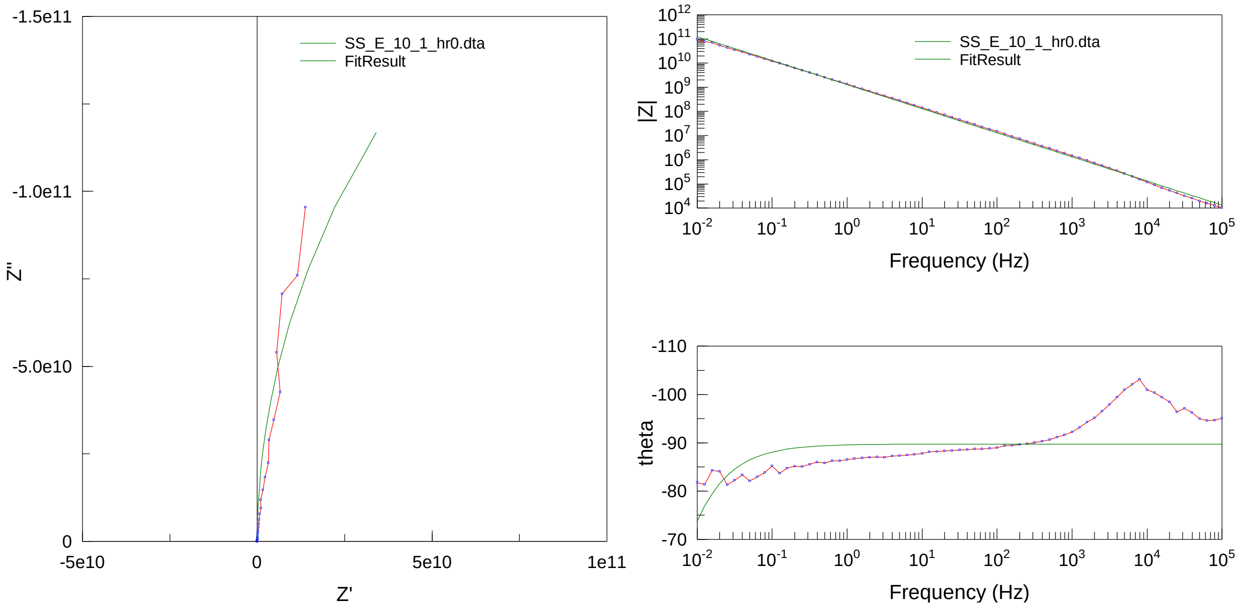

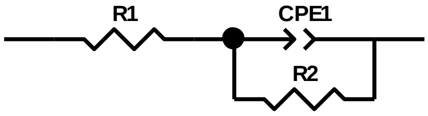

Element	Freedom	Value	Error	Error %
R1	Fixed(X)	10	N/A	N/A
CPE1-T	Free(±)	1.2455E-10	2.5E-12	2.0072
CPE1-P	Free(±)	0.99699	0.0029214	0.29302
R2	Free(±)	4.4264E11	1.0419E11	23.538

Chi-Squared:	1.2943
Weighted Sum of Squares:	179.91
Data File:	C:\Users\Abhijit\Desktop\CRS\SS_E_10_1_hr0.dta
Circuit Model File:	
Mode:	Run Fitting / All Data Points (1 - 71)
Maximum Iterations:	100
Optimization Iterations:	0
Type of Fitting:	Complex
Type of Weighting:	Calc-Modulus

Figure A.37. Equivalent Circuit Model for Epoxy coating on Cold Rolled Steel with 10% cerium capsules after 0 hours of immersion in 5% NaCl solution.

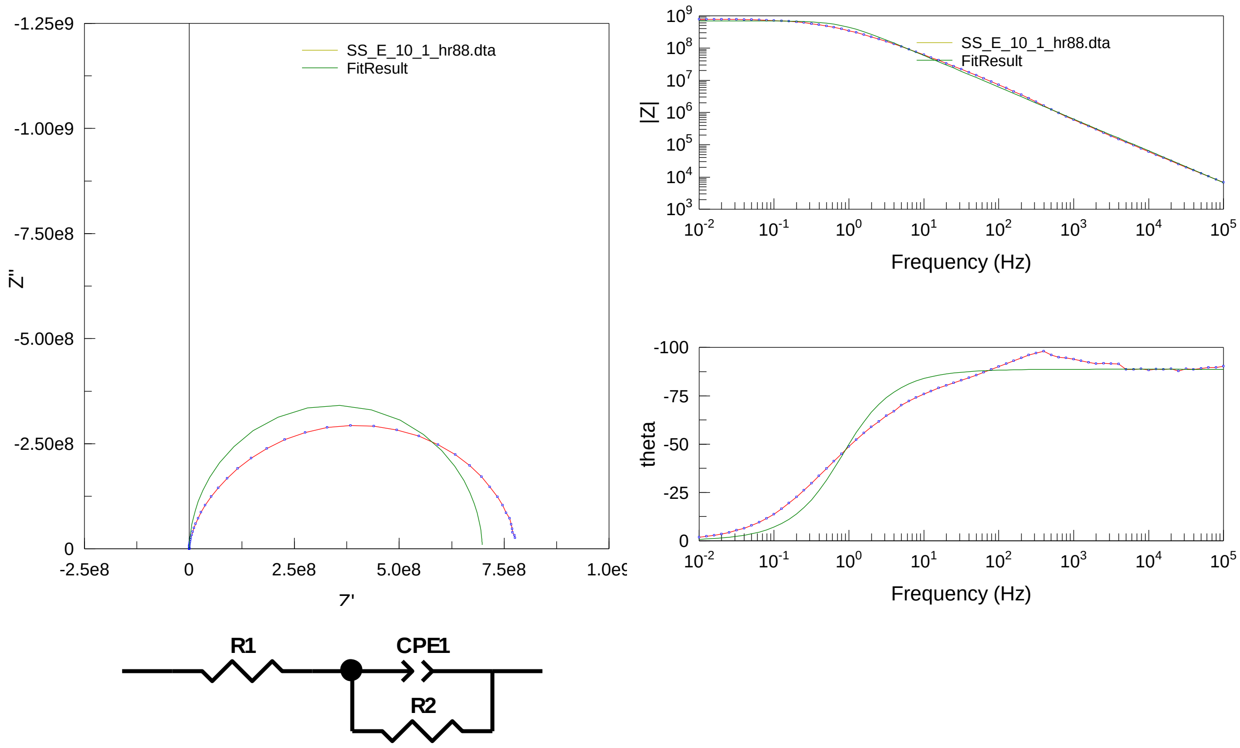

Element	Freedom	Value	Error	Error %
R1	Fixed(X)	10	N/A	N/A
CPE1-T	Free(±)	2.8597E-10	9.2722E-12	3.2424
CPE1-P	Free(±)	0.98589	0.0039434	0.39998
R2	Free(±)	6.9806E08	1.5631E07	2.2392

Chi-Squared: 0.18365
Weighted Sum of Squares: 25.527

Data File: C:\Users\Abhijit\Desktop\CRS\SS_E_10_1_hr88.dta
Circuit Model File:
Mode: Run Fitting / All Data Points (1 - 71)
Maximum Iterations: 100
Optimization Iterations: 0
Type of Fitting: Complex
Type of Weighting: Calc-Modulus

Figure A.38. Equivalent Circuit Model for Epoxy coating on Cold Rolled Steel with 10% cerium capsules after 96 hours of immersion in 5% NaCl solution.

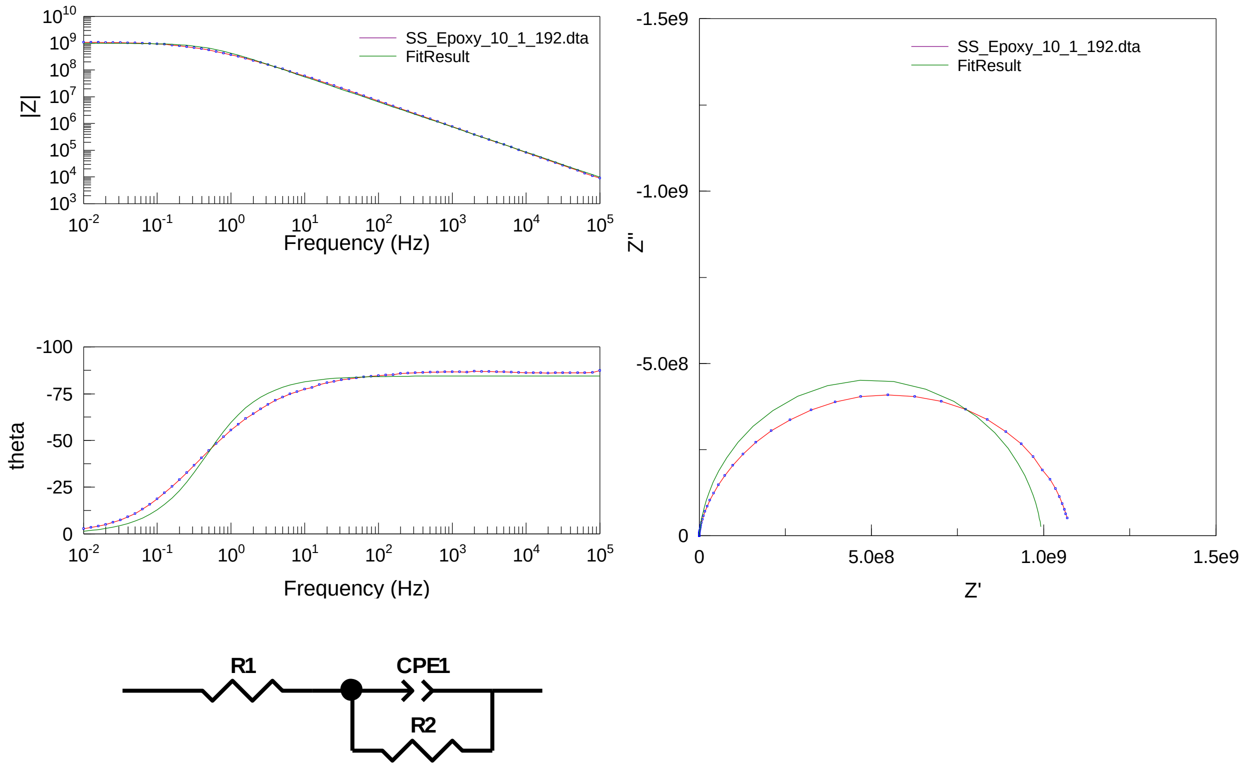

Element	Freedom	Value	Error	Error %
R1	Fixed(X)	10	N/A	N/A
CPE1-T	Free(+)	3.6549E-10	7.1044E-12	1.9438
CPE1-P	Free(+)	0.93929	0.0024185	0.25748
R2	Free(+)	9.9501E08	1.5665E07	1.5744

Chi-Squared:	0.032694
Weighted Sum of Squares:	4.5444

Figure A.39. Equivalent Circuit Model for Epoxy coating on Cold Rolled Steel with 10% cerium capsules after 192 hours of immersion in 5% NaCl solution.

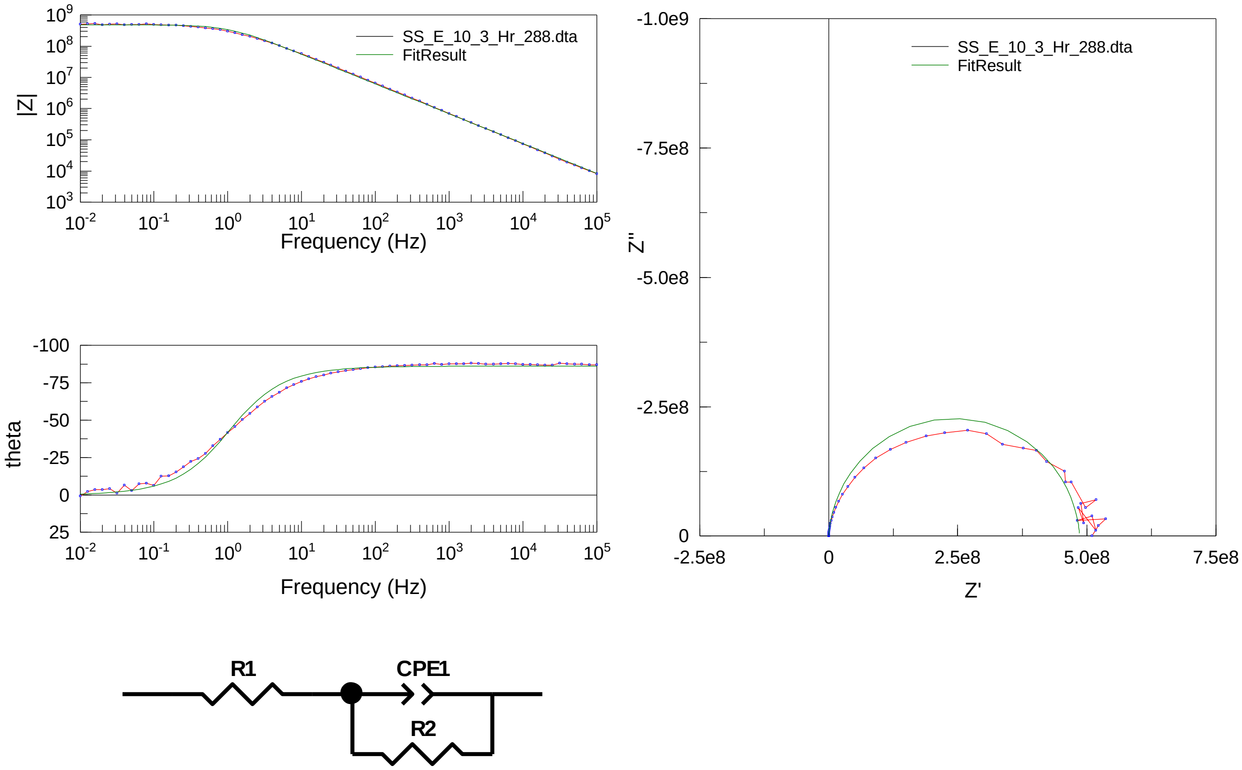

Element	Freedom	Value	Error	Error %
R1	Fixed(X)	10	N/A	N/A
CPE1-T	Free(+)	3.3783E-10	5.4963E-12	1.6269
CPE1-P	Free(+)	0.95705	0.0019409	0.2028
R2	Free(+)	4.8611E08	5.2473E06	1.0794

Chi-Squared:	0.024439
Weighted Sum of Squares:	3.397

Figure A.40. Equivalent Circuit Model for Epoxy coating on Cold Rolled Steel with 10% cerium capsules after 288 hours of immersion in 5% NaCl solution.

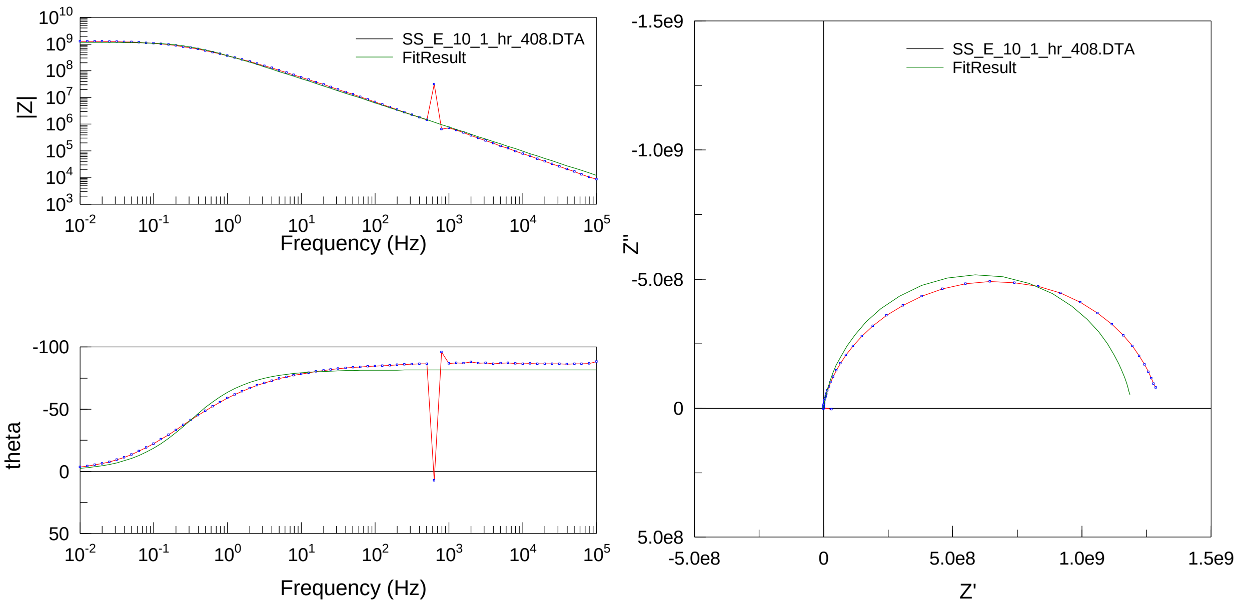

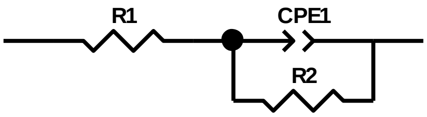

Element	Freedom	Value	Error	Error %
R1	Fixed(X)	10	N/A	N/A
CPE1-T	Free(+)	4.5808E-10	2.6255E-10	57.315
CPE1-P	Free(+)	0.90731	0.03101	3.4178
R2	Free(+)	1.1954E09	1.7278E08	14.454

Chi-Squared:	2.2686
Weighted Sum of Squares:	315.33

Figure A.41. Equivalent Circuit Model for Epoxy coating on Cold Rolled Steel with 10% cerium capsules after 408 hours of immersion in 5% NaCl solution.

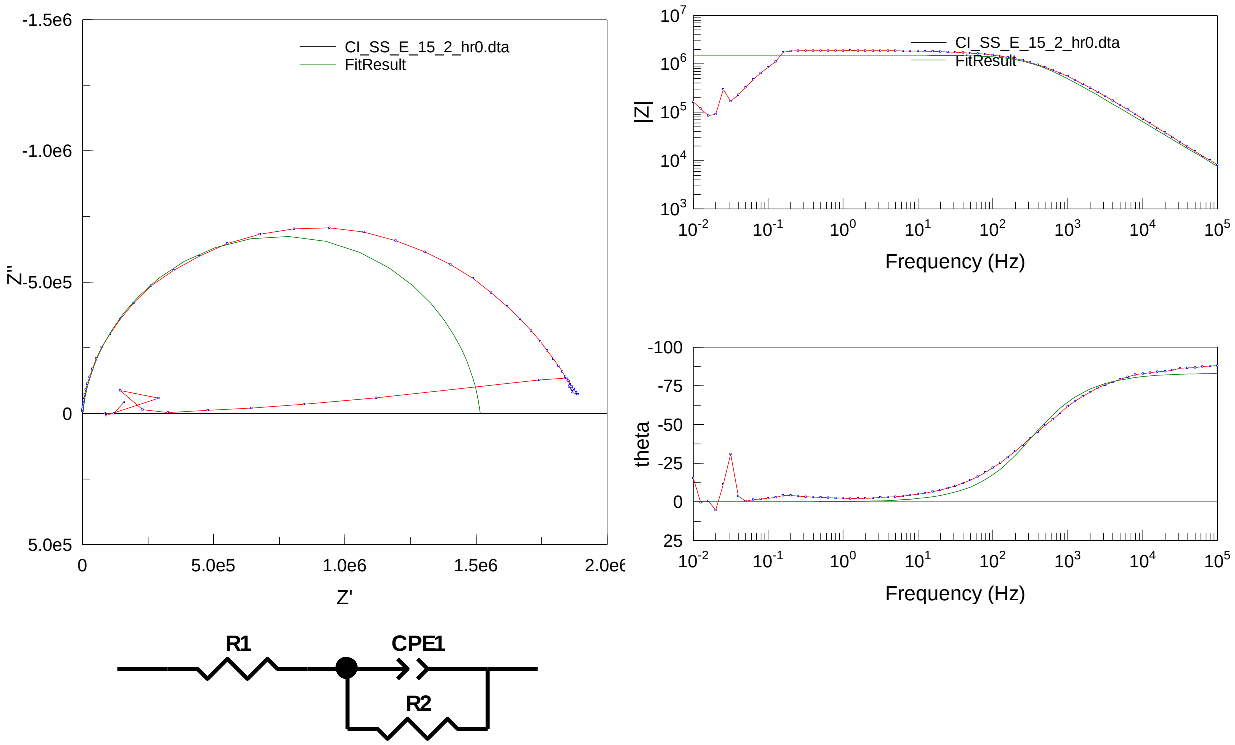

Element	Freedom	Value	Error	Error %
R1	Fixed(X)	10	N/A	N/A
CPE1-T	Free(±)	5.5985E-10	1.2835E-10	22.926
CPE1-P	Free(±)	0.92586	0.021381	2.3093
R2	Free(±)	1.5161E06	59680	3.9364

Chi-Squared:	2.7356
Weighted Sum of Squares:	380.25
Data File:	C:\Users\Abhijit\Desktop\CRS\CI_SS_E_15_2_hr0.dta
Circuit Model File:	
Mode:	Run Fitting / All Data Points (1 - 71)
Maximum Iterations:	100
Optimization Iterations:	0
Type of Fitting:	Complex
Type of Weighting:	Calc-Modulus

Figure A.42. Equivalent Circuit Model for Epoxy coating on Cold Rolled Steel with 15% cerium capsules after 0 hours of immersion in 5% NaCl solution.

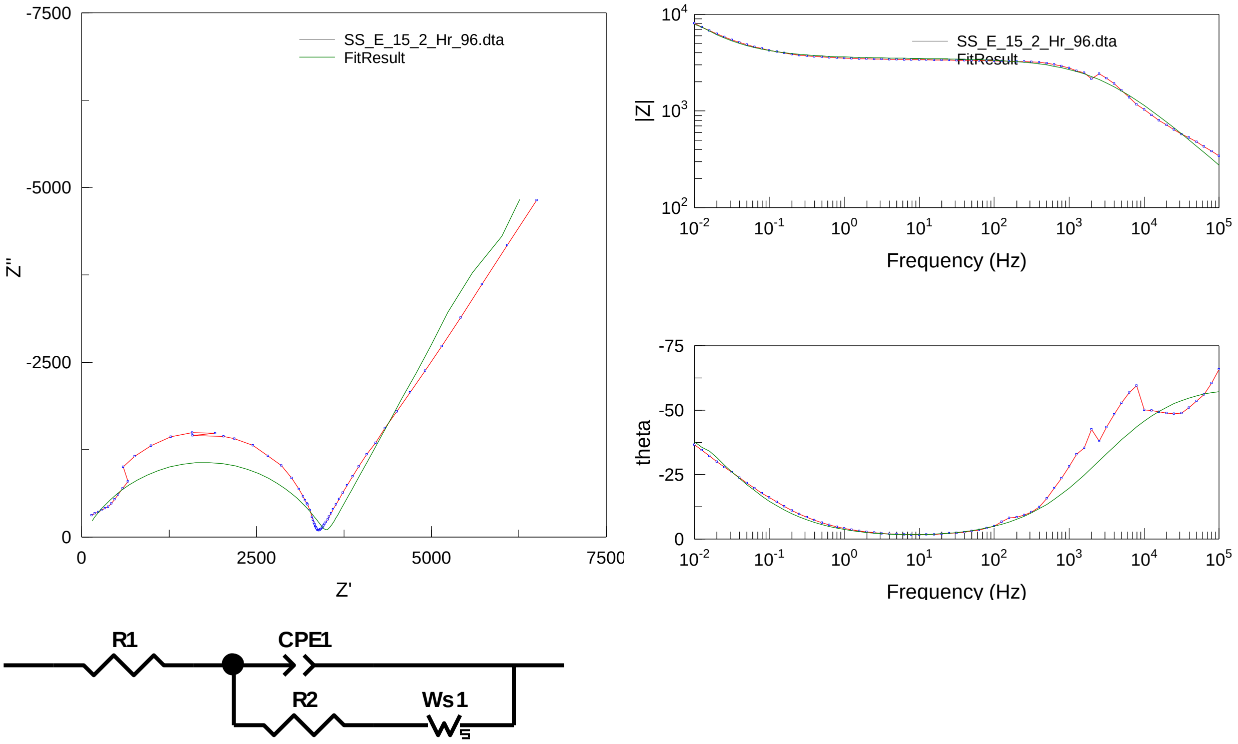

Element	Freedom	Value	Error	Error %
R1	Fixed(X)	10	N/A	N/A
CPE1-T	Free(±)	3.1308E-07	4.0757E-08	13.018
CPE1-P	Free(±)	0.69945	0.010875	1.5548
R2	Free(±)	3488	53.42	1.5315
Ws1-R	Free(±)	22180	5041.5	22.73
Ws1-T	Free(±)	112.9	43.046	38.128
Ws1-P	Free(±)	0.68127	0.028853	4.2352

Chi-Squared:	0.036022
Weighted Sum of Squares:	4.899
Data File:	C:\Users\Abhijit\Desktop\CRS\SS_E_15_2_Hr_96.dta
Circuit Model File:	
Mode:	Run Fitting / All Data Points (1 - 71)
Maximum Iterations:	100
Optimization Iterations:	0
Type of Fitting:	Complex
Type of Weighting:	Calc-Modulus

Figure A.43. Equivalent Circuit Model for Epoxy coating on Cold Rolled Steel with 15% cerium capsules after 96 hours of immersion in 5% NaCl solution.

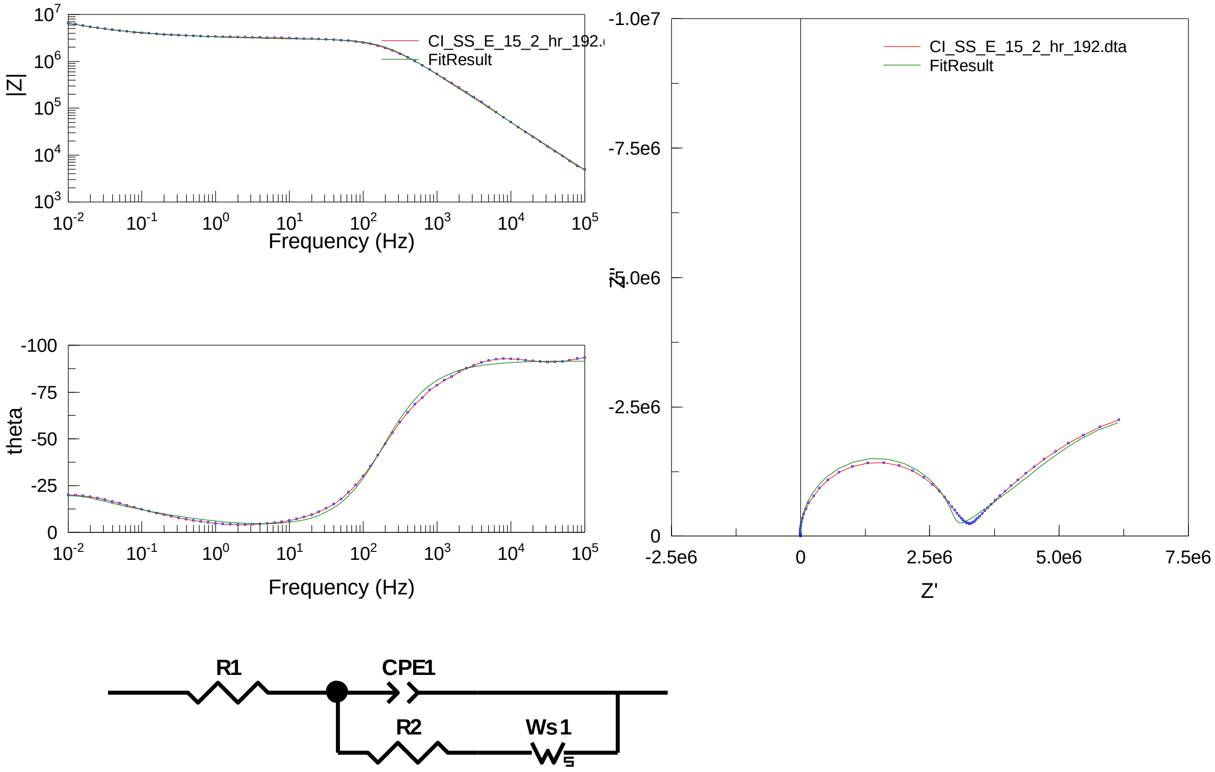

Element	Freedom	Value	Error	Error %
R1	Fixed(X)	10	N/A	N/A
CPE1-T	Free(+)	3.4639E-10	7.2566E-12	2.0949
CPE1-P	Free(+)	0.98054	0.0025423	0.25928
R2	Free(+)	2.9629E06	14870	0.50187
Ws1-R	Free(+)	6.6452E06	3.4762E05	5.2311
Ws1-T	Free(+)	61.72	7.9676	12.909
Ws1-P	Free(+)	0.43742	0.0059894	1.3693

Chi-Squared:	0.0012995
Weighted Sum of Squares:	0.13774

Figure A.44. Equivalent Circuit Model for Epoxy coating on Cold Rolled Steel with 15% cerium capsules after 192 hours of immersion in 5% NaCl solution.

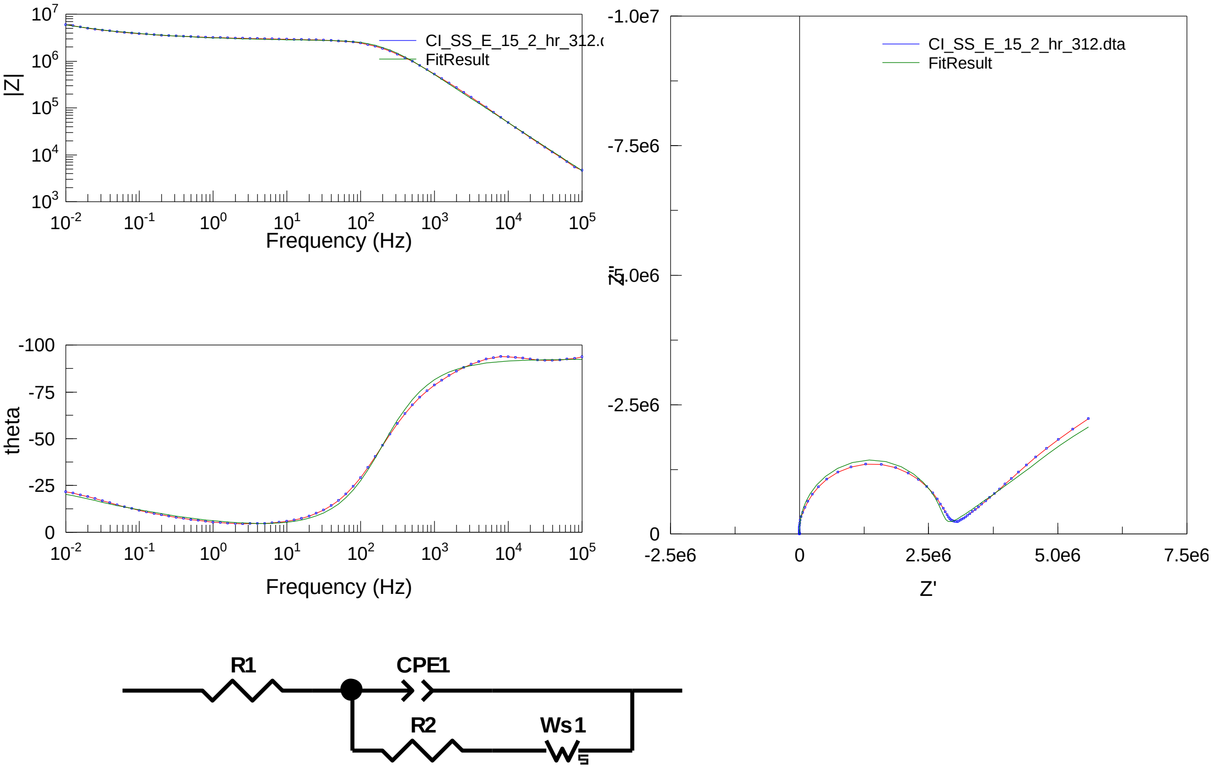

Element	Freedom	Value	Error	Error %
R1	Fixed(X)	10	N/A	N/A
CPE1-T	Free(+)	3.4166E-10	5.9218E-12	1.7332
CPE1-P	Free(+)	0.98346	0.0021602	0.21965
R2	Free(+)	2.7889E06	11758	0.4216
Ws1-R	Free(+)	7.7915E06	7.3417E05	9.4227
Ws1-T	Free(+)	107.7	24.904	23.123
Ws1-P	Free(+)	0.42944	0.004915	1.1445

Chi-Squared:	0.00092795
Weighted Sum of Squares:	0.098363

Figure A.45. Equivalent Circuit Model for Epoxy coating on Cold Rolled Steel with 15% cerium capsules after 312 hours of immersion in 5% NaCl solution.

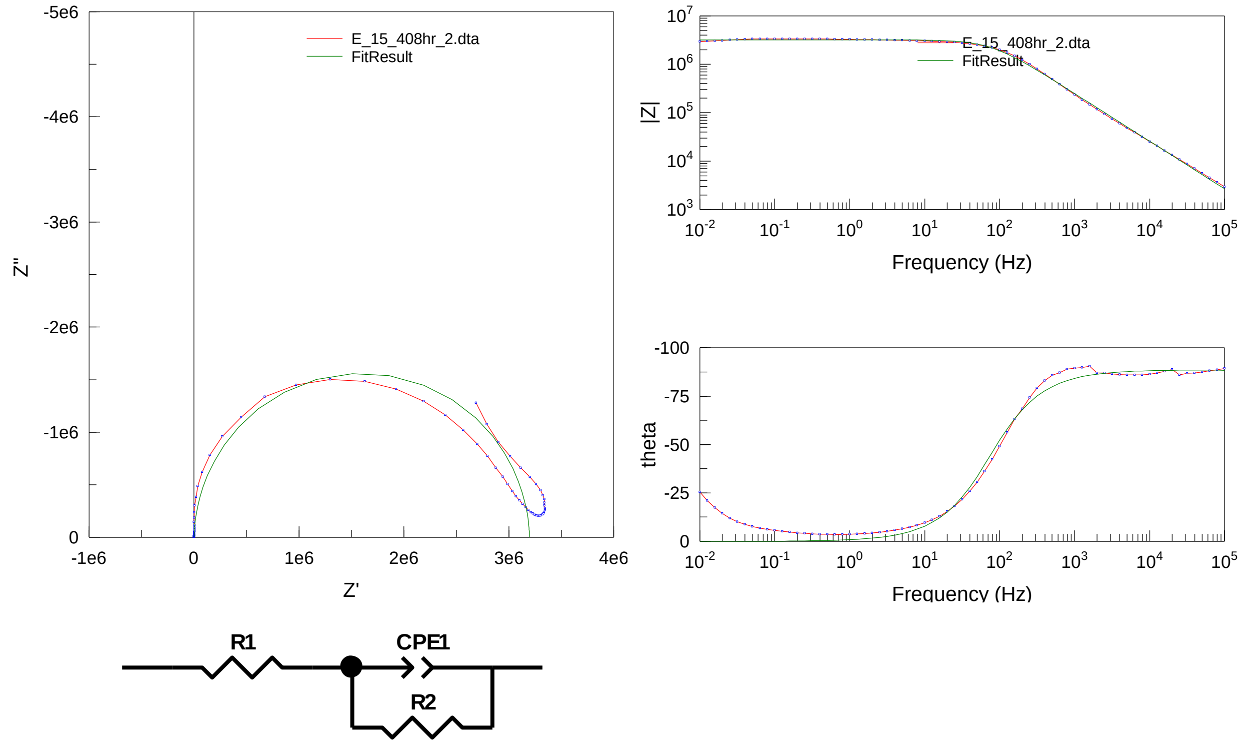

Element	Freedom	Value	Error	Error %
R1	Fixed(X)	10	N/A	N/A
CPE1-T	Free(±)	7.3124E-10	3.848E-11	5.2623
CPE1-P	Free(±)	0.98456	0.0051764	0.52576
R2	Free(±)	3.1971E06	42116	1.3173

Chi-Squared: 0.25425
Weighted Sum of Squares: 35.341

Data File: C:\Users\Abhijit\Desktop\CRS\E_15_408hr_2.dta
Circuit Model File:
Mode: Run Fitting / All Data Points (1 - 71)
Maximum Iterations: 100
Optimization Iterations: 0
Type of Fitting: Complex
Type of Weighting: Calc-Modulus

Figure A.46. Equivalent Circuit Model for Epoxy coating on Cold Rolled Steel with 15% cerium capsules after 408 hours of immersion in 5% NaCl solution.

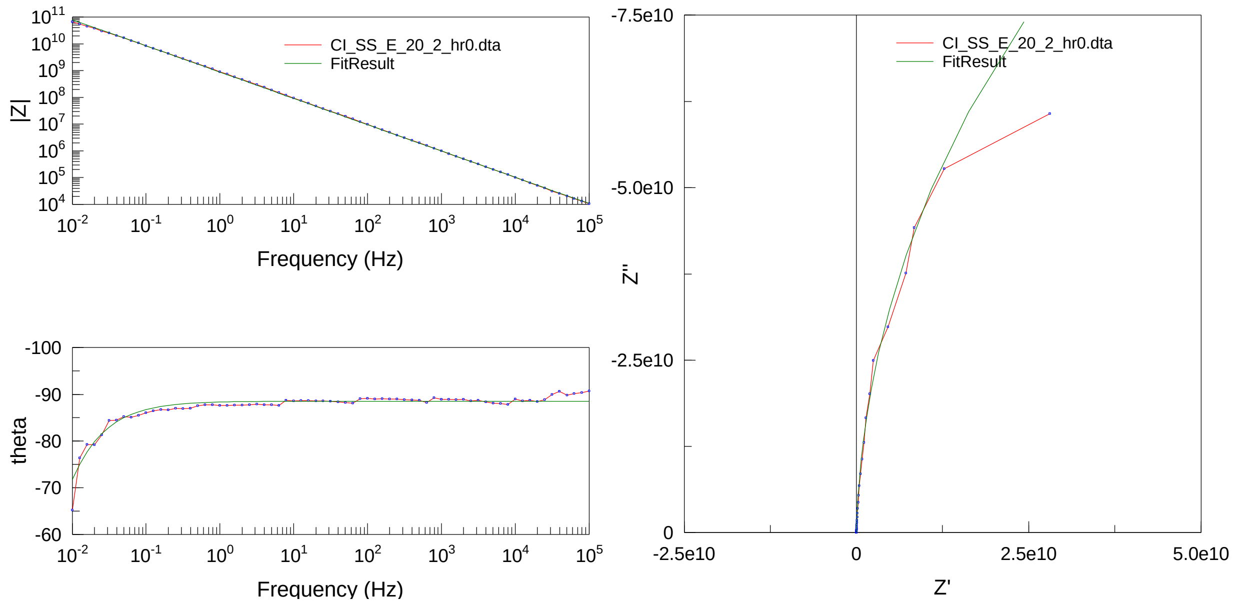

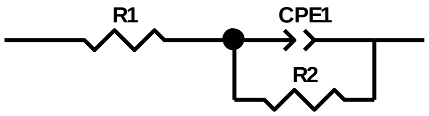

<u>Element</u>	<u>Freedom</u>	<u>Value</u>	<u>Error</u>	<u>Error %</u>
R1	Fixed(X)	10	N/A	N/A
CPE1-T	Free(+)	1.8564E-10	9.9855E-13	0.5379
CPE1-P	Free(+)	0.98381	0.00075184	0.076421
R2	Free(+)	2.7091E11	1.1039E10	4.0748

Chi-Squared: 0.025911
Weighted Sum of Squares: 3.6017

Figure A.47. Equivalent Circuit Model for Epoxy coating on Cold Rolled Steel with 20% cerium capsules after 0 hours of immersion in 5% NaCl solution.

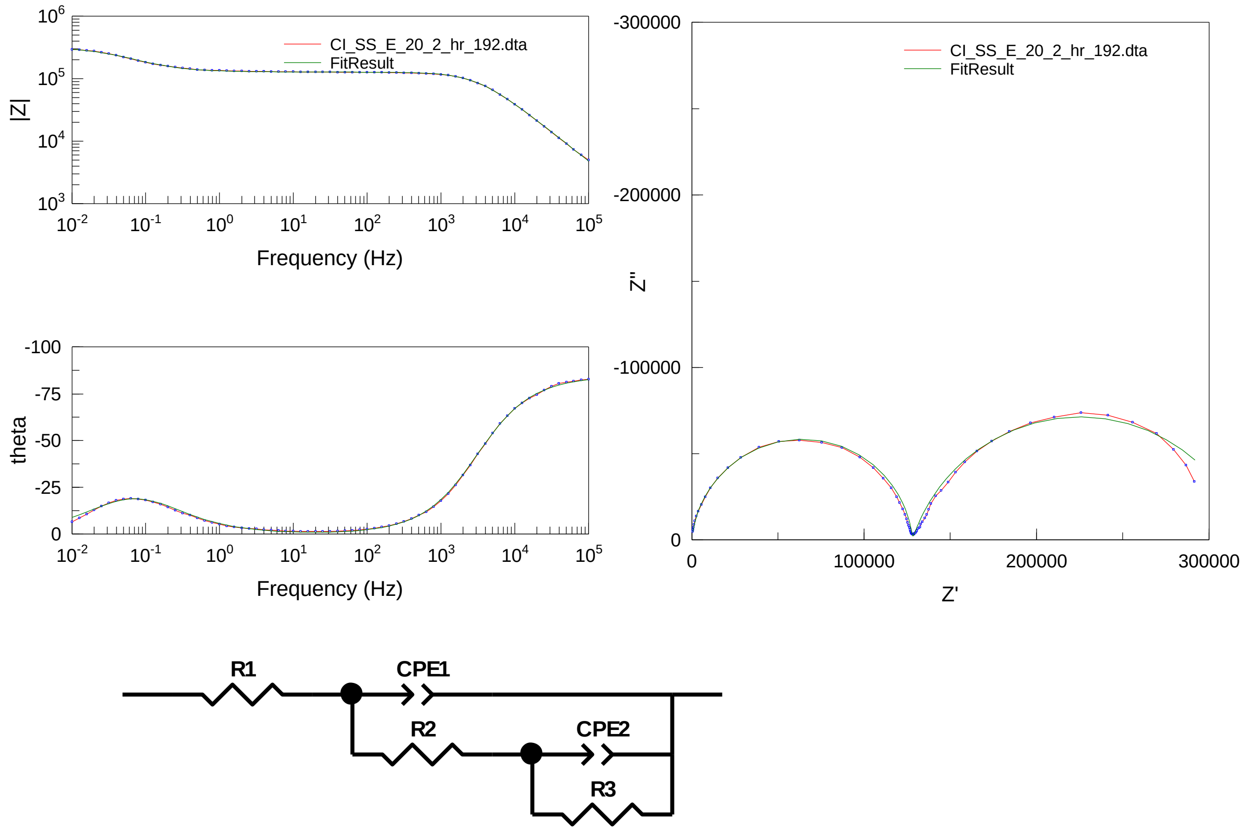

Element	Freedom	Value	Error	Error %
R1	Fixed(X)	10	N/A	N/A
CPE1-T	Free(+)	7.1304E-10	1.0748E-11	1.5073
CPE1-P	Free(+)	0.94229	0.0012726	0.13505
R2	Free(+)	1.2804E05	221.36	0.17288
CPE2-T	Free(+)	1.5583E-05	1.5182E-07	0.97427
CPE2-P	Free(+)	0.80627	0.0065466	0.81196
R3	Free(+)	1.9428E05	2267.6	1.1672

Chi-Squared: 0.00072198

Weighted Sum of Squares: 0.09819

Figure A.48. Equivalent Circuit Model for Epoxy coating on Cold Rolled Steel with 20% cerium capsules after 96 hours of immersion in 5% NaCl solution.

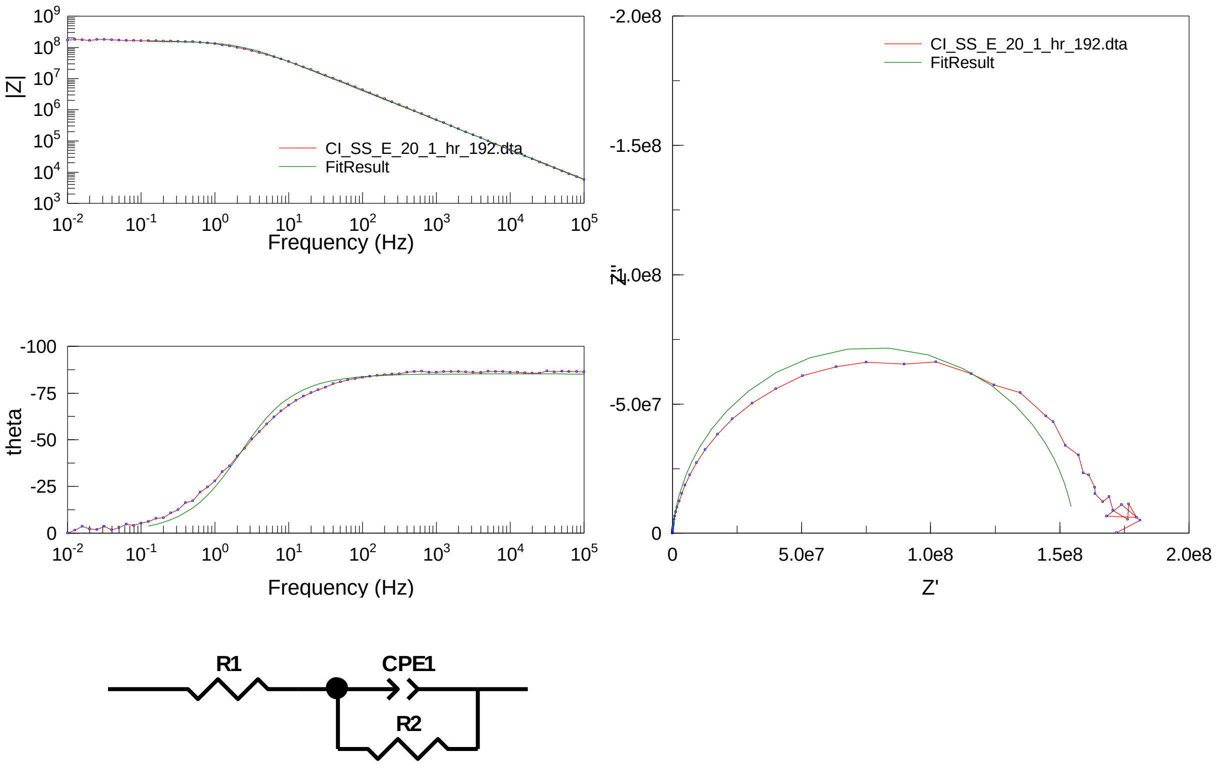

Element	Freedom	Value	Error	Error %
R1	Fixed(X)	10	N/A	N/A
CPE1-T	Free(+)	5.388E-10	8.3406E-12	1.548
CPE1-P	Free(+)	0.94811	0.0017894	0.18873
R2	Free(+)	1.5585E08	1.8378E06	1.1792

Chi-Squared: 0.012837

Weighted Sum of Squares: 1.5019

Figure A.49. Equivalent Circuit Model for Epoxy coating on Cold Rolled Steel with 20% cerium capsules after 192 hours of immersion in 5% NaCl solution.

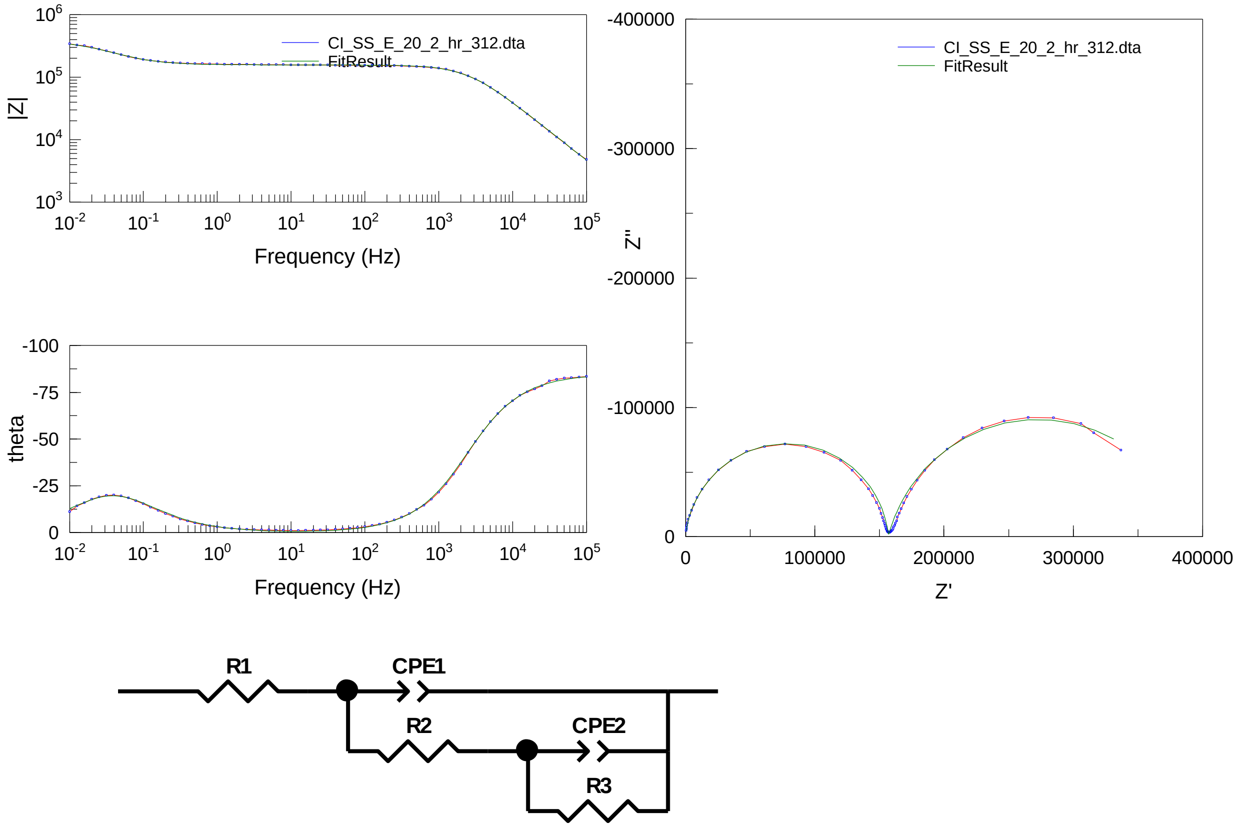

Element	Freedom	Value	Error	Error %
R1	Fixed(X)	10	N/A	N/A
CPE1-T	Free(+)	7.0389E-10	8.8058E-12	1.251
CPE1-P	Free(+)	0.94534	0.0010781	0.11404
R2	Free(+)	1.5695E05	233.43	0.14873
CPE2-T	Free(+)	2.2359E-05	2.404E-07	1.0752
CPE2-P	Free(+)	0.84452	0.0066101	0.7827
R3	Free(+)	2.321E05	3307.6	1.4251

Chi-Squared: 0.00064683
Weighted Sum of Squares: 0.087969

Figure A.50. Equivalent Circuit Model for Epoxy coating on Cold Rolled Steel with 20% cerium capsules after 312 hours of immersion in 5% NaCl solution.

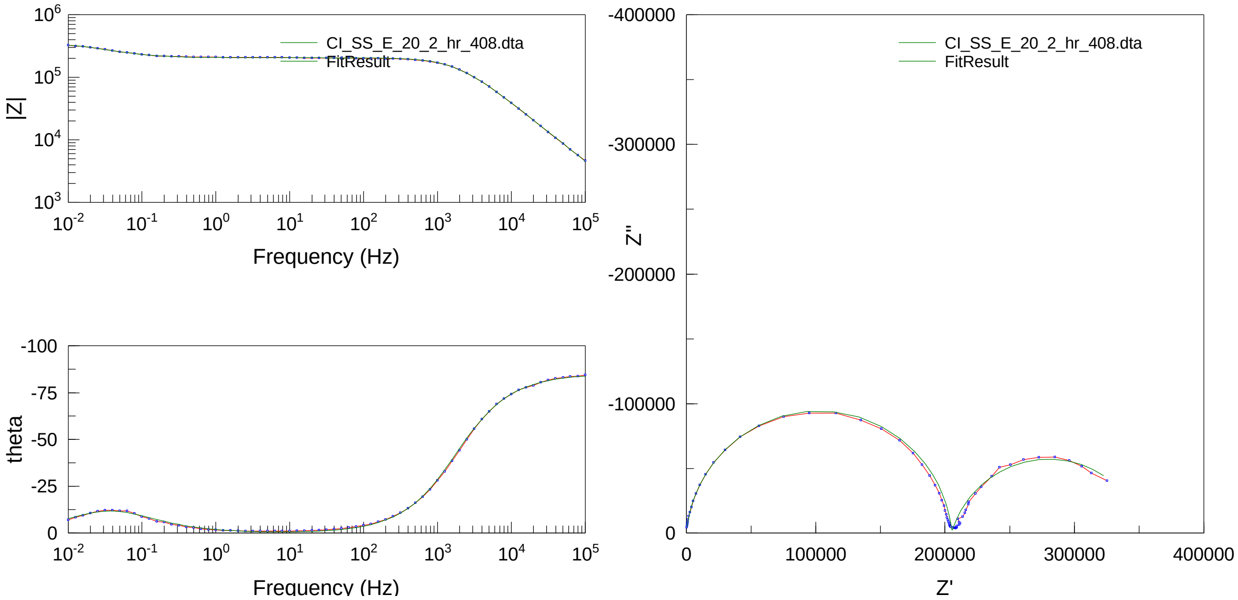

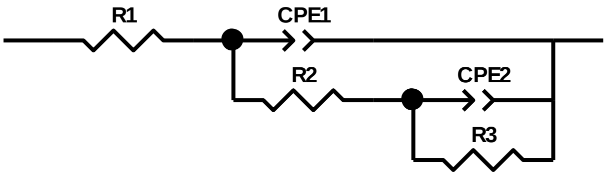

Element	Freedom	Value	Error	Error %
R1	Fixed(X)	10	N/A	N/A
CPE1-T	Free(+)	7.0879E-10	8.3267E-12	1.1748
CPE1-P	Free(+)	0.94692	0.001025	0.10825
R2	Free(+)	2.0523E05	317.24	0.15458
CPE2-T	Free(+)	2.908E-05	5.3998E-07	1.8569
CPE2-P	Free(+)	0.82914	0.011366	1.3708
R3	Free(+)	1.4987E05	3209.1	2.1413

Chi-Squared: 0.00078198

Weighted Sum of Squares: 0.10635

Figure A.51. Equivalent Circuit Model for Epoxy coating on Cold Rolled Steel with 20% cerium capsules after 408 hours of immersion in 5% NaCl solution.

APPENDIX B. COATINGS PROPERTIES OF CERIUM CAPSULES CONTAINING COATINGS

B.1. Results and discussion

One of the key elements in designing an autonomic coating system is not only to improve corrosion performance of the intended coating system but also to improve or at the least retain the existing coating properties of the virgin coating system. In order to evaluate the coating properties, various weight percentages of dry capsules were blended into a 2K waterborne epoxy system and coatings were applied on to steel and AA2024 T-3 substrates using a drawdown applicator at 8 mils wet film thickness and allowed to ambient cure for two days before evaluating coating properties. ASTM coating evaluation procedures as described in chapter 2 were followed to determine the properties of the coatings.

After the coatings were cured it was observed that the roughness of the coating surface increased as a function of the weight percent of the capsules added. This may be because of the buoyancy of the capsules due to the density difference in the resin system and the capsules. The dry film thickness of the coating was measured on both steel and aluminum using Positector ® 6000 thickness measurement gauge. It was observed that with increase in the weight percent of capsules the thickness of the coating was found to increase on steel surface. It may be because of the tendency of the capsules to float to the surface of the coating resulting in the increased thickness than that of virgin epoxy coating. It is also observed that with increase in the weight percent of capsules lesser percentage of the smooth epoxy coating was exposed to the tip of the film thickness gauge thus large deviations in the measurements at higher weight percent capsule containing coatings were recorded. Thickness of all the microcapsules containing coatings was greater on the steel substrate than the epoxy coatings on aluminum substrates. It was also noted that in case of aluminum substrates the standard deviation at lower weight percentages was higher than that of the steel samples indicating that the differences observed were more experimental than the actual thickness of the sample. The percent solids also play a role in the thickness of the coating as well, as water was added to adjust the viscosity of the admixed epoxy system at higher weight percent capsules.

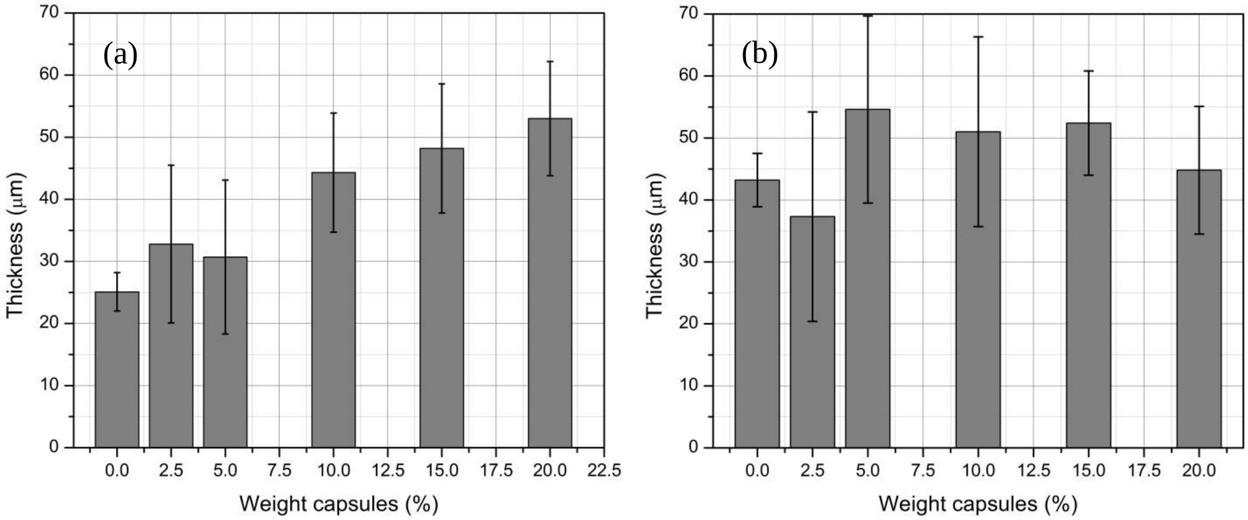

Figure B.1. Dry film thickness of epoxy coatings containing various weight percent of capsules on (a) Cold rolled steel and (b) AA 2024 T-3.

The increase in the roughness of the coating as a result of the floating of the micro-capsules to the surface was evidenced in the gloss measurements. It was observed that with increase in the weight percent the 20°, 60° and 85° reflectance values decreased. The decrease in the observed reflectance was a direct consequence of the roughness introduced by the capsules on the surface of the coating.

The hardness of the coating as a result of the addition of capsules in coatings was characterized using pendulum, pencil and impact hardness procedures. The hardness coating was evaluated using Konig pendulum hardness (ASTM D 4366) on both steel and AA2024 T-3 and it was observed that with increase in the the percent of capsules incorporated in the coating, the pendulum hardness decreased.

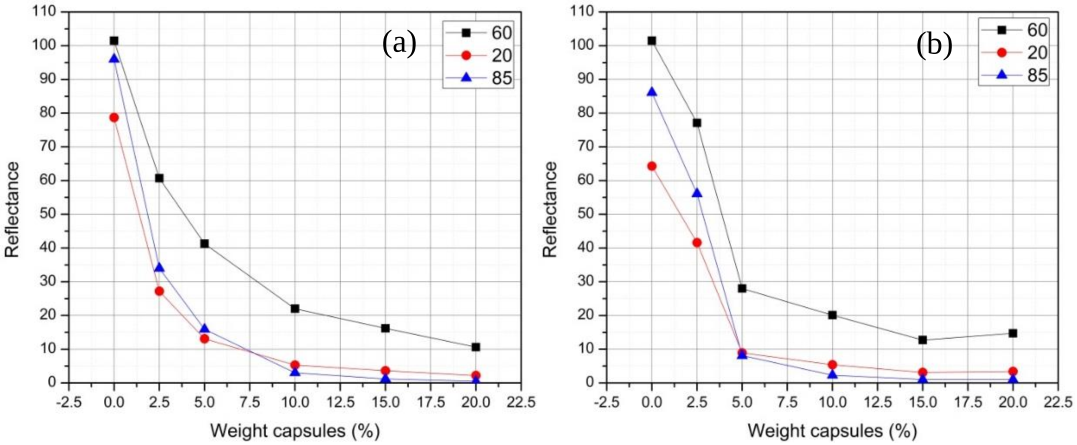

Figure B.2. Gloss measurements of epoxy coatings containing various weight percent of capsules on (a) Cold rolled steel and (b) AA 2024 T-3.

This indicated that with increase in the capsule concentration a dampening of the pendulum oscillation was observed, which can be explained by the microcapsules available at the surface which act as a soft interface dampening the oscillations.

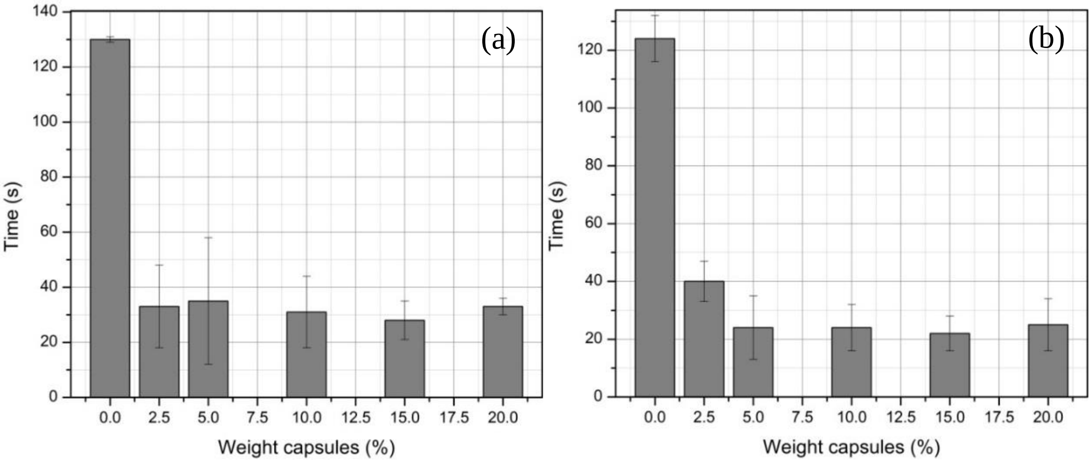

Figure B.3. Pendulum hardness of epoxy coatings containing various weight percent of capsules on (a) Cold rolled steel and (b) AA 2024 T-3.

Pencil hardness of the coatings was also evaluated and a similar trend as that of the pendulum hardness was noted. With increase in the weight percent of capsule, due to the availability of capsules on the surface, reduced pencil hardness was observed. The trend was irrespective of the metal substrate used. The impact hardness (ASTM D 2794) of the coating however was unaffected by the addition of capsule. All the coatings demonstrated hardness greater than 172 lb.cm without sign of crazing indicating that the properties of the underlying coating were intact after the addition of the capsules in the coating.

Table B.1. Coating properties of capsule containing epoxy coatings on cold roll steel.

Weight microcapsules (%)	0	2.5	5	10	15	20
Pendulum hardness(s)	124±8	40±7	24±11	24±8	22±6	25±9
Pencil hardness	2H	H	H	H	F	F
Cross hatch adhesion	0/25	0/25	0/25	0/25	0/25	0/25
Impact Hardness (lb.cm)	>172	>172	>172	>172	>172	>172
MEK double rubs (#)	110	100	50	50	30	30

Table B.2. Coating properties of capsule containing epoxy coatings on AA 2024 T-3.

Weight microcapsules (%)	0	2.5	5	10	15	20
Pendulum hardness(s)	130±1	33±15	35±23	31±13	28±7	33±3
Pencil hardness	2H	2H	2H	H	F	F
Cross hatch adhesion	0/25	0/25	0/25	0/25	0/25	0/25
Impact Hardness (lb.cm)	>172	>172	>172	>172	>172	>172
MEK double rubs (#)	120	30	70	50	40	30

The effect of incorporation of microcapsules on adhesion was evaluated using crosshatch adhesion test (ASTM D 3359). The crosshatch adhesion measurements were performed to evaluate the adhesion of the coating upon scribing the surface. In case of the cross adhesion test, no delamination was observed in the coatings containing capsules. The solvent resistance of the coating was also evaluated using MEK double rub test (ASTM D 7835). It was observed that with increase in the microcapsule concentration in the coating, the solvent resistance decreases on both the metal surfaces. The roughness introduced in the coating due to the capsules may have resulted in the poor solvent resistance due to the particle acting as little sand particles removing the coating with each double rub.

The addition of cerium containing capsules to a traditional 2 K epoxy coating system did not deteriorate the coating properties drastically. The deterioration in the coating system was primarily observed due to the non-uniform distribution and the buoyancy of the capsules in the epoxy coating systems. Upon application of a topcoat the surface defects were eliminated.